Characterization of Time-dependent Behavior of Semi-crystalline Polymers

by

Furui Shi

A thesis submitted in partial fulfillment of the requirements for the degree of

Doctor of Philosophy

Department of Mechanical Engineering
University of Alberta

Abstract

This thesis is concerned with the experiments and modelling for the time-dependent behavior of semicrystalline polymers. Relaxation test had long been used to evaluate the performance of materials. In this study, a novel multi-relaxation-recovery test was proposed based on cyclic stages of stress relaxation and stress recovery. Three nonlinear viscoelastic models, that is, the standard model and two models with two dashpots connected either in parallel or in series, were examined for the analysis of the test results. Each model contains a time-dependent, viscous branch and a time-independent, quasi-static branch. The examination suggests that the standard model can determine the long-term, load-carrying performance of polyethylene and identify a transition point for the onset of plastic deformation in the crystalline phase, but the models with two dashpots connected either in parallel or in series are needed to provide a close simulation of the experimentally measured stress response in both relaxation and recovery stages of the multi-relaxation-recovery test. In this work, the mechanical performance of two types of polyethylene was compared based on multi-relaxation-recovery test results at room temperature. The multi-relaxation-recovery tests were also conducted at elevated temperatures to explore the possibility of quantifying the activation energies for deformation of the dashpots at the relaxation stage. It was found the multi-relaxation-recovery test has the advantage of separating the time-dependent and time-independent

components of stiffness of the materials. The study concludes that the multi-relaxation-recovery test can provide data for determining parameters in Eyring's model in order to characterize the contribution of time-dependent and time-independent components of the stress response to polyethylene's deformation.

This study also presents an analysis of the stress evolution of high-density polyethylene at loading, relaxation, and recovery stages in a multi-relaxation-recovery test. The analysis is based on a three-branch spring-dashpot model that uses the Eyring's law to govern the viscous behavior. The spring-dashpot model comprises two viscous branches to represent the short- and long-term time-dependent stress responses to deformation, and a quasi-static branch to represent the time-independent stress response. A fast numerical analysis framework based on genetic algorithms was developed to determine values for the model parameters so that the difference between the simulation and the experimental data could be less than 0.08 MPa. Using this approach, values of the model parameters were determined as functions of deformation and time so that the model can simulate the stress response at loading, relaxation, and recovery stages of the multi-relaxation-recovery test. The simulation also generated ten sets of model parameter values to examine their consistency. The study concludes that the three-branch model can serve as a suitable tool for ana-

lyzing the mechanical properties of high-density polyethylene, and values for the model parameters can potentially be used to characterize the difference among different types of polyethylene for their mechanical performance.

It is important to explore the possibility of identifying a unique set of the parameter values so that the parameters can be used to establish the relationship between deformation and microstructural changes. The study developed an approach for this purpose based on stress variation during loading, relaxation, and recovery of polyethylene. One thousand sets of parameter values were determined for fitting data at the relaxation stages with discrepancy within 0.08 MPa. The study found that even with such a small discrepancy, the 1000 sets of parameter values showed a wide range of variation, but one of the model parameters, $\sigma_{v,L}(0)$, followed two distinct paths rather than showing a random distribution. The study further found that five selected sets of parameter values which showed discrepancy below 0.04 MPa yielded highly consistent values for the model parameters, except for the characteristic relaxation time. Therefore, the study concludes that a unique set of model parameter values can be identified to characterize mechanical behavior of polyethylene. This approach was then applied to four types of polyethylene pipes, to determine their quasi-static stress. The results showed that these polyethylene pipes have very close quasi-static stress despite the clear difference in the measured stress. This indicates that a unique set of

model parameter values could be identified for the spring-dashpot model, enabling a further study of using spring-dashpot models to characterize microstructural changes of polyethylene during deformation.

Preface

This thesis is an original work by Furui Shi under the supervision of Dr. Ben Jar. The main body of this thesis includes four published/under review journal papers.

Chapter 1 of this thesis includes the published work in section 1.2.1, with modifications, which has been published in a journal: Furui Shi and P-Y. Ben Jar. " Studies on the time-dependent behavior of semi-crystalline polymers." *Research and Development in Polymer Science* (2023), 2. 1. For this mini review paper, I was responsible for literature collection and manuscript composition. Dr. Jar was the supervisory author and assisted with manuscript edits and review.

Chapter 2 of this thesis, with minor revision, has been published in journal paper: Furui Shi and P-Y. Ben Jar. "Characterization of Polyethylene Using a New Test Method Based on Stress Response to Relaxation and Recovery." *Polymers* (2022). 14.14, 2763. I was responsible for the data collection and analysis as well as the manuscript composition. Dr. Jar was the supervisory author and assisted with data collection and manuscript editing.

Chapter 3 is based on the published paper: Furui Shi and P-Y. Ben Jar. " Characterization of loading, relaxation, and recovery behaviors of high-density polyethylene using a three-branch spring-dashpot model." *Polymer Engineering & Science* (2024). I was responsible for experiments, data collection, modelling, simulation, and analysis as well as the manuscript composition. Dr. Jar was the supervisory author and assisted with data collection, modelling, simulation, and manuscript editing.

Chapter 4 of this thesis is based on the journal paper under review: Furui Shi and P-Y. Ben Jar. "Simulation and analysis of loading, relaxation and recovery behavior of polyethylene and its pipes" *Polymers (under review)*. I was responsible for modelling, simulation, and analysis as well as the manuscript composition. Dr. Jar was the supervisory author and assisted with data collection, modelling, simulation, and manuscript editing.

Acknowledgements

I am deeply grateful to my supervisor, Professor Ben Jar, for his unwavering support, guidance, and feedback throughout this research. We began our work with a glorious purpose: to fully characterize polymers. This goal remained steadfast, even during the pandemic, thanks to his strong financial and emotional support. His dedication and commitment were particularly evident during those challenging times, as he continued to guide and support me persistently toward our shared purpose. His mentorship has been instrumental in the successful completion of this work. The more than five-year study journey with Professor Ben Jar is the most valuable experience of my life.

I would also like to extend my sincere thanks to my committee members, Professor Chong Qing Ru and Professor Morris Flynn, for their invaluable insights and constructive criticism, which greatly contributed to the refinement and improvement of my research.

My gratitude goes to the Natural Sciences and Engineering Research Council of Canada for their financial support, without which this research would not have been possible.

I am also thankful to the China Scholarship Council (CSC) for their generous funding and support during my studies.

I would like to express my appreciation to the machine shop staff for their technical assistance, which was crucial in the experimental phases of this project. Their expertise and help were vital to the successful execution of my research.

Finally, I want to thank my friends Jie Zheng, Chao Fan, and Congshan Mao for their encouragement, and my roommate, Wanke Yu, who has been like an older brother to me.

Table of Contents

List of Tables

List of Figures

List of Symbols and Abbreviations

E	Spring stiffness, MPa/mm
E_{qs}	Spring stiffness in the quasi-static branch, MPa/mm
E_v	Stiffness of the spring in the viscous branch, MPa/mm
$K_{v,L}$	Stiffness of the spring in the long-term branch, MPa/mm
$K_{v,S}$	Stiffness of the spring in the short-term branch, MPa/mm
$\dot{e}_{0,1}$	Pre-exponential factor of dashpot 1, mm/s
$\dot{e}_{0,2}$	Pre-exponential factor of dashpot 2, mm/s
HDPE	High-density polyethylene
MDPE	Medium-Density Polyethylene
k	Boltzmann's constant, kJ/(mol·K)
L	Long-term branch
MR	Multiple-relaxation
RR	Multiple-relaxation-recovery
PE	Polyethylene
RX	Relaxation
RY	Recovery
S	Short-term branch
SCP	Semi-crystalline Polymer

T	Temperature, K
t	Time, s
VBOP	Viscoplasticity theory based on overstress for polymers
ΔH_1	Activation energy of dashpot 1, kJ/mol
ΔH_2	Activation energy of dashpot 2, kJ/mol
$\dot{\delta}_{0E}$	Reference stroke rate, mm/s
$\dot{\delta}_{0E,1}$	Reference stroke rate of dashpot 1, mm/s
$\dot{\delta}_{0E,2}$	Reference stroke rate of dashpot 2, mm/s
δ_A	Applied stroke, mm
δ_v	Stroke of the dashpot, mm
$\delta_{v,1}$	Stroke of the dashpot 1, mm
$\delta_{v,2}$	Stroke of the dashpot 2, mm
$\dot{\delta}_{0E,L}$	Reference stroke rate of long-term branch, mm/s
$\dot{\delta}_{0E,S}$	Reference stroke rate of short-term branch, mm/s
$\dot{\delta}_A$	Time derivative of applied stroke, mm/s
$\dot{\delta}_v$	Stroke rate of the dashpot, mm/s
η	Dashpot constant, MP·s/mm
σ_0	Reference stress, MPa
$\sigma_{0,1}$	Reference stress of dashpot 1, MPa

$\sigma_{0,2}$	Reference stress of dashpot 2, MPa
$\sigma_{0,L}$	Reference stress of dashpot in the long-term branch, MPa
$\sigma_{0,S}$	Reference stress of dashpot in the short-term branch, MPa
σ_A	Applied stress, MPa
$\sigma_A(0)$	Applied stress at the beginning of the relaxation or recovery, MPa
σ_{qs}	Quasi-static stress, MPa
σ_v	Viscous stress, MPa
$\sigma_{v,1}$	Viscous stress of the dashpot 1, MPa
$\sigma_{v,2}$	Viscous stress of the dashpot 2, MPa
$\dot{\sigma}_v$	Time derivative of viscous stress, MPa/s
$\sigma_{v,L}$	Viscous stress of long-term branch, MPa
$\dot{\sigma}_{v,L}$	Time derivative of viscous stress for long-term branch, MPa/s
$\sigma_{v,S}$	Viscous stress of short-term branch, MPa
$\dot{\sigma}_{v,S}$	Time derivative of viscous stress for long-term branch, MPa/s
τ_v	Characteristic time for stress relaxation or stress recovery, s
$\tau_{v,1}$	Characteristic time for stress relaxation or stress recovery of dashpot 1, s
$\tau_{v,2}$	Characteristic time for stress relaxation or stress recovery of dashpot 2, s
$\sigma_{v,L}(0)$	Viscous stress of long-term branch at the origin of relaxation or recovery, MPa

$\sigma_{v,S}(0)$ Viscous stress of short-term branch at the origin of relaxation or recovery, MPa

Chapter 1 Introduction

Chapter 1 is an overview of this thesis, which presents the research background, motivations, and literature review, objectives, and methodologies. The thesis organization is also outlined at the end of this chapter.

1.1 Background and motivation

It is widely accepted that the ages of human civilization are defined by the utilization of materials. For instance, people in the Stone Age learned how to use stones and boosted the development of society. We are currently living in the Polymer Age [1,2]. Nowadays, more than two-thirds of global polymer production are semi-crystalline polymers (SCPs) [3]. SCPs such as polyethylene (PE) are materials made of large molecules, which are a class of thermoplastics that possess a complicated microstructure [4,5]. The study of SCPs has attracted enormous attention throughout the world, and the number of publications about SCPs steadily increases recently, which is shown in Figure 1.1 [6]. Utilization of SCPs has increased considerably in industrial sectors such as fluid transportation, packaging, electronics, civil engineering, aerospace, medical and automotive industries due to SCPs' potential for fulfilling the performance requirements, with the advantages of chemical inertness and attractive mechanical properties [7–10]. As the most popular SCP, PE has a global demand of 100 million metric tons in 2018, equivalent to approximately US$164 billion, with an annual growth of 4.0% [11,12]. Figure 1.2. shows that U.S. miles of plastic main by materials in 2021, and it was noticed that more than 98% of plastic pipes are made of PE, which suggests that PE is very popular for gas pipe applications in the U.S. [13]. SCPs possess complex microstructures composed of crystalline and amorphous phases, hence they exhibit nonlinear time-dependent behaviors [8], including relaxation and creep [4,14–19], which significantly impact their performance in various applications. The winner of Nobel Prize in Physics, Richard Feynman, clearly showed how time-dependent behavior of polymers is significant in practical engineering after explosion of the space shuttle Challenger caused by the failure of the O-ring in 1986 [20]. This suggests the time-dependent behavior of SCPs is not well understood [21].

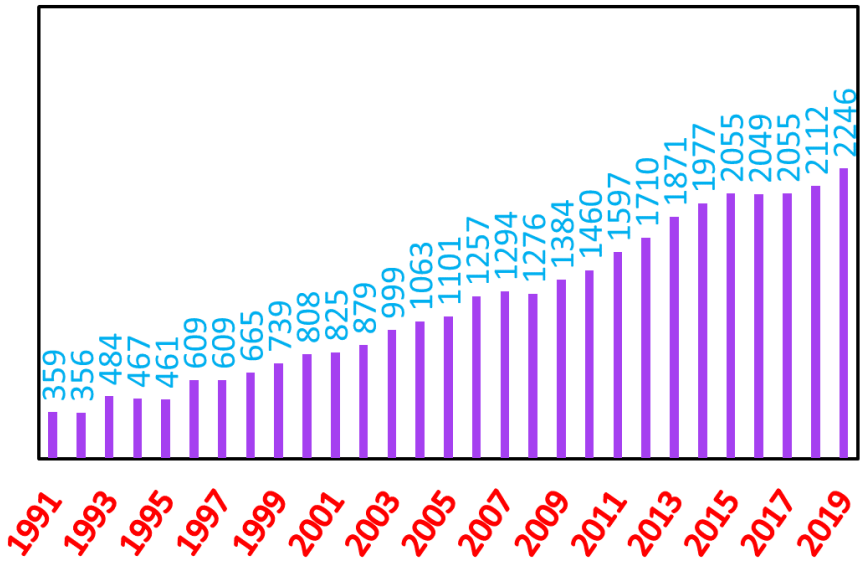

Figure 1.1. The number of publications in the field of SCPs in recent years.

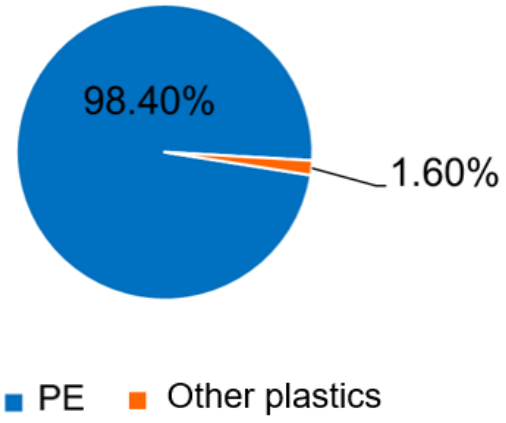

Figure 1.2. U.S. miles of plastic main by materials in 2021.

Polymer crystallization-related study can date back to 1805 when the concept of macromolecules was known. The British philosopher Gough reported the sensation of warmth in his lips while fast stretching natural rubber [6,22]. In 1920, Staudinger [23,24] first proposed that natural and man-made polymers are covalently linked macromolecules, rather than colloidal systems or aggregates of smaller organic molecules, marking the beginning of modern polymer science and engineering. In 1925, Katz [25] first observed strain-induced crystallization of natural rubber under large deformation using wide angle X-ray diffraction (WAXD). In 1946, Eyring and Halsey [26] showed the connection between the mechanical properties of textiles and molecular structure. In 1947, Flory [27] first predicted that the orientation of the polymer chain molecules under stretched state causes conformational entropy loss, which shifts up the melting point of the crystalline phase and hence favors polymer crystallization. Recently, Lambri et al. [28] in 2019 performed dynamic mechanical analysis (DMA) on crosslinked low-density polyethylene (XLPE) and determined the activation energy at the relaxation peak. Wilhelm et al. [29] in 2019 developed the nano-creep test for HDPE using a rheometer and measured the activation energy and volume in the amorphous phase according to Eyring's equation. Eichelter et al. [30] in 2020 proposed that mechanical relaxations in polyolefins are related to the mobility of polymer chains and performed dynamic mechanical thermal analysis (DMTA) using isotactic polypropylene (iPP) to measure the activation energy in α relaxation. Izraylit et al. [31] in 2020 performed relaxation experiments to investigate the performance of polymer blends and obtained values for the three parameters in Eyring's equation based on the Hong-Strobl model. Although SCP's properties have been improved in recent years, sometimes this cannot guarantee the designed service life of SCP structures as unexpected failure can happen, which leads to tremendous economic losses and sometimes fatalities [32–34]. Therefore, it is necessary to fully characterize the time-dependent behavior of SCPs.

There have been numerous experimental studies addressing different characteristics of the time-dependent behavior of SCPs [35,36]. The time-dependent behavior can be characterized by relaxation and creep tests [37,38]. According to Khan and Lopez-Pamies, detailed knowledge of the relaxation and creep processes on polymers is essential for developing a good understanding of their mechanical behavior [39]. Relaxation (i.e., at constant deformation) and creep (i.e., at constant load) behavior of SCPs can be observed at room temperature [40,41]. Over 50 years ago, stress relaxation tests were introduced to assess the material properties of plastic pipes under constant strain [42,43]. Moser et al. [43] demonstrated the usefulness of stress relaxation tests for predicting the performance of plastic pipes because buried pipes are subjected to fixed deformation in the presence of the equilibrium condition between the pipe and soil systems [44]. Modern PE pipes have a lifespan exceeding 50 years [13,45–49], and 98% of plastic pipes in the United States are made of PE [13,50–53]. However, stress relaxation can lead to the failure at the fitting and joints of PE pipe, which can result in the leakage of the pipe transportation system [54]. Therefore, it is necessary to conduct corresponding experiments and modelling for the study of the relaxation behavior of PE.

It is well known that the stress in relaxation decreases dramatically at the beginning of the relaxation, and after a short period the stress reaches an asymptotic-like limit [8,55]. Zhang and Jar found the curve profile for stress-time in relaxation can be affected by the crosshead speed in the loading path before the relaxation [50]. Recovery behavior could be observed after unloading down to a constant deformation level. According to Castagnet [56], the stress responses in relaxation and recovery are different for SCPs, and a larger stress change is measured in relaxation after loading, in comparison to that observed in recovery behavior after unloading. It is also well known

that the creep behavior contains 3 distinctive states, including primary, the secondary and the tertiary creep stages [57,58]. It was observed that the creep strain rate drops rapidly from an initially high value during primary creep, then almost reaches a constant in the secondary creep, and the strain rate increases in the tertiary creep [15,59]. According to Khan, test methods containing complex loading histories can reveal some singular deformation characteristics [41]. It was reported that although a particular attention has been paid often on creep and relaxation after the tensile loading on SCPs [15,57,60–63], only a few studies investigated creep and recovery behavior after unloading [36,64–66]. It was observed that recovery and creep behavior after strain reversal could show unusual stress and deformation responses respectively [36,64,65,67].

For many years, considerable models about the time-dependent behavior of polymers have been developed. According to Khan and Zhang, most of these models have been aimed at different aspects of these observations for the time-dependent behavior of polymers, and frequently one model describes only one of time-dependent behaviors (creep, relaxation, or tensile test with constant strain rate) and the other time-dependent behaviors of the same polymer are not considered [35]. Ayoub et al. [68] presented that most of the modelling work in the literature has been devoted to description of amorphous polymers which are monophasic, in contrast to SCPs that show coexistence of amorphous and crystalline phases [69,70]. The interaction between the amorphous and crystalline phases in responding to applied deformation is an important issue for determination of the overall mechanical behavior [63,71]. Jar proposed that the level of involvement of amorphous and crystalline phases changes in the deformation process for SCPs [72]. Spring-dashpot models are common for the description of the time-dependent behavior of polymers [73,74]. It was reported that the spring-dashpot model has the advantage of being able to visualize the deformation easily and directly [75]. According to Haward and Thackray, suitable models should be as simple

as possible [76]. The simplest models are Maxwell model and Voigt model, which can be applied to represent the relaxation and creep behavior, respectively [55,77]. However, these linear models are insufficient to describe the complex time-dependent behavior of SCPs [78]. It was reported that some models could qualitatively describe the recovery and creep behavior after strain reversal, but with poor accuracy [36,79]. Some models are good at the description of the time-dependent behavior of SCPs, but they incorporate a large number of material parameters [69,80,81]. Khan and Zhang reported that it is very complicated and time consuming to determine material parameters of complex models [35].

It is also worth mentioning that many models used for the analysis of the mechanical test results require assumptions that are practically unrealistic. For example, characteristic relaxation time for the viscous deformation has often been assumed to be constant, independent of the deformation levels or the materials [60,63]. The modulus of the spring in the viscous branch was assumed to be constant during tensile deformation [15,63,76]. It was also assumed that viscous stress for the Eyring's equation is a function of the total strain rate, rather than the strain rate across the Eyring's dashpot [15,82].

1.2 Literature review

1.2.1 Mechanical characterization of time-dependent behavior

SCPs have long been use for industrial applications such as fluid transportation, packaging, electronics, civil infrastructures, aerospace, medicines and automotive [7–10]. One of the challenges for these applications lies on the proper characterization and prediction of SCP's time-dependent properties which are often demonstrated through the relaxation and creep behavior. So

far, numerous experimental studies have been carried out using changes in the relaxation or creep behavior to characterize SCP's time-dependent properties.

Time-dependent behavior of SCP is often characterized using relaxation and creep tests [37,38]. From literature, knowledge of the relaxation and creep processes is essential for developing a good understanding of SCP's mechanical behavior [39]. Relaxation and creep can be observed in many polymers at room temperature [40,41], which for some SCP is known to show a drastic stress decrease at the beginning of the relaxation, but the stress decrease reaches an asymptotic-like limit after a short period [8,55]. Strobl and coworkers [61,63] determined the viscous stress and quasi-static stress in the relaxation behavior. Zhang and Jar constructed the master curves for relaxation modulus versus time based on the horizontal and vertical shift of a series of relaxation tests, found two transitions for the drop of relaxation modulus with time [50]. Stress recovery could be observed after unloading to a predetermined deformation level. According to Castagnet [56], the stress responses in relaxation and recovery are different for SCP, and the stress change in relaxation after loading is larger than that in recovery after unloading when the strain change is the same for the loading and unloading before relaxation and recovery respectively. It is also known that creep behavior contains three distinctive stages, which are primary, secondary, and tertiary creep stages [15,16]. The creep strain rate drops rapidly at the primary stage, followed by a nearly constant creep strain rate at the secondary stage, and then increase of the strain rate at the tertiary stage [17]. Khan performed numerous experimental investigations on time-dependent behavior considering diverse loading histories, proposed that test methods containing complex loading histories can reveal some singular deformation characteristics, which could present challenges for the simulation of SCP's deformation behavior [41]. Recently, Tan and Jar [60] proposed the use of a multiple-relaxation (MR) test to characterize SCP's relaxation behavior. One cycle of

a MR test contained loading and relaxation stages and a MR test contained multiple stages, which demonstrated the change of relaxation behavior with the increase of the deformation.

Although work in the past have paid particular attentions to creep and relaxation behavior after tensile loading [15,57,60–63], studies on the creep and recovery behaviors after unloading are limited in the literature [36,64–66]. Studies reported so far showed that recovery and creep behavior after strain reversal could show unusual stress and deformation responses, respectively [36,64,65,67]. For the creep behavior after the strain reversal, Dusunceli [64] found that strain could change non-monotonically with the increase of time. For the recovery behavior after unloading, the stress can increase first and then drop, which shows a non-monotonic stress change. Kitagawa et al. [67] first observed this stress drop and regarded the drop as an "anomalous" phenomenon. Drozdov et al. [83] reported this stress drop as an "unusual" stress response and the accurate modelling of it was unresolved.

1.2.2 Modelling of time-dependent behavior

The microstructure of SCP consists of crystalline and amorphous phases, and their stress response to deformation could be nonlinear and time-dependent [8]. Therefore, characterization of SCP's mechanical properties has long been known to be complex [84], and often required models that are based on either deformation kinetics or global deformation behavior. The former are often known to be the physics-based models [81,85–98], which were investigated by some researchers for the modeling of the deformation behavior of solid polymers, such as Dupaix and Krishnan [85], Hao et al. [86], Ayoub et al. [87], Sweeney et al. [99], Garcia-Gonzalez et al. [89], Adams et al. [90], Govaert and coworkers [91], Ahzi et al. [92], Ames et al. [81], Anand and Gurtin [93], Arruda et al. [94], Uchida and Tada [95], Boyce et al. [96], Buckley and Jones [97], and Zaïri et al. [98]. These models are usually complex due to dealing with complex interactions among molecules,

and yet to be able to provide close simulation of the experimentally observed deformation behavior. The physics based models are usually complex and not accurate for numerical simulation [100,101]. As a result, validity of these physics-based models has often been questioned for their capability to quantify SCP's long-term deformation behavior [101–107].

Alternatively, many researchers relied on the global-deformation-based models, also known as phenomenological models [61,107–109], such as Strobl and coworkers [61,63], Drozdov [110], Qi et al. [107], Colak [109], Khan and Zhang [35], Balieu et al. [102], Nguyen et al. [111], Zhang and Moore [112], Dusunceli and Colak [113], and Popelar et al. [114]. Most of these models consist of springs and dashpots that may not reflect SCP's microstructure [73,74,115–118], but have the advantage of being able to mimic closely the deformation behavior observed from the experimental testing [119,120]. Therefore, there has been some confidence in the use of these phenomenological models to predict SCP's deformation behavior in the long-term service [107,111].

Spring-dashpot models have long been used to describe the time-dependent behavior of polymers due to the advantage of being able to visualize the deformation easily and directly. Two-element models for viscoelasticity, such as the Maxwell and the Voigt models, are the basic spring-dashpot models for describing the viscous behavior of materials, but are incapable of capturing SCP's intricate and time-dependent characteristics [78]. The three-element model, also known as the standard model [121], is to combine a spring and the Voigt model in series to simulate PE's long-term stress response in relaxation at different deformation levels [60,62], but it fails to simulate the short-term stress response. In slightly different approaches, Drozdov [122] used a two-phase constitutive model to examine the transition from relaxation to recovery behavior of isotactic polypropylene, and Dusunceli [64] employed the viscoplasticity theory based on overstress

(VBOP) to predict the recovery behavior of polyethylene (PE). However, these models consist of over twenty parameters for which the values are difficult to determine using limited experimental data. The three-branch spring-dashpot model has been commonly used to mimic the stress response to deformation of a variety of materials, such as isotactic polypropylene [123], finger pad [124], cortical bone [125,126], and shape-memory polymers [127]. Sweeney and colleagues [66] proposed a model that consists of three parallel Maxwell branches to simulate data that include single relaxation and recovery stages in one test. This model has successfully described the loading, relaxation, and recovery behavior, but the approach used to determine the model parameter values was not given in detail. Furthermore, as a nonlinear model the work provided only one set of model parameter values. The possibility of having multiple sets of the parameter values to mimic the experimental data was not considered. Therefore, it is not clear whether these multiple sets of the model parameter values follow the same trend of change with deformation as the set of values presented in the work, let alone the trend of change reveals the relationship between deformation behavior and the SCP's microstructures. The uniqueness of the estimated model parameter values remains an open question, as this model has multiple solutions for simulating time-dependent behavior. Therefore, developing an analysis approach for parameter identification is necessary.

Zaïri et al. [128] suggested that the primary challenge in dealing with constitutive models is the identification of parameters. To estimate the model parameters, many researchers have developed optimization methods that minimize the error between experiments and models, including global optimization [129–134], local optimization [135–139], or a combination of them [140–143]. Pyrz and Zaïri [144] formulated parameter identification as an optimization problem and used evolutionary algorithms (EA) to stochastically search for the material parameters of polycarbonate (PC), simplifying parameter identification to a similar curve-fitting problem. Dusunceli et al. [130]

presented a parameter identification procedure based on a genetic algorithm (GA) in MATLAB to determine the material parameters of a viscoplastic model for high-density polyethylene (HDPE). However, they did not apply their parameter identification approaches to the spring-dashpot models. Recently, Xu et al. [145] developed a generalized reduced gradient optimization algorithm to determine parameter values of the three-branch model, and they developed three sets of model parameter values. However, the coefficient of variation for model parameter values is more than 50%. Therefore, it is necessary to develop an analysis approach to determine more unique model parameter values for the characterization of polymers.

1.3 Research objectives and methodology

The overall objective of this research three folded, to develop new testing methods for SCPs, to develop phenomenological models to describe the time-dependent behavior, and to determine the model parameter values for the characterization of SCPs. In this study, the time-dependent behavior of SCPs in different loading and temperature conditions is investigated. PE is selected as the SCP for the analysis. It is planned to determine time-dependent behavior experimentally, including stress-time and deformation-time relations. The effect of deformation rate and temperature is also investigated. Novel experimental methods are developed to generate rich data for the deformation behavior. Spring-dashpot models based on the Eyring's law are considered for the analysis. A new spring-dashpot model is developed to accurately describe the unusual response in the recovery and relaxation tests. The model parameters are then calibrated and verified using experimental results. So that, the model will be applicable to the prediction of stress and deformation response of SCPs.

Here are the detailed objectives for this research:

(1). To develop a new test to characterize the time-dependent behavior of PEs.

(2). To construct the spring-dashpot model to reproduce experimental data from objective #1.

(3). To develop a novel analysis method to determine the model parameter values as functions of deformation for the characterization for the mechanical behavior of SCPs during deformation.

(4). To determine the criteria for estimation of the performance of PE and its pipes at different deformation levels.

Details of the objectives are given below.

(1). The new test is to obtain additional data points and remove the assumptions during the data analysis. In this study, a systematic experimental investigation based on stress relaxation and recovery has been carried out to characterize the time-dependent behavior as a function of deformation. It is necessary to characterize relaxation and recovery behavior and investigate the relationship between their stress variations. As shown in Figure 1.3, a new test method named multiple relaxation and recovery (RR) test has been developed in which one cycle contains 6 modes, including 2 loadings, 1 relaxation, 1 stabilization, 1 recovery, and 1 unloading. Because the relaxation and recovery are introduced at the same stroke they share the same quasi-static stress, which can be used to cancel one parameter (quasi-static stress) that needs to be determined through the curve fitting. The stabilization stage is designed to reduce the effect of the relaxation stage on the following recovery stage. The time durations for relaxation, stabilization, and recovery, of 10000 s each, are long enough to minimize the residual viscous stress left from each stage. In addition, 1 mm/min was used for the crosshead speed for the loading and the unloading stages.

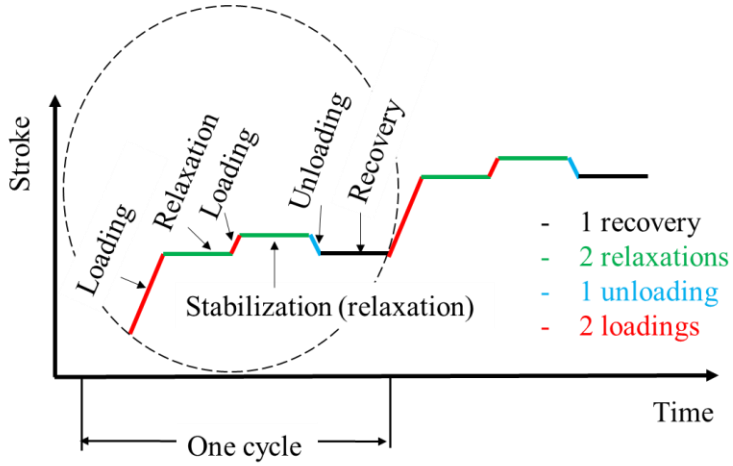

Figure 1.3. Schematic of RR test, and stroke profile as a function of time.

(2). The spring-dashpot models are used for simulating time-dependent behavior. Basic models, such as Maxwell and Voigt models, were found to be insufficient for simulating the highly nonlinear behavior of polymers. In addition, Eyring's equation was used to govern the deformation of the dashpot element in the spring-dashpot model. The Eyring's law is a simple equation and is widely accepted for the description of the time-dependent behavior of SCPs. The Eyring's law is expressed in Equation (1.1) below:

$$\dot{\delta}_v = \dot{\delta}_{0E} \sinh(\sigma_v / \sigma_0) \qquad (1.1)$$

where $\dot{\delta}_v$ represents the stroke rate of the dashpot, $\dot{\delta}_{0E}$ the reference stroke rate, σ_v the viscous stress and σ_0 the reference stress. Hooke's law was adopted to govern the deformation of springs. In this study, the spring-dashpot models with single Eyring's dashpot and multiple dashpots were examined to regenerate the experimental data from the RR tests. Matlab ode solvers were used to solve the ordinary differential equations derived from the spring-dashpot models.

(3). A fast numerical analysis framework, based on genetic algorithms, was developed to determine values for the model parameters so that difference between the simulation and the experimental data could be minimized. Using this approach, values of the model parameters were determined as functions of deformation and time so that the model can simulate the stress response at loading, relaxation, and recovery stages of the RR test. The simulation also generated multiple sets of model parameter values to determine the variation range of model parameter values and examine consistency among the values. The spring stiffness as functions of stroke, determined using stress variation at the loading stages, could also be used to detect the material performance changes during deformation of the RR test.

(4). In view that the spring-dashpot models can produce multiple sets of parameter values that can reproduce the test results, this study explores the possibility of identifying a unique set of model parameter values for fitting the experimental data. A hybrid method by combining the genetic algorithm and trust-region-reflective algorithm is used to minimize the maximum difference of the stress response between the experiments and the model. This maximum difference is compared with the determined experimental resolution so that the maximum difference can be lowered to an acceptable level. The parameter values with the minimum of the maximum difference will be selected to narrow down the variation of them. The uniqueness of these model parameter values should be evaluated and discussed. Finally, these model parameter values are used to characterize the mechanical performance of PE and its pipes.

1.3 Thesis organization

The thesis provides a detailed description of the proposed RR test, simulation using spring-dashpot models, and usefulness of the spring-dashpot model for characterization of PE and its pipes. The remainder of this thesis is composed of four chapters as follows:

In Chapter 2, RR tests are used to differentiate the quasi-static stress response from the viscous stress counterpart during deformation. As the name implies, an RR test involves multiple cycles of stress relaxation, recovery, loading, and unloading. These stages are repeated with increasing deformation to characterize the quasi-static and the viscous stress responses as functions deformation, which is applied to evaluate the spring-dashpot models for the identification of the appropriate model parameters that can be used to reproduce the experimentally observed stress response as functions of deformation and time. Specifically, this study examines three models, the standard model, the model with two dashpots connected either in parallel (referred to as the Parallel model), or in series (referred to as the Series model). All three models are based on the Eyring's law for the stress response as functions of deformation rate in the dashpot. Each model comprises two branches: a viscous branch to capture the time-dependent stress response to deformation, and a quasi-static branch to capture the time-independent stress response. This study outlines the RR test procedure and the corresponding analysis approach used to determine values for all model parameters. The analysis also explores the potential of using RR test results to identify the critical strokes representing the onset of plastic deformation in the crystalline phase of PE. Additionally, two case studies for the further application of the RR tests are presented. The first compares the mechanical performance of two types of high-density polyethylene (HDPE), while the second uses the relaxation behavior from RR test results at different temperatures to calculate the activation energies.

Chapter 3 presents a study in which the RR test was applied to a pipe-grade HDPE to demonstrate a data analysis process utilizing a three-branch spring-dashpot model to simulate the viscous stress response as functions of deformation and time. Following the previous work in the literature, deformation applied to the specimens used in the current study is represented by the stroke of the test machine. By adopting some assumptions, a computer program based on the GA in Matlab was developed to determine values for the model parameters so that the model could closely mimic the experimental data at all loading, relaxation, and recovery stages. Through this computer program, ten sets of parameter values were determined, all of which met the criteria for mimicking the stress response to deformation in the RR test. Based on the ten sets of the parameter values as functions of deformation, feasibility of using the three-branch model to characterize the mechanical behavior of HDPE is discussed.

In Chapter 4, an analysis method was developed based on global and local optimization to simulate the relaxation, recovery, and loading behaviors of PE and its pipes using the three-branch spring dashpot model based on the Eyring's law. This analysis method removed all the assumptions in Chapter 3. Data from RR test on cylindrical specimens and notched pipe ring (NPR) specimens cut from pipes were used in the simulation, to generate 1000 sets of parameter values to mimic closely stress drop at the relaxation stages. The range of variation for these parameter values was examined and discussed. The experimental resolution was evaluated and was compared with the maximum difference of stress response between the model and experiments. The best five sets with the minimum of the maximum difference of stress response between experiments and model were selected from the 1000 sets and they were evaluated for the characterization of the materials. Then, the analysis method was applied to four types of PE pipes, and their quasi-static stress as a function of specimen displacement was determined and discussed.

Chapter 5 summarizes the key contributions of this study and offers recommendations for the future work.

References

1. Sparks, T.D.; Banerjee, D. Materials Informatics and Polymer Science: Pushing the Frontiers of Our Understanding. *Matter* 2021, *4*, 1454–1456, doi:10.1016/j.matt.2021.04.003.

2. Stepto, R.; Horie, K.; Kitayama, T.; Abe, A. Mission and challenges of polymer science and technology. *Pure and Applied Chemistry* 2003, *75*, 1359–1369, doi:10.1351/pac200375101359.

3. Men, Y. Critical Strains Determine the Tensile Deformation Mechanism in Semicrystalline Polymers. *Macromolecules* 2020, *53*, 9155–9157, doi:10.1021/acs.macromol.0c02076.

4. Felder, S.; Holthusen, H.; Hesseler, S.; Pohlkemper, F.; Gries, T.; Simon, J.-W.; Reese, S. Incorporating Crystallinity Distributions into a Thermo-Mechanically Coupled Constitutive Model for Semi-Crystalline Polymers. *International Journal of Plasticity* 2020, *135*, 102751, doi:10.1016/j.ijplas.2020.102751.

5. Farge, L.; Boisse, J.; Dillet, J.; André, S.; Albouy, P.-A.; Meneau, F. Wide-Angle X-Ray Scattering Study of the Lamellar/Fibrillar Transition for a Semi-Crystalline Polymer Deformed in Tension in Relation with the Evolution of Volume Strain. *J. Polym. Sci. Part B: Polym. Phys.* 2015, *53*, 1470–1480, doi:10.1002/polb.23790.

6. Li, C.Y. The Rise of Semicrystalline Polymers and Why Are They Still Interesting. *Polymer* 2020, *211*, 123150, doi:10.1016/j.polymer.2020.123150.

7. Barba, D.; Arias, A.; Garcia-Gonzalez, D. Temperature and Strain Rate Dependences on Hardening and Softening Behaviours in Semi-Crystalline Polymers: Application to PEEK. *International Journal of Solids and Structures* 2020, *182–183*, 205–217, doi:10.1016/j.ijsolstr.2019.08.021.

8. Ayoub, G.; Zaïri, F.; Naït-Abdelaziz, M.; Gloaguen, J.M. Modelling Large Deformation Behaviour under Loading–Unloading of Semicrystalline Polymers: Application to a High Density Polyethylene. *International Journal of Plasticity* 2010, *26*, 329–347, doi:10.1016/j.ijplas.2009.07.005.

9. Atiq, O.; Ricci, E.; Baschetti, M.G.; De Angelis, M.G. Modelling Solubility in Semi-Crystalline Polymers: A Critical Comparative Review. *Fluid Phase Equilibria* 2022, *556*, 113412, doi:10.1016/j.fluid.2022.113412.

10. Nunes dos Santos, W.; Augusto Marcondes Agnelli, J.; Mummery, P.; Wallwork, A. Effect of Recycling on the Thermal Properties of Polymers. *Polymer Testing* 2007, *26*, 216–221, doi:10.1016/j.polymertesting.2006.10.004.

11. Alsabri, A.; Al-Ghamdi, S.G. Carbon Footprint and Embodied Energy of PVC, PE, and PP Piping: Perspective on Environmental Performance. *Energy Reports* 2020, *6*, 364–370, doi:10.1016/j.egyr.2020.11.173.

12. Ivanov, D.A. Semicrystalline Polymers. In *Polymer Science: A Comprehensive Reference*; Elsevier, 2012; pp. 227–258 ISBN 978-0-08-087862-1.

13. Zha, S.; Lan, H.; Huang, H. Review on Lifetime Predictions of Polyethylene Pipes: Limitations and Trends. *International Journal of Pressure Vessels and Piping* 2022, *198*, 104663, doi:10.1016/j.ijpvp.2022.104663.

14. Li, Y.; He, Y.; Liu, Z. A Viscoelastic Constitutive Model for Shape Memory Polymers Based on Multiplicative Decompositions of the Deformation Gradient. *International Journal of Plasticity* 2017, *91*, 300–317, doi:10.1016/j.ijplas.2017.04.004.

15. Liu, P.; Peng, L.; Chen, J.; Yang, B.; Chen, Y.; Luo, Z.; Han, C.C.; Huang, X.; Men, Y. Tensile Creep Failure of Isotactic Polypropylene under the Strain Criterion. *Macromolecules* 2022, *55*, 9663–9670, doi:10.1021/acs.macromol.2c01263.

16. Xu, S.; Zhou, J.; Pan, P. Strain-Induced Multiscale Structural Evolutions of Crystallized Polymers: From Fundamental Studies to Recent Progresses. *Progress in Polymer Science* 2023, 101676.

17. Sedighiamiri, A.; Govaert, L.E.; Kanters, M.J.W.; van Dommelen, J.A.W. Micromechanics of Semicrystalline Polymers: Yield Kinetics and Long-Term Failure. *J. Polym. Sci. B Polym. Phys.* 2012, *50*, 1664–1679, doi:10.1002/polb.23136.

18. Lim, S.D.; Rhee, J.M.; Nah, C. Predicting the Long-Term Creep Behavior of Plastics Using the Short-Term Creep Test. 2004, 7.

19. Kubát, J. Stress Relaxation in Solids. *Nature* 1965, *205*, 378–379.

20. Schiavi, A.; Prato, A. Evidences of Non-Linear Short-Term Stress Relaxation in Polymers. *Polymer Testing* 2017, *59*, 220–229.

21. Janssen, R. Deformation and Failure in Semi-Crystalline Polymer Systems. 53.

22. Nie, Y.; Gao, H.; Yu, M.; Hu, Z.; Reiter, G.; Hu, W. Competition of Crystal Nucleation to Fabricate the Oriented Semi-Crystalline Polymers. *Polymer* 2013, *54*, 3402–3407, doi:10.1016/j.polymer.2013.04.047.

23. Percec, V.; Xiao, Q. The Legacy of Hermann Staudinger: Covalently Linked Macromolecules. *Chem* 2020, *6*, 2855–2861, doi:10.1016/j.chempr.2020.10.007.

24. Mülhaupt, R. Hermann Staudinger and the Origin of Macromolecular Chemistry. *Angewandte Chemie International Edition* 2004, *43*, 1054–1063, doi:10.1002/anie.200330070.

25. Ulu, K.N.; Dragičević, M.; Albouy, P.-A.; Huneau, B.; Béranger, A.-S.; Heuillet, P. Strain-Induced Crystallization Ability of Hydrogenated Nitrile Butadiene Rubber. In *Constitutive Models for Rubber X*; Lion, A., Johlitz, M., Eds.; CRC Press, 2017; pp. 279–282 ISBN 978-1-315-22327-8.

26. Eyring, H.; Halsey, G. Mechanical Properties of Textiles, V: The Three-Element Model Under Any Experimental Condition. *Textile Research Journal* 1946, *16*, 124–129, doi:10.1177/004051754601600303.

27. Candau, N.; Vives, E.; Fernández, A.I.; Maspoch, M.L. Elastocaloric Effect in Vulcanized Natural Rubber and Natural/Wastes Rubber Blends. *Polymer* 2021, *236*, 124309, doi:10.1016/j.polymer.2021.124309.

28. Lambri, O.A.; Bonifacich, F.G.; García, J.Á.; Giordano, E.D.V.; Zelada, G.I.; Sánchez, F.A.; Mocellini, R.R.; Plazaola, F. Mechanical Energy Losses in Commercial Crosslinked Low-Density Polyethylene in the Temperature Range between 200 and 400 K. *J Appl Polym Sci* 2019, *136*, 47605, doi:10.1002/app.47605.

29. Wilhelm, H.; Spieckermann, F.; Fischer, C.; Polt, G.; Zehetbauer, M. Characterization of Strain Bursts in High Density Polyethylene by Means of a Novel Nano Creep Test. *International Journal of Plasticity* 2019, *116*, 297–313, doi:10.1016/j.ijplas.2019.01.010.

30. Eichelter, J.; Wilhelm, H.; Eder, A.; Mautner, A.; Bismarck, A. Influence of the α-Relaxation on the High-Velocity Stretchability of Isotactic Polypropylene. *Polymer* 2020, *200*, 122593, doi:10.1016/j.polymer.2020.122593.

31. Izraylit, V.; Heuchel, M.; Gould, O.E.C.; Kratz, K.; Lendlein, A. Strain Recovery and Stress Relaxation Behaviour of Multiblock Copolymer Blends Physically Cross-Linked with PLA Stereocomplexation. *Polymer* 2020, *209*, 122984, doi:10.1016/j.polymer.2020.122984.

32. Zhang, Y.; Ben Jar, P.-Y.; Xue, S.; Li, L. Quantification of Strain-Induced Damage in Semi-Crystalline Polymers: A Review. *J Mater Sci* 2019, *54*, 62–82, doi:10.1007/s10853-018-2859-2.

33. Zhang, Y.; Ben Jar, P.-Y.; Nguyen, K.-C.T.; Le, L.H. Characterization of Ductile Damage in Polyethylene Plate Using Ultrasonic Testing. *Polymer Testing* 2017, *62*, 51–60, doi:10.1016/j.polymertesting.2017.06.010.

34. Zakar, F. Installation Errors in Polyethylene Pipe for Natural Gas Service: Recent Case Histories by the National Transportation Safety Board (NTSB). In Proceedings of the Volume 2: Pipeline Safety Management Systems; Project Management, Design, Construction, and Environmental Issues; Strain Based Design; Risk and Reliability; Northern, Offshore, and Production Pipelines; American Society of Mechanical Engineers: Virtual, Online, September 28 2020; p. V002T02A015.

35. Khan, A.; Zhang, H. Finite Deformation of a Polymer: Experiments and Modeling. *International Journal of Plasticity* 2001, *17*, 1167–1188, doi:10.1016/S0749-6419(00)00073-5.

36. Drozdov, A.D. Time-Dependent Response of Polypropylene after Strain Reversal. *International Journal of Solids and Structures* 2010, 13.

37. de Melo, C.C.; Macêdo, S.; Sciuti, V.F.; Canto, R.B. A Novel Mechanical Test for the Stress Relaxation Analysis of Polymers. *Polymer Testing* 2019, *73*, 276–283, doi:10.1016/j.polymertesting.2018.11.027.

38. Bakbak, O.; Birkan, B.E.; Acar, A.; Colak, O. Mechanical Characterization of Araldite LY 564 Epoxy: Creep, Relaxation, Quasi-Static Compression and High Strain Rate Behaviors. *Polym. Bull.* 2022, *79*, 2219–2235, doi:10.1007/s00289-021-03624-x.

39. Khan, A.S.; Lopez-Pamies, O. Time and Temperature Dependent Response and Relaxation of a Soft Polymer. *International Journal of Plasticity* 2002, *18*, 1359–1372, doi:10.1016/S0749-6419(02)00003-7.

40. Wilding, M.A.; Ward, I.M. Creep and Recovery of Ultra High Modulus Polyethylene. *Polymer* 1981, *22*, 870–876, doi:10.1016/0032-3861(81)90259-7.

41. Khan, F. Loading History Effects on the Creep and Relaxation Behavior of Thermoplastics. *Journal of Engineering Materials and Technology* 2006, *128*, 564–571, doi:10.1115/1.2345448.

42. Malpass, V.E. Prediction of Long-Term ABS Relaxation Behavior. *Journal of Applied Polymer Science* 1968, *12*, 771–788, doi:10.1002/app.1968.070120415.

43. Moser, A.P.; Folkman, S.L. *Buried Pipe Design*; 3rd ed.; McGraw-Hill: New York, 2008; ISBN 978-0-07-147689-8.

44. Moser, A.P. Structural Performance of Buried Profile-Wall High-Density Polyethylene Pipe and Influence of Pipe Wall Geometry. *Transportation Research Record* 1998, *1624*, 206–213, doi:10.3141/1624-24.

45. Frank, A.; Pinter, G.; Lang, R.W. Prediction of the Remaining Lifetime of Polyethylene Pipes after up to 30 Years in Use. *Polymer Testing* 2009, *28*, 737–745, doi:10.1016/j.polymertesting.2009.06.004.

46. Frank, A.; Berger, I.J.; Arbeiter, F.; Hutař, P.; Pinter, G. Lifetime Prediction of PE100 and PE100-RC Pipes Based on Slow Crack Growth Resistance. 2016, doi:10.13140/RG.2.2.27467.80165.

47. Hoàng, E.M.; Lowe, D. Lifetime Prediction of a Blue PE100 Water Pipe. *Polymer Degradation and Stability* 2008, *93*, 1496–1503, doi:10.1016/j.polymdegradstab.2008.05.008.

48. Brown, N. Intrinsic Lifetime of Polyethylene Pipelines. *Polym. Eng. Sci.* 2007, *47*, 477–480, doi:10.1002/pen.20696.

49. Frank, A.; Arbeiter, F.J.; Berger, I.J.; Hutař, P.; Náhlík, L.; Pinter, G. Fracture Mechanics Lifetime Prediction of Polyethylene Pipes. *J. Pipeline Syst. Eng. Pract.* 2019, *10*, 04018030, doi:10.1061/(ASCE)PS.1949-1204.0000356.

50. Zhang, Y.; Jar, P.-Y.B. Time-Strain Rate Superposition for Relaxation Behavior of Polyethylene Pressure Pipes. *Polymer Testing* 2016, *50*, 292–296, doi:10.1016/j.polymertesting.2015.12.014.

51. Zhang, Y.; Jar, P.-Y.B.; Xue, S.; Han, L.; Li, L. Measurement of Environmental Stress Cracking Resistance of Polyethylene Pipe: A Review. In Proceedings of the ASME 2019 Asia Pacific Pipeline Conference; American Society of Mechanical Engineers: Qingdao, China, May 15 2019; p. V001T10A001.

52. Zhang, Y.; Jar, P.-Y.B.; Xue, S.; Li, L. Numerical Simulation of Ductile Fracture in Polyethylene Pipe with Continuum Damage Mechanics and Gurson-Tvergaard-Needleman Damage Models. *Proceedings of the IMechE* 2019, *233*, 2455–2468, doi:10.1177/1464420719863458.

53. Zhang, Y.; Qiao, L.; Fan, J.; Xue, S.; Jar, P.B. Molecular Dynamics Simulation of Plastic Deformation in Polyethylene under Uniaxial and Biaxial Tension. *Proceedings of the Institution of Mechanical Engineers, Part L: Journal of Materials: Design and Applications* 2021, 146442072110458, doi:10.1177/14644207211045821.

54. Khademi Zahedi, R.; Alimouri, P.; Khademi Zahedi, H.; Shishesaz, M. Investigating Peak Stresses in Fitting and Repair Patches of Buried Polyethylene Gas Pipes. *Front. Struct. Civ. Eng.* 2020, *14*, 147–168, doi:10.1007/s11709-019-0587-6.

55. Fancey, K.S. A Mechanical Model for Creep, Recovery and Stress Relaxation in Polymeric Materials. *J Mater Sci* 2005, *40*, 4827–4831, doi:10.1007/s10853-005-2020-x.

56. Castagnet, S. High-Temperature Mechanical Behavior of Semi-Crystalline Polymers and Relationship to a Rubber-like "Relaxed" State. *Mechanics of Materials* 2009, *41*, 75–86, doi:10.1016/j.mechmat.2008.10.001.

57. Tan, N.; Ben Jar, P.-Y. Reanalysis of the Creep Test Data and Failure Behavior of Polyethylene and Its Copolymers. *J. of Materi Eng and Perform* 2022, *31*, 2182–2192, doi:10.1007/s11665-021-06360-5.

58. Drozdov, A.D. Creep Rupture and Viscoelastoplasticity of Polypropylene. *Engineering Fracture Mechanics* 2010, *77*, 2277–2293, doi:10.1016/j.engfracmech.2010.05.010.

59. Duxbury, J.; Ward, I.M. The Creep Behaviour of Ultra-High Modulus Polypropylene. *J Mater Sci* 1987, *22*, 1215–1222, doi:10.1007/BF01233111.

60. Tan, N.; Jar, P.-Y.B. Determining Deformation Transition in Polyethylene under Tensile Loading. *Polymers* 2019, *11*, 1415, doi:10.3390/polym11091415.

61. Hong, K.; Rastogi, A.; Strobl, G. Model Treatment of Tensile Deformation of Semicrystalline Polymers: Static Elastic Moduli and Creep Parameters Derived for a Sample of Polyethylene. *Macromolecules* 2004, *37*, 10174–10179, doi:10.1021/ma049172x.

62. Tan, N.; Jar, P.B. Multi-Relaxation Test to Characterize PE Pipe Performance. *Plastics Engineering* 2019, *75*, 40–45, doi:10.1002/peng.20184.

63. Hong, K.; Rastogi, A.; Strobl, G. A Model Treating Tensile Deformation of Semicrystalline Polymers: Quasi-Static Stress−Strain Relationship and Viscous Stress Determined for a Sample of Polyethylene. *Macromolecules* 2004, *37*, 10165–10173, doi:10.1021/ma049174h.

64. Dusunceli, N. The Unusual Creep and Relaxation Behaviour of Polypropylene. *Journal of Polymer Engineering* 2012, *32*, doi:10.1515/polyeng-2011-0159.

65. Zhang, C.; Moore, I.D. Nonlinear Mechanical Response of High Density Polyethylene. Part I: Experimental Investigation and Model Evaluation. *Polym. Eng. Sci.* 1997, *37*, 404–413, doi:10.1002/pen.11683.

66. Sweeney, J.; Bonner, M.; Ward, I.M. Modelling of Loading, Stress Relaxation and Stress Recovery in a Shape Memory Polymer. *Journal of the Mechanical Behavior of Biomedical Materials* 2014, *37*, 12–23, doi:10.1016/j.jmbbm.2014.05.011.

67. Kitagawa, M.; Zhou, D.; Qui, J. Stress-Strain Curves for Solid Polymers. *Polym. Eng. Sci.* 1995, *35*, 1725–1732, doi:10.1002/pen.760352202.

68. Ayoub, G.; Zaïri, F.; Fréderix, C.; Gloaguen, J.M.; Naït-Abdelaziz, M.; Seguela, R.; Lefebvre, J.M. Effects of Crystal Content on the Mechanical Behaviour of Polyethylene under Finite Strains: Experiments and Constitutive Modelling. *International Journal of Plasticity* 2011, *27*, 492–511, doi:10.1016/j.ijplas.2010.07.005.

69. Okereke, M.I.; Akpoyomare, A.I. Two-Process Constitutive Model for Semicrystalline Polymers across a Wide Range of Strain Rates. *Polymer* 2019, *183*, 121818, doi:10.1016/j.polymer.2019.121818.

70. Arzhakov, M. *Relaxation in Physical and Mechanical Behavior of Polymers*; 1st ed.; CRC Press, 2019; ISBN 978-0-429-24452-0.

71. Vandommelen, J.; Parks, D.; Boyce, M.; Brekelmans, W.; Baaijens, F. Micromechanical Modeling of the Elasto-Viscoplastic Behavior of Semi-Crystalline Polymers. *Journal of the Mechanics and Physics of Solids* 2003, *51*, 519–541, doi:10.1016/S0022-5096(02)00063-7.

72. Jar, P.B. Revisiting Creep Test on Polyethylene Pipe—Data Analysis and Deformation Mechanisms. *Polym Eng Sci* 2021, *61*, 586–599, doi:10.1002/pen.25603.

73. Bouvard, J.L.; Ward, D.K.; Hossain, D.; Marin, E.B.; Bammann, D.J.; Horstemeyer, M.F. A General Inelastic Internal State Variable Model for Amorphous Glassy Polymers. *Acta Mech* 2010, *213*, 71–96, doi:10.1007/s00707-010-0349-y.

74. Bouvard, J.L.; Francis, D.K.; Tschopp, M.A.; Marin, E.B.; Bammann, D.J.; Horstemeyer, M.F. An Internal State Variable Material Model for Predicting the Time, Thermomechanical, and

Stress State Dependence of Amorphous Glassy Polymers under Large Deformation. *International Journal of Plasticity* 2013, *42*, 168–193, doi:10.1016/j.ijplas.2012.10.005.

75. Brazel, C.S.; Rosen, S.L. Fundamental Principles of Polymeric Materials. 427.

76. Haward, R.N.; Thackray, G. The Use of a Mathematical Model to Describe Isothermal Stress-Strain Curves in Glassy Thermoplastics. *Proceedings of the Royal Society of London. Series A, Mathematical and Physical Sciences* 1968, *302*, 453–472.

77. Serra-Aguila, A.; Puigoriol-Forcada, J.M.; Reyes, G.; Menacho, J. Viscoelastic Models Revisited: Characteristics and Interconversion Formulas for Generalized Kelvin–Voigt and Maxwell Models. *Acta Mech. Sin.* 2019, *35*, 1191–1209, doi:10.1007/s10409-019-00895-6.

78. Brusselle-Dupend, N.; Lai, D.; Feaugas, X.; Guigon, M.; Clavel, M. Mechanical Behavior of a Semicrystalline Polymer before Necking. Part II: Modeling of Uniaxial Behavior. *Polym. Eng. Sci.* 2003, *43*, 501–518, doi:10.1002/pen.10041.

79. Drozdov, A.D. Modelling an Anomalous Stress Relaxation in Glassy Polymers (the Kitagawa Effect). *Mathematical and Computer Modelling* 1998, *27*, 45–67, doi:10.1016/S0895-7177(98)00072-7.

80. Muliana, A.; Rajagopal, K.R.; Tscharnuter, D.; Pinter, G. A Nonlinear Viscoelastic Constitutive Model for Polymeric Solids Based on Multiple Natural Configuration Theory. *International Journal of Solids and Structures* 2016, *100–101*, 95–110, doi:10.1016/j.ijsolstr.2016.07.017.

81. Ames, N.M.; Srivastava, V.; Chester, S.A.; Anand, L. A Thermo-Mechanically Coupled Theory for Large Deformations of Amorphous Polymers. Part II: Applications. *International Journal of Plasticity* 2009, *25*, 1495–1539, doi:10.1016/j.ijplas.2008.11.005.

82. Fritsch, J.; Hiermaier, S.; Strobl, G. Characterizing and Modeling the Non-Linear Viscoelastic Tensile Deformation of a Glass Fiber Reinforced Polypropylene. *Composites Science and Technology* 2009, *69*, 2460–2466, doi:10.1016/j.compscitech.2009.06.021.

83. Drozdov, A.D.; Christiansen, J. deC. Cyclic Viscoplasticity of High-Density Polyethylene: Experiments and Modeling. *Computational Materials Science* 2007, *39*, 465–480, doi:10.1016/j.commatsci.2006.07.014.

84. Brusselle-Dupend, N.; Cangémi, L. A Two-Phase Model for the Mechanical Behaviour of Semicrystalline Polymers. Part I: Large Strains Multiaxial Validation on HDPE. *Mechanics of Materials* 2008, *40*, 743–760, doi:10.1016/j.mechmat.2008.03.011.

85. Dupaix, R.B.; Krishnan, D. A Constitutive Model for Strain-Induced Crystallization in Poly(Ethylene Terephthalate) (PET) during Finite Strain Load-Hold Simulations. *Journal of Engineering Materials and Technology* 2005, *128*, 28–33, doi:10.1115/1.1924564.

86. Hao, P.; Laheri, V.; Dai, Z.; Gilabert, F.A. A Rate-Dependent Constitutive Model Predicting the Double Yield Phenomenon, Self-Heating and Thermal Softening in Semi-Crystalline Polymers. *International Journal of Plasticity* 2022, *153*, 103233, doi:10.1016/j.ijplas.2022.103233.

87. Ayoub, G.; Rodriguez, A.K.; Mansoor, B.; Colin, X. Modeling the Visco-Hyperelastic–Viscoplastic Behavior of Photodegraded Semi-Crystalline Low-Density Polyethylene Films. *International Journal of Solids and Structures* 2020, *204–205*, 187–198, doi:10.1016/j.ijsolstr.2020.08.025.

88. Sweeney, J.; Collins, T.L.D.; Coates, P.D.; Unwin, A.P.; Duckett, R.A.; Ward, I.M. Application of a Large Deformation Model to Unstable Tensile Stretching of Polyethylene. *International Journal of Plasticity* 2002, *18*, 399–414, doi:10.1016/S0749-6419(00)00104-2.

89. Garcia-Gonzalez, D.; Zaera, R.; Arias, A. A Hyperelastic-Thermoviscoplastic Constitutive Model for Semi-Crystalline Polymers: Application to PEEK under Dynamic Loading Conditions. *International Journal of Plasticity* 2017, *88*, 27–52, doi:10.1016/j.ijplas.2016.09.011.

90. Adams, A.M.; Buckley, C.P.; Jones, D.P. Biaxial Hot Drawing of Poly(Ethylene Terephthalate): Measurements and Modelling of Strain-Stiffening. *Polymer* 2000, *41*, 771–786, doi:10.1016/S0032-3861(98)00834-9.

91. Tervoort, T.A.; Smit, R.J.M.; Brekelmans, W.A.M.; Govaert, L.E. A Constitutive Equation for the Elasto-Viscoplastic Deformation of Glassy Polymers. *Mechanics of Time-Dependent Materials* 1997, *1*, 269–291, doi:10.1023/A:1009720708029.

92. Ahzi, S.; Makradi, A.; Gregory, R.V.; Edie, D.D. Modeling of Deformation Behavior and Strain-Induced Crystallization in Poly(Ethylene Terephthalate) above the Glass Transition Temperature. *Mechanics of Materials* 2003, *35*, 1139–1148, doi:10.1016/S0167-6636(03)00004-8.

93. Anand, L.; Gurtin, M.E. A Theory of Amorphous Solids Undergoing Large Deformations, with Application to Polymeric Glasses. *International Journal of Solids and Structures* 2003, *40*, 1465–1487, doi:10.1016/S0020-7683(02)00651-0.

94. Arruda, E.M.; Boyce, M.C.; Jayachandran, R. Effects of Strain Rate, Temperature and Thermomechanical Coupling on the Finite Strain Deformation of Glassy Polymers. *Mechanics of Materials* 1995, *19*, 193–212, doi:10.1016/0167-6636(94)00034-E.

95. Uchida, M.; Tada, N. Micro-, Meso- to Macroscopic Modeling of Deformation Behavior of Semi-Crystalline Polymer. *International Journal of Plasticity* 2013, *49*, 164–184, doi:10.1016/j.ijplas.2013.03.007.

96. Boyce, M.C.; Socrate, S.; Llana, P.G. Constitutive Model for the Finite Deformation Stress–Strain Behavior of Poly(Ethylene Terephthalate) above the Glass Transition. *Polymer* 2000, *41*, 2183–2201, doi:10.1016/S0032-3861(99)00406-1.

97. Buckley, C. Glass-Rubber Constitutive Model for Amorphous Polymers near the Glass Transition. *Polymer* 1995, *36*, 3301–3312, doi:10.1016/0032-3861(95)99429-X.

98. Zaïri, F.; Naït-Abdelaziz, M.; Gloaguen, J.M.; Lefebvre, J.M. A Physically-Based Constitutive Model for Anisotropic Damage in Rubber-Toughened Glassy Polymers during Finite Deformation. *International Journal of Plasticity* 2011, *27*, 25–51, doi:10.1016/j.ijplas.2010.03.007.

99. Sweeney, J.; Collins, T.L.D.; Coates, P.D.; Unwin, A.P.; Duckett, R.A.; Ward, I.M. Application of a Large Deformation Model to Unstable Tensile Stretching of Polyethylene. *International Journal of Plasticity* 2002, *18*, 399–414.

100. Khan, A.S.; Lopez-Pamies, O.; Kazmi, R. Thermo-Mechanical Large Deformation Response and Constitutive Modeling of Viscoelastic Polymers over a Wide Range of Strain Rates and Temperatures. *International Journal of Plasticity* 2006, *22*, 581–601.

101. Argon, A.S.; Bulatov, V.V.; Mott, P.H.; Suter, U.W. Plastic Deformation in Glassy Polymers by Atomistic and Mesoscopic Simulations. *Journal of Rheology* 1995, *39*, 377–399, doi:10.1122/1.550728.

102. Balieu, R.; Lauro, F.; Bennani, B.; Delille, R.; Matsumoto, T.; Mottola, E. A Fully Coupled Elastoviscoplastic Damage Model at Finite Strains for Mineral Filled Semi-Crystalline Polymer. *International Journal of Plasticity* 2013, *51*, 241–270, doi:10.1016/j.ijplas.2013.05.002.

103. Xiang, Y.; Zhong, D.; Wang, P.; Yin, T.; Zhou, H.; Yu, H.; Baliga, C.; Qu, S.; Yang, W. A Physically Based Visco-Hyperelastic Constitutive Model for Soft Materials. *Journal of the Mechanics and Physics of Solids* 2019, *128*, 208–218, doi:10.1016/j.jmps.2019.04.010.

104. Lan, T.; Shao, T.; Zhang, Y.; Zhang, Y.; Zhu, J.; Jiang, Y.; Wu, P. A Physically-Based Constitutive Model for Amorphous Glassy Polymers in Large Deformations. *European Journal of Mechanics - A/Solids* 2023, 105015, doi:10.1016/j.euromechsol.2023.105015.

105. Diani, J.; Fayolle, B.; Gilormini, P. A Review on the Mullins Effect. *European Polymer Journal* 2009, *45*, 601–612, doi:10.1016/j.eurpolymj.2008.11.017.

106. Khan, A.S.; Lopez-Pamies, O.; Kazmi, R. Thermo-Mechanical Large Deformation Response and Constitutive Modeling of Viscoelastic Polymers over a Wide Range of Strain Rates and Temperatures. *International Journal of Plasticity* 2006, *22*, 581–601, doi:10.1016/j.ijplas.2005.08.001.

107. Qi, Z.; Hu, N.; Li, G.; Zeng, D.; Su, X. Constitutive Modeling for the Elastic-Viscoplastic Behavior of High Density Polyethylene under Cyclic Loading. *International Journal of Plasticity* 2019, *113*, 125–144, doi:10.1016/j.ijplas.2018.09.010.

108. Drozdov, A.D. Mullins' Effect in Semicrystalline Polymers. *International Journal of Solids and Structures* 2009, *46*, 3336–3345, doi:10.1016/j.ijsolstr.2009.05.001.

109. Colak, O. Modeling Deformation Behavior of Polymers with Viscoplasticity Theory Based on Overstress. *International Journal of Plasticity* 2005, *21*, 145–160, doi:10.1016/j.ijplas.2004.04.004.

110. Drozdov, A.D. Mullins' Effect in Semicrystalline Polymers. *International Journal of Solids and Structures* 2009, *46*, 3336–3345.

111. Nguyen, V.-D.; Lani, F.; Pardoen, T.; Morelle, X.P.; Noels, L. A Large Strain Hyperelastic Viscoelastic-Viscoplastic-Damage Constitutive Model Based on a Multi-Mechanism Non-Local Damage Continuum for Amorphous Glassy Polymers. *International Journal of Solids and Structures* 2016, *96*, 192–216, doi:10.1016/j.ijsolstr.2016.06.008.

112. Zhang, C.; Moore, I.D. Nonlinear Mechanical Response of High Density Polyethylene. Part II: Uniaxial Constitutive Modeling. *Polym. Eng. Sci.* 1997, *37*, 414–420, doi:10.1002/pen.11684.

113. Dusunceli, N.; Colak, O.U. Modelling Effects of Degree of Crystallinity on Mechanical Behavior of Semicrystalline Polymers. *International Journal of Plasticity* 2008, *24*, 1224–1242, doi:10.1016/j.ijplas.2007.09.003.

114. Popelar, C.F.; Popelar, C.H.; Kenner, V.H. Viscoelastic Material Characterization and Modeling for Polyethylene. *Polym. Eng. Sci.* 1990, *30*, 577–586, doi:10.1002/pen.760301004.

115. Sack, I. Magnetic Resonance Elastography from Fundamental Soft-Tissue Mechanics to Diagnostic Imaging. *Nat Rev Phys* 2022, *5*, 25–42, doi:10.1038/s42254-022-00543-2.

116. Wang, B.; Yang, W.; McKittrick, J.; Meyers, M.A. Keratin: Structure, Mechanical Properties, Occurrence in Biological Organisms, and Efforts at Bioinspiration. *Progress in Materials Science* 2016, *76*, 229–318, doi:10.1016/j.pmatsci.2015.06.001.

117. Collinson, D.W.; Sheridan, R.J.; Palmeri, M.J.; Brinson, L.C. Best Practices and Recommendations for Accurate Nanomechanical Characterization of Heterogeneous Polymer Systems with Atomic Force Microscopy. *Progress in Polymer Science* 2021, *119*, 101420, doi:10.1016/j.progpolymsci.2021.101420.

118. Webber, M.J.; Tibbitt, M.W. Dynamic and Reconfigurable Materials from Reversible Network Interactions. *Nat Rev Mater* 2022, *7*, 541–556, doi:10.1038/s41578-021-00412-x.

119. Brazel, C.S.; Rosen, S.L. Fundamental Principles of Polymeric Materials. *John Wiley & Sons* 2012, 427.

120. Coleman, B.D.; Noll, W. Foundations of Linear Viscoelasticity. *Rev. Mod. Phys.* 1961, *33*, 239–249, doi:10.1103/RevModPhys.33.239.

121. *Theoretical Analyses, Computations, and Experiments of Multiscale Materials: A Tribute to Francesco Dell'Isola*; Giorgio, I., Placidi, L., Barchiesi, E., Abali, B.E., Altenbach, H., Eds.; Advanced Structured Materials; Springer International Publishing: Cham, 2022; Vol. 175; ISBN 978-3-031-04547-9.

122. Drozdov, A.D. Time-Dependent Response of Polypropylene after Strain Reversal. *International Journal of Solids and Structures* 2010, *47*, 3221–3233, doi:10.1016/j.ijsolstr.2010.08.001.

123. Yakimets, I.; Lai, D.; Guigon, M. Model to Predict the Viscoelastic Response of a Semi-Crystalline Polymer under Complex Cyclic Mechanical Loading and Unloading Conditions. *Mech Time-Depend Mater* 2007, *11*, 47–60, doi:10.1007/s11043-007-9031-8.

124. Kumar, S.; Liu, G.; Schloerb, D.; Srinivasan, M. Viscoelastic Characterization of the Primate Finger Pad In Vivo by Microstep Indentation and Three-Dimensional Finite Element Models for Tactile Sensation Studies. *Journal of biomechanical engineering* 2015, *137*, doi:10.1115/1.4029985.

125. Johnson, T.P.M.; Socrate, S.; Boyce, M.C. A Viscoelastic, Viscoplastic Model of Cortical Bone Valid at Low and High Strain Rates. *Acta Biomater.* 2010, *6*, 4073–4080, doi:10.1016/j.actbio.2010.04.017.

126. Blake, Y. Review of Viscoelastic Models Applied to Cortical Bone.

127. Heuchel, M.; Cui, J.; Kratz, K.; Kosmella, H.; Lendlein, A. Relaxation Based Modeling of Tunable Shape Recovery Kinetics Observed under Isothermal Conditions for Amorphous Shape-Memory Polymers. *Polymer* 2010, *51*, 6212–6218, doi:10.1016/j.polymer.2010.10.051.

128. Abdul-Hameed, H.; Messager, T.; Zaïri, F.; Naït-Abdelaziz, M. Large-Strain Viscoelastic–Viscoplastic Constitutive Modeling of Semi-Crystalline Polymers and Model Identification by Deterministic/Evolutionary Approach. *Computational Materials Science* 2014, *90*, 241–252, doi:10.1016/j.commatsci.2014.03.043.

129. Meißner, P.; Watschke, H.; Winter, J.; Vietor, T. Artificial Neural Networks-Based Material Parameter Identification for Numerical Simulations of Additively Manufactured Parts by Material Extrusion. *Polymers* 2020, *12*, 2949, doi:10.3390/polym12122949.

130. Dusunceli, N.; Colak, O.U.; Filiz, C. Determination of Material Parameters of a Visco-plastic Model by Genetic Algorithm. *Materials & Design* 2010, *31*, 1250–1255, doi:10.1016/j.matdes.2009.09.023.

131. Fatima Brondani, M. de; Sausen, A.T.Z.R.; Sausen, P.S.; Binelo, M.O. Parameter Estimation of Lithium Ion Polymer Battery Mathematical Model Using Genetic Algorithm. *Comp. Appl. Math.* 2018, *37*, 296–313, doi:10.1007/s40314-017-0537-7.

132. Mitra, K. Genetic Algorithms in Polymeric Material Production, Design, Processing and Other Applications: A Review. *International Materials Reviews* 2008, *53*, 275–297, doi:10.1179/174328008X348174.

133. Costa, A.L.H.; Silva, F.P.T. da; Pessoa, F.L.P. Parameter Estimation of Thermodynamic Models for High-Pressure Systems Employing a Stochastic Method of Global Optimization. *Braz. J. Chem. Eng.* 2000, *17*, 349–354, doi:10.1590/S0104-66322000000300011.

134. Erodotou, P.; Voutsas, E.; Sarimveis, H. A Genetic Algorithm Approach for Parameter Estimation in Vapour-Liquid Thermodynamic Modelling Problems. *Computers & Chemical Engineering* 2020, *134*, 106684, doi:10.1016/j.compchemeng.2019.106684.

135. Hossain, M.; Vu, D.K.; Steinmann, P. Experimental Study and Numerical Modelling of VHB 4910 Polymer. *Computational Materials Science* 2012, *59*, 65–74, doi:10.1016/j.commatsci.2012.02.027.

136. Weizel, A.; Distler, T.; Detsch, R.; Boccaccini, A.R.; Bräuer, L.; Paulsen, F.; Seitz, H.; Budday, S. Hyperelastic Parameter Identification of Human Articular Cartilage and Substitute Materials. *Journal of the Mechanical Behavior of Biomedical Materials* 2022, *133*, 105292, doi:10.1016/j.jmbbm.2022.105292.

137. Pappas, G.; Canal, L.P.; Botsis, J. Characterization of Intralaminar Mode I Fracture of AS4/PPS Composite Using Inverse Identification and Micromechanics. *Composites Part A: Applied Science and Manufacturing* 2016, *91*, 117–126, doi:10.1016/j.compositesa.2016.09.018.

138. Hartmann, S.; Gilbert, R.R. Identifiability of Material Parameters in Solid Mechanics. *Arch Appl Mech* 2018, *88*, 3–26, doi:10.1007/s00419-017-1259-4.

139. Kyaw, S.T.; Rouse, J.P.; Lu, J.; Sun, W. Determination of Material Parameters for a Unified Viscoplasticity-Damage Model for a P91 Power Plant Steel. *International Journal of Mechanical Sciences* 2016, *115–116*, 168–179, doi:10.1016/j.ijmecsci.2016.06.014.

140. Raponi, E.; Fiumarella, D.; Boria, S.; Scattina, A.; Belingardi, G. Methodology for Parameter Identification on a Thermoplastic Composite Crash Absorber by the Sequential Response Surface Method and Efficient Global Optimization. *Composite Structures* 2021, *278*, 114646, doi:10.1016/j.compstruct.2021.114646.

141. Qu, J.; Jin, Q.; Xu, B. Parameter Identification Theory of a Complex Model Based on Global Optimization Method. *Sci. China Ser. G-Phys. Mech. Astron.* 2008, *51*, 1722–1732, doi:10.1007/s11433-008-0177-4.

142. Rehman, D.; Lienhard, J.H. Global Optimization for Accurate and Efficient Parameter Estimation in Nanofiltration. *Journal of Membrane Science Letters* 2022, *2*, 100034, doi:10.1016/j.memlet.2022.100034.

143. Qu, J.; Jin, Q.; Xu, B. Parameter Identification for Improved Viscoplastic Model Considering Dynamic Recrystallization. *International Journal of Plasticity* 2005, *21*, 1267–1302, doi:10.1016/j.ijplas.2004.04.009.

144. Pyrz, M.; Zairi, F. Identification of Viscoplastic Parameters of Phenomenological Constitutive Equations for Polymers by Deterministic and Evolutionary Approach. *Modelling Simul. Mater. Sci. Eng.* 2007, *15*, 85–103, doi:10.1088/0965-0393/15/2/006.

145. Xu, Q.; Engquist, B.; Solaimanian, M.; Yan, K. A New Nonlinear Viscoelastic Model and Mathematical Solution of Solids for Improving Prediction Accuracy. *Scientific reports* 2020, *10*, 2202.

Chapter 2 Characterization of Polyethylene Using a New Test Method Based on Stress Response to Relaxation and Recovery

This chapter proposed a novel multi-relaxation-recovery (RR) test based on cyclic stages of stress relaxation and stress recovery. Three nonlinear visco-elastic models, that is, the standard model and two models with two dashpots connected either in parallel or in series, were examined for the analysis of the test results. Each model contains a time-dependent, viscous branch and a time-independent, quasi-static branch. The examination suggests that the standard model can determine the long-term, load-carrying performance of polyethylene (PE) and identify a transition point for the onset of plastic deformation in the crystalline phase, but the models with two dashpots connected either in parallel or in series are needed to provide a close simulation of the experimentally measured stress response in both relaxation and recovery stages of the RR test. In this work, the mechanical performance of two PEs was compared based on RR test results at room temperature. The RR tests were also conducted at elevated temperatures to explore the possibility of quantifying the activation energies for deformation of the dashpots at the relaxation stage. It was found the RR test has the advantage of separating the time-dependent and time-independent components of stiffness of the materials. The study concludes that the RR test can provide data for determining parameters in Eyring's model in order to characterize the contribution of time-dependent and time-independent components of the stress response to PE's deformation.

2.1. Introduction

Semi-crystalline polymers (SCPs) have been increasingly used in industrial applications due to their potential for fulfilling the performance requirements, with the advantages of chemical resistance and installation flexibility [1–3]. As the most studied SCP, polyethylene (PE) has a global demand of nearly a hundred million metric tons in 2018, equivalent to approximately US$164 billion, with an annual growth of 4.0% [4,5]. With the significant improvement in PE's performance, its applications to engineering structures have steadily increased in recent years [6,7]. A total of 95% of the plastic pipes in the United States are PE pipes [8]. PE pipes are increasingly applied to water and gas transportation [9]. However, PE's failure can also cause tremendous economic losses and sometimes fatalities [10–12]. Therefore, urgent attention is needed for the proper evaluation of PE's performance. As a result, literature has shown tremendous work in experimental testing and performance modeling for the characterization of PE's mechanical behavior [13–15]. Currently, some bottlenecks still exist, especially in linking its mechanical performance with the dominant deformation mechanisms. These bottlenecks are known to be caused by several issues. Firstly, many models used for the analysis of the mechanical test results require assumptions that are practically unrealistic. For example, characteristic relaxation time for the viscous deformation has often been assumed to be constant, independent of the deformation level or of the material [16–18]. Secondly, modeling based on spring and dashpot elements often assumed that the viscous stress component is a function of total strain rate, rather than the strain rate across the dashpot element [16]. Maxwell and Voigt-Kelvin models are the basic models that use spring and dashpot to simulate the viscous deformation [19,20], with the assumption of a linear relationship between viscous stress and strain rate across the dashpot. However, these linear models are insufficient to describe the complex, nonlinear stress response of PE to deformation [19,21], Drozdov et al. have

proposed a model with 15 parameters to simulate the nonlinear deformation behavior, but the model was only used for the analysis prior to the yield point [22]. Alternatively, Anand and coworkers developed a thermo-mechanical-coupled theory with more than thirty parameters to mimic the large deformation, but this theory was only applicable to amorphous polymers [23]. Some other models that consider nonlinear constitutive equations are only applicable to a specific loading mode. For example, Boyce et al. proposed a constitutive model to simulate the loading behavior of poly(ethylene terephthalate), but failed to predict correctly the unloading behavior [24]. Mirkhalaf et al. modeled the post-yield response of amorphous polymers, also without the validation of the unloading behavior [25]. Models in the literature that considered the unloading showed that relaxation and recovery behaviors could not be simulated using the same model parameters. For example, Detrez et al. characterized SCPs for loading, relaxation, and unloading behaviors, but failed to simulate the recovery behavior after the unloading [26].

In this chapter, a new mechanical test, named the multi-relaxation-recovery (RR) test, is proposed to separate the quasi-static stress response to deformation from the viscous counterpart. As suggested by the name, the RR test consists of multiple stages of stress relaxation and recovery and the associated loading and unloading. These stages are repeated during the RR test to characterize the quasi-static and the viscous stress responses to deformation, based on which spring-dashpot models are examined to identify the proper model parameters that can simulate the experimentally-determined stress-deformation curve. Specifically, this chapter considers three models which are the standard model [27], the model with two dashpots connected either in parallel (to be named the Parallel model hereafter), or in series (to be named the Series model), all of which are based on the Eyring's law for the stress response of the dashpot [28–30]. Each of these models

consists of two branches, one being a viscous branch to simulate the time-dependent stress response to deformation, and the other a quasi-static branch to simulate the time-independent stress response. This chapter provides details of the RR test and the analysis for determining parameter values for all spring and dashpot elements in the models. The analysis also examines the possibility of using the RR test results to identify the critical strokes for the onset of deformation transition that has been reported in the previous work [17,31]. Furthermore, two case studies are presented using the RR test. One is to compare two types of high-density polyethylene (HDPE) for their mechanical performance, and the other to use RR test results at different temperatures to determine the activation energies for deformation during the stress relaxation.

2.2. RR Test

Tests that consist of multiple deformation stages have been developed to characterize the time- and strain rate-dependent deformation behaviors of polymers [16,17,31]. In the work that is concerned about the mechanical performance, analysis of the test data is often based on a constant characteristic relaxation time, i.e., independent of deformation level or material [17,31,32].

The idea for the RR test described in this chapter is to address the above deficiency, that is, to collect stress response at both stress relaxation and stress recovery modes and without the assumption of constant characteristic relaxation time. As shown in Figure 2.1(a), each stage of the RR test contains four test modes, including loading, relaxation, unloading, and recovery. Note that stress relaxation is introduced twice, one being labeled as relaxation in Figure 2.1(a) and the other 'stabilization.' The latter is to stabilize the deformation process before the specimen is unloaded

for stress recovery. Loading between relaxation and stabilization is through a much smaller displacement increment than the loading between recovery and the following relaxation. In this study, displacement increment for the former is about one-fifth of that for the latter.

The deformation stage shown in Figure 2.1(a) is repeated cyclically to cover a wide range of deformation levels, which could continue till the specimen fractures. However, for the work reported here, the RR tests were terminated at the point where necking became noticeable to the naked eyes, in order to reduce the amount of data for the analysis in view that the test is in the development stage. A sample curve of engineering stress versus displacement, collected from an RR test, is shown in Figure 2.1(b).

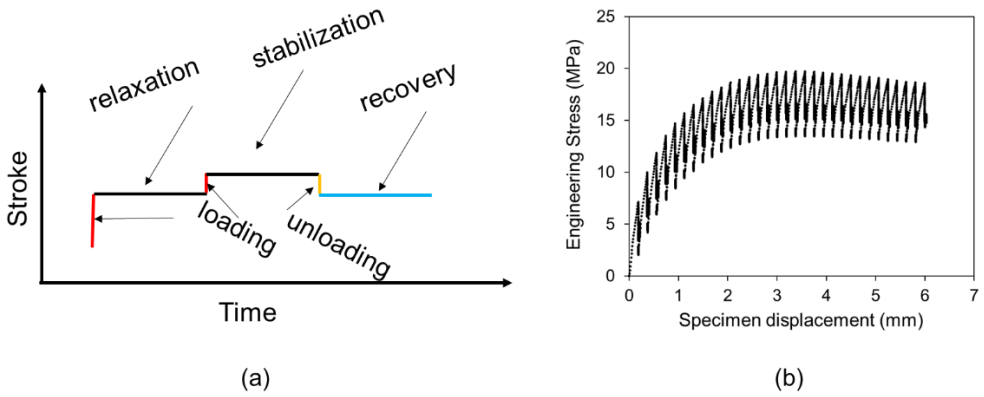

Figure 2.1. Multi-relaxation-recovery test: (a) stroke versus time in one stage of the RR test; (b) a sample curve showing the engineering stress versus displacement (taken from data for HDPE-a).

Three spring-dashpot models, including the standard model [17], the Parallel model, also considered in Ref. [33–36], and the Series model, were applied to simulate the relaxation and re-

covery behavior in the RR test, to extract the model parameters by fitting the experimentally determined engineering stress-displacement curves. Each of these models consists of two branches, one being a viscous branch to simulate the time-dependent stress response to deformation, and the other a quasi-static branch to simulate the time-independent stress response. Quasi-static stress (σ_{qs}) was obtained as a function of stroke by an approach, named combined relaxation-recovery (CRR) approach here, which is based on a widely accepted concept that a common σ_{qs} exists for relaxation and recovery phases at the same specimen displacement. Compared to the analysis of multi-relaxation tests in the literature, the CRR approach allows the variation of characteristic relaxation time (τ_v) with deformation, and thus removes the assumption of a constant τ_v that has been used in the past [17,31,32]. RR test provided a data set for the determination of model parameters, which was then applied to the characterization of the time-dependent and time-independent performance of polymers. In this study, using the results, mechanical performance for two types of high-density polyethylene (HDPE) was compared. In addition, the RR test results at elevated temperatures were used to obtain the activation energies. The methodological procedure of this study is shown in the flow chart, as shown in Figure 2.2.

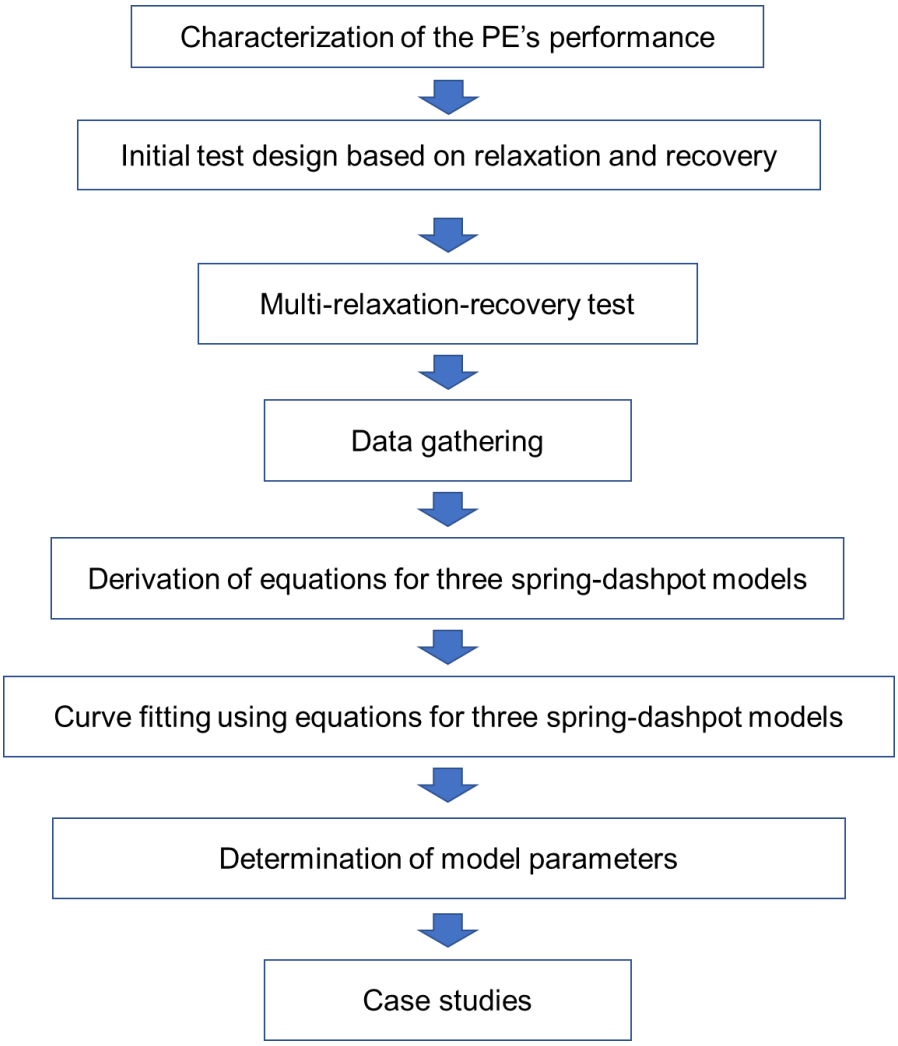

Figure 2.2. Flow chart of the methodological procedure in this study.

2.3. Analysis of RR Test Results Based on Spring-Dashpot Models

Tan and Jar [17] used the standard model for the simulation of relaxation behavior of PE, and they determined the quasi-static stress by removing the viscous stress. Sweeney et al. [34] proposed that one Eyring's dashpot is not sufficient to fully describe the relaxation behavior. It is necessary to investigate the spring-dashpot models with different combinations of two Eyring's

dashpots. The three spring-dashpot models considered for the data analysis are depicted in Figure 2.3, namely, the standard model [17], the Parallel model [33–36], and the Series model [37]. For each model, the lower branch in Figure 2.3 represents the σ_{qs} response to deformation and the upper branch the viscous counterpart. Since the two branches are connected in parallel, total specimen displacement is equivalent between the two branches, so is the total stroke rate. Note that displacement and the stroke change measured by the test machine follow a one-to-one relationship. Therefore, displacement is defined as the stroke change of the test machine. For the Parallel model, the equivalence is also applicable to the stroke and the stroke rate for the two dashpots. For the Series model, on the other hand, stress applied to the two dashpots is equivalent, so is the stress rate, but the stroke and the stroke rate for the two dashpots could be different.

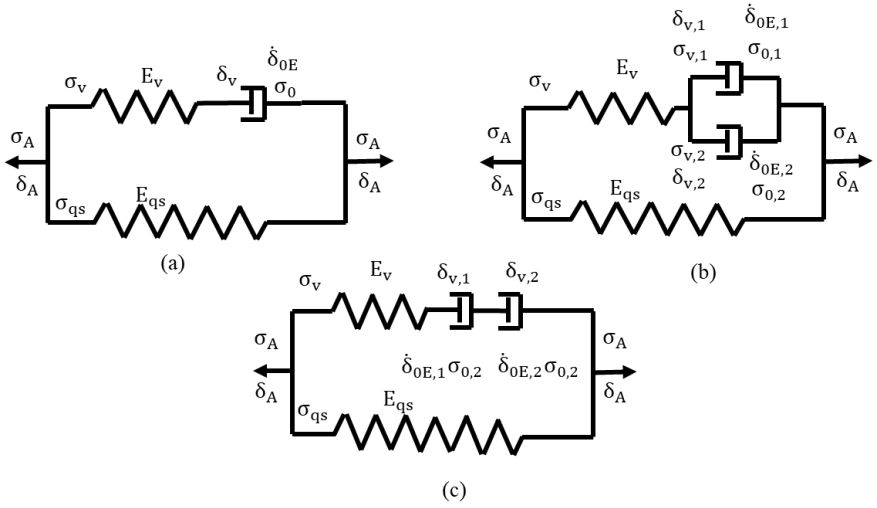

Figure 2.3. Schematic diagrams of three models used for the data analysis: (a) the standard model; (b) the Parallel model; (c) the Series model.

2.3.1. Standard Model

For the standard model in Figure 2.3(a), the applied stress is represented by σ_A, the applied stroke δ_A, the viscous stress component σ_v, the spring constant in the viscous branch E_v, the spring constant in the quasi-static branch E_{qs}, and the quasi-static stress σ_{qs}. Halsey et al. originally proposed Eyring's process for deformation of a polymer [38], and this theory is widely accepted [39,40]. Eyring's equation, as shown below, is adopted to govern the stroke rate ($\dot{\delta}_v$) of the dashpot:

$$\dot{\delta}_v = \dot{\delta}_{0E} \sinh(\sigma_v / \sigma_0) \tag{2.2}$$

where $\dot{\delta}_{0E}$ and σ_0 are the reference stroke rate and the reference stress, respectively, of the dashpot. The relationship between the stroke rate of the spring in the viscous branch $(\dot{\delta}_{E_v})$ and the corresponding stress rate $(\dot{\sigma}_v)$ is given below.

$$\dot{\delta}_{E_v} = \dot{\sigma}_v / E_v \tag{2.3}$$

Based on Equations (2.1) and (2.2), the applied stroke rate for the upper branch, which is equivalent to $\dot{\delta}_A$, can be expressed as

$$\dot{\delta}_A = \dot{\sigma}_v / E_v + \dot{\delta}_{0E} \sinh(\sigma_v / \sigma_0) \tag{2.4}$$

In the mode of stress relaxation or stress recovery at constant δ_A, Equation (2.3) becomes

$$\sigma_v = 2\sigma_0 \tanh^{-1}\{\tanh[\sigma_v(0) / (2\sigma_0)] \exp(-t / \tau_v)\} \tag{2.5}$$

where t is the time measured from the beginning of stress relaxation or stress recovery, $\sigma_v(0)$ is σ_v at t = 0, and τ_v the characteristic time for stress relaxation or stress recovery, which is a combined parameter of σ_0, E_v and $\dot{\delta}_{0E}$:

$$\tau_v = \sigma_0 / (E_v \dot{\delta}_{0E}) \quad (2.6)$$

Since σ_A is the sum of stresses applied to the viscous and quasi-static branches, σ_v and σ_{qs}, σ_A for the standard model can be expressed as

$$\sigma_A = \sigma_{qs} + 2\sigma_0 \tanh^{-1}\{\tanh[\sigma_v(0) / (2\sigma_0)] \exp(-t / \tau_v)\} \quad (2.7)$$

In this study, Equation (2.6) is used to examine the suitability of the standard model for reproducing the RR test results.

2.3.2. Parallel Model

For the Parallel model in Figure 2.3(b), $\dot{\delta}_{v,1}$, $\dot{\delta}_{0E,1}$, $\sigma_{0,1}$ represent stroke rate, reference stroke rate, and reference stress, respectively, of dashpot 1, and the corresponding terms with sub-script 2, i.e., $\dot{\delta}_{v,2}$, $\dot{\delta}_{0E,2}$, and $\sigma_{0,2}$ for dashpot 2. Again, Equation (2.1) is adopted to govern the stroke rate for each dashpot. Here, process 1 is used to represent the process with a larger τ_v value and process 2 the process with a smaller τ_v value. As mentioned earlier, since the two dashpots are connected in parallel, the two dashpots have the same stroke and stroke rate, and the expression for the stroke rate applied to the dashpots is given below.

$$\dot{\delta}_{v,1} = \dot{\delta}_{v,2} = \dot{\delta}_A - \dot{\sigma}_v / E_v \quad (2.8)$$

Since stresses of the two dashpots are additive, based on Equation (2.1), total stress of the viscous branch is

$$\sigma_v = \sigma_A - \sigma_{qs} \quad (2.9)$$

$$= \sigma_{0,1}\,\mathrm{asinh}\left[\left(\dot{\delta}_A - \dot{\sigma}_v / E_v\right) / \dot{\delta}_{0E,1}\right]$$

$$+ \sigma_{0,2}\,\mathrm{asinh}\left[\left(\dot{\delta}_A - \dot{\sigma}_v / E_v\right) / \dot{\delta}_{0E,2}\right]$$

2.3.3. Series Model

For the Series model, in Figure 2.3(c), the total deformation of the viscous branch (equivalent to δ_A)is equal to the summation of deformations of the spring in the branch and the two dashpots. Same as the other two models, Equation (2.1) is adopted to govern the stroke rate for the two dashpots, as a function of the stress applied to the viscous branch (σ_v). Therefore, the stress rate applied to the viscous branch ($\dot{\sigma}_v$) can be expressed using the following expression.

$$\dot{\sigma}_v = E_v\left[\dot{\delta}_A - \dot{\delta}_{0E,1}\sinh\left(\sigma_v / \sigma_{0,1}\right) - \dot{\delta}_{0E,2}\sinh\left(\sigma_v / \sigma_{0,2}\right)\right] \qquad (2.10)$$

Equations (2.6), (2.8) and (2.9) for the three models were solved by curve fitting, and the details are given in Section 5.

2.4. Experimental Details of the RR Test Used in the Study

2.4.1. Materials and Specimen Dimensions

Two types of HDPE were used in the study. One is qualified as a PE100 resin (HDPE-a) and the other not qualified (HDPE-b). Their characteristics are listed in Table 2.1, provided by the material suppliers.

Table 2.1. Characteristics of HDPE-a and HDPE-b used in this study.

Properties	Test Method	Units	HDPE-a	HDPE-b
Density	ASTM D792	g/cm^3	0.949	0.945
Tensile Strength @ Yield	ASTM D638	MPa	24.1	22.5
Ultimate Elongation	ASTM D638	%	500	850
SCG PENT	ASTM F1473	h	>10,000	>100

Specimens used for the RR test had an axisymmetric geometry, as shown in Figure 2.4, with the same dimensions as the specimens used previously in our study [41]. That is, the overall length is 140 mm, and the length and diameter in the gauge section are 20 and 6 mm, respectively. Same as before, the specimens contained a small circumferential groove in the middle of the gauge section, with a groove depth of 0.076 mm, to ensure that necking started there. Each specimen was gripped using a 50-mm-long steel tab at both ends to avoid slippage during the RR test.

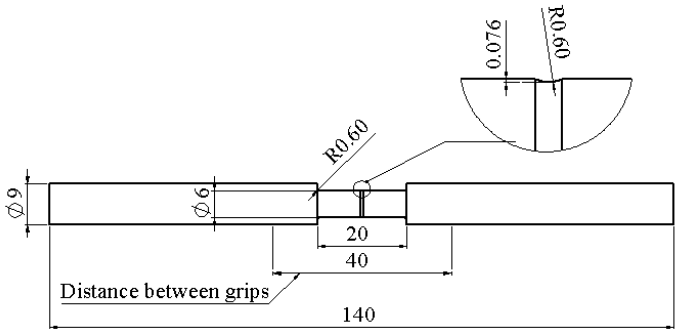

Figure 2.4. Geometry and dimensions of specimens used for the RR tests.

2.4.2. Test Conditions

A computer-controlled universal test machine (Qualitest Quasar100, Lauderdale, FL, USA) was used to conduct the RR tests. The test program was designed to have each stage follow the scheme depicted in Figure 2.1(a) as a function of time. For this study, a loading period of 12 s was used to reach the relaxation phase, and a period of 10,000 s for stress relaxation at a fixed stroke. Note that at the end of the relaxation phase, a loading period of 3 s was given before the stabilization phase which was also for a period of 10,000 s. At the end of the stabilization phase, the specimen was unloaded for 3 s before the recovery phase for a period of 10,000 s as well. Crosshead speed for all loading and unloading phases was set to be 1 mm/min. However, a period of about 1.5 s was needed for the crosshead to reach the specified speed. Therefore, the actual stroke increment for loading was about 0.2 mm between the recovery and the next relaxation phases, and the stroke change of about 0.033 mm between the relaxation and stabilization phases (loading) and between stabilization and recovery phases (unloading). In total, about 30 cycles of the loading scheme shown in Figure 2.1(a) were applied to the specimen, to introduce a total specimen displacement, in terms of stroke of the test machine, of around 6 mm.

Repeated RR tests were conducted at room temperature using at least two specimens for each HDPE, to ensure consistency of the reproducibility as that obtained previously [17,41]. RR tests were also conducted at elevated temperatures of 313, 318, 328, 343, 358, and 368 K, to determine the activation energies, but only for HDPE-a of one specimen at each temperature. The use of one specimen at each temperature was mainly because of the good reproducibility of the test results and a long period of about 11 days required for each RR test. Besides, each RR test provides 30 sets of data for the analysis, with each set including loading, relaxation, unloading, and recovery. Therefore, the limited number of tests at elevated temperatures have actually provided more than 180 sets of data for the analysis.

2.5. Results and Discussion

A typical engineering stress-stroke curve for one cycle of the RR test is shown in Figure 2.5, as complementary to the stroke-time plot in Figure 2.1(a). Figure 2.5 indicates that a commonly observed hysteresis loop from loading-unloading of polymeric materials [42] is hardly visible between unloading before the recovery phase and the initial loading after the recovery phase. Overlap of the unloading curve to the recovery phase and the initial loading curve to the following relaxation phase suggests that the specimen was in a nearly fully relaxed state after the stabilization. The slope for this part of the stress-stroke curve is presented in Figure 2.6 as a function of stroke for the two HDPEs [43], representing the total stiffness (E_{total}) of the material in the fully relaxed state. The figure indicates that an early, relatively fast rate of E_{total} drop occurred in HDPE-a. For HDPE-b, the E_{total} drop has a constant rate which is close to the drop rate of E_{total} for HDPE-a at the large stroke.

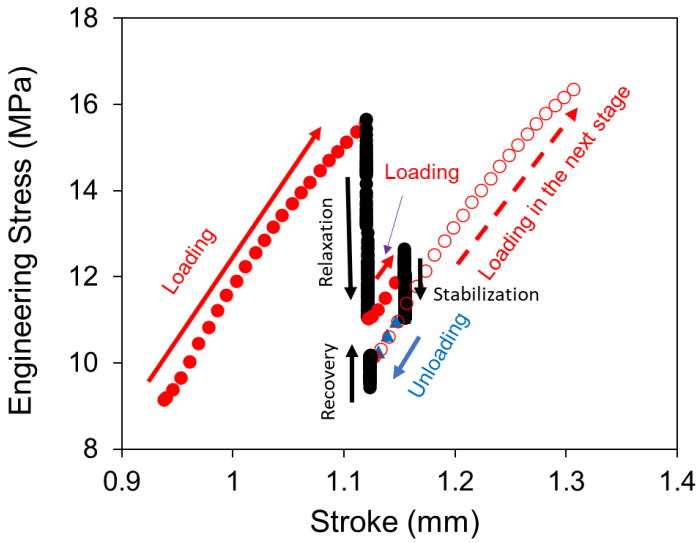

Figure 2.5. A sample curve of engineering stress versus stroke, from one cycle of the RR test on HDPE-a at room temperature.

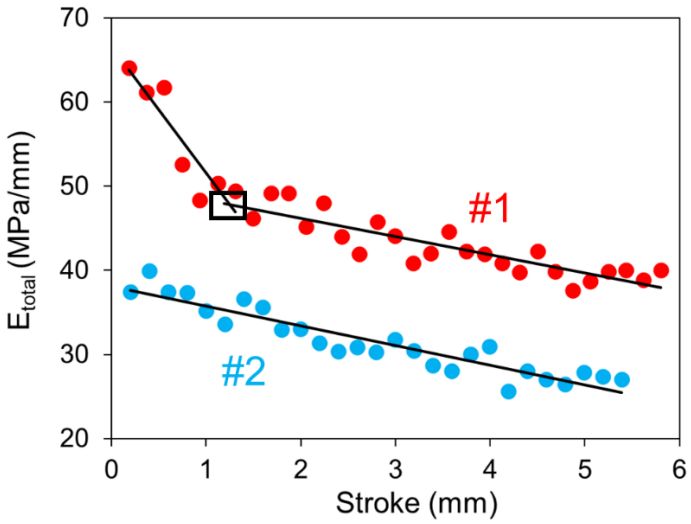

Figure 2.6. Total stiffness (E_{total}) versus stroke for HDPE-a and HDPE-b at room temperature.

Three models, as described in Section 3, were used to analyze the RR test results. For each model, the CRR approach was used to determine values for the model parameters, based on the assumption that σ_{qs} is only a function of specimen displacement (in terms of stroke of the test machine). This assumption is consistent with the common belief that relaxation and recovery processes at a given stroke should eventually reach the same stress level [44]. In the CRR approach, a σ_{qs} value was firstly selected within the stress range between the end of the relaxation phase and the end of the following recovery phase. Values for parameters in each of the three models in Figure 2.3 were then searched to provide the best fit to the experimental curve in the relaxation and recovery phases. A two-folded fitting criterion was applied to determine the most suitable σ_{qs} value. One was the number of experimental data points in a given marker size passed by the model-generated curve, and the other the consistency of the overall trend of the model-generated curve with the trend shown by the experimental data.

In this study, σ_{qs} was determined using the standard model based on Equation (2.6), with $\sigma_v(0)$ being the difference between σ_A and σ_{qs} at the beginning of the relaxation or the recovery phase. The σ_{qs} values were then applied to the other two models to determine their model parameters.

Two case studies are presented below to demonstrate results from the CRR approach. The first case study is to compare the quality of the curve fitting generated by the three models, and to investigate the pros and cons of the three models for mimicking the experimentally-obtained curves. The second case study is to explore the possibility of using the RR tests at elevated temperatures to determine the activation energies for Eyring's model. Note that both HDPE-a and HDPE-b were used in the first case study, but for the second case study, only HDPE-a was used. Determination of the activation energies in the second case study was based on the Parallel model because results from the first case study have indicated that among the three models considered here, the Parallel model is most suitable for mimicking the stress response to deformation in the RR test.

2.5.1. Case Study 1: Comparison of Three Models Depicted in Figure 2.3

The simulation of relaxation and recovery using the standard model can be completed using Equation (2.6). Curve fitting was performed by firstly choosing a σ_{qs} value, and then adjusting the σ_0 and τ_v values for the standard model to fit the experimentally obtained stress-time curves from the relaxation and recovery phases. Note that for the five unknowns at a given stroke, i.e., σ_{qs} and the two sets of σ_0 and τ_v (one set for the relaxation phase and the other set for the recovery phase), were the values that could provide the best fit to the experimental data obtained

from the two phases. This fitting procedure was repeated through the whole RR tests to establish the variation of values for the five parameters as a function of stroke.

The simulation of relaxation and recovery using the Parallel and the Series models was performed using Equations (2.8) and (2.9), respectively. It was assumed that σ_{qs} values used for the Parallel and the Series models are the same as those determined from the standard model. Since $\dot{\delta}_A$ is 0 in the relaxation and recovery phases, there were four unknowns in each of Equations (2.8) and (2.9), to be determined from the curve fitting: $\sigma_{0,1}$, $\sigma_{0,2}$, $E_v\dot{\delta}_{0E,1}$, and $E_v\dot{\delta}_{0E,2}$. Equations (2.8) and (2.9) are ordinary differential equations involving the unknown function $\sigma_v(t)$ and its derivatives with respect to time t. Matlab was applied to solve these ordinary differential equations. To solve these ordinary differential equations using Matlab, function "ode15i" in Matlab was used to determine these four parameters in the Parallel model, based on Equation (2.8), as this equation is a fully implicit differential equation which can be solved using "ode15i" [45]. Matlab function "decic" was used to compute the consistent initial conditions for "ode15i" as "ode15i" requires consistent initial conditions for σ_v and $\dot{\sigma}_v$. For the Series model, on the other hand, the four parameters were determined using the function "ode45" in Matlab, as this function is designed to solve a nonstiff differential equation like Equation (2.9) [46]. As mentioned earlier, the model-generated curves were checked by naked eyes to ensure that the fitting criterion of passing through as many experimental data points as possible and showing the same trend as the experimental curves were met.

Sample curves generated from the above CRR approach for the three models in Figure 2.3 are presented in Figure 2.7, for HDPE-a at the stroke of 2.24 mm. Figure 2.7(a) indicates that the curves generated by the Parallel and the Series models are close to the experimental data. For the standard model, although a pretty good agreement was achieved with the experimental curve, some

deviation is shown in the section from 1 to 1000 s. Nevertheless, these results are consistent with those reported in the literature [17,34,47].

Figure 2.7(b) indicates that all simulation curves mimicked reasonably well the experimental curve in the recovery phase before the maximum stress is reached, but failed to regenerate a small stress drop before the end of the recovery phase. The stress drops in the recovery phase were also reported in the literature. Kitagawa et al. first observed this stress drop and regarded the drop as an "anomalous" phenomenon [48]. Drozdov et al. reported this stress drop as an "unusual" stress response and suggested that accurate modeling of this behavior remains unresolved [22]. Figure 2.7(b) shows that the three models considered here also failed to regenerate this stress drop phenomenon. The stress drop is the long-term relaxation behavior caused by the loading stage before the relaxation stage. The stress increase in the initial stage of recovery is caused by the unloading before the recovery, and the effect of the unloading was reduced with increasing time during recovery. Therefore, it shows the stress decrease of the long-term relaxation behavior at the end of recovery stage as the stoke change during the loading before relaxation is much larger than the stroke change during the unloading. The stress continues to decrease over a longer recovery period, as the effect of unloading diminishes progressively with time. Even though the stress drop during the recovery phase could not be simulated using the models considered in this study, the maximum difference between the experimental data and data generated by the models in the relaxation phase, apart from the very first relaxation phase that did not go through the stress recovery process, is 0.127 MPa for the Series model and 0.116 MPa for the Parallel model. Such a difference is slightly better than the difference reported in the literature, e.g., 0.17 MPa [44], 0.3 MPa [34], and about 1 MPa [49,50]. In view that the Parallel and the Series models show similar closeness

in simulating the experimental data, with the former being slightly better than the latter, the Parallel model will be used in the second case study to determine activation energies for HDPE-a.

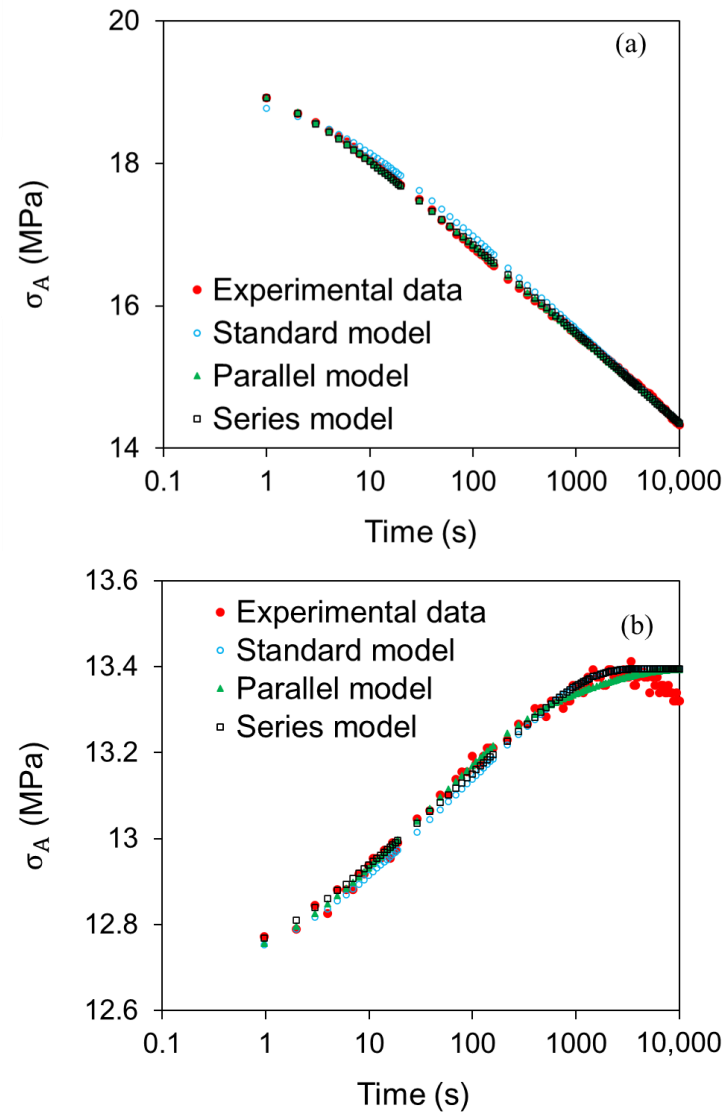

Figure 2.7. Sample curves for simulation of stress response in the relaxation and recovery phases using the three models in Figure 2.3, taken from RR test data at stroke of 2.24 mm of HDPE-a: (a) for the relaxation phase; (b) for the recovery phase.

Figure 2.8 compares stress responses to deformation in the RR tests for the 2 HDPEs. Figure 2.8(a) depicts the applied stress as a function of stroke at the beginning of the relaxation phase, $\sigma_A(0)$, which indicates that $\sigma_A(0)$ for HDPE-a is higher than that for HDPE-b. The corresponding σ_{qs} and $\sigma_v(0)$ values are presented in Figures 2.8(b), and (c), respectively. Qualitative difference of the two HDPEs in these stress responses to deformation is expected, but further study is needed using PE of clear difference in the material characteristics, such as molecular weight and its distribution and side branch length, its distribution and density, would be needed to quantify the difference among these stress responses.

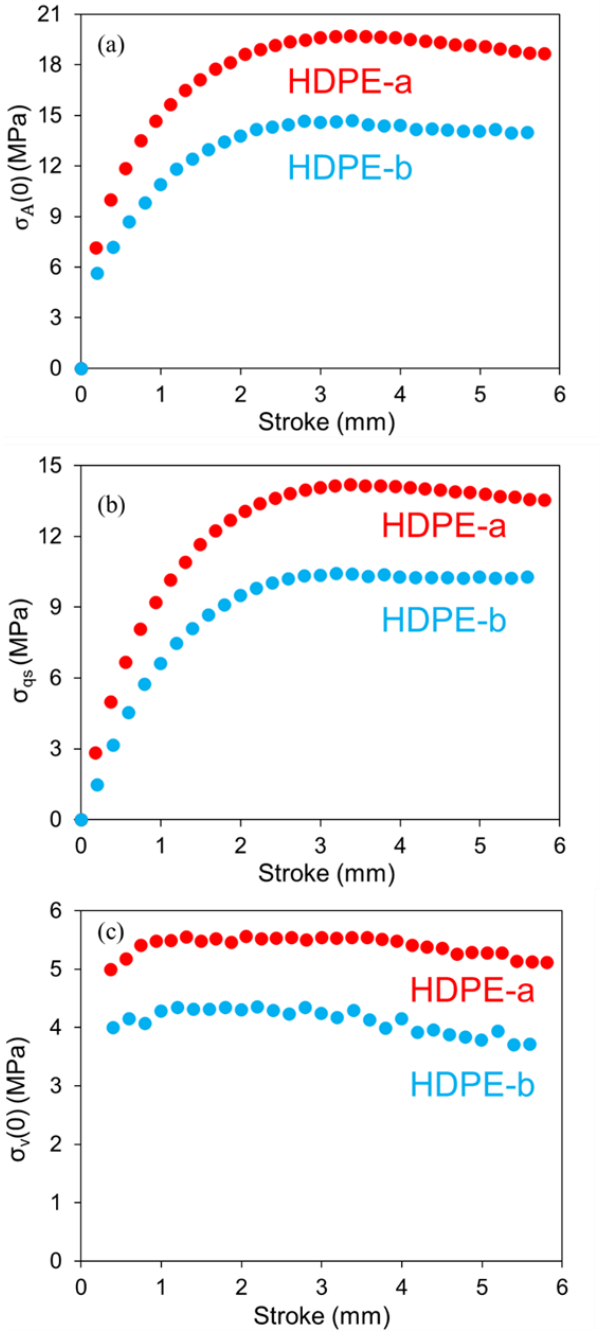

Figure 2.8. Comparison of stress responses at the beginning of the relaxation phases for the two HDPEs at 294 K: (a) $\sigma_A(0)$; (b) σ_{qs}; (c) $\sigma_v(0)$.

Values for parameters in viscous branches of the three models in Figure 2.3 are summarized in Figure 2.9. For the standard model, as shown in Figure 2.9(a), and (b), a critical stroke can be detected using the change of σ_0 values. However, further study is needed to examine the influence of allowing the τ_v change on the critical stroke value and whether the critical stroke indicates the change of mechanisms involved in the deformation process [17]. For the Parallel model, Figure 2.9(c), and (d) shows changes of $\sigma_{0,1}$ and $\sigma_{0,2}$, respectively, in the relaxation phase as functions of stroke. Unlike Figure 2.9(a) for the standard model, none of the curves in Figure 2.9(c), and (d) shows a clear transition of the trend line that occurs at a common stroke. A similar phenomenon is shown in, Figure 2.9(e), and (f) for the Series model. In addition, Figure 2.9(e) indicates a strong change in the trend line for HDPE-b, but not for HDPE-a. Therefore, the critical stroke detected using the standard model, and a critical stroke reported in the past using models with a single dashpot [17,31,51], may need further investigation.

Figure 2.9(g)–(j) indicates that values for $E_v\dot{\delta}_{0E,1}$ and $E_v\dot{\delta}_{0E,2}$ in both Parallel and the Series models can maintain constant for the entire RR test. Therefore, a constant value could be chosen for the E_v value for each HDPE, and the difference between the corresponding $E_v\dot{\delta}_{0E,1}$ and $E_v\dot{\delta}_{0E,2}$ comes from the difference in the $\dot{\delta}_{0E,1}$ and $\dot{\delta}_{0E,2}$values. However, in view that neither the Parallel nor the Series model could simulate the stress drop in the recovery phase, as shown in Figure 2.7(b), determination of the E_v value was not pursued here. Rather, a study is being conducted when this manuscript is prepared, to develop a model that could mimic the stress drop in the recovery phase, for which the E_v value will be determined in the future.

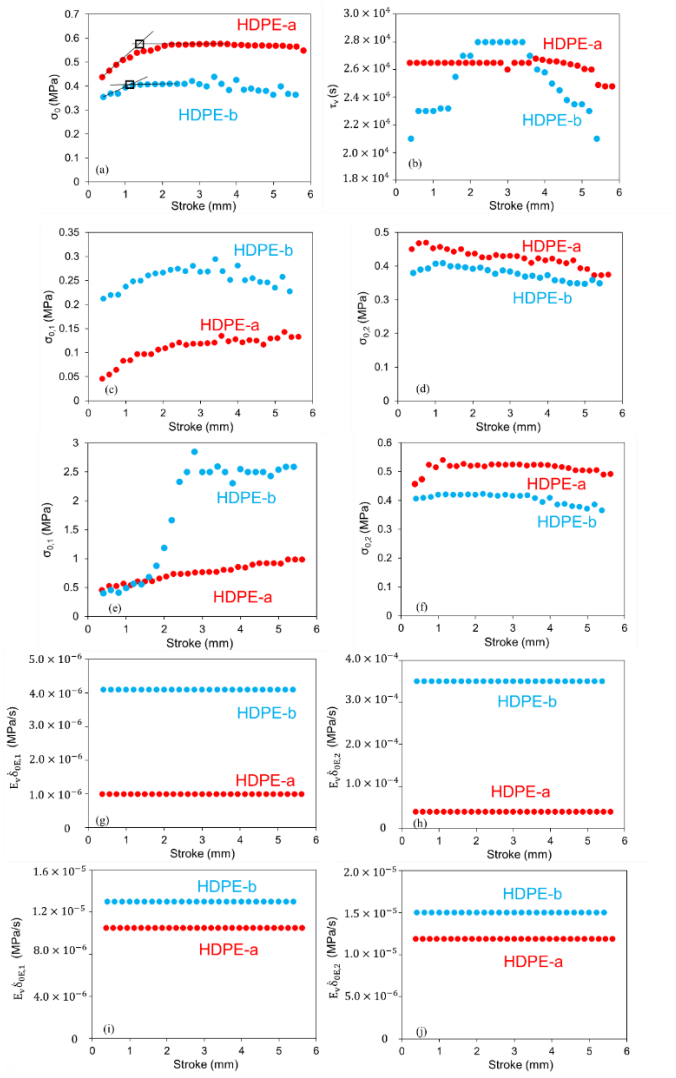

Figure 2.9. Comparison of model parameters in Figure 2.9, to simulate stress variation of HDPE-a and HDPE-b as functions of time in the relaxation phases at 294 K: (a) σ_0 for the standard model; (b) τ_v for the standard model; (c) $\sigma_{0,1}$ for the Parallel model; (d) $\sigma_{0,2}$ for the Parallel model; (e) $\sigma_{0,1}$ for the Series model; (f) $\sigma_{0,2}$ for the Series model; (g) $E_v\dot{\delta}_{0E,1}$ for the Parallel model; (h) $E_v\dot{\delta}_{0E,2}$ for the Parallel model; (i) $E_v\dot{\delta}_{0E,1}$ for the Series model; (j) $E_v\dot{\delta}_{0E,2}$ for the Series model.

2.5.2. Case Study 2: Determination of Activation Energies for the Eyring's Model

Determination of activation energies was based on RR test results at different temperatures, and analyzed using the Parallel model. Based on Eyring's law [52], the reference stroke rate ($\dot{\delta}_{0E,i}, i = 1, 2$) for the dashpot can be expressed as:

$$\dot{\delta}_{0E,1} = \dot{e}_{0,1}\exp(-\frac{\Delta H_1}{kT}) \quad (2.11)$$

$$\dot{\delta}_{0E,2} = \dot{e}_{0,2}\exp(-\frac{\Delta H_2}{kT}) \quad (2.12)$$

where $\dot{e}_{0,i}$ and ΔH_i, with i = 1, 2, are the pre-exponential factor and the activation energies, respectively, for the Eyring's process i, k the Boltzmann's constant, and T temperature in K. Values for $\dot{\delta}_{0E,1}$ and $\dot{\delta}_{0E,2}$ at different temperatures were determined by fitting the RR test data in the relaxation phase and the last three points in the prior loading phase. To determine the activation energies, the stroke function of σ_{qs} was first determined using the RR test results at different temperatures, based on the standard model, as shown in Figure 2.10(a). Equation (8) was used for the simulation of relaxation phase and the last three data points in the loading phase before the relaxation phase. Equation (2.8) was first applied to fit the relaxation phase, to determine values for $E_v\dot{\delta}_{0E,1}$, $E_v\dot{\delta}_{0E,2}$, $\sigma_{0,1}$, $\sigma_{0,2}$, and then values for E_v, $\dot{\delta}_{0E,1}$ and $\dot{\delta}_{0E,2}$ were determined by fitting the last three data points in the loading phase prior to the relaxation phase. This part of curve fitting was based on the assumption that E_v, $\sigma_{0,1}$, $\sigma_{0,2}$, $\dot{\delta}_{0E,1}$, and $\dot{\delta}_{0E,2}$ at the end of the loading phase, before the relaxation, remained constant, with their values to be the same as the corresponding values in the relaxation phase. Since $\dot{\delta}_A$ was 0 in the relaxation phase and 0.0167 mm/s for the last three data points in the loading phase, with values for $\sigma_{0,1}$, $\sigma_{0,2}$, $E_v\dot{\delta}_{0E,1}$, and $E_v\dot{\delta}_{0E,2}$

determined in the fitting process for data in the relaxation phase, using the parallel model described in Section 5.1, values for E_v, $\dot{\delta}_{0E,1}$ and $\dot{\delta}_{0E,2}$ were then adjusted to fit the last three data points in the loading phase.

As shown in Figure 2.10(a), σ_{qs} values decrease with the increase of the temperatures. Sample curves in the relaxation phase, from simulation and experiments, are shown in Figure 2.10(b) in which the open circles are the experimental data and the solid lines from the simulation. These sample curves depict a good agreement between simulation using the Parallel model and the experimental data, with the maximum difference of 0.125 MPa in the stress value.

Figure 2.11 shows a sample of the simulation curve for the last three data points in the loading phase and all experimental data for the loading phase. The maximum difference in the stress value for all fittings conducted in this case study was 0.069 MPa. Figure 2.12 summarizes the value for $\sigma_{0,1}$, $\sigma_{0,2}$, $\dot{\delta}_{0E,1}$, $\dot{\delta}_{0E,2}$, and E_v as a function of stroke using the above process. The figure 2. suggests that values for $\dot{\delta}_{0E,1}$, $\dot{\delta}_{0E,2}$, and E_v show little dependence on the stroke, but values for $\sigma_{0,1}$ and $\sigma_{0,2}$ did show some variations with the change of stroke, though the extent of variation decreased with the temperature increase. Figure 2.12 also suggests that similar to Figure 2.9(c), and (d), $\sigma_{0,1}$ and $\sigma_{0,2}$ determined using the Parallel model did not show any clear transition in their dependence on the stroke variation.

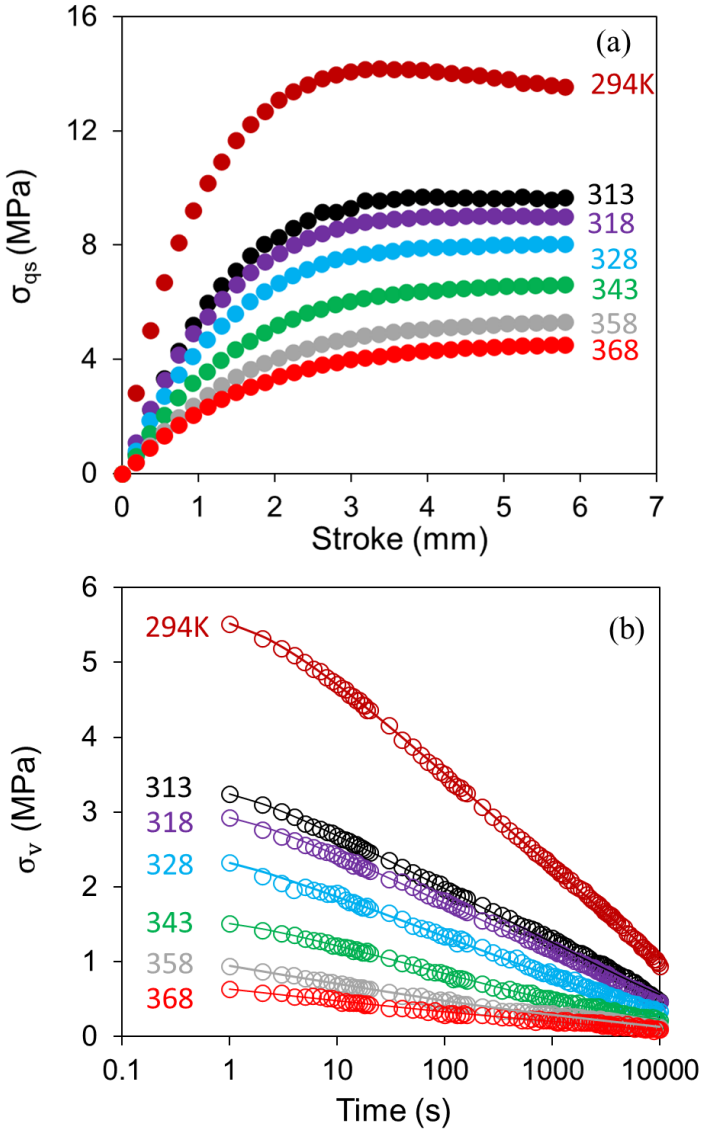

Figure 2.10. Summary of σ_{qs} (a) and σ_v (b) as a function of stroke and time, respectively, at different temperatures (σ_v was taken from relaxation at the stroke of 3.75 mm at each temperature).

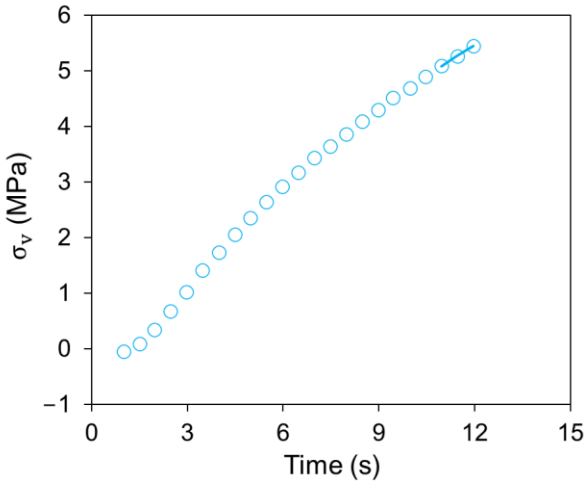

Figure 2.11. A sample curve of σ_v versus time in the loading phase between recovery and relaxation, and the fitting line for the last three points based on the Parallel model.

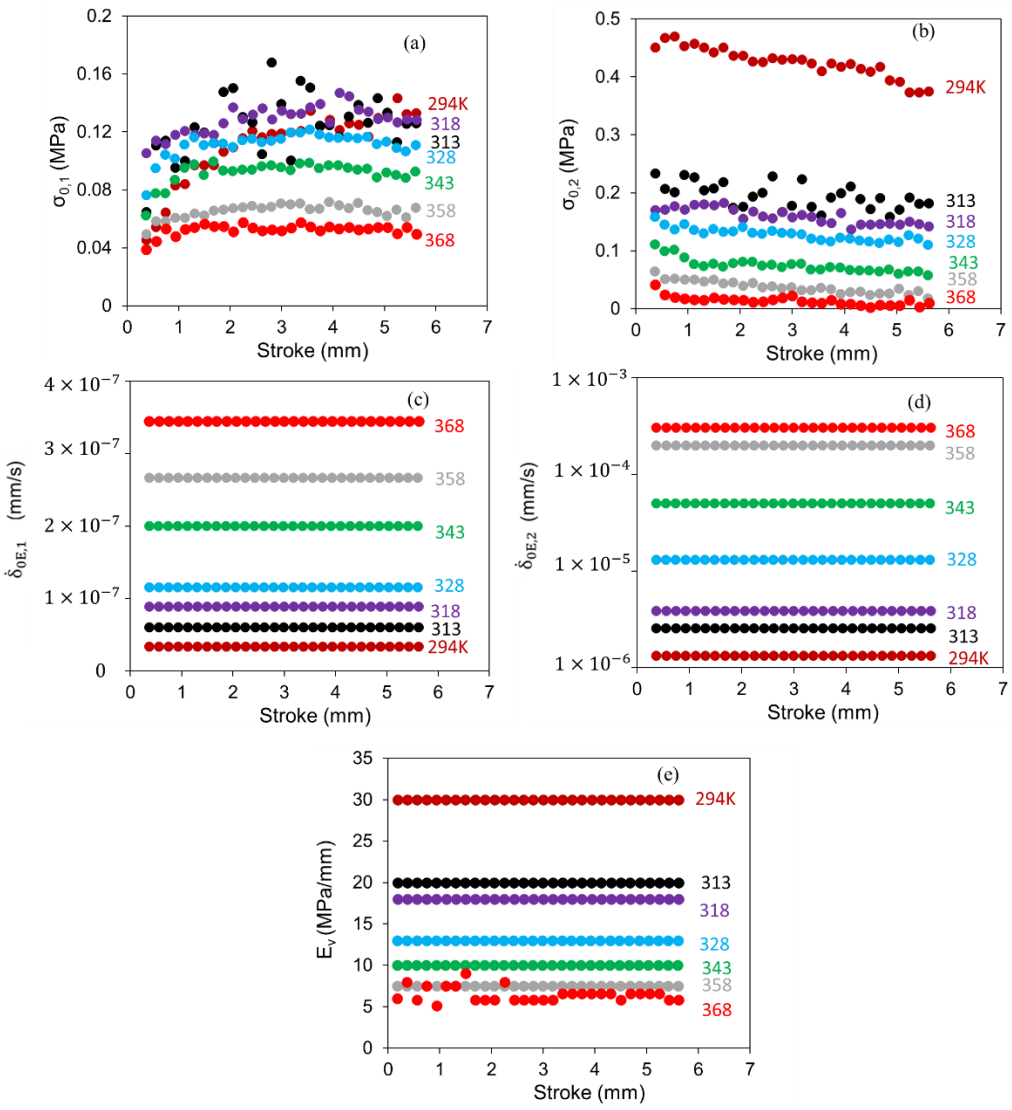

Figure 2.12. Stroke dependence of parameters used in the Parallel model to simulate the stress response in the relaxation phase at different temperatures: (a) $\sigma_{0,1}$; (b) $\sigma_{0,2}$; (c) $\dot{\delta}_{0E,1}$; (d) $\dot{\delta}_{0E,2}$; (e) E_v.

Figure 2.13 presents the plots of $\ln(\dot{\delta}_{0E,1})$ and $\ln(\dot{\delta}_{0E,2})$ as a function of $1/T$, where T is temperature in K. It should be noted that the slopes of the two curves for process 1 and process 2

are $-\Delta H_1 / k$ and $-\Delta H_2 / k$, respectively, and the unit for the slope is K as activation energy has the unit of kJ/mol and Boltzmann constant k is 8.3145×10^{-3} kJ/(mol·K). The figure shows that slopes of data points for processes 1 and 2, based on the linear curve fitting, are -3485 K and -8815 K, respectively. Based on Equations (2.10) and (2.11), the corresponding activation energies for processes 1 and 2 are 28.96 and 73.25 kJ/mol, respectively. Activation energy is the energy barrier that must be surpassed to enable molecular motions [53]. From Gao et al. [54], the molecular and structural interpretations behind the activation energy have not been clarified. Tan and Jar proposed that these two Eyring's processes should represent different mechanisms during deformation. It was reported that one process is associated with the crystalline phase and the other with the molecular network [55]. The activation energies from this study can be used to quantify the energy barriers for relaxation introduced in the RR test. These values are in the same order of magnitude as those reported in the literature, such as Wilhelm et al. [56] who used creep test data for PE100 pipe resin and determined the activation energy for one Eyring's process to be 30 kJ/mol and Truss et al. [57] who used torsion test data for HDPE with the density of 0.972 g/cm^3 and determined the activation energies for yielding using two Eyring's process connected in parallel to be 243 and 100 kJ/mol.

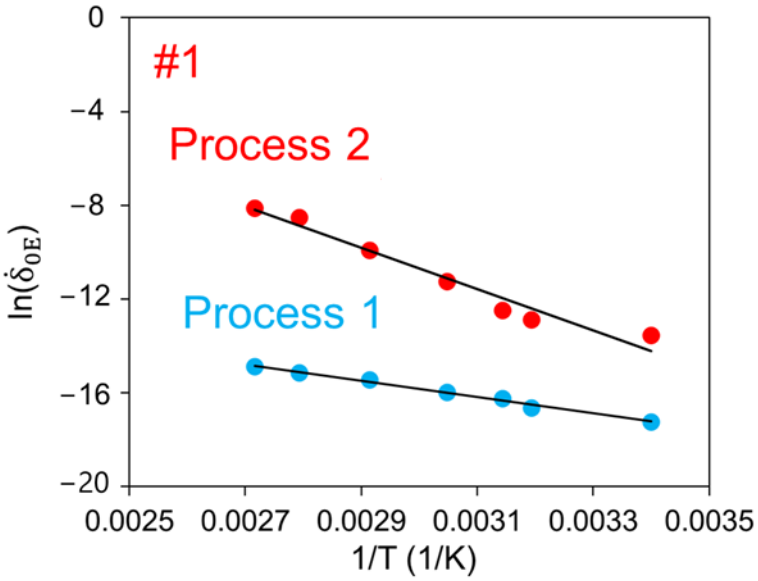

Figure 2.13. Plot of $\ln(\dot{\delta}_{0E})$ versus 1/T for the Parallel model, and the corresponding equations for the linear curve fitting.

As suggested by André and Cruz-Pinto [58], in addition to the dependence on materials, different loading modes may also yield different values for the activation energies. Therefore, a further study on the effect of the loading mode on the activation energy will be conducted based on the principle of the RR test presented here.

2.6. Conclusions

A novel RR test was developed, which contains multiple cycles with six stages in one cycle of the test. The test was designed to separate the viscous stress response to deformation from the quasi-static counterpart. The study discovered that a commonly observed hysteresis loop from loading-unloading of polymeric materials is hardly visible between unloading before the recovery phase and the initial loading after the recovery phase in the RR test. Three models were examined to explore their feasibility to analyze the RR test results. It was found that the standard model could

not mimic closely the stress drop during the entire relaxation process of 10,000 s, but, the Parallel and the Series models could. It was found that the standard model could determine the long-term performance of polyethylene and reveal a transition point for the onset of plastic deformation in the crystalline phase. However, none of the three models was able to generate a stress drop in the recovery phase after the maximum point which was shown in the experimental data.

The viscous and quasi-static stress responses for two HDPEs were characterized using the RR test based on the three models for the data analysis. It was found that the RR test has the advantage of determining the total stiffness of the materials at different deformation levels, which can be applied to the evaluation of PE's mechanical performance. The study shows that the RR test provides a data set that can be used to evaluate the suitability of spring-dashpot models for characterizing the time-dependent and time-independent mechanical performance of PE, and the possibility of determining the activation energy for deformation in the stress relaxation mode. A study is being conducted when this manuscript is prepared, to develop a suitable model that can mimic the complex stress response to deformation introduced in the RR test, and determine the corresponding activation energy for deformation introduced in the RR test.

References

1. Geyer, R.; Jambeck, J.R.; Law, K.L. Production, Use, and Fate of All Plastics Ever Made. *Sci. Adv.* 2017, *3*, e1700782, doi:10.1126/sciadv.1700782.

2. Nguyen, K.Q.; Mwiseneza, C.; Mohamed, K.; Cousin, P.; Robert, M.; Benmokrane, B. Long-Term Testing Methods for HDPE Pipe-Advantages and Disadvantages: A Review. *Eng. Fract. Mech.* 2021, *246*, 107629, doi:10.1016/j.engfracmech.2021.107629.

3. Qi, Z.; Hu, N.; Li, G.; Zeng, D.; Su, X. Constitutive Modeling for the Elastic-Viscoplastic Behavior of High Density Polyethylene under Cyclic Loading. *Int. J. Plast.* 2019, *113*, 125–144, doi:10.1016/j.ijplas.2018.09.010.

4. Alsabri, A.; Al-Ghamdi, S.G. Carbon Footprint and Embodied Energy of PVC, PE, and PP Piping: Perspective on Environmental Performance. *Energy Rep.* 2020, *6*, 364–370, doi:10.1016/j.egyr.2020.11.173.

5. Ivanov, D.A. Semicrystalline Polymers. In *Polymer Science: A Comprehensive Reference*; Elsevier: Amsterdam, The Netherlands, 2012; pp. 227–258, ISBN 978-0-08-087862-1.

6. Wu, K.; Zhang, H.; Liu, X.; Bolati, D.; Liu, G.; Chen, P.; Zhao, Y. Stress and Strain Analysis of Buried PE Pipelines Subjected to Mechanical Excavation. *Eng. Fail. Anal.* 2019, *106*, 104171, doi:10.1016/j.engfailanal.2019.104171.

7. Krishnaswamy, P.; Shim, D.-J.; Kalyanam, S. Comparison of Parent and Butt-Fusion Material Properties of Unimodal High-Density Polyethylene. *J. Press. Vessel Technol.* 2017, *139*, 041413, doi:10.1115/1.4036658.

8. Zha, S.; Lan, H.; Huang, H. Review on Lifetime Predictions of Polyethylene Pipes: Limitations and Trends. *Int. J. Press. Vessel. Pip.* 2022, *198*, 104663, doi:10.1016/j.ijpvp.2022.104663.

9. Brown, N. Intrinsic Lifetime of Polyethylene Pipelines. *Polym. Eng. Sci.* 2007, *47*, 477–480, doi:10.1002/pen.20696.

10. Zhang, Y.; Jar, P.-Y.B. Characterization of Ductile Damage in Polyethylene Based on Effective Stress Concept. *Mech. Mater.* 2019, *136*, 103080, doi:10.1016/j.mechmat.2019.103080.

11. Venkatesh, C. Performance Comparison of High Density Polyethylene Pipe (Hdpe) in Municipal Water Applications. Master's Thesis, University of Texas at Arlington, Arlington, TX, USA, 2012.

12. Majid, Z.A.; Mohsin, R.; Yaacob, Z.; Hassan, Z. Failure Analysis of Natural Gas Pipes. *Eng. Fail. Anal.* 2010, *17*, 818–837, doi:10.1016/j.engfailanal.2009.10.016.

13. Zhang, Y.; Chang, P.; Qiao, L.; Fan, J.; Xue, S.; Zhou, B. On the Estimation of Tensile Yield Stress for Polymer Materials Based on Punch Tests. *Polym. Test.* 2021, *100*, 107249, doi:10.1016/j.polymertesting.2021.107249.

14. Zrida, M.; Laurent, H.; Rio, G.; Pimbert, S.; Grolleau, V.; Masmoudi, N.; Bradai, C. Experimental and Numerical Study of Polypropylene Behavior Using an Hyper-Visco-Hysteresis Constitutive Law. *Comput. Mater. Sci.* 2009, *45*, 516–527, doi:10.1016/j.commatsci.2008.11.017.

15. Yeh, I.-C.; Andzelm, J.W.; Rutledge, G.C. Mechanical and Structural Characterization of Semicrystalline Polyethylene under Tensile Deformation by Molecular Dynamics Simulations. *Macromolecules* 2015, *48*, 4228–4239, doi:10.1021/acs.macromol.5b00697.

16. Fritsch, J.; Hiermaier, S.; Strobl, G. Characterizing and Modeling the Non-Linear Viscoelastic Tensile Deformation of a Glass Fiber Reinforced Polypropylene. *Compos. Sci. Technol.* 2009, *69*, 2460–2466, doi:10.1016/j.compscitech.2009.06.021.

17. Tan, N.; Jar, P.-Y.B. Determining Deformation Transition in Polyethylene under Tensile Loading. *Polymers* 2019, *11*, 1415, doi:10.3390/polym11091415.

18. Izraylit, V.; Gould, O.E.C.; Rudolph, T.; Kratz, K.; Lendlein, A. Controlling Actuation Performance in Physically Cross-Linked Polylactone Blends Using Polylactide Stereocomplexation. *Biomacromolecules* 2020, *21*, 338–348, doi:10.1021/acs.biomac.9b01279.

19. Alotta, G.; Barrera, O.; Pegg, E.C. Viscoelastic Material Models for More Accurate Polyethylene Wear Estimation. *J. Strain Anal. Eng. Des.* 2018, *53*, 302–312, doi:10.1177/0309324718765512.

20. Cangemi, L.; Meimon, Y. A Two-Phase Model for the Mechanical Behavior of Semicrystalline Polymers. *Oil Gas Sci. Technol. Rev. IFP* 2001, *56*, 555–580, doi:10.2516/ogst:2001045.

21. Brusselle-Dupend, N.; Lai, D.; Feaugas, X.; Guigon, M.; Clavel, M. Mechanical Behavior of a Semicrystalline Polymer before Necking. Part II: Modeling of Uniaxial Behavior. *Polym. Eng. Sci.* 2003, *43*, 501–518, doi:10.1002/pen.10041.

22. Drozdov, A.D.; de Claville Christiansen, J. Cyclic Viscoplasticity of High-Density Polyethylene: Experiments and Modeling. *Comput. Mater. Sci.* 2007, *39*, 465–480, doi:10.1016/j.commatsci.2006.07.014.

23. Ames, N.M.; Srivastava, V.; Chester, S.A.; Anand, L. A Thermo-Mechanically Coupled Theory for Large Deformations of Amorphous Polymers. Part II: Applications. *Int. J. Plast.* 2009, *25*, 1495–1539, doi:10.1016/j.ijplas.2008.11.005.

24. Boyce, M.C.; Socrate, S.; Llana, P.G. Constitutive Model for the Finite Deformation Stress–Strain Behavior of Poly(Ethylene Terephthalate) above the Glass Transition. *Polymer* 2000, *41*, 2183–2201, doi:10.1016/S0032-3861(99)00406-1.

25. Mirkhalaf, S.M.; Andrade Pires, F.M.; Simoes, R. Modelling of the Post Yield Response of Amorphous Polymers under Different Stress States. *Int. J. Plast.* 2017, *88*, 159–187, doi:10.1016/j.ijplas.2016.10.008.

26. Detrez, F.; Cantournet, S.; Séguéla, R. A Constitutive Model for Semi-Crystalline Polymer Deformation Involving Lamellar Fragmentation. *Comptes Rendus Mécanique* 2010, *338*, 681–687, doi:10.1016/j.crme.2010.10.008.

27. Ward, I.M.; Sweeney, J. *Mechanical Properties of Solid Polymers*, 3rd ed.; Wiley: Chichester, UK, 2013; ISBN 978-1-4443-1950-7.

28. O'Connor, T.C.; Robbins, M.O. Molecular Models for Creep in Oriented Polyethylene Fibers. *J. Chem. Phys.* 2020, *153*, 144904, doi:10.1063/5.0021286.

29. Baled, H.O.; Gamwo, I.K.; Enick, R.M.; McHugh, M.A. Viscosity Models for Pure Hydrocarbons at Extreme Conditions: A Review and Comparative Study. *Fuel* 2018, *218*, 89–111, doi:10.1016/j.fuel.2018.01.002.

30. Yang, J.-L.; Zhang, Z.; Schlarb, A.K.; Friedrich, K. On the Characterization of Tensile Creep Resistance of Polyamide 66 Nanocomposites. Part II: Modeling and Prediction of Long-Term Performance. *Polymer* 2006, *47*, 6745–6758, doi:10.1016/j.polymer.2006.07.060.

31. Hong, K.; Rastogi, A.; Strobl, G. A Model Treating Tensile Deformation of Semicrystalline Polymers: Quasi-Static Stress−Strain Relationship and Viscous Stress Determined for a Sample of Polyethylene. *Macromolecules* 2004, *37*, 10165–10173, doi:10.1021/ma049174h.

32. Izraylit, V.; Heuchel, M.; Gould, O.E.C.; Kratz, K.; Lendlein, A. Strain Recovery and Stress Relaxation Behaviour of Multiblock Copolymer Blends Physically Cross-Linked with PLA Stereocomplexation. *Polymer* 2020, *209*, 122984, doi:10.1016/j.polymer.2020.122984.

33. Olley, P.; Sweeney, J. A Multiprocess Eyring Model for Large Strain Plastic Deformation. *J. Appl. Polym. Sci.* 2011, *119*, 2246–2260, doi:10.1002/app.32951.

34. Sweeney, J.; Bonner, M.; Ward, I.M. Modelling of Loading, Stress Relaxation and Stress Recovery in a Shape Memory Polymer. *J. Mech. Behav. Biomed. Mater.* 2014, *37*, 12–23, doi:10.1016/j.jmbbm.2014.05.011.

35. Chivers, R.A.; Bonner, M.J.; Hine, P.J.; Ward, I.M. Shape Memory and Stress Relaxation Behaviour of Oriented Mono-Dispersed Polystyrene. *Polymer* 2014, *55*, 1055–1060, doi:10.1016/j.polymer.2014.01.002.

36. Johnsen, J.; Clausen, A.H.; Grytten, F.; Benallal, A.; Hopperstad, O.S. A Thermo-Elasto-Viscoplastic Constitutive Model for Polymers. *J. Mech. Phys. Solids* 2019, *124*, 681–701, doi:10.1016/j.jmps.2018.11.018.

37. Xu, Q.; Solaimanian, M. Modelling Linear Viscoelastic Properties of Asphalt Concrete by the Huet–Sayegh Model. *Int. J. Pavement Eng.* 2009, *10*, 401–422, doi:10.1080/10298430802524784.

38. Halsey, G.; White, H.J.; Eyring, H. Mechanical Properties of Textiles, I. *Text. Res.* 1945, *15*, 295–311, doi:10.1177/004051754501500901.

39. Zhou, H.; Wilkes, G.L. Creep Behaviour of High Density Polyethylene Films Having Well-Defined Morphologies of Stacked Lamellae with and without an Observable Row-Nucleated Fibril Structure. *Polymer* 1998, *39*, 3597–3609, doi:10.1016/S0032-3861(97)10359-7.

40. Siviour, C.R.; Jordan, J.L. High Strain Rate Mechanics of Polymers: A Review. *J. Dyn. Behav. Mater.* 2016, *2*, 15–32, doi:10.1007/s40870-016-0052-8.

41. Jar, P.-Y.B. Effect of Tensile Loading History on Mechanical Properties for Polyethylene. *Polym. Eng. Sci.* 2015, *55*, 2002–2010, doi:10.1002/pen.24042.

42. Bao, Q.; Yang, Z.; Lu, Z. Molecular Dynamics Simulation of Amorphous Polyethylene (PE) under Cyclic Tensile-Compressive Loading below the Glass Transition Temperature. *Polymer* 2020, *186*, 121968, doi:10.1016/j.polymer.2019.121968.

43. Gu, G.; Xia, Y.; Lin, C.; Lin, S.; Meng, Y.; Zhou, Q. Experimental Study on Characterizing Damage Behavior of Thermoplastics. *Mater. Des.* 2013, *44*, 199–207, doi:10.1016/j.matdes.2012.07.062.

44. Bergstrom, J. Constitutive Modeling of the Large Strain Time-Dependent Behavior of Elastomers. *J. Mech. Phys. Solids* 1998, *46*, 931–954, doi:10.1016/S0022-5096(97)00075-6.

45. Shampine, L.F. Solving 0 = F(t, y(t), Y′(t)) in Matlab. *J. Numer. Math.* 2002, *291-310*, doi:10.1515/JNMA.2002.291.

46. Senan, N.A.F. A Brief Introduction to Using Ode45 in MATLAB. University of California at Berkeley, USA, 2007. https://www.eng.auburn.edu/~tplacek/courses/3600/ode45berkley.pdf.

47. Tan, N.; Jar, P.B. Multi-Relaxation Test to Characterize PE Pipe Performance. *Plast. Eng.* 2019, *75*, 40–45, doi:10.1002/peng.20184.

48. Kitagawa, M.; Zhou, D.; Qui, J. Stress-Strain Curves for Solid Polymers. *Polym. Eng. Sci.* 1995, *35*, 1725–1732, doi:10.1002/pen.760352202.

49. Richeton, J.; Ahzi, S.; Daridon, L.; Rémond, Y. A Formulation of the Cooperative Model for the Yield Stress of Amorphous Polymers for a Wide Range of Strain Rates and Temperatures. *Polymer* 2005, *46*, 6035–6043, doi:10.1016/j.polymer.2005.05.079.

50. Natarajan, V.D. Constitutive Behavior of a Twaron® Fabric/Natural Rubber Composite: Experiments and Modeling. *Mech. Adv. Mater. Struct.* 2011, *17*, 246–259.

51. Na, B.; Zhang, Q.; Fu, Q.; Men, Y.; Hong, K.; Strobl, G. Viscous-Force-Dominated Tensile Deformation Behavior of Oriented Polyethylene. *Macromolecules* 2006, *39*, 2584–2591, doi:10.1021/ma052496g.

52. Senden, D.J.A.; van Dommelen, J.A.W.; Govaert, L.E. Physical Aging and Deformation Kinetics of Polycarbonate. *J. Polym. Sci. B Polym. Phys.* 2012, *50*, 1589–1596. https://doi.org/10.1002/polb.23161.

53. Yeo, S.-S.; Hsuan, Y. G. Evaluation of Creep Behavior of High Density Polyethylene and Polyethylene-Terephthalate Geogrids. Geotextiles and Geomembranes 2010, 28 (5), 409–421, doi:10.1016/j.geotexmem.2009.12.003.

54. Gao, R.; Kuriyagawa, M.; Nitta, K.-H.; He, X.; Liu, B. Structural Interpretation of Eyring Activation Parameters for Tensile Yielding Behavior of Isotactic Polypropylene Solids. Journal of Macromolecular Science, Part B 2015, 54 (10), 1196–1210, doi:10.1080/00222348.2015.1079088.

55. Ward, I. M.; Wilding, M. A. Creep Behavior of Ultrahigh-Modulus Polyethylene: Influence of Draw Ratio and Polymer Composition. Journal of Polymer Science: Polymer Physics Edition 1984, 22 (4), 561–575, doi: 10.1002/pol.1984.180220403.

56. Wilhelm, H.; Spieckermann, F.; Fischer, C.; Polt, G.; Zehetbauer, M. Characterization of Strain Bursts in High Density Polyethylene by Means of a Novel Nano Creep Test. *Int. J. Plast.* 2019, *116*, 297–313, doi:10.1016/j.ijplas.2019.01.010.

57. Truss, R.W.; Duckett, R.A.; Ward, I.M. Effect of Hydrostatic Pressure on the Yield and Fracture of Polyethylene in Torsion. *J. Mater. Sci* 1981, *16*, 1689–1699, doi:10.1007/BF02396889.

58. André, J.R.S.; Cruz Pinto, J.J.C. Modeling Nonlinear Stress Relaxation of Polymers. *Polym. Eng. Sci.* 2014, *54*, 404–416, doi:10.1002/pen.23581.

Chapter 3 Characterization of loading, relaxation, and recovery behaviors of high-density polyethylene using a three-branch spring-dashpot model

This chapter presents an analysis of the stress evolution of high-density polyethylene (HDPE) at loading, relaxation, and recovery stages in a multi-relaxation-recovery (RR) test. The analysis is based on a three-branch spring-dashpot model that uses the Eyring's law to govern the viscous behavior. The spring-dashpot model comprises two viscous branches to represent the short- and long-term time-dependent stress responses to deformation, and a quasi-static branch to represent the time-independent stress response. A fast numerical analysis framework based on genetic algorithms was developed to determine values for the model parameters so that the difference between the simulation and the experimental data could be less than 0.08 MPa. Using this approach, values of the model parameters were determined as functions of deformation and time so that the model can simulate the stress response at loading, relaxation, and recovery stages of the RR test. The simulation also generated ten sets of model parameter values to examine their consistency. The study concludes that the three-branch model can serve as a suitable tool for analyzing the mechanical properties of HDPE, and values for the model parameters can potentially be used to characterize the difference among PEs for their mechanical performance.

3.1. Introduction

Semi-crystalline polymers (SCP) such as polyethylene (PE) have long been used in industries due to their advantages in the physical and chemical properties [1]. The microstructure of SCP consists of crystalline and amorphous phases of which the stress responses to deformation could be nonlinear and time-dependent [2]. Therefore, characterization of SCP's mechanical properties is complex [3], and has often been done using models based on either deformation kinetics or global deformation behavior. The former are known to be the physics-based models [4–18], to deal with the complex interactions among molecules, but yet to be able to provide close simulation of the experimentally observed deformation behavior. As a result, validity of these physics-based models has been questioned for their capability to predict SCP's long-term deformation behavior [19–25]. The global-deformation-based models are also known as phenomenological models [20,25–34], most of which consist of springs and dashpots that may not reflect SCP's microstructures [35–40], but have the advantage of being able to mimic closely the deformation behavior observed from the experimental testing [41,42]. Therefore, there is some confidence in the use of these phenomenological models to predict SCP's deformation behavior in the long-term service [25,31].

Two-element spring-dashpot models for viscoelasticity, such as the Maxwell and the Voigt models, are the basic models for describing the viscous behavior of materials. However, they are incapable of capturing SCP's intricate and time-dependent characteristics [43]. The three-element model, also known as the standard model [44], is to combine a spring in series with the Voigt model to simulate PE's long-term stress response in relaxation at different deformation levels [45,46], but it fails to simulate the short-term stress response. In slightly different approaches, Drozdov [47] used a two-phase constitutive model to examine the transition from relaxation to

recovery behavior of isotactic polypropylene, and Dusunceli [48] employed the viscoplasticity theory based on overstress for polymers (VBOP) to predict the recovery behavior of PE. However, these models consist of over twenty parameters for which the values are difficult to determine using limited experimental data. Dusunceli et al. [49] proposed the use of a theory based on overstress to describe the loading, unloading, creep, and relaxation behavior of high-density PE (HDPE), and determined the material parameters using Matlab genetic algorithm (GA). They have successfully determined the material parameter values to generate a trend similar to the experimental data, but only one set of values was provided. Sweeney et al. [50] proposed a model which consists of three parallel Maxwell branches to simulate data that contains single relaxation and recovery stages in one test. This model has successfully described the loading, relaxation, and recovery behavior, but the approach used to determine the model parameter values was not given in detail. Furthermore, as a nonlinear model their work provided only one set of model parameter values, without consideration of the possibility of having multiple sets of the parameter values all of which could mimic the experimental data. Therefore, it is not known whether the multiple sets of the model parameter values show the same trend of variation with deformation as the set of values obtained in the study.

The possibility of using spring-dashpot models to characterize SCP's deformation behavior also relies on the availability of experimental data that provide a wide range of deformation behavior in order to validate the models. The literature has shown that a tremendous amount of efforts have been made by the scientific community to provide comprehensive data for characterization of SCP's time-dependent behavior [51,52], and most of the studies were based on stress relaxation and creep deformation [53,54] which have long been known to provide the essential information about SCP's time-dependent deformation behavior [55]. Since PE shows significant relaxation and

creep behaviors at room temperature [56,57], occurrence of these deformation behaviors has a significant influence on the feasibility of using PE in load-bearing applications. Zhang and Moore [26] investigated the time-dependent stress response of HDPE in stress relaxation and recovery tests under uniaxial compression, and examined the unusual stress response in recovery after the unloading which is about the stress drop during the recovery after a long period of stress increase. Zhang and Jar [58] compared the results of stress variation during the relaxation at the same strain after being subjected to uniaxial tensile loading at different strain rates, and found that the data could be used to construct a master curve of the relaxation modulus to increase the time span covered in the study. Recently, Tan and Jar [45] developed a multiple-relaxation (MR) test and confirmed the occurrence of a transition [27] induced by the tensile loading. Following that work, we proposed a multiple-relaxation-recovery (RR) test to increase the complexity of the loading process so that various spring-dashpot models could be evaluated for their suitability to mimic SCP's viscous deformation behavior [59].

This chapter presents a study in which the RR test was applied to a pipe-grade HDPE to demonstrate a data analysis process that uses a three-branch spring-dashpot model to simulate the viscous stress response to deformation. Following the previous work [59], deformation introduced to the specimens used in the current study is represented by the stroke of the test machine. A computer program based on the GA in Matlab was developed to determine values for the model parameters so that the model could closely mimic the experimental data at all loading, relaxation, and recovery stages. Using this computer program, ten sets of parameter values were determined, all of which met the criteria for mimicking the stress response to deformation in the RR test. Based on the ten sets of the parameter values, feasibility of using the three-branch model to characterize the mechanical behavior of HDPE is discussed.

3.2. Material and RR test

Geometry and dimensions of the HDPE specimens used in this study were the same as those used previously [59,60]. Material characteristics of the HDPE can also be found as HDPE-a in the previous work [59], for which the supplier would like to remain anonymous.

The RR test provides a cyclic loading process which consists of six stages in each cycle, including the first loading, relaxation, the second loading, stabilization, unloading, and then recovery, with the stress response at the recovery stages showing the unusual stress drop similar to that reported in the literature [47,61]. These stages are to reflect the modes of polymer deformation in load-carrying applications, such as loading [45], unloading [62,63], relaxation [46,64], and recovery [50,65]. For instance, a PE pipe could experience multiple pressure surges throughout its lifespan including loading and unloading, with a relatively constant deformation level in between.

Details of the RR test scheme are the same as those given in a previous publication [59]. In the current study, the RR tests were conducted using a computer-controlled universal test machine (Qualitest Quasar100, Lauderdale, FL, USA) at room temperature. Two RR tests were carried out to ensure repeatability of the test results, one containing 14 cycles and the other 30 cycles, from which the engineering stress-stroke curves are presented in Figure 3.1. Note that the small number of 14 cycles for the first test was because of an unexpected power outage in the laboratory. However, in view of the good reproducibility between the two sets of data in the first 14 cycles, the analysis presented here was based on the RR test of 30 cycles with the total displacement of about 5.8 mm, which could be used to represent the general analysis of the PE used in this study. Additional RR tests were conducted on other PE-based materials, and the same data analysis process was conducted to ensure the consistency of the results. However, in view that focus of this

manuscript is on the development of an analysis approach, only two sets of test results on one PE, named HDPE-a in the previous work[59], are presented.

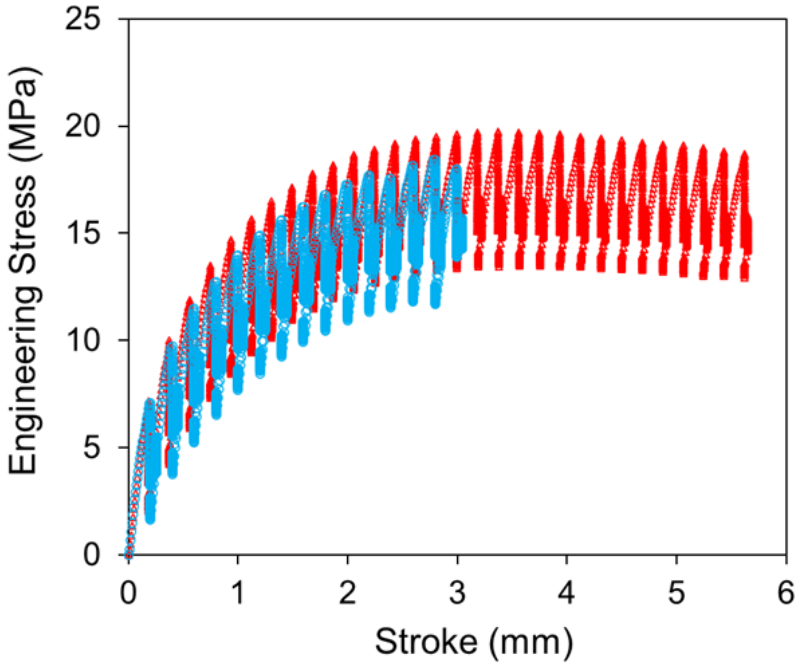

Figure 3.1. Engineering stress–stroke curves from two RR tests with 14 (blue symbols) or 30 (red symbols) cycles.

Data analysis presented here is to use a spring-dashpot model, as detailed in Section 3, to provide a close simulation of the stress response in the RR test. The stress response is based on engineering stress, and this study is to simulate the stress response during loading, relaxation and recovery stages of the HDPE as functions of the deformation (represented by stroke generated by the test machine). Although strain should be used to represent the deformation variation, in view that all comparisons in the study will be made among specimens of the same geometry, stroke is used to represent the deformation variation, which has been adopted by many researchers [66–71].

3.3. The three-branch spring-dashpot model

Based on the conclusion from the previous work [66], a model with one viscous branch is insufficient for simulating the highly nonlinear stress drop of PE at the relaxation stage. However, many researchers [50,72,73] have shown that models with two viscous branches could provide a close simulation of the stress response of polymers under loading. The three-branch model used in the current work is one of the phenomenological models that utilize a combination of springs and dashpots to mimic the stress response to deformation of a diverse range of materials, such as finger pad [74], cortical bone [75,76], polymer snap [77], shape-memory polymers [78], polymethyl methacrylate (PMMA) [67], and HDPE [79].

The use of a spring-dashpot model in the data analysis is because such models have the advantage of providing clear visualization of the deformation behavior [41,42], and can divide the total stress into the time-independent (quasi-static) and the time-dependent (viscous) components [80–86]. Currently, the main challenge for this type of model is two-folded. One is the ability to extract quasi-static stress from the applied stress, and the other to mimic the viscous stress variation with time during the deformation. Work in the literature has suggested that a model with two Eyring's processes could mimic reasonably well the viscous stress variation as a function of time [87–89]. However, as shown in our previous work [59], not all spring-dashpot models with two Eyring's processes could generate a close simulation of the stress responses to deformation of HDPE, especially for the unusual stress drop that was detected during the recovery stage after the unloading. As a result, we have developed a computer program for the data analysis, with the capability to mimic the stress drop observed at the recovery stages of the RR test. The computer program is to determine values for all parameters in the three-branch model so that the stress change during the entire RR test could be closely regenerated.

Figure 3.2 depicts the three-branch model used in this study. Two of the branches contain a spring and a dashpot connected in series and the third branch a spring only. It should be noted that the three branches in Figure 3.2 are denoted using subscripts L, S, and qs, representing long-term viscous, short-term viscous, and quasi-static, respectively. The long- and short-terms are assigned based on the characteristic time (τ_v) required to generate the viscous stress response to deformation, which is defined as

$$\tau_{v,i} = \sigma_{0,i} / (K_{v,i}\dot{\delta}_{0,i}) \tag{3.1}$$

where $\tau_{v,i}$, $\sigma_{0,i}$, $K_{v,i}$ and $\dot{\delta}_{0,i}$ are characteristic relaxation time, reference stress, spring stiffness and reference stroke rate, respectively, with $i = L$ or S.

Note that the original Eyring's model [90] was used to describe the relationship between viscous stress and strain rate applied to the dashpot, but in this work the strain rate is represented by the displacement rate of the dashpot, named stroke rate here which is different from the applied stroke rate, as the latter represents the crosshead speed of the test machine.

Using the long-term viscous branch in Figure 3.2 as an example, the Eyring's process defines the relationship between viscous stress ($\sigma_{v,L}$) and stroke rate of the dashpot ($\dot{\delta}_{v,L}$) as [46,59]

$$\dot{\delta}_{v,L} = d\delta_{v,L} / dt = \dot{\delta}_{0,L}\, sinh(\sigma_{v,L} / \sigma_{0,L}) \tag{3.2}$$

where t is time measured from the beginning of the loading, relaxation or recovery stage.

The relationship between $\sigma_{v,L}$ and stroke generated in the spring ($\delta_A - \delta_{v,L}$) is

$$\sigma_{v,L} = K_{v,L}(\delta_A - \delta_{v,L}) \tag{3.3}$$

where δ_A is the stroke applied by the test machine, $\delta_{v,L}$ the stroke of the dashpot and $K_{v,L}$ the spring stiffness in the long-term viscous branch.

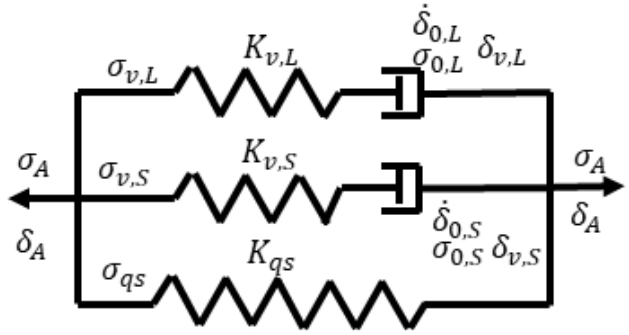

Figure 3.2. Schematic depiction of the three-branch spring-dashpot model used in this study.

By differentiating Eq. (3.3) with time and then combining it with Eq. (3.2), the total stroke rate of the branch, which is equivalent to $\dot{\delta}_A$, can be expressed as [27]

$$\dot{\delta}_A = d\delta_A / dt = \dot{\sigma}_{v,L} / K_{v,L} + \dot{\delta}_{0,L} sinh(\sigma_{v,L} / \sigma_{0,L}) \quad (3.4)$$

In the relaxation or the recovery process, δ_A is fixed, i.e. $\dot{\delta}_A = 0$, and therefore

$$0 = \dot{\sigma}_{v,L} / K_{v,L} + \dot{\delta}_{0,L} sinh(\sigma_{v,L} / \sigma_{0,L}) \quad (3.5)$$

Following the derivation given in the previous work [27,45,85], Eq. (3.5) leads to the following equation.

$$\sigma_{v,L} = 2\sigma_{0,L} tanh^{-1}\{tanh\,[\sigma_{v,L}(0) / (2\sigma_{0,L})]\exp(-t / \tau_{v,L})\} \quad (3.6)$$

where $\sigma_{v,L}(0)$ is $\sigma_{v,L}$ at $t = 0$.

Similarly, during the relaxation and recovery stages the viscous stress in the short-term viscous branch ($\sigma_{v,S}$) can be expressed as

$$\sigma_{v,S} = 2\sigma_{0,S} tanh^{-1}\{tanh\,[\sigma_{v,S}(0) / (2\sigma_{0,S})]\, exp(-t / \tau_{v,S})\} \quad (3.7)$$

where $\sigma_{v,S}(0)$ is $\sigma_{v,S}$ at $t = 0$.

The applied stress (σ_A) is the summation of quasi-static stress (σ_{qs}), stress in the long-term viscous branch ($\sigma_{v,L}$), and stress in the short-term viscous branch ($\sigma_{v,S}$), i.e.,

$$\sigma_A = \sigma_{qs} + \sigma_{v,L} + \sigma_{v,S} \quad (3.8)$$

Total stress decay ($\Delta\sigma_A$) during the relaxation and the recovery stages is the summation of the stress decay in the two viscous branches, i.e.,

$$\begin{aligned} \Delta\sigma_A &= \sigma_A(0) - \sigma_A(t) = \sigma_{v,L}(0) + \sigma_{v,S}(0) \\ &- 2\sigma_{0,L} tanh^{-1}\{tanh\,[\sigma_{v,L}(0) / (2\sigma_{0,L})]\exp(-t / \tau_{v,L})\} \\ &- 2\sigma_{0,S} tanh^{-1}\{tanh\,[\sigma_{v,S}(0) / (2\sigma_{0,S})]\, exp(-t / \tau_{v,S})\} \end{aligned} \quad (3.9)$$

At the loading stages, Eq. (3.4) can be converted to the following two expressions for the long- and the short-term viscous branches, respectively:

$$\dot{\sigma}_{v,L} = K_{v,L}\dot{\delta}_A - (\sigma_{0,L} / \tau_{v,L}) \sinh(\sigma_{v,L} / \sigma_{0,L}) \quad (3.10)$$

$$\dot{\sigma}_{v,S} = K_{v,S}\dot{\delta}_A - (\sigma_{0,S} / \tau_{v,S}) \sinh(\sigma_{v,S} / \sigma_{0,S}) \quad (3.11)$$

3.4. Data analysis

In view that the number of fitting parameters for Eqs. (3.6) to (3.11), i.e. $\sigma_{v,L}(0)$, $\sigma_{0,L}$, $\tau_{v,L}$, $K_{v,L}$, $\sigma_{v,S}(0)$, $\sigma_{0,S}$, $\tau_{v,S}$, and $K_{v,S}$, is bigger than the number of equations governing the

stress-deformation relationship, an inverse approach [91–96] was used to determine the fitting parameter values so that stress generated by the model could mimic the stress response obtained from the RR test. Using the inverse approach, accuracy of the parameter values is expected to depend on the difference between the simulation results and the experimental data [97–101], and with the nonlinear nature of the Eyring's model, there should be more than one set of fitting parameter values that could generate the same level of accuracy for mimicking the experimental data. In the literature, however, most of the works using this approach provided only one set of fitting parameter values [28,45,50,80,81], and the difference of the simulation results from the experimental data ranged from 0.17 to about 1 MPa [50,88,102–105]. To our knowledge, neither the accuracy of the fitting parameter values nor their possible range for the same fitting quality was evaluated. This was possibly because of the tedious nature in searching for the fitting parameter values in order to simulate the experimental data [106–110]. In view of this deficiency, one of the key objectives of the presented work was to develop a computer program in order to obtain multiple sets of the fitting parameter values in a reasonable timeframe to meet the same level of accuracy.

Matlab was used to develop the program for determining the fitting parameter values for the model in Figure 3.2. The maximum difference allowed between the stress from the simulation results and that from the experimental data was set to be 0.08 MPa. GA [111–116], which belongs to a branch of biomathematics [117,118] and has been widely used in the field of materials science [111,114,115,119–126], was used to determine values for the fitting parameters. For data collected at the relaxation and recovery stages, Eq. (3.9) was used to generate the simulation results from the model in Figure 3.2, and for the data collected at the loading stages, Eqs. (3.8), (3.10), and (3.11) were used. Function ODE45 in Matlab was used to solve Eqs. (3.10) and (3.11).

In the data analysis, values for six fitting parameters in the two viscous branches, $\sigma_{v,L}(0)$, $\sigma_{0,L}$, $\tau_{v,L}$, $\sigma_{v,S}(0)$, $\sigma_{0,S}$, and $\tau_{v,S}$, were firstly determined as functions of stroke so that stress generated from the model in Figure 3.2 could fit the experimentally measured stress data at the relaxation stages, and then value for $\tau_{v,L}$ was fixed and values for the other five parameters for the recovery stages were determined by curve fitting using the process similar to that used at the relaxation stages. A similar curve fitting process was used for simulation of stress variation at the loading stages, but the six fitting parameters used were $\tau_{v,L}$, $\sigma_{0,L}$, $K_{v,L}$, $\tau_{v,S}$, $\sigma_{0,S}$, and $K_{v,S}$, which was to replace $\sigma_{v,L}(0)$ and $\sigma_{v,S}(0)$ by $K_{v,L}$ and $K_{v,S}$. Noted that the above fitting processes were based on the assumptions that values for $\tau_{v,L}$ and $\tau_{v,S}$ remained constant for all relaxation or recovery stages of the RR test, and $\tau_{v,L}$ has the same value between the relaxation and the recovery stages. The above assumptions were an extended version of the assumption made in the previous works [27,45] in which SCP's quasi-static stress was determined using a model with a single dashpot. Consistent with the work reported in the literature [45], $\sigma_{v,L}(0)$ at relaxation stages for PE shows a plateau region in a curve as a function of stroke. The computer program developed in this study assumes that $\sigma_{0,S}$ at both relaxation and recovery stages, and $\sigma_{v,S}(0)$ and $\sigma_{0,L}$ at recovery stages may vary with stroke introduced in the RR test. Range of the fitting parameters is specified based on results provided in the literature [66,127–129] to limit the number of solutions. According to the literature [66,128,130,131], the reference stress ($\sigma_{0,i}$) and the reference stroke rate ($\dot{\delta}_{0,i}$) of the dashpot, i standing for L or S, are related to activation volume and activation energy, respectively, for the viscous deformation. Therefore, with the success of determining the range of model parameters, we would like to explore the possibility of using the results to understand the physical meanings for these model parameters.

Computer programs were developed for determination of the fitting parameters. The key concept of the computer programs is to use the algorithm based on GA in the Matlab to search for the optimal values for the fitting parameters and their variation with stroke introduced in the RR test. Flow charts of these computer programs are given in the appendix that is available from the publisher, to limit the stress difference between the simulation results and the experimental data within 0.08 MPa.

3.5.5. Results and discussion

3.5.1 Relaxation and recovery stages

Figure 3.3 presents some examples of the simulation curves (solid lines) that were generated using the model in Figure 3.2 to fit the stress response of the experimental data (markers) at some relaxation (Figure 3. 3(a)) and recovery (Figure 3.3(b)) stages, based on the fitting parameters determined from the programs with the algorithms depicted in the appendix that is available from the publisher. The figures show that stress changes at the relaxation and the recovery stages can be well reproduced by the model, including the unusual stress response at the recovery stages in the time range from 2000 to 10000 s, with the maximum difference between the simulation curves and the experimental data within 0.08 MPa, as depicted in a figure in the appendix, Figure S1(d). Note that the difference between the simulation results and the experimental data reported in the literature is in the range from 0.17 to about 1 MPa [50,88,102–105].

A close examination of Figure 3.3 suggests that the curves produced by the model for the relaxation stages in the time range from 100 to 1000 seconds did not match the experimental data as well as the rest of the curves, though still with the difference within 0.08 MPa, suggesting that

there is still room of improvement for the computer programs used for the curve fitting. This is being investigated when this manuscript is prepared.

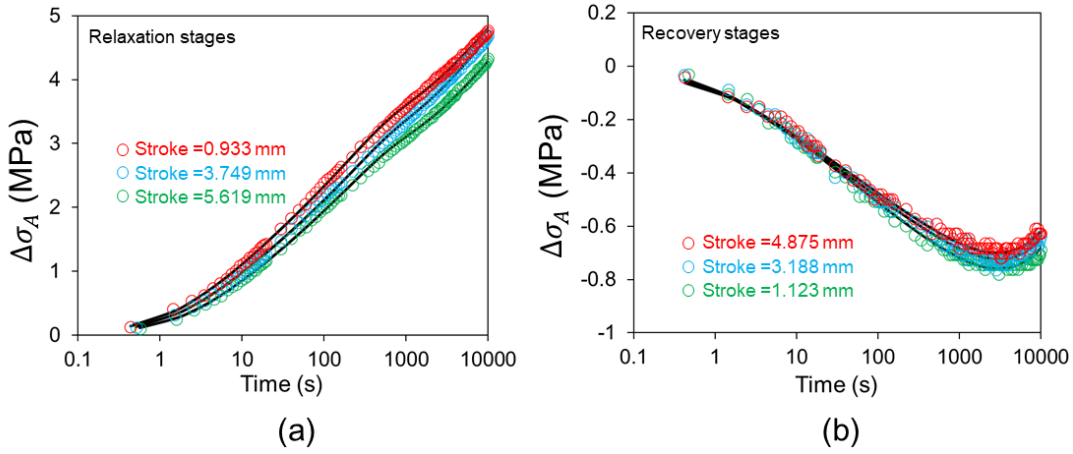

Figure 3.3. Sample plots of experimental data (markers) for stress change at (a) relaxation and (b) recovery stages, and the corresponding fitting curves (lines) generated from the model in Figure 3.2 (strokes for the relaxation and recovery stages are given in the figures).

Figure 3.4 shows values for $\sigma_{v,S}$, $\sigma_{v,L}$, and total viscous stress (σ_v) as functions of time at a relaxation stage, Figure 3.4(a), and the corresponding recovery stage, Figure 3.4(b). As depicted in Figure 3.4(a), $\sigma_{v,S}$, $\sigma_{v,L}$, and σ_v all decreased with the increase of time at a given relaxation stage, whereas at the recovery stage, $\sigma_{v,S}$ and σ_v increased but $\sigma_{v,L}$ decreased with the increase of time. It should be noted that the σ_v and $\sigma_{v,L}$ eventually became close to each other at both relaxation and recovery stages, while the corresponding $\sigma_{v,S}$ became close to zero.

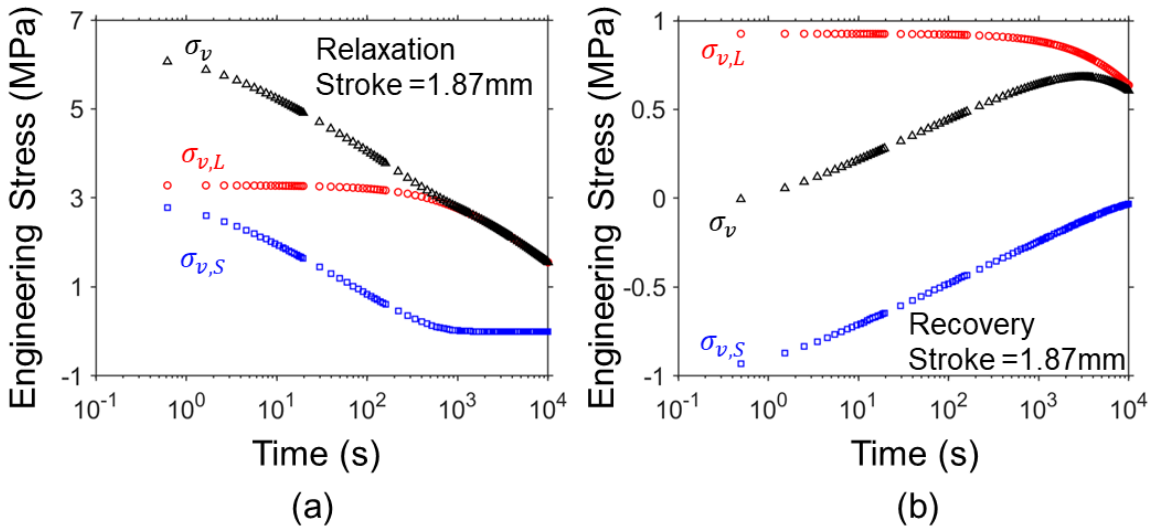

Figure 3.4. Sample curves for $\sigma_{v,S}$ (blue squares), $\sigma_{v,L}$ (red circles), and σ_v (black triangles) at (a) relaxation and (b) recovery stages as functions of time at the stroke of 1.87 mm.

To examine the possible range of variation for the fitting parameter values to fit the experimental data with the maximum stress difference within 0.08 MPa, ten sets of values for the six fitting parameters were generated for each of the relaxation and the recovery stages. The results for the relaxation stages are summarized in Figures 3.5 and 3.6. The corresponding values for the recovery stages are given in the appendix for this work. Each plot in these figures also includes the coefficients of variation for the ten sets of values, defined as the ratio of the standard deviation of the ten sets of values to their average.

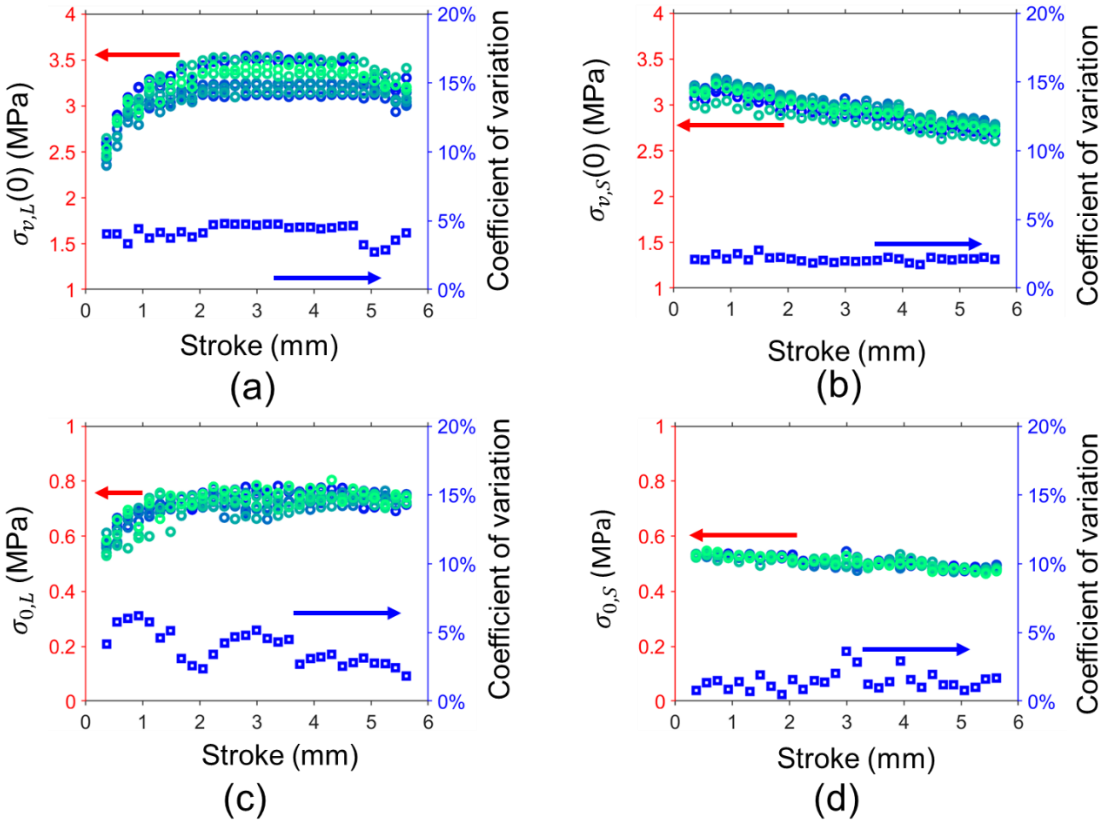

Figure 3.5. Summary of ten sets of values (in open circles) for fitting parameters of the model in Figure 3.2 at the relaxation stages, and the corresponding coefficient of variation (in open squares): (a) $\sigma_{v,L}(0)$, (b) $\sigma_{v,S}(0)$, (c) $\sigma_{0,L}$, and (d) $\sigma_{0,S}$.

Among the fitting parameters for the relaxation stages, $\sigma_{v,L}(0)$ and $\sigma_{0,L}$ in Figures 3.5(a) and 3.5(c), respectively, show similar strokes where a transition occurs for the trend of variation, i.e., a transition from an initial increase to a plateau and then another from the plateau to a decrease. This suggests that both $\sigma_{v,L}(0)$ and $\sigma_{0,L}$ could be used to indicate the possible changes in the

deformation behaviors that were represented by the long-term viscous branch of the model in Figure 3.2. This is consistent with the transition phenomenon reported in the literature using models with a single dashpot to mimic the stress response to deformation under tensile loading [27,28,45].

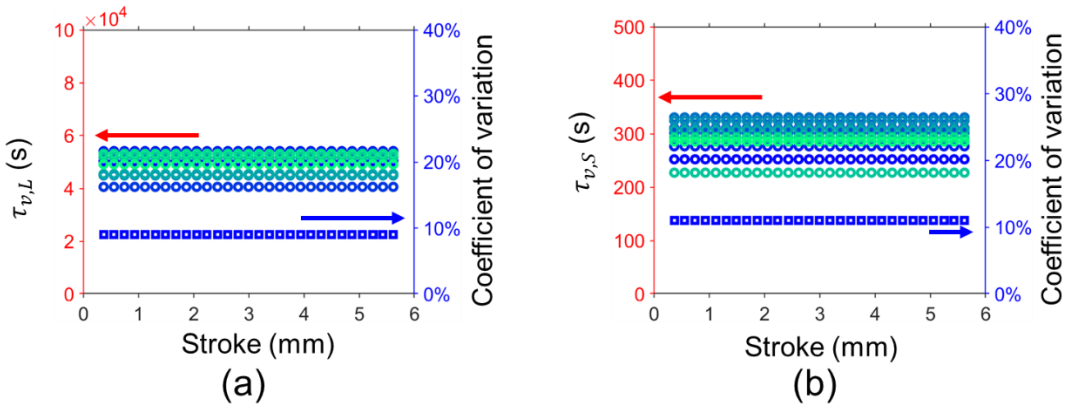

Figure 3.6. Summary of ten sets of values (in open circles) for fitting parameters of the model in Figure 3.2 at the relaxation stages, and the corresponding coefficient of variation (in open squares): (a) $\tau_{v,L}$ and (b) $\tau_{v,S}$.

Figures 3.5(b) and 5(d), for $\sigma_{v,S}(0)$ and $\sigma_{0,S}$ respectively at the relaxation stages, show a continuous decrease with the increase of the stroke without any clear indication of the trend line change. In view that the maximum coefficient of variation for $\sigma_{v,S}(0)$ was only about 2.5% and for $\sigma_{0,S}$ about 5%, any transition, if occurring in the short-term viscous branch, should have been shown in Figures 3.5(b) and 5(d). Therefore, no transition was detected in the short-term viscous branch that represents the change of the deformation behavior. In view that the long-term viscous branch showed the transitional phenomena but the short-term viscous branch did not, the two viscous branches could possibly represent different aspects of the deformation behaviors, and thus models with a single viscous branch could not provide close simulation of the experimental data.

However, deformation behaviors that are represented by the two viscous branches are not clear at this stage, and would require a further study to clarify.

Figures 3.6(a) and 3.6(b) show the ten sets of values for $\tau_{v,L}$ and $\tau_{v,S}$, respectively, at the relaxation stages and their corresponding coefficients of variation. These figures suggest that the $\tau_{v,L}$ and $\tau_{v,S}$ values could be constant during the RR test, but their variation among the ten sets could be significant, and much bigger than the variation of the other four fitting parameters shown in Figure 3.5. The large values for the coefficient of variation also suggest that the choice of $\tau_{v,L}$ and $\tau_{v,S}$ values should not have a significant influence on the use of the spring-dashpot model to simulate the stress drop at the relaxation stages, which is consistent with the suggestion given in the literature [80].

Note that the corresponding fitting parameters for the recovery stages are available in the appendix but no additional information could be obtained from the recovery stages.

Figure 3.7 summarizes the applied stress values determined at the beginning of the relaxation stages ($\sigma_A(0)$) and the ten sets of σ_{qs} values, as well as the coefficient of variation for σ_{qs}. The figure suggests that σ_{qs} is very consistent among the ten sets of values, with the coefficient of variation less than 1.5%, and that the maximum σ_{qs} occurs at the stroke in the range from 3.2 to 3.6 mm, which is consistent with the stroke for the yield point indicated by $\sigma_A(0)$.

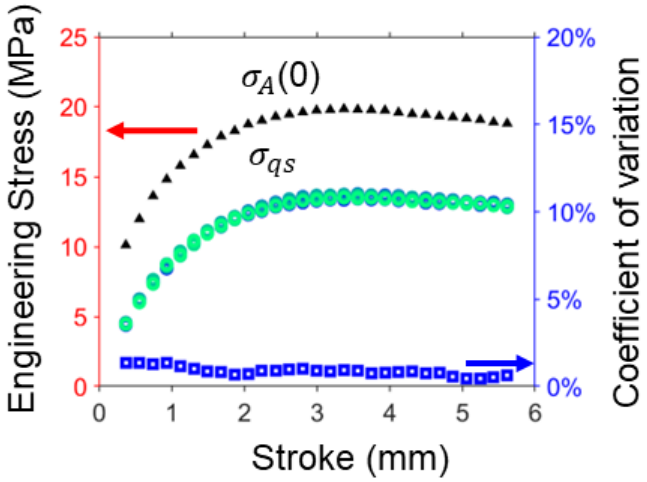

Figure 3.7. Summary of $\sigma_A(0)$ (black triangles), σ_{qs} (circles which include ten sets of values) and the coefficient of variation for the ten sets of σ_{qs} as a function of stroke (blue squares).

3.5.2 Loading stages

Figure 3.8 presents sample curves from the analysis of data at the loading stages, with the stroke ranges covered for the loading given in each figure. Figure 3.8(a) compares the experimentally measured applied stress data (markers) with the fitting curves from the model in Figure 3.2 (lines). The corresponding σ_{qs}, $\sigma_{v,L}$, and $\sigma_{v,S}$ are presented in Figures 3.8(b), 3.8(c), and 3.8(d), respectively. The figures suggest that both $\sigma_{v,L}$ and $\sigma_{v,S}$ increase monotonically at the loading stage, with the former increasing almost linearly with time.

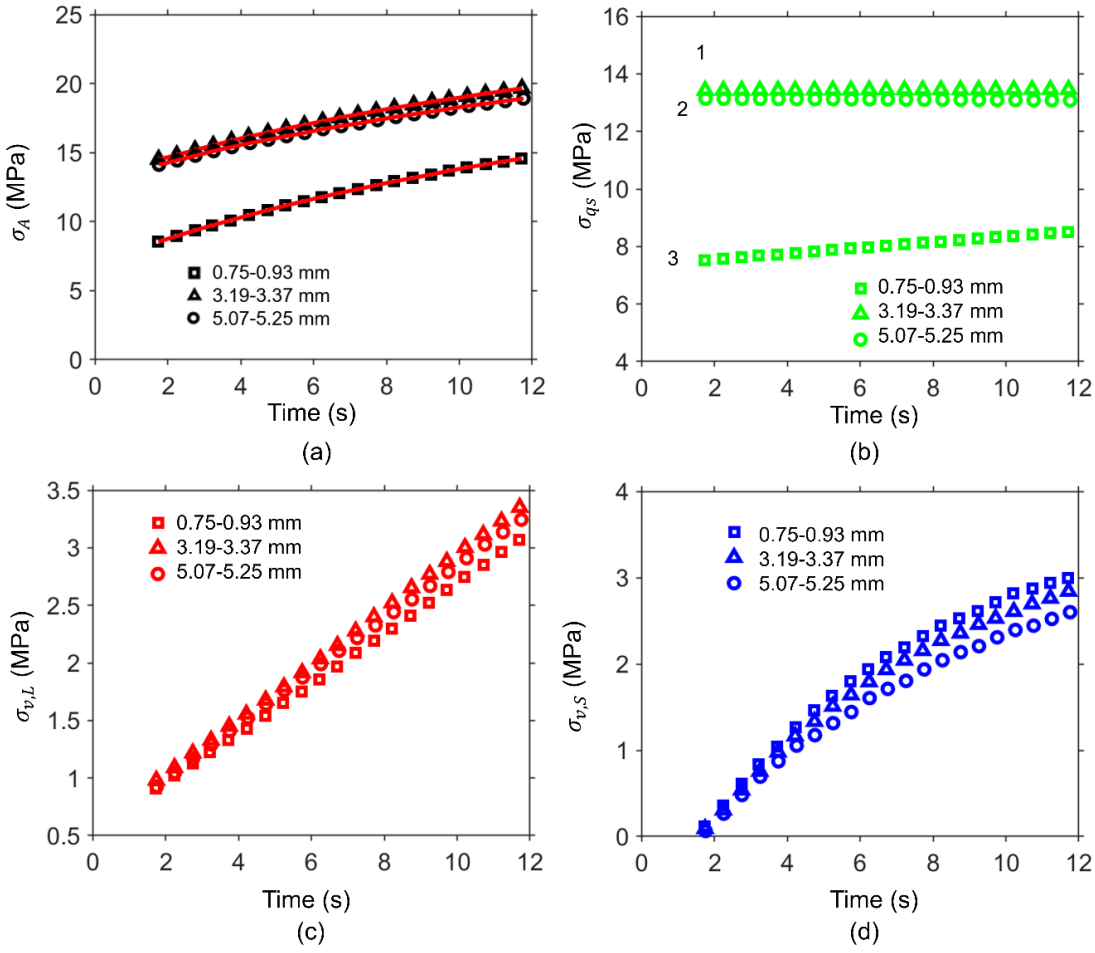

Figure 3.8. Summary of sample curves from the loading stages: (a) the experimentally measured stress (markers) and the simulation results (lines), (b) σ_{qs}, (c) $\sigma_{v,L}$, and (d) $\sigma_{v,S}$.

Figure 3.9 summarizes $K_{v,L}$ and $K_{v,S}$ values determined using the algorithm described in the appendix based on Eqs. (3.8), (3.10), and (3.11). Figure 3.9(a) shows the ten sets of $K_{v,L}$ and $K_{v,S}$ values, using the ten sets of values for the fitting parameters for the relaxation and the corresponding recovery stages as the boundary conditions. The figure suggests that $K_{v,L}$ and $K_{v,S}$ values are fairly consistent among the ten sets, with slightly bigger scattering at strokes smaller than

1 mm. However, with the further increase of stroke, $K_{v,S}$ values became fairly consistent. For clarity, Figure 3.9(b) shows sample curves for one set of $K_{v,L}$ and $K_{v,S}$ values determined based on one set of fitting parameter values determined for the relaxation and the corresponding recovery stages. Overall, Figure 3.9 suggests that with the increase of stroke, $K_{v,S}$ decreases from around 30 to 25 MPa/mm, and $K_{v,L}$ increases slightly before the stroke of 3 mm and then decreases after the stroke of around 4 mm. The overall range of $K_{v,L}$ values are between 10 and 20 MPa/mm.

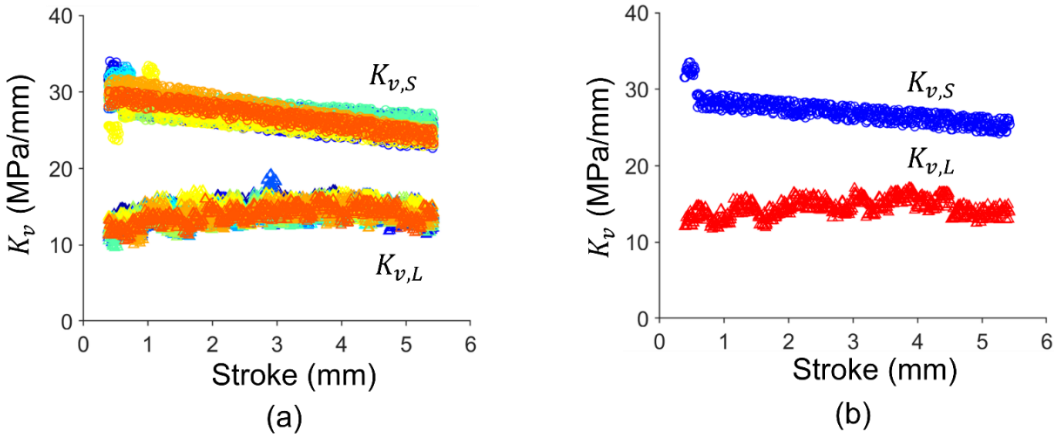

Figure 3.9. Summary of ten sets of $K_{v,L}$ and $K_{v,S}$ values determined from the loading stages using the ten sets of fitting parameter values determined from the relaxation and recovery stages, and (b) sample curves for one set of $K_{v,L}$ and $K_{v,S}$ values using one set of fitting parameter values selected from the relaxation and recovery stages

The above analysis was applied to evaluation of the time-dependent behavior of HDPE represented by the long- and short-term viscous branches of the model in Figure 3.2.

First of all, in view that $\sigma_{v,L}$ remained positive even after the unloading stages, while the corresponding $\sigma_{v,S}$ was negative, it is questionable whether the stress response of the long-term viscous branch at the recovery stages was due to a new process that started at the commencement

of the recovery stage. Because $\sigma_{v,L}$ value remained positive in the RR test at both relaxation and recovery stages, it is conceivable that the stress drop in the long-term viscous branch could continue from the relaxation stage to the following recovery stage. If it was indeed the case, the stress response in the long-term viscous branch might not be synchronized with the global deformation introduced in the RR test. To explore this possibility, Figure 3.10 presents the variation of stress and stroke as functions of test time, using data from the 10th and 20th cycles as examples. These examples suggest general similarity of the stress variation among different cycles in the RR test. Figure 3.10 also includes values labeled as 'prediction of $\sigma_{v,L}$' that were the $\sigma_{v,L}$ values predicted after the relaxation stages, using the parameters from the relaxation stage in the same cycle and with the time starting from the commencement of the relaxation stages but without the consideration of the second loading, stabilization and the unloading stages. Values for the 'prediction of $\sigma_{v,L}$' show a consistent trend of variation with the corresponding stress values at the recovery stages even though the second loading, stabilization and unloading stages were not considered. The difference between $\sigma_{v,L}$ (red circles) and 'prediction of $\sigma_{v,L}$' (green triangles) at the recovery stages shown in Figure 3.10 is believed to come primarily from the second loading and unloading stages that were not considered in the calculation of the 'prediction of $\sigma_{v,L}$' values. The phenomenon shown in Figure 3.10 suggests that the stress response from the long-term viscous branch at the recovery stages might not start after the unloading. Rather, the stress response could have been the result of the combined effect of the loading history prior to the recovery stage. Therefore, using the point where the recovery stages commenced as time zero for the calculation of $\sigma_{v,L}$ at the recovery stages is merely an assumption for the data analysis.

For $\sigma_{v,S}$, on the other hand, Figure 3.10 shows that its value was almost zero before the end of the relaxation and recovery stages. Therefore, it is reasonable to use the commencement of the recovery stage of the RR test as time zero for the calculation of $\sigma_{v,S}$ at the recovery stages.

The above findings suggest that the stress increase measured from the recovery stages in the RR test was the result of two different components of the stress response of the HDPE. One part was the stress recovery from the short-term viscous branch, consistent with the expectation of stress recovery response of HDPE after the unloading. The other part was the continuation of the stress drop due to relaxation after the first loading stage. The above findings also provide a reasonable explanation for the stress drop in the later part of the recovery stages, as reported in the literature [47,61–63,132–135]. These findings offer an opportunity that could lead to identification of the mechanisms in HDPE which are represented by the two viscous branches in the proposed spring-dashpot model. A study to identify these mechanisms was being planned when this manuscript was prepared.

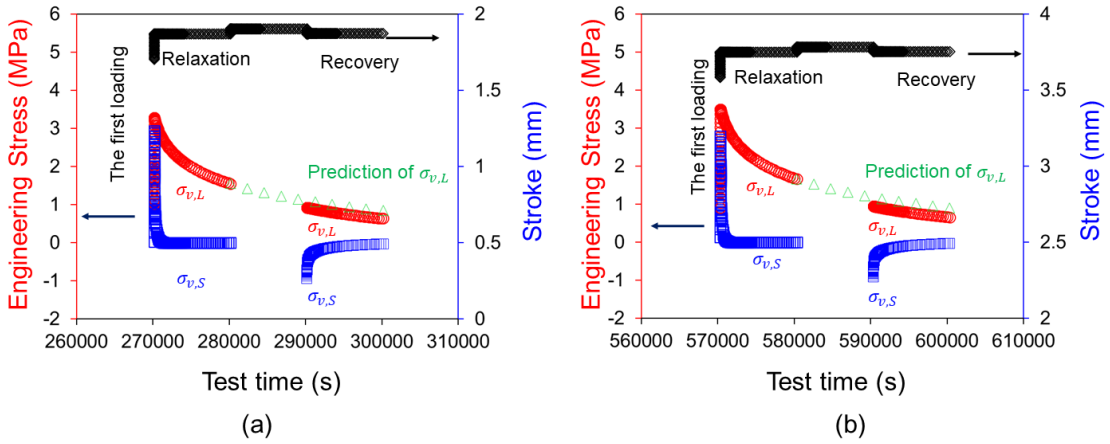

Figure 3.10. Sample curves for $\sigma_{v,S}$ (blue), $\sigma_{v,L}$ (red) and stroke (black) at the first loading, relaxation, and recovery stages, and the predicted values for $\sigma_{v,L}$ (green) by extending the curves at the relaxation stages beyond 10,000 s using the model in Figure 3.2 in (a) the 10th cycle and (b) the 20th cycle of the RR test.

3.6. Conclusions

The study shows that stress response at various stages of the RR test could be simulated very closely using the proposed model, including the unusual stress drop at the recovery stages, with the maximum difference between experimental data and simulation results within 0.08 MPa. It was found that fitting parameters $\sigma_{v,L}(0)$ and $\sigma_{0,L}$ for the relaxation stages show the same transitions in the trend of change with the increase of stroke. On the other hand, the corresponding fitting parameters for the short-term viscous branch, $\sigma_{v,S}(0)$ and $\sigma_{0,S}$, did not indicate the occurrence of any transition at either the relaxation or the recovery stages. Therefore, the transition detected by the long-term viscous branch could represent some deformation mechanism that was not detected by the short-term viscous branch. A further study is being planned to find out the source for the difference in the stress response between the long- and short-term viscous branches.

The study also shows that σ_{qs} as a function of stroke is highly consistent among predictions based on the ten sets of fitting parameter values, and the stroke for the maximum σ_{qs} is close to the stroke for the yield point based on $\sigma_A(0)$. In addition, values for $K_{v,L}$ as a function of stroke, determined using stress variation at the loading stages, showed the trend of change that indicates the occurrence of degradation from the early stage of the RR test. The study also found that stress drop at the relaxation stages in the long-term viscous branch could continue after the end of the relaxation stages, and contributed to the stress variation at the following recovery stages. Stress drop in the short-term viscous branch, on the other hand, ceased before the end of the relaxation stages, similarly for its stress increase at the recovery stages. Therefore, the conventional concept for the stress response of polymers, that is, stress drop after loading and stress increase after unloading, represents only part of the stress response of HDPE to deformation, which could be represented by the short-term viscous branch of the three-branch spring-dashpot model. The long-term viscous branch showed stress drop at both relaxation and recovery stages, which provides a reasonable explanation for the 'abnormal' stress drop observed during the stress recovery that has been reported in the literature.

The study demonstrates that the three-branch spring-dashpot model is capable of simulating the stress response of HDPE in a complex deformation scenario. The proposed data analysis has successfully divided the applied stress into quasi-static, long-term viscous, and short-term viscous components. The algorithms developed in the study enabled the quick determination of ten sets of values for the fitting parameters, to allow the assessment of the range of variation for the fitting parameter values. These algorithms will be used in a follow-up study to examine the difference among HDPEs of various material characteristics and to identify deformation mechanisms that are responsible for the difference.

References

1. Zhang, Y.; Ben Jar, P.-Y.; Xue, S.; Li, L. Quantification of Strain-Induced Damage in Semi-Crystalline Polymers: A Review. *J Mater Sci* 2019, *54*, 62–82, doi:10.1007/s10853-018-2859-2.

2. Ayoub, G.; Zaïri, F.; Naït-Abdelaziz, M.; Gloaguen, J.M. Modelling Large Deformation Behaviour under Loading–Unloading of Semicrystalline Polymers: Application to a High Density Polyethylene. *International Journal of Plasticity* 2010, *26*, 329–347, doi:10.1016/j.ijplas.2009.07.005.

3. Brusselle-Dupend, N.; Cangémi, L. A Two-Phase Model for the Mechanical Behaviour of Semicrystalline Polymers. Part I: Large Strains Multiaxial Validation on HDPE. *Mechanics of Materials* 2008, *40*, 743–760, doi:10.1016/j.mechmat.2008.03.011.

4. Dupaix, R.B.; Krishnan, D. A Constitutive Model for Strain-Induced Crystallization in Poly(Ethylene Terephthalate) (PET) during Finite Strain Load-Hold Simulations. *Journal of Engineering Materials and Technology* 2005, *128*, 28–33, doi:10.1115/1.1924564.

5. Hao, P.; Laheri, V.; Dai, Z.; Gilabert, F.A. A Rate-Dependent Constitutive Model Predicting the Double Yield Phenomenon, Self-Heating and Thermal Softening in Semi-Crystalline Polymers. *International Journal of Plasticity* 2022, *153*, 103233, doi:10.1016/j.ijplas.2022.103233.

6. Ayoub, G.; Rodriguez, A.K.; Mansoor, B.; Colin, X. Modeling the Visco-Hyperelastic–Viscoplastic Behavior of Photodegraded Semi-Crystalline Low-Density Polyethylene Films. *International Journal of Solids and Structures* 2020, *204–205*, 187–198, doi:10.1016/j.ijsolstr.2020.08.025.

7. Sweeney, J.; Collins, T.L.D.; Coates, P.D.; Unwin, A.P.; Duckett, R.A.; Ward, I.M. Application of a Large Deformation Model to Unstable Tensile Stretching of Polyethylene. *International Journal of Plasticity* 2002, *18*, 399–414, doi:10.1016/S0749-6419(00)00104-2.

8. Garcia-Gonzalez, D.; Zaera, R.; Arias, A. A Hyperelastic-Thermoviscoplastic Constitutive Model for Semi-Crystalline Polymers: Application to PEEK under Dynamic Loading Conditions. *International Journal of Plasticity* 2017, *88*, 27–52, doi:10.1016/j.ijplas.2016.09.011.

9. Adams, A.M.; Buckley, C.P.; Jones, D.P. Biaxial Hot Drawing of Poly(Ethylene Terephthalate): Measurements and Modelling of Strain-Stiffening. *Polymer* 2000, *41*, 771–786, doi:10.1016/S0032-3861(98)00834-9.

10. Tervoort, T.A.; Smit, R.J.M.; Brekelmans, W.A.M.; Govaert, L.E. A Constitutive Equation for the Elasto-Viscoplastic Deformation of Glassy Polymers. *Mechanics of Time-Dependent Materials* 1997, *1*, 269–291, doi:10.1023/A:1009720708029.

11. Ahzi, S.; Makradi, A.; Gregory, R.V.; Edie, D.D. Modeling of Deformation Behavior and Strain-Induced Crystallization in Poly(Ethylene Terephthalate) above the Glass Transition Temperature. *Mechanics of Materials* 2003, *35*, 1139–1148, doi:10.1016/S0167-6636(03)00004-8.

12. Ames, N.M.; Srivastava, V.; Chester, S.A.; Anand, L. A Thermo-Mechanically Coupled Theory for Large Deformations of Amorphous Polymers. Part II: Applications. *International Journal of Plasticity* 2009, *25*, 1495–1539, doi:10.1016/j.ijplas.2008.11.005.

13. Anand, L.; Gurtin, M.E. A Theory of Amorphous Solids Undergoing Large Deformations, with Application to Polymeric Glasses. *International Journal of Solids and Structures* 2003, *40*, 1465–1487, doi:10.1016/S0020-7683(02)00651-0.

14. Arruda, E.M.; Boyce, M.C.; Jayachandran, R. Effects of Strain Rate, Temperature and Thermomechanical Coupling on the Finite Strain Deformation of Glassy Polymers. *Mechanics of Materials* 1995, *19*, 193–212, doi:10.1016/0167-6636(94)00034-E.

15. Uchida, M.; Tada, N. Micro-, Meso- to Macroscopic Modeling of Deformation Behavior of Semi-Crystalline Polymer. *International Journal of Plasticity* 2013, *49*, 164–184, doi:10.1016/j.ijplas.2013.03.007.

16. Boyce, M.C.; Socrate, S.; Llana, P.G. Constitutive Model for the Finite Deformation Stress–Strain Behavior of Poly(Ethylene Terephthalate) above the Glass Transition. *Polymer* 2000, *41*, 2183–2201, doi:10.1016/S0032-3861(99)00406-1.

17. Buckley, C. Glass-Rubber Constitutive Model for Amorphous Polymers near the Glass Transition. *Polymer* 1995, *36*, 3301–3312, doi:10.1016/0032-3861(95)99429-X.

18. Zaïri, F.; Naït-Abdelaziz, M.; Gloaguen, J.M.; Lefebvre, J.M. A Physically-Based Constitutive Model for Anisotropic Damage in Rubber-Toughened Glassy Polymers during Finite Deformation. *International Journal of Plasticity* 2011, *27*, 25–51, doi:10.1016/j.ijplas.2010.03.007.

19. Argon, A.S.; Bulatov, V.V.; Mott, P.H.; Suter, U.W. Plastic Deformation in Glassy Polymers by Atomistic and Mesoscopic Simulations. *Journal of Rheology* 1995, *39*, 377–399, doi:10.1122/1.550728.

20. Balieu, R.; Lauro, F.; Bennani, B.; Delille, R.; Matsumoto, T.; Mottola, E. A Fully Coupled Elastoviscoplastic Damage Model at Finite Strains for Mineral Filled Semi-Crystalline Polymer. *International Journal of Plasticity* 2013, *51*, 241–270, doi:10.1016/j.ijplas.2013.05.002.

21. Xiang, Y.; Zhong, D.; Wang, P.; Yin, T.; Zhou, H.; Yu, H.; Baliga, C.; Qu, S.; Yang, W. A Physically Based Visco-Hyperelastic Constitutive Model for Soft Materials. *Journal of the Mechanics and Physics of Solids* 2019, *128*, 208–218, doi:10.1016/j.jmps.2019.04.010.

22. Lan, T.; Shao, T.; Zhang, Y.; Zhang, Y.; Zhu, J.; Jiang, Y.; Wu, P. A Physically-Based Constitutive Model for Amorphous Glassy Polymers in Large Deformations. *European Journal of Mechanics - A/Solids* 2023, 105015, doi:10.1016/j.euromechsol.2023.105015.

23. Diani, J.; Fayolle, B.; Gilormini, P. A Review on the Mullins Effect. *European Polymer Journal* 2009, *45*, 601–612, doi:10.1016/j.eurpolymj.2008.11.017.

24. Khan, A.S.; Lopez-Pamies, O.; Kazmi, R. Thermo-Mechanical Large Deformation Response and Constitutive Modeling of Viscoelastic Polymers over a Wide Range of Strain Rates and Temperatures. *International Journal of Plasticity* 2006, *22*, 581–601, doi:10.1016/j.ijplas.2005.08.001.

25. Qi, Z.; Hu, N.; Li, G.; Zeng, D.; Su, X. Constitutive Modeling for the Elastic-Viscoplastic Behavior of High Density Polyethylene under Cyclic Loading. *International Journal of Plasticity* 2019, *113*, 125–144, doi:10.1016/j.ijplas.2018.09.010.

26. Zhang, C.; Moore, I.D. Nonlinear Mechanical Response of High Density Polyethylene. Part I: Experimental Investigation and Model Evaluation. *Polym. Eng. Sci.* 1997, *37*, 404–413, doi:10.1002/pen.11683.

27. Hong, K.; Rastogi, A.; Strobl, G. A Model Treating Tensile Deformation of Semicrystalline Polymers: Quasi-Static Stress−Strain Relationship and Viscous Stress Determined for a Sample of Polyethylene. *Macromolecules* 2004, *37*, 10165–10173, doi:10.1021/ma049174h.

28. Hong, K.; Rastogi, A.; Strobl, G. Model Treatment of Tensile Deformation of Semicrystalline Polymers: Static Elastic Moduli and Creep Parameters Derived for a Sample of Polyethylene. *Macromolecules* 2004, *37*, 10174–10179, doi:10.1021/ma049172x.

29. Drozdov, A.D. Mullins' Effect in Semicrystalline Polymers. *International Journal of Solids and Structures* 2009, *46*, 3336–3345, doi:10.1016/j.ijsolstr.2009.05.001.

30. Colak, O. Modeling Deformation Behavior of Polymers with Viscoplasticity Theory Based on Overstress. *International Journal of Plasticity* 2005, *21*, 145–160, doi:10.1016/j.ijplas.2004.04.004.

31. Nguyen, V.-D.; Lani, F.; Pardoen, T.; Morelle, X.P.; Noels, L. A Large Strain Hyperelastic Viscoelastic-Viscoplastic-Damage Constitutive Model Based on a Multi-Mechanism Non-Local Damage Continuum for Amorphous Glassy Polymers. *International Journal of Solids and Structures* 2016, *96*, 192–216, doi:10.1016/j.ijsolstr.2016.06.008.

32. Dusunceli, N.; Colak, O.U. Modelling Effects of Degree of Crystallinity on Mechanical Behavior of Semicrystalline Polymers. *International Journal of Plasticity* 2008, *24*, 1224–1242, doi:10.1016/j.ijplas.2007.09.003.

33. Popelar, C.F.; Popelar, C.H.; Kenner, V.H. Viscoelastic Material Characterization and Modeling for Polyethylene. *Polym. Eng. Sci.* 1990, *30*, 577–586, doi:10.1002/pen.760301004.

34. Zhang, C.; Moore, I.D. Nonlinear Mechanical Response of High Density Polyethylene. Part II: Uniaxial Constitutive Modeling. *Polym. Eng. Sci.* 1997, *37*, 414–420, doi:10.1002/pen.11684.

35. Bouvard, J.L.; Ward, D.K.; Hossain, D.; Marin, E.B.; Bammann, D.J.; Horstemeyer, M.F. A General Inelastic Internal State Variable Model for Amorphous Glassy Polymers. *Acta Mech* 2010, *213*, 71–96, doi:10.1007/s00707-010-0349-y.

36. Bouvard, J.L.; Francis, D.K.; Tschopp, M.A.; Marin, E.B.; Bammann, D.J.; Horstemeyer, M.F. An Internal State Variable Material Model for Predicting the Time, Thermomechanical, and Stress State Dependence of Amorphous Glassy Polymers under Large Deformation. *International Journal of Plasticity* 2013, *42*, 168–193, doi:10.1016/j.ijplas.2012.10.005.

37. Sack, I. Magnetic Resonance Elastography from Fundamental Soft-Tissue Mechanics to Diagnostic Imaging. *Nat Rev Phys* 2022, *5*, 25–42, doi:10.1038/s42254-022-00543-2.

38. Wang, B.; Yang, W.; McKittrick, J.; Meyers, M.A. Keratin: Structure, Mechanical Properties, Occurrence in Biological Organisms, and Efforts at Bioinspiration. *Progress in Materials Science* 2016, *76*, 229–318, doi:10.1016/j.pmatsci.2015.06.001.

39. Collinson, D.W.; Sheridan, R.J.; Palmeri, M.J.; Brinson, L.C. Best Practices and Recommendations for Accurate Nanomechanical Characterization of Heterogeneous Polymer Systems with Atomic Force Microscopy. *Progress in Polymer Science* 2021, *119*, 101420, doi:10.1016/j.progpolymsci.2021.101420.

40. Webber, M.J.; Tibbitt, M.W. Dynamic and Reconfigurable Materials from Reversible Network Interactions. *Nat Rev Mater* 2022, *7*, 541–556, doi:10.1038/s41578-021-00412-x.

41. Brazel, C.S.; Rosen, S.L. Fundamental Principles of Polymeric Materials. *John Wiley & Sons* 2012, 427.

42. Coleman, B.D.; Noll, W. Foundations of Linear Viscoelasticity. *Rev. Mod. Phys.* 1961, *33*, 239–249, doi:10.1103/RevModPhys.33.239.

43. Brusselle-Dupend, N.; Lai, D.; Feaugas, X.; Guigon, M.; Clavel, M. Mechanical Behavior of a Semicrystalline Polymer before Necking. Part II: Modeling of Uniaxial Behavior. *Polym. Eng. Sci.* 2003, *43*, 501–518, doi:10.1002/pen.10041.

44. *Theoretical Analyses, Computations, and Experiments of Multiscale Materials: A Tribute to Francesco Dell'Isola*; Giorgio, I., Placidi, L., Barchiesi, E., Abali, B.E., Altenbach, H., Eds.; Advanced Structured Materials; Springer International Publishing: Cham, 2022; Vol. 175; ISBN 978-3-031-04547-9.

45. Tan, N.; Jar, P.-Y.B. Determining Deformation Transition in Polyethylene under Tensile Loading. *Polymers* 2019, *11*, 1415, doi:10.3390/polym11091415.

46. Tan, N.; Jar, P.B. Multi-Relaxation Test to Characterize PE Pipe Performance. *Plastics Engineering* 2019, *75*, 40–45, doi:10.1002/peng.20184.

47. Drozdov, A.D. Time-Dependent Response of Polypropylene after Strain Reversal. *International Journal of Solids and Structures* 2010, *47*, 3221–3233, doi:10.1016/j.ijsolstr.2010.08.001.

48. Dusunceli, N. The Unusual Creep and Relaxation Behaviour of Polypropylene. *Journal of Polymer Engineering* 2012, *32*, doi:10.1515/polyeng-2011-0159.

49. Dusunceli, N.; Colak, O.U.; Filiz, C. Determination of Material Parameters of a Viscoplastic Model by Genetic Algorithm. *Materials & Design* 2010, *31*, 1250–1255, doi:10.1016/j.matdes.2009.09.023.

50. Sweeney, J.; Bonner, M.; Ward, I.M. Modelling of Loading, Stress Relaxation and Stress Recovery in a Shape Memory Polymer. *Journal of the Mechanical Behavior of Biomedical Materials* 2014, *37*, 12–23, doi:10.1016/j.jmbbm.2014.05.011.

51. Shi, F. Studies on the Time-Dependent Behavior of Semi-Crystalline Polymers. *Res Dev Polymer Sci* 2023, *2*, 1–2, doi:10.54026/RDPS/1006.

52. Lee, H.-N.; Paeng, K.; Swallen, S.F.; Ediger, M.D. Direct Measurement of Molecular Mobility in Actively Deformed Polymer Glasses. *Science* 2009, *323*, 231–234, doi:10.1126/science.1165995.

53. de Melo, C.C.; Macêdo, S.; Sciuti, V.F.; Canto, R.B. A Novel Mechanical Test for the Stress Relaxation Analysis of Polymers. *Polymer Testing* 2019, *73*, 276–283, doi:10.1016/j.polymertesting.2018.11.027.

54. Bakbak, O.; Birkan, B.E.; Acar, A.; Colak, O. Mechanical Characterization of Araldite LY 564 Epoxy: Creep, Relaxation, Quasi-Static Compression and High Strain Rate Behaviors. *Polym. Bull.* 2022, *79*, 2219–2235, doi:10.1007/s00289-021-03624-x.

55. Khan, A.S.; Lopez-Pamies, O. Time and Temperature Dependent Response and Relaxation of a Soft Polymer. *International Journal of Plasticity* 2002, *18*, 1359–1372, doi:10.1016/S0749-6419(02)00003-7.

56. Wilding, M.A.; Ward, I.M. Creep and Recovery of Ultra High Modulus Polyethylene. *Polymer* 1981, *22*, 870–876, doi:10.1016/0032-3861(81)90259-7.

57. Khan, F. Loading History Effects on the Creep and Relaxation Behavior of Thermoplastics. *Journal of Engineering Materials and Technology* 2006, *128*, 564–571, doi:10.1115/1.2345448.

58. Zhang, Y.; Jar, P.-Y.B. Time-Strain Rate Superposition for Relaxation Behavior of Polyethylene Pressure Pipes. *Polymer Testing* 2016, *50*, 292–296, doi:10.1016/j.polymertesting.2015.12.014.

59. Shi, F.; Jar, P.-Y.B. Characterization of Polyethylene Using a New Test Method Based on Stress Response to Relaxation and Recovery. *Polymers* 2022, *14*, 2763, doi:10.3390/polym14142763.

60. Ben Jar, P.-Y. Transition of Neck Appearance in Polyethylene and Effect of the Associated Strain Rate on the Damage Generation. *Polym Eng Sci* 2014, *54*, 1871–1878, doi:10.1002/pen.23735.

61. Dusunceli, N. An Observation of the Evolution of Equilibrium Stress on Poly(Lactic Acid) and Poly(Lactic Acid)/Hydroxyapatite Nanocomposites. *Proceedings of the Institution of Mechanical Engineers, Part C: Journal of Mechanical Engineering Science* 2021, *235*, 1026–1044, doi:10.1177/0954406220939598.

62. Dusunceli, N.; Drozdov, A.D.; Theilgaard, N. Influence of Temperature on Viscoelastic–Viscoplastic Behavior of Poly(Lactic Acid) under Loading–Unloading. *Polymer Engineering & Sci* 2017, *57*, 239–247, doi:10.1002/pen.24404.

63. Drozdov, A.D.; Dusunceli, N. TWO-PHASE MODEL IN VISCOELASTICITY AND VISCOPLASTICITY OF SEMICRYSTALLINE POLYMERS. *Int. J. Comp. Mat. Sci. Eng.* 2012, *01*, 1250015, doi:10.1142/S2047684112500157.

64. Humphrey, D.; Duggan, C.; Saha, D.; Smith, D.; Käs, J. Active Fluidization of Polymer Networks through Molecular Motors. *Nature* 2002, *416*, 413–416.

65. Koerner, H.; Price, G.; Pearce, N.A.; Alexander, M.; Vaia, R.A. Remotely Actuated Polymer Nanocomposites—Stress-Recovery of Carbon-Nanotube-Filled Thermoplastic Elastomers. *Nature materials* 2004, *3*, 115–120.

66. Tan, N.; Jar, P.-Y.B. Determining Deformation Transition in Polyethylene under Tensile Loading. *Polymers* 2019, *11*, 1415, doi:10.3390/polym11091415.

67. Wayne Chen, W.; Jane Wang, Q.; Huan, Z.; Luo, X. Semi-Analytical Viscoelastic Contact Modeling of Polymer-Based Materials. *Journal of Tribology* 2011, *133*, 041404, doi:10.1115/1.4004928.

68. Puchaty, R.; De Vita, G.; Vaidyanathan, R. Load–Displacement Behavior of Helical Shape Memory Alloy Spring Actuators with Small Spring Diameter to Wire Diameter Ratios. *Shap. Mem. Superelasticity* 2020, *6*, 301–310, doi:10.1007/s40830-020-00295-x.

69. Fontenier, B.; Hault-Dubrulle, A.; Drazetic, P.; Fontaine, C.; Naceur, H. On the Mechanical Characterization and Modeling of Polymer Gel Brain Substitute under Dynamic Rotational Loading. *Journal of the Mechanical Behavior of Biomedical Materials* 2016, *63*, 44–55, doi:10.1016/j.jmbbm.2016.06.008.

70. Cui, X.; Jar, P.-Y.B. Prediction of Quasi-Static Elastic Modulus for Polyethylene-Terephthalate-Glycol Prepared from Fused Deposition Modeling. *SPE Polymers* 2023, *4*, 49–62.

71. Choi, J.; Quagliato, L.; Shin, J.; Kim, N. Investigation on the Static and Cyclic Anisotropic Mechanical Behavior of Polychloroprene Rubber (CR) Reinforced with Tungsten Nano-Particles. *Engineering Fracture Mechanics* 2020, *235*, 107183, doi:10.1016/j.engfracmech.2020.107183.

72. Duxbury, J.; Ward, I.M. The Creep Behaviour of Ultra-High Modulus Polypropylene. *J Mater Sci* 1987, *22*, 1215–1222, doi:10.1007/BF01233111.

73. Yakimets, I.; Lai, D.; Guigon, M. Model to Predict the Viscoelastic Response of a Semi-Crystalline Polymer under Complex Cyclic Mechanical Loading and Unloading Conditions. *Mech Time-Depend Mater* 2007, *11*, 47–60, doi:10.1007/s11043-007-9031-8.

74. Kumar, S.; Liu, G.; Schloerb, D.; Srinivasan, M. Viscoelastic Characterization of the Primate Finger Pad In Vivo by Microstep Indentation and Three-Dimensional Finite Element Models for Tactile Sensation Studies. *Journal of biomechanical engineering* 2015, *137*, doi:10.1115/1.4029985.

75. Johnson, T.P.M.; Socrate, S.; Boyce, M.C. A Viscoelastic, Viscoplastic Model of Cortical Bone Valid at Low and High Strain Rates. *Acta Biomater.* 2010, *6*, 4073–4080, doi:10.1016/j.actbio.2010.04.017.

76. Blake, Y. Review of Viscoelastic Models Applied to Cortical Bone.

77. Hansen, T.S.; Kristiansen, B.U. Achieving a More Accurate Prediction of a Polymer Snap Deformation Pattern. 2011.

78. Heuchel, M.; Cui, J.; Kratz, K.; Kosmella, H.; Lendlein, A. Relaxation Based Modeling of Tunable Shape Recovery Kinetics Observed under Isothermal Conditions for Amorphous Shape-Memory Polymers. *Polymer* 2010, *51*, 6212–6218, doi:10.1016/j.polymer.2010.10.051.

79. Shahin, A.; Barsoum, I.; Islam, M.D. Constitutive Model Calibration of the Time and Temperature-Dependent Behavior of High Density Polyethylene. *Polymer Testing* 2020, *91*, 106800, doi:10.1016/j.polymertesting.2020.106800.

80. Fritsch, J.; Hiermaier, S.; Strobl, G. Characterizing and Modeling the Non-Linear Viscoelastic Tensile Deformation of a Glass Fiber Reinforced Polypropylene. *Composites Science and Technology* 2009, *69*, 2460–2466, doi:10.1016/j.compscitech.2009.06.021.

81. Liu, P.; Peng, L.; Chen, J.; Yang, B.; Chen, Y.; Luo, Z.; Han, C.C.; Huang, X.; Men, Y. Tensile Creep Failure of Isotactic Polypropylene under the Strain Criterion. *Macromolecules* 2022, *55*, 9663–9670, doi:10.1021/acs.macromol.2c01263.

82. Hong, K.; Strobl, G. Characterizing and Modeling the Tensile Deformation of Polyethylene: The Temperature and Crystallinity Dependences. *Polym. Sci. Ser. A* 2008, *50*, 483–493, doi:10.1134/S0965545X08050027.

83. Kazempour, M.; Baniassadi, M.; Shahsavari, H.; Remond, Y.; Baghani, M. Homogenization of Heterogeneous Brain Tissue under Quasi-Static Loading: A Visco-Hyperelastic Model of a 3D RVE. *Biomech Model Mechanobiol* 2019, *18*, 969–981, doi:10.1007/s10237-019-01124-6.

84. Na, B. High Viscous Stress of Oriented Polyolefins Under Uniaxial Tensile Deformation. *Chinese J. Polym. Sci.* 2007, *25*, 285, doi:10.1142/S0256767907002126.

85. Zhang, Y.; Jar, P.-Y.B. Comparison of Mechanical Properties Between PE80 and PE100 Pipe Materials. *J. of Materi Eng and Perform* 2016, *25*, 4326–4332, doi:10.1007/s11665-016-2274-2.

86. Na, B.; Zhang, Q.; Fu, Q.; Men, Y.; Hong, K.; Strobl, G. Viscous-Force-Dominated Tensile Deformation Behavior of Oriented Polyethylene. *Macromolecules* 2006, *39*, 2584–2591, doi:10.1021/ma052496g.

87. Truss, R.W.; Clarke, P.L.; Duckett, R.A.; Ward, I.M. The Dependence of Yield Behavior on Temperature, Pressure, and Strain Rate for Linear Polyethylenes of Different Molecular Weight

and Morphology. *J. Polym. Sci. Polym. Phys. Ed.* 1984, *22*, 191–209, doi:10.1002/pol.1984.180220205.

88. Richeton, J.; Ahzi, S.; Daridon, L.; Rémond, Y. A Formulation of the Cooperative Model for the Yield Stress of Amorphous Polymers for a Wide Range of Strain Rates and Temperatures. *Polymer* 2005, *46*, 6035–6043, doi:10.1016/j.polymer.2005.05.079.

89. Sweeney, J.; Caton-Rose, P.; Spares, R.; Coates, P.D. Unified Model of Necking and Shear Banding in Amorphous and Semicrystalline Polymers. *J. Appl. Polym. Sci.* 2007, *106*, 1095–1105, doi:10.1002/app.26546.

90. Halsey, G.; White, H.J.; Eyring, H. Mechanical Properties of Textiles, I. *Textile Research* 1945, *15*, 295–311, doi:10.1177/004051754501500901.

91. Schemmann, M.; Brylka, B.; Gajek, S.; Böhlke, T. Parameter Identification by Inverse Modelling of Biaxial Tensile Tests for Discontinous Fiber Reinforced Polymers. *PAMM* 2015, *15*, 355–356, doi:10.1002/pamm.201510168.

92. Xu, H.; Jiang, X. Creep Constitutive Models for Viscoelastic Materials Based on Fractional Derivatives. *Computers & Mathematics with Applications* 2017, *73*, 1377–1384, doi:10.1016/j.camwa.2016.05.002.

93. Ponthot, J.-P.; Kleinermann, J.-P. A Cascade Optimization Methodology for Automatic Parameter Identification and Shape/Process Optimization in Metal Forming Simulation. *Computer Methods in Applied Mechanics and Engineering* 2006, *195*, 5472–5508, doi:10.1016/j.cma.2005.11.012.

94. Petrica, M.; Popescu, I. Inverse Problem for Parameters Identification in a Modified SIRD Epidemic Model Using Ensemble Neural Networks. *BioData Mining* 2023, *16*, 22, doi:10.1186/s13040-023-00337-x.

95. Rèpaci, A.; Vacca, M.T. Parameter Identification by Solution of Inverse Problem Referred to Mathematical Models of Continuum Physics. *Mathematical and Computer Modelling* 1990, *13*, 79–84, doi:10.1016/0895-7177(90)90034-K.

96. Mahnken, R.; Stein, E. A Unified Approach for Parameter Identification of Inelastic Material Models in the Frame of the Finite Element Method. *Computer Methods in Applied Mechanics and Engineering* 1996, *136*, 225–258, doi:10.1016/0045-7825(96)00991-7.

97. Lyu, Y.; Pathirage, M.; Ramyar, E.; Liu, W.K.; Cusatis, G. Machine Learning Meta-Models for Fast Parameter Identification of the Lattice Discrete Particle Model. *Comput Mech* 2023, *72*, 593–612, doi:10.1007/s00466-023-02320-z.

98. Yoshida, F.; Urabe, M.; Hino, R.; Toropov, V.V. Inverse Approach to Identification of Material Parameters of Cyclic Elasto-Plasticity for Component Layers of a Bimetallic Sheet. *International Journal of Plasticity* 2003, *19*, 2149–2170, doi:10.1016/S0749-6419(03)00063-9.

99. Yun, G.J.; Shang, S. A Self-Optimizing Inverse Analysis Method for Estimation of Cyclic Elasto-Plasticity Model Parameters. *International Journal of Plasticity* 2011, *27*, 576–595, doi:10.1016/j.ijplas.2010.08.003.

100. Unger, J.F.; Könke, C. An Inverse Parameter Identification Procedure Assessing the Quality of the Estimates Using Bayesian Neural Networks. *Applied Soft Computing* 2011, *11*, 3357–3367, doi:10.1016/j.asoc.2011.01.007.

101. Soares, C.M.M.; De Freitas, M.M.; Araújo, A.L.; Pedersen, P. Identification of Material Properties of Composite Plate Specimens. *Composite Structures* 1993, *25*, 277–285, doi:10.1016/0263-8223(93)90174-O.

102. Bergstrom, J.; Boyce, M.C. Constitutive Modeling of the Large Strain Time-Dependent Behavior of Elastomers. *Journal of the Mechanics and Physics of Solids* 1998, *46*, 931–954, doi:10.1016/S0022-5096(97)00075-6.

103. Li, Y.; He, Y.; Liu, Z. A Viscoelastic Constitutive Model for Shape Memory Polymers Based on Multiplicative Decompositions of the Deformation Gradient. *International Journal of Plasticity* 2017, *91*, 300–317, doi:10.1016/j.ijplas.2017.04.004.

104. Natarajan, V.D. *Constitutive Behavior of a Twaron® Fabric/Natural Rubber Composite: Experiments and Modeling*; 2011;

105. Popa, C.M.; Fleischhauer, R.; Schneider, K.; Kaliske, M. Formulation and Implementation of a Constitutive Model for Semicrystalline Polymers. *International Journal of Plasticity* 2014, *61*, 128–156, doi:10.1016/j.ijplas.2014.05.010.

106. Spathis, G.; Kontou, E. Creep Failure Time Prediction of Polymers and Polymer Composites. *Composites Science and Technology* 2012, *72*, 959–964, doi:10.1016/j.compscitech.2012.03.018.

107. Song, L.; Evans, J.W. Electrochemical-Thermal Model of Lithium Polymer Batteries. *J. Electrochem. Soc.* 2000, *147*, 2086, doi:10.1149/1.1393490.

108. Bruns, M.C.; Koo, J.H.; Ezekoye, O.A. Population-Based Models of Thermoplastic Degradation: Using Optimization to Determine Model Parameters. *Polymer Degradation and Stability* 2009, *94*, 1013–1022, doi:10.1016/j.polymdegradstab.2009.02.007.

109. Burgess, S.K.; Mikkilineni, D.S.; Yu, D.B.; Kim, D.J.; Mubarak, C.R.; Kriegel, R.M.; Koros, W.J. Water Sorption in Poly(Ethylene Furanoate) Compared to Poly(Ethylene Terephthalate). Part 2: Kinetic Sorption. *Polymer* 2014, *55*, 6870–6882, doi:10.1016/j.polymer.2014.10.065.

110. Abdul-Hameed, H.; Messager, T.; Zaïri, F.; Naït-Abdelaziz, M. Large-Strain Viscoelastic–Viscoplastic Constitutive Modeling of Semi-Crystalline Polymers and Model Identification by Deterministic/Evolutionary Approach. *Computational Materials Science* 2014, *90*, 241–252, doi:10.1016/j.commatsci.2014.03.043.

111. Pyrz, M.; Zairi, F. Identification of Viscoplastic Parameters of Phenomenological Constitutive Equations for Polymers by Deterministic and Evolutionary Approach. *Modelling Simul. Mater. Sci. Eng.* 2007, *15*, 85–103, doi:10.1088/0965-0393/15/2/006.

112. Belaadi, A.; Boumaaza, M.; Alshahrani, H.; Bourchak, M. Delamination in Drilling of Jute/Cork-Reinforced Polymer Biosandwich Materials: Optimization by Response Surface Methodology and Genetic Algorithm. *Int J Adv Manuf Technol* 2022, *122*, 2095–2111, doi:10.1007/s00170-022-10001-z.

113. Chen, Y.; Li, J.; Chen, C. Optimization Design of Thin Wall Angular Contact Ball Bearing Based on MATLAB Genetic Algorithm. *J. Phys.: Conf. Ser.* 2023, *2459*, 012104, doi:10.1088/1742-6596/2459/1/012104.

114. Holland, J.H. *Adaptation in Natural and Artificial Systems: An Introductory Analysis with Applications to Biology, Control, and Artificial Intelligence*; MIT Press, 1992; ISBN 978-0-262-58111-0.

115. Booker, L.B.; Goldberg, D.E.; Holland, J.H. Classifier Systems and Genetic Algorithms. *Artificial Intelligence* 1989, *40*, 235–282, doi:10.1016/0004-3702(89)90050-7.

116. Mayer, M.J.; Szilágyi, A.; Gróf, G. Environmental and Economic Multi-Objective Optimization of a Household Level Hybrid Renewable Energy System by Genetic Algorithm. *Applied Energy* 2020, *269*, 115058, doi:10.1016/j.apenergy.2020.115058.

117. Al-Solami, H.M.; Alhebshi, A.M.S.; Abdo, H.; Mahmuod, S.R.; Alwabli, A.S.; Alkenani, N. A Bio-Mathematical Approach to Control the Anopheles Mosquito Using Sterile Males Technology. *Int. J. Biomath.* 2022, *15*, 2250037, doi:10.1142/S1793524522500371.

118. Sabir, Z. Stochastic Numerical Investigations for Nonlinear Three-Species Food Chain System. *Int. J. Biomath.* 2022, *15*, 2250005, doi:10.1142/S179352452250005X.

119. Paszkowicz, W. Genetic Algorithms, a Nature-Inspired Tool: A Survey of Applications in Materials Science and Related Fields: Part II. *Materials and Manufacturing Processes* 2013, *28*, 708–725, doi:10.1080/10426914.2012.746707.

120. Lin, J.; Yang, J. GA-Based Multiple Objective Optimisation for Determining Viscoplastic Constitutive Equations for Superplastic Alloys. *International Journal of Plasticity* 1999, *15*, 1181–1196, doi:10.1016/S0749-6419(99)00031-5.

121. Mahnken, R.; Stein, E. Parameter Identification for Viscoplastic Models Based on Analytical Derivatives of a Least-Squares Functional and Stability Investigations. *International Journal of Plasticity* 1996, *12*, 451–479, doi:10.1016/S0749-6419(95)00016-X.

122. Rahman, S.M.; Hassan, T.; Corona, E. Evaluation of Cyclic Plasticity Models in Ratcheting Simulation of Straight Pipes under Cyclic Bending and Steady Internal Pressure. *International Journal of Plasticity* 2008, *24*, 1756–1791, doi:10.1016/j.ijplas.2008.02.010.

123. Lin, J. Selection of Material Models for Predicting Necking in Superplastic Forming. *International Journal of Plasticity* 2003, *19*, 469–481, doi:10.1016/S0749-6419(01)00059-6.

124. Muthusamy, S.; Manickam, L.P.; Murugesan, V.; Muthukumaran, C.; Pugazhendhi, A. Pectin Extraction from Helianthus Annuus (Sunflower) Heads Using RSM and ANN Modelling by a Genetic Algorithm Approach. *International Journal of Biological Macromolecules* 2019, *124*, 750–758, doi:10.1016/j.ijbiomac.2018.11.036.

125. Zaferani, S.P.G.; Emami, M.R.S.; Amiri, M.K.; Binaeian, E. Optimization of the Removal Pb (II) and Its Gibbs Free Energy by Thiosemicarbazide Modified Chitosan Using RSM and ANN Modeling. *International Journal of Biological Macromolecules* 2019, *139*, 307–319, doi:10.1016/j.ijbiomac.2019.07.208.

126. Daneshgar, P.; Moosavi-Movahedi, A.A.; Norouzi, P.; Ganjali, M.R.; Madadkar-Sobhani, A.; Saboury, A.A. Molecular Interaction of Human Serum Albumin with Paracetamol: Spectroscopic and Molecular Modeling Studies. *International Journal of Biological Macromolecules* 2009, *45*, 129–134, doi:10.1016/j.ijbiomac.2009.04.011.

127. Hong, K.; Rastogi, A.; Strobl, G. Model Treatment of Tensile Deformation of Semicrystalline Polymers: Static Elastic Moduli and Creep Parameters Derived for a Sample of Polyethylene. *Macromolecules* 2004, *37*, 10174–10179, doi:10.1021/ma049172x.

128. Hong, K.; Rastogi, A.; Strobl, G. A Model Treating Tensile Deformation of Semicrystalline Polymers: Quasi-Static Stress- Strain Relationship and Viscous Stress Determined for a Sample of Polyethylene. *Macromolecules* 2004, *37*, 10165–10173.

129. Fritsch, J.; Hiermaier, S.; Strobl, G. Characterizing and Modeling the Non-Linear Viscoelastic Tensile Deformation of a Glass Fiber Reinforced Polypropylene. *Composites Science and Technology* 2009, *69*, 2460–2466, doi:10.1016/j.compscitech.2009.06.021.

130. Gao, R.; Kuriyagawa, M.; Nitta, K.-H.; He, X.; Liu, B. Structural Interpretation of Eyring Activation Parameters for Tensile Yielding Behavior of Isotactic Polypropylene Solids. *Journal of Macromolecular Science, Part B* 2015, *54*, 1196–1210, doi:10.1080/00222348.2015.1079088.

131. Sweeney, J.; Ward, I.M. *Mechanical Properties of Solid Polymers*; John Wiley & Sons, 2012;

132. Kitagawa, M.; Zhou, D.; Qui, J. Stress-Strain Curves for Solid Polymers. *Polym. Eng. Sci.* 1995, *35*, 1725–1732, doi:10.1002/pen.760352202.

133. Drozdov, A.D.; Christiansen, J. deC. Time-Dependent Response of Polypropylene/Clay Nanocomposites under Tension and Retraction. *Polymer Engineering & Science* 2013, *53*, 931–940, doi:10.1002/pen.23340.

134. Drozdov, A.D.; Dusunceli, N. Inverse Relaxation in Polypropylene. *Iran Polym J* 2012, *21*, 701–711, doi:10.1007/s13726-012-0077-3.

135. Drozdov, A.D.; Dusunceli, N. Unusual Mechanical Response of Carbon Black-Filled Thermoplastic Elastomers. *Mechanics of Materials* 2014, *69*, 116–131, doi:10.1016/j.mechmat.2013.09.019.

Chapter 4 Simulation and analysis of loading, relaxation and recovery behavior of polyethylene and its pipes

Spring-dashpot models have long been used to simulate mechanical behavior of polymers, but usefulness of these models is limited due to multiple model parameter values that can reproduce the experimental data. In view of this limitation, objective of this study is to explore the possibility of identifying a unique set of the parameter values so that the parameters can be used to establish the relationship between deformation and microstructural changes. The study developed an approach for this purpose based on stress variation during loading, relaxation, and recovery of polyethylene. One thousand sets of parameter values were determined for fitting data at the relaxation stages with discrepancy within 0.08 MPa. The study found that even with such a small discrepancy, the 1000 sets of parameter values showed a wide range of variation, but one of the model parameters, $\sigma_{v,L}(0)$*, followed two distinct paths rather than showing a random distribution. The study further found that based on five selected sets of parameter values which showed discrepancy below 0.04 MPa yielded highly consistent values for the model parameters, except for the characteristic relaxation time. Therefore, the study concludes that a unique set of model parameter values can be identified to characterize mechanical behavior of polyethylene. This approach was then applied to four types of polyethylene pipes, to determine their quasi-static stress. The results showed that these polyethylene pipes have very close quasi-static stress despite the clear difference in the measured stress. This indicates that a unique set of model parameter values could be identified for the spring-dashpot model, enabling a further study of using spring-dashpot models to characterize microstructural changes of polyethylene during deformation.*

4.1. Introduction

Polymers are widely used in our daily life [1,2], among which more than two-thirds are semi-crystalline polymers (SCPs) [3]. SCPs, such as polyethylene (PE), are a class of thermoplastics with complicated microstructures [4–8], which have attracted significant attention from many research groups [9–17]. In view that SCPs are increasingly used in various industrial sectors, for fluid transportation [18], packaging [19], electronics [20], civil engineering [21], aerospace [22], medical devices [23], automotive components [24], etc., due to their chemical inertness and attractive mechanical properties [25–29], it is important to provide a proper characterization of their stress response to deformation. However, SCPs exhibit complex time-dependent behaviors, including relaxation and creep [4,30–35], which could significantly impact their performance in all applications. Therefore, full characterization of SCPs for their mechanical behavior which includes the time-dependent stress response to deformation, is essential to ensure their reliable performance in the entire designed lifetime [36].

Stress relaxation under a constant deformation level has long been used to assess performance of plastic pipes [37,38]. Moser and Folkman [38] demonstrated the usefulness of using stress relaxation tests to predict the long-term performance of plastic pipes and their interaction with soil systems [39]. In view that plastic pipes are designed to have a lifespan exceeding 50 years [40–45], with about 95% of the plastic pipes made of PE [44,46–49], stress relaxation tests and the corresponding data analysis based on modeling have been widely used to study the long-term mechanical performance of PE and its pipes [44].

In a relaxation test at a constant deformation level, stress decrease is very significant at the beginning, but eventually reaches an asymptotic limit [26,50]. The stress-time curve during the

relaxation process is known to be influenced by the loading rate prior to the relaxation [46], and a transition of the mechanism involved in the deformation process could be detected by characterizing the relaxation behavior before and after the transition [51,52]. Although relaxation and recovery processes are known to give different stress responses to deformation, as the former is introduced after loading and the latter after unloading, both are carried out at a constant deformation level, with a bigger stress change in the former than in the latter [53]. At the same deformation level, the two processes are expected to reach the same stress level that is known as quasi-static stress. We have recently developed a test for characterizing SCP's viscous behavior, named multiple-relaxation-recovery test (RR test), in which a recovery process is generated right after a relaxation process at a similar deformation level, and the two processes are repeated multiple times with the increase of specimen displacement [54,55] .

Various models have been used to analyze mechanical test results of SCPs [56–68], among which models consisting of springs and dashpots have been used to mimic the stress response to deformation. Basic spring-dashpot models are known as Maxwell [69] and Voigt models, which represent the basic relaxation and creep behaviors, but are insufficient for simulating SCPs' highly nonlinear behavior [64]. However, if the Eyring's equation is used to govern the stress response of the dashpot element [70–77], some success has been obtained. Recently, the three-branch model proposed by Hong et al. [78,79] and Izraylit et al. [80], with only one branch containing an Eyring dashpot, has been successfully used to mimic the relaxation behavior. However, this model was not applicable to the recovery behavior after unloading [81]. Our recent work [82] also showed that some three-branch spring-dashpot models are not able to provide a full description of the stress change during relaxation and recovery phases of the RR test, especially for the unusual stress drop detected during the recovery. A three-branch model with two Maxwell branches and one spring

branch, on the other hand, has been able to simulate fairly accurately both relaxation and recovery behavior. Most of the works using a three-branch model [83–88] only provided a single set of parameter values to mimic the experimental data, even though it is commonly believed that multiple sets of the parameter values exist for a model to mimic the experimental data [89,89–91]. As a result, the use of a spring-dashpot model to reproduce the experimental data is often considered merely a curve fitting exercise. The parameter values were not used to characterize the viscous part of the mechanical properties of SCPs. Therefore, it is necessary to develop a novel approach to determine unique model parameters for accurate simulation and characterization of SCPs' mechanical behavior.

In this work, an analysis method was developed based on global and local optimization to simulate the relaxation, recovery, and loading behaviors of PE and its pipes using the three-branch spring dashpot model based on the Eyring's law. Data from RR test on cylindrical specimens and notched pipe ring (NPR) specimens were used in the simulation, to generate 1000 sets of parameter values to mimic stress drop at the relaxation stages. The range of variation for these parameter values was examined and discussed. Then, the analysis method was applied to four PE types of pipes, and their quasi-static stress as a function of specimen displacement was determined and discussed.

4.2. Experimental

4.2.1. Materials

One type of cylindrical specimen [82], and four types of NPR specimens were used in the study. The cylindrical specimen, HDPE-b, has characteristics detailed in previous work [82]. The four types of NPR specimens were from four PE pipes, with their characteristics summarized in

Table 4.1 which lists materials of the four pipes, pipe name, density, yield strength and hydrostatic design basis (HDB). All pipes have the ratio of pipe outer diameter to wall thickness (SDR) of 11.

Table 4.1. Characteristics of pipes used in this study.

Material	Pipe name	Density (g/cc)	Yield strength (MPa)	HDB @23 °C (MPa)
HDPE	PE4710- black	0.949	24.8	11.03
HDPE	PE4710- yellow	0.949	>24.1	11.03
PEX	PE-Xa	0.938	19	8.62
MDPE	PE2708	0.940	19.3	8.62

Samples of cylindrical and NPR specimens are shown in Figure 4.1(a) and (b), respectively. The cylindrical specimens of HDPE-b were also used for mechanical tests in ref [92]. The NPR specimens from PE4710-black, PE4710-yellow, and PE2708 pipes were also used for the MR tests in ref [93]. Dimensions of the specimens in Figure 4.1 are depicted in Figure 4.2(a) and (b), for cylindrical and NPR specimens, respectively.

The set-up of the RR test in the universal test machine was depicted in refs [92–96].

(a)

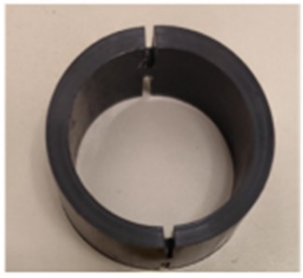

(b)

Figure 4.1. Specimens used in the RR tests: (a) cylindrical specimen and (b) NPR specimen (PEX pipe).

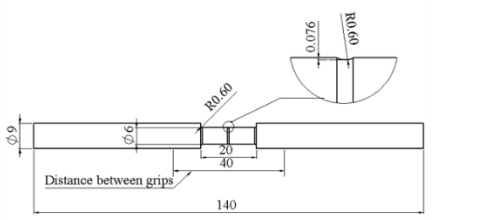

(a)

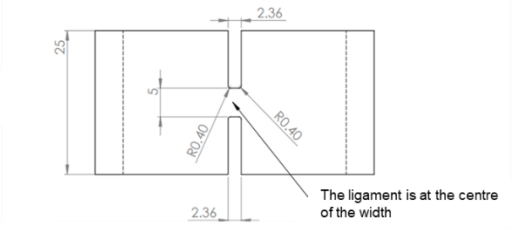

(b)

Figure 4.2. Schematic diagrams of dimensions and geometry of specimens in Figure 4.1: (a) cylindrical specimen and (b) NPR specimen. All units are in millimeters.

4.2.2. Mechanical characterization

RR tests were carried out using a Qualitest Quasar 100 universal test machine, with data collected by a personal computer [51]. The stroke-time relation and the engineering stress-stroke relation of the RR tests were described in the previous work [82,97]. The RR test consists of six stages in one cycle: 1st loading, relaxation, 2nd loading, stabilization (at a constant stroke), unloading, and recovery stages. The maximum deformation introduced in the RR tests was set to exceed the yield point, at which approximately 30 cycles were generated [51]. Sample curves of the RR tests on cylindrical specimens are available in the previous publications [82,97]. The crosshead speed was set to be 1 mm/min, with 10000 seconds allocated for each relaxation, stabilization, or recovery stage. To ensure repeatability and reliability, two specimens were tested for each material, except PE4710-black pipe for which only one RR test was conducted due to the laboratory shutdown in the COVID-19 pandemic period.

4.3. Data analysis

4.3.1. Three-branch Model

In this study, the three-branch, spring-dashpot model employed for the simulation of relaxation, recovery, and loading behaviors of the results from RR tests is depicted in Figure 4.3. This model is known as the Maxwell-Weichert model which has been commonly used to mimic the stress response to deformation of a variety of materials [56,84,86,98–101]. As shown in Figure 4.3, the model incorporates three springs governed by Hooke's law [52,102–106] and two dashpots governed by the Eyring's law [107–114]. The left, middle and right branches represent long-term viscous stress, short-term viscous stress, and quasi-static stress, respectively, denoted by the subscripts L, S, and qs [115].

From our previous publication on the three-branch model [97], the equations governing stress response as a function of time during relaxation, recovery, and loading stages were derived. The stress change [108] during each relaxation or recovery stage can be expressed as follows:

$$\begin{aligned}\Delta\sigma_A &= \sigma_A(0) - \sigma_A(t) \\ &= \sigma_{v,L}(0) + \sigma_{v,S}(0) \\ &- 2\sigma_{0,L}tanh^{-1}\{tanh\,[\sigma_{v,L}(0)\,/\,(2\sigma_{0,L})]\exp\,(-t\,/\,\tau_{v,L})\} \\ &- 2\sigma_{0,S}tanh^{-1}\{tanh\,[\sigma_{v,S}(0)\,/\,(2\sigma_{0,S})]\,exp(-\,t\,/\,\tau_{v,S})\}\end{aligned} \tag{4.1}$$

$$\tau_{v,i} = \sigma_{0,i}\,/\,(K_{v,i}\dot{\delta}_{0,i}) \tag{4.2}$$

where σ_A represents the applied engineering stress, t the time from the beginning of the stage, $\sigma_{v,i}(0)$ the viscous stress at the beginning of the stage, $\sigma_{0,i}$ reference stress, $\tau_{v,i}$ characteristic relaxation time, $K_{v,i}$ the spring stiffness, $\dot{\delta}_{0,i}$ the reference stroke rate, with $i = L$ or S.

For each loading stage, the stress responses for the long-term and short-term branches were determined as follows:

$$\dot{\sigma}_{v,L} = K_{v,L}\dot{\delta}_A - (\sigma_{0,L}\,/\,\tau_{v,L})\,\sinh(\sigma_{v,L}\,/\,\sigma_{0,L}) \tag{4.3}$$

$$\dot{\sigma}_{v,S} = K_{v,S}\dot{\delta}_A - (\sigma_{0,S}\,/\,\tau_{v,S})\,\sinh(\sigma_{v,S}\,/\,\sigma_{0,S}) \tag{4.4}$$

where $\dot{\delta}_A$ is crosshead speed of the test machine and $\dot{\sigma}_{v,i}$ the first derivative of $\sigma_{v,i}$ with respect to time t, for $i = L$ or S.

To estimate values for the fitting parameters in Equations (4.1), (4.3), and (4.4), the inverse analysis method [116–128] was employed by simulating the experimental data of the RR tests.

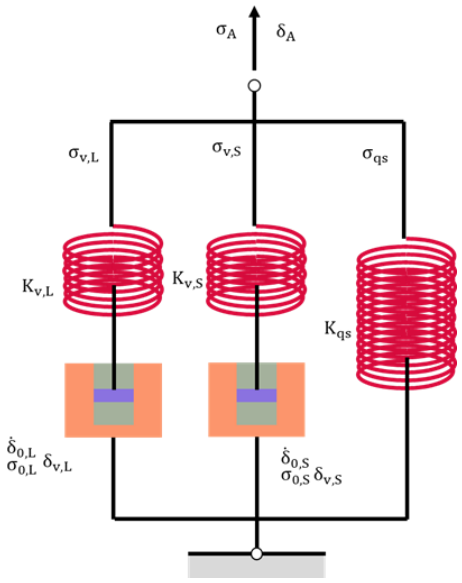

Figure 4.3. Three-branch spring-dashpot model used in this study.

4.3.2. Method for data analysis

This section describes a new analysis method for simulation of relaxation, recovery, and loading behavior of PE and its pipes. The analysis method uses a new optimization approach that combines global and local optimization techniques.

In our previous work [97], genetic algorithm (GA) in MATLAB was used to determine model parameter values via the inverse approach. However, that method was constrained by several assumptions that have limited its applicability to a specific type of loading range. For example, the method depends on the presence of a plateau region [51] of the stress-displacement curve to determine one of the model parameter values. For test data that do not have such a clear plateau region, the method could not be used.

In the current study, a method was developed without the requirement of a plateau region. Rather, the new method focuses solely on minimization of the maximum difference between the

experimental data and values generated by the model in Figure 4.3, based on the principle known as minimax in approximation theory [129,130]. Setiyoko et al. [131] reported minimax as an approach that is contrasted from the widely used least squares for determining values for parameters [83,86,132–139]. Many researchers have typically determined a single set of values for their model parameters [140–143], but whether values for the model parameters are unique remains a challenging question. In our previous work [97], ten sets of values for the model parameters in Figure 4.3 were determined to examine variation of the values [97], however, time for determining the ten sets of values was long due to constraints imposed in the algorithms, such as assumption of the plateau region. By removing these assumptions, it became possible to obtain 1,000 sets of the parameter values within a reasonable timeframe.

All programs developed in this study were coded in MATLAB, and values for the model parameters in Equations (4.1), (4.3), and (4.4) were determined using experimental data at the relaxation, the recovery, and the first loading stages of the RR tests. At each of the relaxation or recovery stages, values for the parameters in Figure 4.3 are assumed to remain fixed as the material microstructure during the relaxation and recovery is deemed to remain unchanged [144]. At each of the first loading stages, values for $K_{v,L}$ and $K_{v,S}$ were assumed to remain fixed as the deformation range introduced at each of the first loading stages was deemed to be small enough to allow values for $K_{v,L}$ and $K_{v,S}$ to remain constant. However, values for $\sigma_{0,L}$, $\tau_{v,L}$, $\sigma_{0,S}$, and $\tau_{v,S}$ were allowed to vary at each of the first loading stages.

Figure 4.4 depicts the entire procedure used to determine values for the fitting parameters in Figure 4.3, including the initial 1000 sets of parameter values based on the experimental data at the relaxation stages, and then 5 best sets of parameter values at each of the recovery and the 1st

loading stages. The objective function of the analysis was to minimize the maximum difference between the experimental data and values generated by the model.

The programs are based on the hybrid combination of global and local optimization approaches [146], also known as combined two-phase strategy [145]. According to Renders and Flasse [146], global optimization inherently involves a fundamental conflict between accuracy, reliability, and computing time. As a result, Mahinthakumar and Sayeed [147] suggested that the strength of GA could be decreased when the population was converged to a narrow location in the search space and difference between solutions was small. It was also reported that GA often requires extensive iterations and tends to converge slowly [148–150]. On the other hand, local optimization is more efficient in narrow search areas and thus is increasingly hybridized with GA to accelerate the computation [151–155]. As a result, a hybrid global-local approach was developed, by using GA and lsqnonlin [156–159] in MATLAB for the global and local optimization [146] respectively, to identify the fitting parameters for the relaxation stages of the RR tests. For example, GA was used to identify values for the six fitting parameters in Equation (4.1), and the identified values were then set as the initial guesses of lsqnonlin based on the trust-region-reflective algorithm [160].

In the first step illustrated in Figure 4.4, a numerical method was developed using the inverse approach to search for 1000 sets of values for the fitting parameters in the three-branch model in Figure 4.3 in order to mimic the experimental data at the relaxation. The initial value ranges were set to be the same as those in the previous work [97], i.e., [0.1, 20] (in MPa) for $\sigma_{v,L}(0)$, [0.01, 2] (in MPa) for $\sigma_{0,L}$, [1000, 90000] (in second) for $\tau_{v,L}$, [0.1, 20] (in MPa) for $\sigma_{v,S}(0)$, [0.01, 2] (in MPa) for $\sigma_{0,S}$, and [1, 900] (in second) for $\tau_{v,S}$. In addition, experimental data for

the very first relaxation stage were ignored in the analysis, because it did not have any prior recovery stage, and thus not with the same deformation history as the relaxation stages in other cycles. In other words, the analysis conducted in this study always started from the relaxation stage in the second cycle of the RR test.

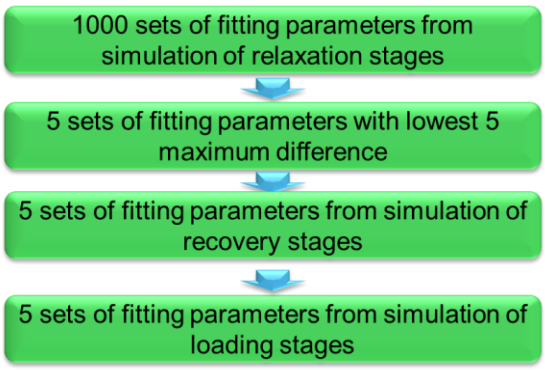

Figure 4.4. Procedure for the determination of fitting parameters in relaxation, recovery, and loading stages of RR tests.

The analysis developed in this study used a hybrid global-local approach that combines GA and lsqnonlin [156–159] in MATLAB to identify the fitting parameter values for the relaxation stages. GA was used to identify the six fitting parameters in Equation (4.1), and the generated fitting parameter values were set as the initial guesses of lsqnonlin which were based on the trust-region-reflective algorithm [160]. That is, GA was used for global optimization and lsqnonlin was used for local optimization [146].

The objective function of GA is the maximum difference of stress response between the experiments and the model, which needs to be minimized. The population size was set to be 200, and the maximum number of generations was 600. In view that speed of the computer program could be increased using parallel computing [161], parallel computing was implemented using

'parfor' in MATLAB, following the work in ref [162], to speed up the simulation so that 1000 sets of model parameter values could be determined at the first step in a reasonable timeframe.

In the second step of Figure 4.4, five sets of fitting parameter values with the smallest maximum difference between the experimental data at the relaxation stages and the simulation results were selected. In the third step, each of the five sets of values from the second step was used to determine one set of fitting parameter values for the recovery stages at similar deformation levels. The initial values of the fitting parameters at the recovery stages, for example in the mth cycle of the RR tests, were set to be $[0.01,\ \alpha]$ (in MPa) for $\sigma_{v,L}(0)$, $[0.001, \beta]$ (in MPa) for $\sigma_{0,L}$, [1000, 90000] (in second) for $\tau_{v,L}$, $[-20,\ -0.001]$ (in MPa) for $\sigma_{v,S}(0)$, [0.001, 2] (in MPa) for $\sigma_{0,S}$, and [1, 10000] (in second) for $\tau_{v,S}$, where α and β are values for $\sigma_{v,L}(0)$ in the relaxation stage of the mth cycle and $\sigma_{0,L}$ values in the next relaxation stage, i.e. in the $(m+1)$th cycle. In view that the range of stress variation at the recovery stages was much less than that at the corresponding relaxation stages, it was deemed unnecessary to determine 1000 sets of parameter values for the simulation of the recovery stages.

The final step in Figure 4.4 is to determine five sets of fitting parameter values for Equations (4.3) and (4.4) to simulate the stress variation at the 1st loading stage in each cycle, based on the parameter values determined for the relaxation and recovery stages in steps 2 and 3, respectively. For this purpose, the method was similar to that used in our previous work [97], based on GA in MATLAB, but with the improvement by combining GA with the lsqnonlin. However, in this case lsqnonlin automatically employed Levenberg-Marquardt algorithm as the original method [97] was designed to fit only one data point at a time but the trust-region-reflective algorithm requires the number of data points (equations) to be at least equal to the number of parameters (variables).

It should be noted that in literature, many researchers [51,52,93,96] have used constant characteristic relaxation time for their simulation. However, as suggested in ref [163], the effect of characteristic relaxation time on the determination of σ_{qs} should be evaluated and characteristic relaxation time should be allowed to vary with deformation. The novelty of the proposed method, as described above, originates from its ability to allow change of the characteristic relaxation time during the deformation. The proposed method also enables the evaluation of the influence of the characteristic relaxation time on the determination of other model parameter values. In addition, the combination of global and local optimization also reduced significantly the searching time for the 1000 parameters values, allowing the selection of the best five sets parameter values and thus evaluating uniqueness of the parameter values for the characterization of viscous behavior of SCPs.

4.3.3 Resolution of the experimental measurements

Many researchers have studied the material properties using mechanical tests [109,142,164–170], but few have considered the resolution of the test data [171]. For example, Mulliken and Boyce [172] successfully predicted the stress response of polymers in tension and compression tests using a constitutive model, but resolution of the experimental measurements was not reported to justify quality of the prediction. According to Jar [166,173], uncertainty of the experimental measurements affects accuracy of the test results. Therefore, a model that provides a good fitting to experimental data with a poor resolution does not provide a clear indication on the validity of the model. In view of this potential issue, resolution of the stress measurements obtained from the study was determined to assess the accuracy of the test results.

For the cylindrical specimens, σ_A was calculated using the following expression:

$$\sigma_A = \frac{4F}{(\pi D^2)} \tag{4.5}$$

where F is the measured tensile force using the universal testing machine, and D the initial diameter of the gage section measured using a digital caliper. Therefore, the resolution of σ_A for the cylindrical specimens, $d\sigma_A$, can be expressed as follows [171,174]:

$$d\sigma_A = \left|\frac{4dF}{(\pi D^2)}\right| + \left|\frac{8FdD}{(\pi D^3)}\right| \tag{4.6}$$

where *dF* and *dD* are resolution of force and diameter measurements, respectively.

Similarly, the resolutions for the NPR specimens can be calculated using the following equation.

$$\begin{aligned} d\sigma_A = & \left|\frac{dF}{t_1w_1+t_2w_2}\right| + \left|\frac{Fw_1dt_1}{(t_1w_1+t_2w_2)^2}\right| + \left|\frac{Ft_1dw_1}{(t_1w_1+t_2w_2)^2}\right| \\ & + \left|\frac{Fw_2dt_2}{(t_1w_1+t_2w_2)^2}\right| + \left|\frac{Ft_2dw_2}{(t_1w_1+t_2w_2)^2}\right| \end{aligned} \tag{4.7}$$

where t_j is the initial thickness of the gauge section j of the NPR specimens, w_j the corresponding initial width of the gauge section (j is 1 or 2, representing the two ligaments of the NPR specimens).

In this study, resolution of the universal test machine for the force measurement was 0.5 N and the resolution of the digital caliper for the dimensional measurement was 0.01 mm. As an example, for a cylindrical specimen with *D* of 5.90 mm and the maximum force of 402.5 N, resolution of its stress measurement, $d\sigma_A$, is

$$d\sigma_A = \left|\frac{4dF}{(\pi D^2)}\right| + \left|\frac{8FdD}{(\pi D^3)}\right| = 0.0682 \text{ MPa} \tag{4.8}$$

Similarly, resolution for the stress measurement of NPR specimens from different PE pipes can be determined based on the dimensions and maximum force generated in the RR tests.

4.4. Results and discussion

4.4.1 Accuracy of the simulation

This section presents 1000 sets of parameter values for simulation of the relaxation stages in the RR tests, including the maximum difference between the simulation and the experimental data and comparison of the simulation results with the resolution of the experimental data.

In the previous study, we found that the three-branch model can accurately describe results at the relaxation, recovery, and loading stages of the RR tests [97]. The previous analysis relied on several assumptions, such as constant $\tau_{v,L}$ and $\tau_{v,S}$ values [52,175], and considered the continuity of the parameter values with the increase of deformation. In this study, the method presented in section 3.2 was used to generate 1000 sets of parameter values for simulation of experimental data at the relaxation stages of the RR tests, on cylindrical specimens and NPR specimens. Table 4.2 summarizes resolution of the measured stress data and their maximum difference with the modelling results, the latter based on the 1000 sets of fitting parameter values.

Table 4.2. Resolution of the measured stress data and maximum difference of the stress response between experiments and model.

Sample specimens	Resolution (MPa)	Max difference (MPa)
HDPE-b, cylindrical	0.0682	0.0618
PE-Xa, NPR pipe	0.0767	0.0759
PE4710-yellow, NPR pipe	0.0746	0.0666
PE4710-black, NPR pipe	0.0743	0.0591
PE2708, NPR pipe	0.0590	0.0524

Table 4.2 shows the values for the experimental resolution and maximum difference for cylindrical and NPR pipe specimens. From Table 4.2, it should be noted that the values of the maximum difference are less than 0.07 MPa, which is smaller than 0.08 MPa reported in our previous work [97]. In literature, the maximum difference between the experiments and model was reported to the range from 0.17 to about 1 MPa [30,86,176–179]. In addition, the difference between the resolution of test data and the value for the maximum difference is less than 0.01 MPa, with the maximum difference of HDPE-b being even smaller than the resolution of the test data. This indicates the analysis method created in this study can provide good agreement between model and experiments. This high accuracy was also achieved for the NPR specimens in Table 4.2, with the maximum differences being less than 0.08 MPa.

Results in Table 4.2 show the capability of the three-branch model based on the proposed analysis method presented in section 3.2, which is consistent with the work in the literature [100]. Jar [180] further validated the close simulation of three-branch model in a new test, named MR test which contains the relaxation behavior at different deformation levels. However, none of the results in these works ensured the maximum difference between experiments and model to be less

than 0.08 MPa. Table 4.2 also suggests that since the inverse approach relies on quality of the experimental measurements, further improvement of the simulation accuracy requires the improvement of the resolution for the experimental data.

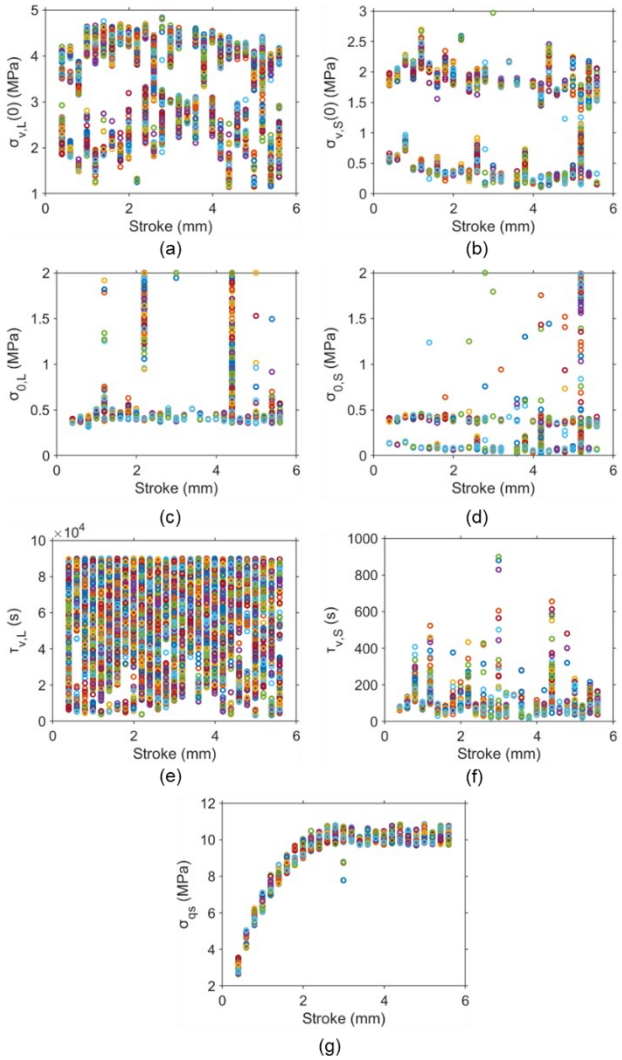

Figure 4.5. One thousand sets of parameter values for simulation at the relaxation stages of different deformation levels in one RR test of HDPE-b: (a) $\sigma_{v,L}(0)$, (b) $\sigma_{v,S}(0)$, (c) $\sigma_{0,L}$, (d) $\sigma_{0,S}$, (e) $\tau_{v,L}$, (f) $\tau_{v,S}$, and (g) σ_{qs}.

Figure 4.5 illustrates 1000 sets of fitting parameter values for simulation of the relaxation stages of different deformation levels of one RR test on HDPE-b cylindrical specimen. As shown in Figure 4.5(a), $\sigma_{v,L}(0)$ follows clearly two distinct paths with the increase of stroke, namely, an upper path and a lower path. Works in the literature always presented a single path of the fitting parameters [93,109,175], even for our previous work showing ten sets of the fitting parameter values [97]. Note that Pyrz and Zaïri [181] identified 20 sets of parameter values but no pattern was identified for these values.

Figure 4.5 also suggests that a two-path pattern exists for the variation of $\sigma_{v,S}(0)$ and $\sigma_{0,S}$ with stroke, in Figures 5(b) and (d), respectively, though $\sigma_{0,L}$ in Figure 4.5(c) shows mainly a single path. With the consideration of the limited resolution for the experimental measurement, this two-path pattern for $\sigma_{v,L}(0)$, $\sigma_{v,S}(0)$, and $\sigma_{0,S}$ values indicates that the fitting parameters could show some identifiable variation with the increase of deformation, rather than the random distribution that has been believed in the past. Therefore, there is a possibility that these model parameters could be linked to microstructural changes of SCPs.

For $\tau_{v,L}$ and $\tau_{v,S}$ values, as shown in Figures 5(e) and (f), their values are scattered across the deformation levels considered in the RR test, indicating that variation of $\tau_{v,L}$ and $\tau_{v,S}$ values may not affect the two-path pattern for the fitting parameters $\sigma_{v,L}(0)$, $\sigma_{v,S}(0)$, and $\sigma_{0,S}$. These results confirm the previous suggest that inaccurate values for the characteristic relaxation time have minor influence on the simulation [168]. In the literature, the characteristic relaxation time was often fixed as a constant for different deformation levels and materials [51,175,182]. Although Izraylit et al. [80] determined the values of characteristic relaxation time at different deformation levels, they did not give clearly the curve fitting process used in their study. Jar [180] obtained

values of characteristic relaxation time as functions of deformation levels but only provided one set of fitting parameters.

Even with a two-path distribution for some of the fitting parameters, a single trend of variation with stroke could be established for σ_{qs}, as shown in Figure 4.5(g). The band of variation for σ_{qs} is quite small, suggesting that the σ_{qs} values are not sensitive to the variation of the fitting parameter values. These findings suggest that the determination of σ_{qs} does not require a unique set of values for the fitting parameters, as long as the fitting parameter could provide a reasonable simulation of the test results.

Figure 4.6 summaries $\sigma_{v,L}(0)$ values for the pipe specimens, which shows clearly a two-path pattern also exists for PE-Xa, PE2708, PE4710-yellow, and PE4710-black pipes, suggesting that the presence of two distinct paths for variation of $\sigma_{v,L}(0)$ with deformation is a common phenomenon. Figure 4.6 also shows that the $\sigma_{v,L}(0)$ increase significantly at the early stage of the RR test, which is consistent with the observations reported in the literature [93]. Note that in the literature, Liu et al. [183], and Moore et al. [184–186] also compared modelling and experimental testing for the stress response of HDPE pipes but they did not provide the viscous stress component of the stress response. Zhang and Jar [182] determined the viscous stress in the pipes but with the assumption that the characteristic relaxation time should be kept constant.

The above findings suggest that it is possible to have a unique set of model parameter values which could be used to characterize mechanical performance of SCPs. However, further study would be needed to confirm this possibility.

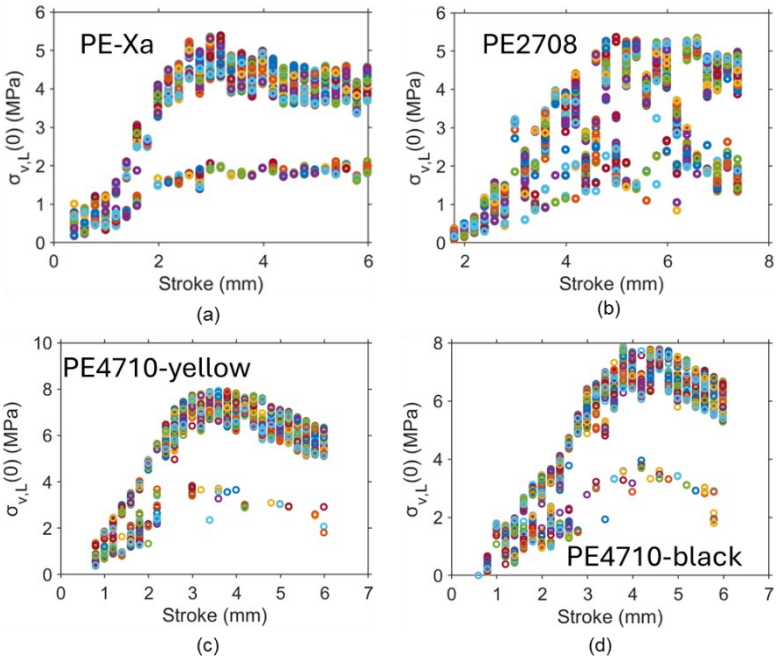

Figure 4.6. A two-path pattern of $\sigma_{v,L}(0)$ as a function of stroke for NPR specimens based on 1000 sets of parameter values: (a) PE-Xa, (b) PE2708, (c) PE4710-yellow, and (d) PE4710-black pipes.

4.4.2 Best five fits

One of the main problems addressed in the literature about the deformation of SCPs is the evolution of the crystalline phase with the increase of deformation [3]. Therefore, if the fitting parameters are to be used to characterize the material's performance, change of the fitting parameter values should reflect the evolution of SCPs microstructures.

Using the procedure depicted in Figure 4.4, five sets fitting parameters were identified which provide the closest simulation of the stress variation at the relaxation stages. These fitting parameters for HDPE-b, along with its σ_{qs}, are summarized in Figure 4.7 as functions of stroke.

Note that some outliers exist, especially for $\sigma_{v,S}(0)$ and $\sigma_{0,S}$, but apart from these outliers, a general trend for $\sigma_{v,L}(0)$, $\sigma_{v,S}(0)$, $\sigma_{0,L}$, and $\sigma_{0,S}$ values is clearly given with the increase of stroke.

It should be pointed out that the five sets of parameter values shown in Figure 4.7 gave the maximum difference of less than 0.04 MPa between the simulation and the experimental data. In view that this value is significantly smaller than the resolution of the test measurement, 0.0682 MPa as shown in Table 4.2, a further study using a test setup that will give a better resolution than that in the current study would be needed to verify the validity of the five sets of parameter values. Nevertheless, Figure 4.7 clearly shows that fitting parameter values with a clear trend of dependence with deformation could be determined using the proposed approach for the data analysis.

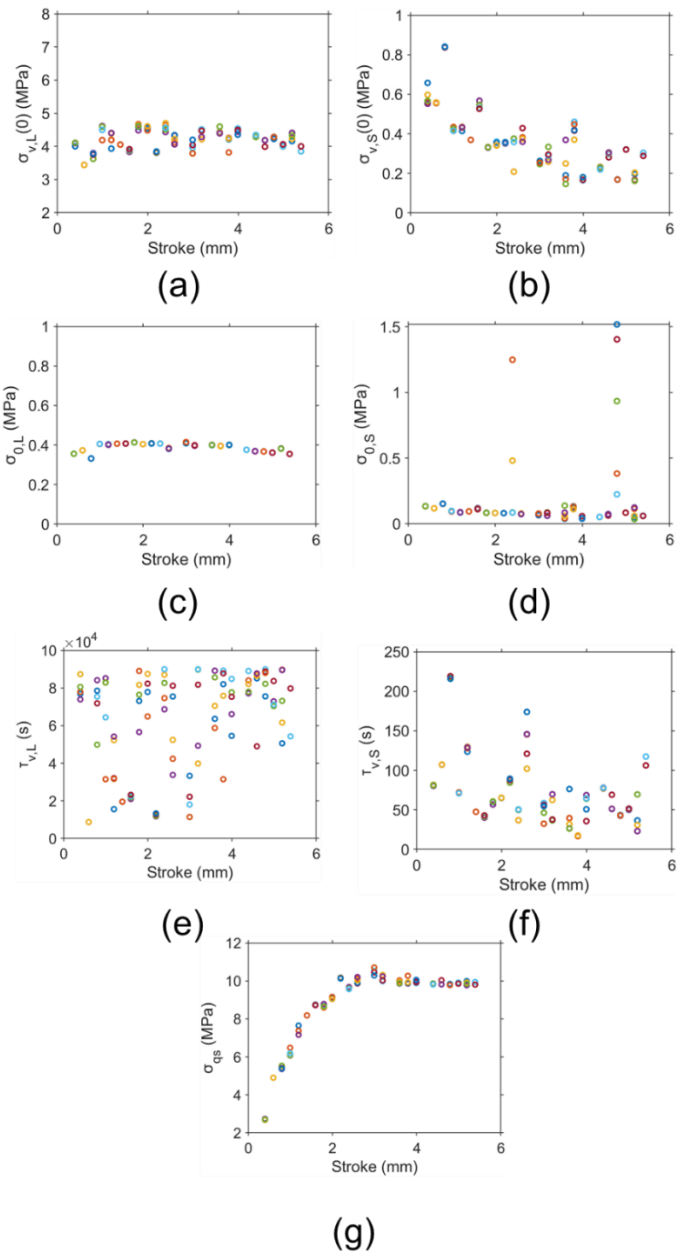

Figure 4.7. Best five sets of parameter values (in open red circles) selected from 1000 sets for simulation of stress variation at the relaxation stages of HDPE-b and the corresponding σ_{qs}: (a) $\sigma_{v,L}(0)$, (b) $\sigma_{v,S}(0)$, (c) $\sigma_{0,L}$, (d) $\sigma_{0,S}$, (e) $\tau_{v,L}$, (f) $\tau_{v,S}$, and (g) σ_{qs}.

It should also be noted that the $\sigma_{v,L}(0)$ values in Figure 4.7(a) were located along the upper path in Figure 4.5(a). In literature, Sweeney et al. applied the Guiu–Pratt analysis to derive the model parameters for fitting experimental test results for a shape-memory polymer [86], and showed a good prediction for the long-term relaxation behavior of the polymer.

Figure 4.7(b) shows $\sigma_{v,S}(0)$ values for the five best sets of fitting parameters. These $\sigma_{v,S}(0)$ values are much smaller than their $\sigma_{v,L}(0)$ counterpart in Figure 4.7(a), which is consistent with the values determined before by the manual curve fitting [180].

The five sets of $\sigma_{0,L}$ values shown in Figure 4.7(c) indicate that the five values at a given stroke are very consistent, and are in the value range consistent with those obtained before [51] using a different test method (MR test). Figure 4.7(d) presents the $\sigma_{0,S}$ values, showing that apart from those outliers, their values are smaller than the corresponding $\sigma_{0,L}$ values at the same stroke, consistent with the previous observations [180]. The values of $\sigma_{0,L}$ and $\sigma_{0,S}$ in Figures 7(c) and (d) are consistent with the values reported in the literature [51,93,175].

$\tau_{v,L}$ and $\tau_{v,S}$ values shown in Figures 7(e) and (f) show significant scattering with the increase of stroke, though the $\tau_{v,S}$values are smaller than the $\tau_{v,L}$ values. This implies that the $\tau_{v,L}$ values and $\tau_{v,S}$ values exhibited high variability. However, the scattering $\tau_{v,L}$ and $\tau_{v,S}$ values did not affect the consistency of the corresponding fitting parameters $\sigma_{v,L}(0)$, $\sigma_{v,S}(0)$, $\sigma_{0,L}$, and $\sigma_{0,S}$. This aligns with the findings in the literature that values for the characteristic relaxation time play a minor role on the simulation [168].

Figure 4.7(g) shows the σ_{qs} values as a function of stroke, which are consistent with values reported previously based on a different curve fitting approach [82]. The figure suggests that σ_{qs} values increase initially and then reach a plateau, consistent with the trend observed previously

[51]. As expected, even with the significant scattering of $\tau_{v,L}$ and $\tau_{v,S}$ values in Figures 7(e) and (f), some outliers for $\sigma_{0,S}$ in Figure 4.7(d) and some scattering for $\sigma_{v,L}(0)$ and $\sigma_{v,S}(0)$ in Figures 7(a) and (b), respectively, the five sets of σ_{qs} values are still very consistent. In view of the measurement resolution shown in Table 4.2, this suggests that σ_{qs} values determined from the current method are quite unique, not much affected by variation of fitting parameter values determined by the inverse approach.

It should be noted that although with some scattering, consistency of the fitting parameter values shown in Figure 4.7 is much better than that reported in the literature. For example, Xu et al. [89] developed a generalized reduced gradient optimization algorithm, and used the algorithm to determine parameter values for a three-branch model. Their results showed a much more significant scattering than those shown in Figure 4.7. Therefore, the proposed analysis method can capture a much more appropriate set of parameter values for the characterization of SCPs than the approaches currently available in the literature.

Table 4.3. Best five sets of parameter values at the yield point for HDPE-b.

Model parameters	Set 1	Set 2	Set 3	Set 4	Set 5
$\sigma_{v,S}(0)$ (MPa)	0.26	0.27	0.33	0.29	0.30
$\sigma_{0,S}$ (MPa)	0.06	0.06	0.09	0.08	0.08
$\tau_{v,S}$ (s)	62.51	69.78	36.70	37.80	37.88
$\sigma_{v,L}(0)$ (MPa)	4.21	4.28	4.47	4.51	4.47
$\sigma_{0,L}$ (MPa)	0.40	0.40	0.40	0.40	0.40
$\tau_{v,L}$ (s)	39881.24	49320.51	89792.94	89999.71	81756.19

Table 4.3 lists the best five sets of fitting parameters for the HDPE-b at the relaxation stage. It was found the five sets of $\sigma_{0,L}$ values are very close to each other. In the literature, Xu et al. [89] determined three sets of model parameters and the coefficient of variation is more than 50%. This indicates that the best-five-fits method in this study could provide better model parameter values. It was also found the $\sigma_{v,L}(0)$ values are higher than $\sigma_{v,S}(0)$ values, which is consistent with the results reported in the literature [180].

Figure 4.8 shows $K_{v,L}$ and $K_{v,S}$ values of HDPE-b as functions of stroke. Figure 4.8 suggests that most of the $K_{v,L}$ values are higher than the $K_{v,S}$ at the same stroke. Note that difference between $K_{v,L}$ and $K_{v,S}$ values has been an open question in the literature, as works reported indicate that $K_{v,L}$ values could be either larger or smaller than $K_{v,S}$ [84,89,180]. This uncertainty could be explained by the results presented in Figure 4.5, as $K_{v,L}$ values are influenced by the choice of $\sigma_{v,L}(0)$ values from the two paths in Figure 4.5(a). When the lower path in Figure 4.5(a) is used to determine $K_{v,L}$, in view that the corresponding $\sigma_{v,S}(0)$ values belong to the upper path in Figure 4.5(b), $K_{v,S}$ must be larger than $K_{v,L}$. Conversely, $K_{v,L}$ values are larger than $K_{v,S}$. As shown in Figure 4.8, for the best five sets of fitting parameter values, $\sigma_{v,L}(0)$ values belong to the upper path. Therefore, $K_{v,L}$ values for HDPE-b should be larger than $K_{v,S}$ values. The above explanation is based on the identification of the two-path pattern for $\sigma_{v,L}(0)$ and $\sigma_{v,S}(0)$, which would not be possible without the collection of a large number of fitting parameter values (1000 sets). Similarly, it was found that the $K_{v,L}$ values are higher than the $K_{v,S}$ for pipes in this study.

In addition, we believe that $K_{v,L}$ and $K_{v,S}$ values could represent the microstructural changes of PE during the deformation process [180]. Accurate determination of $K_{v,L}$ and $K_{v,S}$ values is essential for examining the possible relationship between microstructural changes and mechanical performance of SCPs. This study provides an approach that could clearly distinguish

the difference between $K_{v,L}$ and $K_{v,S}$ values, which has not been possible using other approaches reported in the literature.

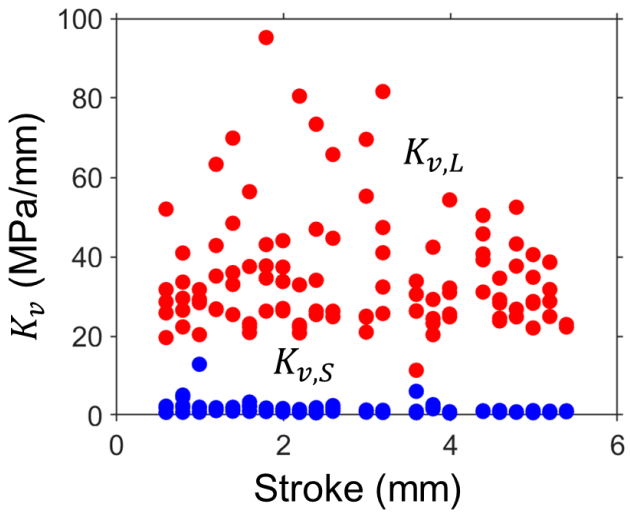

Figure 4.8. $K_{v,L}$ and $K_{v,S}$ as a function of stroke of HDPE-b.

Figure 4.9 compares $\sigma_A(0)$ and σ_{qs} for NPR specimens from the four pipes in Table 4.1. Markers in Figure 4.9(b) represent the averages of the five σ_{qs} values that were determined based on the five sets of the best fitting parameter values using the procedure described in Figure 4.4. Error bars in Figure 4.9(b) depict the standard deviations of the five σ_{qs} values. It was found that although maximum $\sigma_A(0)$ values for PE-Xa and PE2708 are lower than those for PE4710-yellow and PE4710-black at the same stroke, their σ_{qs} values are much closer to each other.

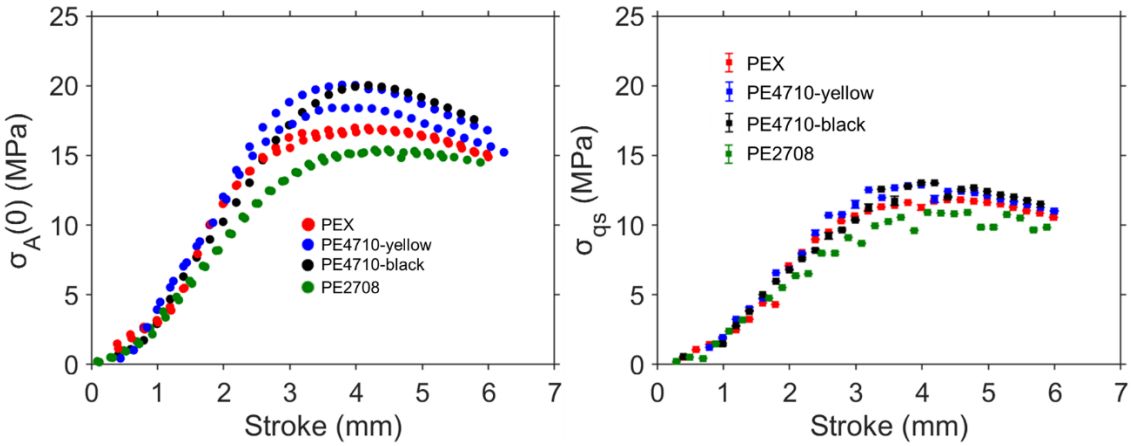

Figure 4.9. Summary RR test results for NPR specimens: (a) applied stress at the onset of relaxation, $\sigma_A(0)$, and (b) σ_{qs}.

The maximum σ_{qs} values in Figure 4.9(b) are summarized and shown in Figure 4.10. Figure 4.10 shows that maximum σ_{qs} values of HDPE (PE4710-balck and PE4710-yellow) are higher than that of MDPE (PE2708), which is consistent with the results in the literature [93]. Although the density of PE-Xa is lower than that of PE2708, the maximum σ_{qs} of PE-Xa is higher than that of PE2708, which indicates that crosslinks improve mechanical performance of PE-Xa pipes [187].

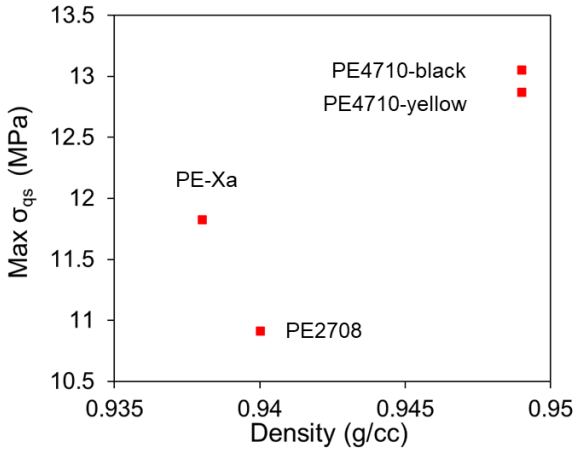

Figure 4.10. Maximum σ_{qs} as functions of densities for the four pipes.

Figure 4.11 summarizes $\sigma_{v,L}(0)$, $\sigma_{v,S}(0)$, $\sigma_{0,L}$, $\sigma_{0,S}$, $\tau_{v,L}$, and $\tau_{v,S}$ from the best five sets for the four pipes listed in Table 4.1. The symbols represent the average values, and the error bars represent the standard deviations. From Figure 4.11(a), the maximum $\sigma_{v,L}(0)$ values for PE4710-black and PE4710-yellow are close, both of which are higher than the maximum $\sigma_{v,L}(0)$ values from PE-Xa and PE2708. Similar phenomenon can be found for the $\sigma_{0,L}$ values of the four pipes. From Figure 4.11(b), the PE-Xa has the highest $\sigma_{v,S}(0)$ values and PE2708 has the lowest $\sigma_{v,S}(0)$ values among the four pipes after 3 mm of stroke. Similarly, $\sigma_{0,S}$ values also show this phenomenon. Figure 4.11(e) shows that most of the $\tau_{v,L}$ values from PE-Xa are consistent, but $\tau_{v,L}$ values from other three pipes are scattering. Figure 4.11(f) depicts that $\tau_{v,S}$ values from the four pipes are close after 4 mm of stroke.

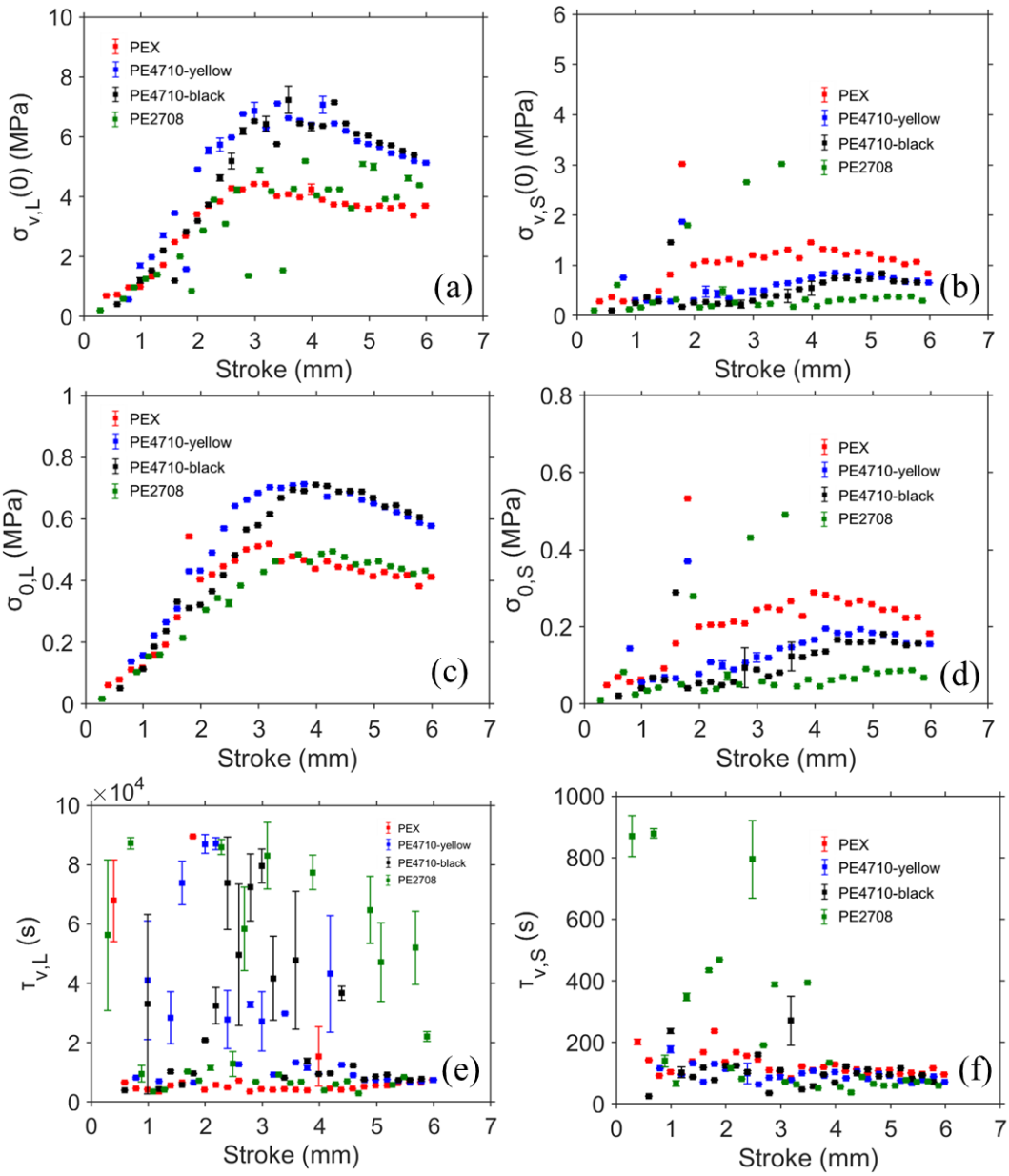

Figure 4.11. Comparison of the model parameter values from the best five sets for the four pipes: (a) $\sigma_{v,L}(0)$, (b) $\sigma_{v,S}(0)$, (c) $\sigma_{0,L}$, (d) $\sigma_{0,S}$, (e) $\tau_{v,L}$, and (f) $\tau_{v,S}$.

4.5. Conclusions

This chapter presents a new analysis method based on the global and local optimization for the simulation of relaxation, recovery, and loading behaviors of PE and its pipes in the RR tests on cylindrical and NPR specimens, respectively. Results from the RR tests can be accurately mimicked using the three-branch model with parameter values determined using the proposed analysis approach, and the maximum difference between the stress measured experimentally and those determined from the model is much smaller than the values reported in the literature.

Based on the proposed analysis method, 1000 sets of fitting parameter values were determined to simulate stress variation at the relaxation stages at different deformation levels, with the discrepancy between the experimental data and simulation results below 0.08 MPa. The 1000 sets of parameter values indicate that the $\sigma_{v,L}(0)$ values show two distinct paths with the increase of the stroke. Results from the best five fits show that the proposed method can determine consistent values and a clear trend for $\sigma_{v,L}(0)$, $\sigma_{v,S}(0)$, $\sigma_{0,L}$ and $\sigma_{0,S}$. The results also indicate that the analysis method is better than any of the methods reported in the literature on parameter identification of spring-dashpot models. Results from the study suggest that it is possible to determine a unique set of parameter values which can then be used to characterize the viscous component of mechanical behavior for SCPs.

Results from the simulation suggest that variation of the characteristic relaxation time does not have much influence on the variation of other fitting parameter values.

Without consideration of the resolution of the test setup used in this study, the proposed analysis approach allows the selection of the best five sets of parameter values to provide precise

prediction on the change of viscous behavior with the increase of deformation. However, further study is needed to improve the resolution of the measured results, so that the accuracy of the values based on the best five sets of fitting parameter values can be verified. The study also confirms that $K_{v,L}$ values for PE should be larger than the $K_{v,S}$ at the same stroke. It was also found that maximum σ_{qs} values of HDPE is higher than that of MDPE. Although the density of PE-Xa is lower than that of PE2708, the maximum σ_{qs} of PE-Xa is higher than that of PE2708.

Overall conclusions of the study are: a unique set parameter values could be identified, if the experimental data have a sufficiently high resolution to reduce uncertainty of the test results. With such experimental data, it is then possible to explore the relationship between these parameters and microstructural changes of polyethylene during the deformation. This study provides a tool to determine the unique model parameter values for a three-branch model, if such values exist.

References

1. Sparks, T.D.; Banerjee, D. Materials Informatics and Polymer Science: Pushing the Frontiers of Our Understanding. *Matter* 2021, *4*, 1454–1456, doi:10.1016/j.matt.2021.04.003.

2. Stepto, R.; Horie, K.; Kitayama, T.; Abe, A. Mission and challenges of polymer science and technology. *Pure and Applied Chemistry* 2003, *75*, 1359–1369, doi:10.1351/pac200375101359.

3. Men, Y. Critical Strains Determine the Tensile Deformation Mechanism in Semicrystalline Polymers. *Macromolecules* 2020, *53*, 9155–9157, doi:10.1021/acs.macromol.0c02076.

4. Felder, S.; Holthusen, H.; Hesseler, S.; Pohlkemper, F.; Gries, T.; Simon, J.-W.; Reese, S. Incorporating Crystallinity Distributions into a Thermo-Mechanically Coupled Constitutive Model for Semi-Crystalline Polymers. *International Journal of Plasticity* 2020, *135*, 102751, doi:10.1016/j.ijplas.2020.102751.

5. Farge, L.; Boisse, J.; Dillet, J.; André, S.; Albouy, P.-A.; Meneau, F. Wide-Angle X-Ray Scattering Study of the Lamellar/Fibrillar Transition for a Semi-Crystalline Polymer Deformed in Tension in Relation with the Evolution of Volume Strain. *J. Polym. Sci. Part B: Polym. Phys.* 2015, *53*, 1470–1480, doi:10.1002/polb.23790.

6. Uchida, M.; Tada, N. Micro-, Meso- to Macroscopic Modeling of Deformation Behavior of Semi-Crystalline Polymer. *International Journal of Plasticity* 2013, *49*, 164–184, doi:10.1016/j.ijplas.2013.03.007.

7. Garcia-Gonzalez, D.; Zaera, R.; Arias, A. A Hyperelastic-Thermoviscoplastic Constitutive Model for Semi-Crystalline Polymers: Application to PEEK under Dynamic Loading Conditions. *International Journal of Plasticity* 2017, *88*, 27–52, doi:10.1016/j.ijplas.2016.09.011.

8. Hao, P.; Laheri, V.; Dai, Z.; Gilabert, F.A. A Rate-Dependent Constitutive Model Predicting the Double Yield Phenomenon, Self-Heating and Thermal Softening in Semi-Crystalline Polymers. *International Journal of Plasticity* 2022, *153*, 103233, doi:10.1016/j.ijplas.2022.103233.

9. Li, C.Y. The Rise of Semicrystalline Polymers and Why Are They Still Interesting. *Polymer* 2020, *211*, 123150, doi:10.1016/j.polymer.2020.123150.

10. Regrain, C.; Laiarinandrasana, L.; Toillon, S.; Saï, K. Multi-Mechanism Models for Semi-Crystalline Polymer: Constitutive Relations and Finite Element Implementation. *International Journal of Plasticity* 2009, *25*, 1253–1279, doi:10.1016/j.ijplas.2008.09.010.

11. Dusunceli, N.; Colak, O.U. Modelling Effects of Degree of Crystallinity on Mechanical Behavior of Semicrystalline Polymers. *International Journal of Plasticity* 2008, *24*, 1224–1242, doi:10.1016/j.ijplas.2007.09.003.

12. Yeh, I.-C.; Andzelm, J.W.; Rutledge, G.C. Mechanical and Structural Characterization of Semicrystalline Polyethylene under Tensile Deformation by Molecular Dynamics Simulations. *Macromolecules* 2015, *48*, 4228–4239, doi:10.1021/acs.macromol.5b00697.

13. Yang, X.; Sun, Y.; Liao, T.; Men, Y. Strain Dependent Evolution of Structure and Stress in Propylene-Based Elastomer during Stress Relaxation. *Polymer* 2020, *201*, 122612, doi:10.1016/j.polymer.2020.122612.

14. Khan, F.; Yeakle, C. Experimental Investigation and Modeling of Non-Monotonic Creep Behavior in Polymers. *International Journal of Plasticity* 2011, *27*, 512–521, doi:10.1016/j.ijplas.2010.06.007.

15. Lendlein, A.; Langer, R. Biodegradable, Elastic Shape-Memory Polymers for Potential Biomedical Applications. *Science* 2002, *296*, 1673–1676, doi:10.1126/science.1066102.

16. Lendlein, A.; Gould, O.E. Reprogrammable Recovery and Actuation Behaviour of Shape-Memory Polymers. *Nature Reviews Materials* 2019, *4*, 116–133.

17. Leterrier, Y. Durability of Nanosized Oxygen-Barrier Coatings on Polymers. *Progress in materials science* 2003, *48*, 1–55.

18. Hutař, P.; Ševčík, M.; Frank, A.; Náhlík, L.; Kučera, J.; Pinter, G. The Effect of Residual Stress on Polymer Pipe Lifetime. *Engineering Fracture Mechanics* 2013, *108*, 98–108, doi:10.1016/j.engfracmech.2013.04.014.

19. Kartalis, C.N.; Papaspyrides, C.D.; Pfaendner, R. Recycling of Post-Used PE Packaging Film Using the Restabilization Technique. *Polymer Degradation and Stability* 2000, *70*, 189–197, doi:10.1016/S0141-3910(00)00106-3.

20. Hou, S.; Qi, S.; Hutt, D.A.; Tyrer, J.R.; Mu, M.; Zhou, Z. Three Dimensional Printed Electronic Devices Realised by Selective Laser Melting of Copper/High-Density-Polyethylene Powder Mixtures. *Journal of Materials Processing Technology* 2018, *254*, 310–324, doi:10.1016/j.jmatprotec.2017.11.020.

21. Sobhan, K.; Mashnad, M. Tensile Strength and Toughness of Soil–Cement–Fly-Ash Composite Reinforced with Recycled High-Density Polyethylene Strips. *Journal of Materials in Civil Engineering* 2002, *14*, 177–184, doi:10.1061/(ASCE)0899-1561(2002)14:2(177).

22. Cha, J.-H.; Kim, Y.; Sathish Kumar, S.K.; Choi, C.; Kim, C.-G. Ultra-High-Molecular-Weight Polyethylene as a Hypervelocity Impact Shielding Material for Space Structures. *Acta Astronautica* 2020, *168*, 182–190, doi:10.1016/j.actaastro.2019.12.008.

23. Zaribaf, F.P. Medical-Grade Ultra-High Molecular Weight Polyethylene: Past, Current and Future. *Materials Science and Technology* 2018, *34*, 1940–1953, doi:10.1080/02670836.2018.1469455.

24. Patil, A.; Patel, A.; Purohit, R. An Overview of Polymeric Materials for Automotive Applications. *Materials Today: Proceedings* 2017, *4*, 3807–3815, doi:10.1016/j.matpr.2017.02.278.

25. Barba, D.; Arias, A.; Garcia-Gonzalez, D. Temperature and Strain Rate Dependences on Hardening and Softening Behaviours in Semi-Crystalline Polymers: Application to PEEK. *International Journal of Solids and Structures* 2020, *182–183*, 205–217, doi:10.1016/j.ijsolstr.2019.08.021.

26. Ayoub, G.; Zaïri, F.; Naït-Abdelaziz, M.; Gloaguen, J.M. Modelling Large Deformation Behaviour under Loading–Unloading of Semicrystalline Polymers: Application to a High Density Polyethylene. *International Journal of Plasticity* 2010, *26*, 329–347, doi:10.1016/j.ijplas.2009.07.005.

27. Atiq, O.; Ricci, E.; Baschetti, M.G.; De Angelis, M.G. Modelling Solubility in Semi-Crystalline Polymers: A Critical Comparative Review. *Fluid Phase Equilibria* 2022, *556*, 113412, doi:10.1016/j.fluid.2022.113412.

28. Nunes dos Santos, W.; Augusto Marcondes Agnelli, J.; Mummery, P.; Wallwork, A. Effect of Recycling on the Thermal Properties of Polymers. *Polymer Testing* 2007, *26*, 216–221, doi:10.1016/j.polymertesting.2006.10.004.

29. Miaudet, P.; Derre, A.; Maugey, M.; Zakri, C.; Piccione, P.M.; Inoubli, R.; Poulin, P. Shape and Temperature Memory of Nanocomposites with Broadened Glass Transition. *Science* 2007, *318*, 1294–1296.

30. Li, Y.; He, Y.; Liu, Z. A Viscoelastic Constitutive Model for Shape Memory Polymers Based on Multiplicative Decompositions of the Deformation Gradient. *International Journal of Plasticity* 2017, *91*, 300–317, doi:10.1016/j.ijplas.2017.04.004.

31. Liu, P.; Peng, L.; Chen, J.; Yang, B.; Chen, Y.; Luo, Z.; Han, C.C.; Huang, X.; Men, Y. Tensile Creep Failure of Isotactic Polypropylene under the Strain Criterion. *Macromolecules* 2022, *55*, 9663–9670, doi:10.1021/acs.macromol.2c01263.

32. Xu, S.; Zhou, J.; Pan, P. Strain-Induced Multiscale Structural Evolutions of Crystallized Polymers: From Fundamental Studies to Recent Progresses. *Progress in Polymer Science* 2023, 101676.

33. Sedighiamiri, A.; Govaert, L.E.; Kanters, M.J.W.; van Dommelen, J.A.W. Micromechanics of Semicrystalline Polymers: Yield Kinetics and Long-Term Failure. *J. Polym. Sci. B Polym. Phys.* 2012, *50*, 1664–1679, doi:10.1002/polb.23136.

34. Lim, S.D.; Rhee, J.M.; Nah, C. Predicting the Long-Term Creep Behavior of Plastics Using the Short-Term Creep Test. 2004, 7.

35. Kubát, J. Stress Relaxation in Solids. *Nature* 1965, *205*, 378–379.

36. Janssen, R. Deformation and Failure in Semi-Crystalline Polymer Systems. 53.

37. Malpass, V.E. Prediction of Long-Term ABS Relaxation Behavior. *Journal of Applied Polymer Science* 1968, *12*, 771–788, doi:10.1002/app.1968.070120415.

38. Moser, A.P.; Folkman, S.L. *Buried Pipe Design*; 3rd ed.; McGraw-Hill: New York, 2008; ISBN 978-0-07-147689-8.

39. Moser, A.P. Structural Performance of Buried Profile-Wall High-Density Polyethylene Pipe and Influence of Pipe Wall Geometry. *Transportation Research Record* 1998, *1624*, 206–213, doi:10.3141/1624-24.

40. Frank, A.; Pinter, G.; Lang, R.W. Prediction of the Remaining Lifetime of Polyethylene Pipes after up to 30 Years in Use. *Polymer Testing* 2009, *28*, 737–745, doi:10.1016/j.polymertesting.2009.06.004.

41. Frank, A.; Berger, I.J.; Arbeiter, F.; Hutař, P.; Pinter, G. Lifetime Prediction of PE100 and PE100-RC Pipes Based on Slow Crack Growth Resistance. 2016, doi:10.13140/RG.2.2.27467.80165.

42. Hoàng, E.M.; Lowe, D. Lifetime Prediction of a Blue PE100 Water Pipe. *Polymer Degradation and Stability* 2008, *93*, 1496–1503, doi:10.1016/j.polymdegradstab.2008.05.008.

43. Brown, N. Intrinsic Lifetime of Polyethylene Pipelines. *Polym. Eng. Sci.* 2007, *47*, 477–480, doi:10.1002/pen.20696.

44. Zha, S.; Lan, H.; Huang, H. Review on Lifetime Predictions of Polyethylene Pipes: Limitations and Trends. *International Journal of Pressure Vessels and Piping* 2022, *198*, 104663, doi:10.1016/j.ijpvp.2022.104663.

45. Frank, A.; Arbeiter, F.J.; Berger, I.J.; Hutař, P.; Náhlík, L.; Pinter, G. Fracture Mechanics Lifetime Prediction of Polyethylene Pipes. *J. Pipeline Syst. Eng. Pract.* 2019, *10*, 04018030, doi:10.1061/(ASCE)PS.1949-1204.0000356.

46. Zhang, Y.; Jar, P.-Y.B. Time-Strain Rate Superposition for Relaxation Behavior of Polyethylene Pressure Pipes. *Polymer Testing* 2016, *50*, 292–296, doi:10.1016/j.polymertesting.2015.12.014.

47. Zhang, Y.; Jar, P.-Y.B.; Xue, S.; Han, L.; Li, L. Measurement of Environmental Stress Cracking Resistance of Polyethylene Pipe: A Review. In Proceedings of the ASME 2019 Asia Pacific Pipeline Conference; American Society of Mechanical Engineers: Qingdao, China, May 15 2019; p. V001T10A001.

48. Zhang, Y.; Jar, P.-Y.B.; Xue, S.; Li, L. Numerical Simulation of Ductile Fracture in Polyethylene Pipe with Continuum Damage Mechanics and Gurson-Tvergaard-Needleman Damage Models. *Proceedings of the IMechE* 2019, *233*, 2455–2468, doi:10.1177/1464420719863458.

49. Zhang, Y.; Qiao, L.; Fan, J.; Xue, S.; Jar, P.B. Molecular Dynamics Simulation of Plastic Deformation in Polyethylene under Uniaxial and Biaxial Tension. *Proceedings of the Institution of Mechanical Engineers, Part L: Journal of Materials: Design and Applications* 2021, 146442072110458, doi:10.1177/14644207211045821.

50. Fancey, K.S. A Mechanical Model for Creep, Recovery and Stress Relaxation in Polymeric Materials. *J Mater Sci* 2005, *40*, 4827–4831, doi:10.1007/s10853-005-2020-x.

51. Tan, N.; Jar, P.-Y.B. Determining Deformation Transition in Polyethylene under Tensile Loading. *Polymers* 2019, *11*, 1415, doi:10.3390/polym11091415.

52. Hong, K.; Rastogi, A.; Strobl, G. Model Treatment of Tensile Deformation of Semicrystalline Polymers: Static Elastic Moduli and Creep Parameters Derived for a Sample of Polyethylene. *Macromolecules* 2004, *37*, 10174–10179, doi:10.1021/ma049172x.

53. Castagnet, S. High-Temperature Mechanical Behavior of Semi-Crystalline Polymers and Relationship to a Rubber-like "Relaxed" State. *Mechanics of Materials* 2009, *41*, 75–86, doi:10.1016/j.mechmat.2008.10.001.

54. Koerner, H.; Price, G.; Pearce, N.A.; Alexander, M.; Vaia, R.A. Remotely Actuated Polymer Nanocomposites—Stress-Recovery of Carbon-Nanotube-Filled Thermoplastic Elastomers. *Nature materials* 2004, *3*, 115–120.

55. Shi, F. Studies on the Time-Dependent Behavior of Semi-Crystalline Polymers. *Res Dev Polymer Sci* 2023, *2*, 1–2, doi:10.54026/RDPS/1006.

56. Yakimets, I.; Lai, D.; Guigon, M. Model to Predict the Viscoelastic Response of a Semi-Crystalline Polymer under Complex Cyclic Mechanical Loading and Unloading Conditions. *Mech Time-Depend Mater* 2007, *11*, 47–60, doi:10.1007/s11043-007-9031-8.

57. Wilding, M.A.; Ward, I.M. Creep and Recovery of Ultra High Modulus Polyethylene. *Polymer* 1981, *22*, 870–876, doi:10.1016/0032-3861(81)90259-7.

58. Wilding, M.A.; Ward, I.M. Tensile Creep and Recovery in Ultra-High Modulus Linear Polyethylenes. *Polymer* 1978, *19*, 969–976, doi:10.1016/0032-3861(78)90208-2.

59. Sweeney, J.; Ward, I.M. A Unified Model of Stress Relaxation and Creep Applied to Oriented Polyethylene. *J Mater Sci* 1990, *25*, 697–705, doi:10.1007/BF00714097.

60. Okereke, M.I.; Akpoyomare, A.I. Two-Process Constitutive Model for Semicrystalline Polymers across a Wide Range of Strain Rates. *Polymer* 2019, *183*, 121818, doi:10.1016/j.polymer.2019.121818.

61. Detrez, F.; Cantournet, S.; Séguéla, R. A Constitutive Model for Semi-Crystalline Polymer Deformation Involving Lamellar Fragmentation. *Comptes Rendus Mécanique* 2010, *338*, 681–687, doi:10.1016/j.crme.2010.10.008.

62. Olley, P.; Sweeney, J. A Multiprocess Eyring Model for Large Strain Plastic Deformation. *J. Appl. Polym. Sci.* 2011, *119*, 2246–2260, doi:10.1002/app.32951.

63. Johnsen, J.; Clausen, A.H.; Grytten, F.; Benallal, A.; Hopperstad, O.S. A Thermo-Elasto-Viscoplastic Constitutive Model for Polymers. *Journal of the Mechanics and Physics of Solids* 2019, *124*, 681–701, doi:10.1016/j.jmps.2018.11.018.

64. Brusselle-Dupend, N.; Lai, D.; Feaugas, X.; Guigon, M.; Clavel, M. Mechanical Behavior of a Semicrystalline Polymer before Necking. Part II: Modeling of Uniaxial Behavior. *Polym. Eng. Sci.* 2003, *43*, 501–518, doi:10.1002/pen.10041.

65. DeMaio, A.; Patterson, T. Rheological Modeling of the Tensile Creep Behavior of Paper: Tensile Creep Behavior of Paper. *J. Appl. Polym. Sci.* 2007, *106*, 3543–3554, doi:10.1002/app.26895.

66. Duxbury, J.; Ward, I.M. The Creep Behaviour of Ultra-High Modulus Polypropylene. *J Mater Sci* 1987, *22*, 1215–1222, doi:10.1007/BF01233111.

67. Guedes, R.M.; Singh, A.; Pinto, V. Viscoelastic Modelling of Creep and Stress Relaxation Behaviour in PLA-PCL Fibres. *Fibers Polym* 2017, *18*, 2443–2453, doi:10.1007/s12221-017-7479-y.

68. Daneshyar, A.; Ghaemian, M.; Du, C. A Fracture Energy–Based Viscoelastic–Viscoplastic–Anisotropic Damage Model for Rate-Dependent Cracking of Concrete. *Int J Fract* 2023, *241*, 1–26, doi:10.1007/s10704-022-00685-5.

69. Jordan, B.; Gorji, M.B.; Mohr, D. Neural Network Model Describing the Temperature- and Rate-Dependent Stress-Strain Response of Polypropylene. *International Journal of Plasticity* 2020, *135*, 102811, doi:10.1016/j.ijplas.2020.102811.

70. Nechad, H.; Helmstetter, A.; El Guerjouma, R.; Sornette, D. Andrade and Critical Time-to-Failure Laws in Fiber-Matrix Composites: Experiments and Model. *Journal of the Mechanics and Physics of Solids* 2005, *53*, 1099–1127.

71. Naraghi, M.; Kolluru, P.V.; Chasiotis, I. Time and Strain Rate Dependent Mechanical Behavior of Individual Polymeric Nanofibers. *Journal of the Mechanics and Physics of Solids* 2014, *62*, 257–275, doi:10.1016/j.jmps.2013.10.006.

72. Xu, P.; Zhou, Z.; Liu, T.; Pan, S.; Tan, X.; Chen, Z. The Investigation of Viscoelastic Mechanical Behaviors of Bolted GLARE Joints: Modeling and Experiments. *International Journal of Mechanical Sciences* 2020, *175*, 105538.

73. Agbossou, A.; Cohen, I.; Muller, D. Effects of Interphase and Impact Strain Rates on Tensile Off-Axis Behaviour of Unidirectional Glass Fibre Composite: Experimental Results. *Engineering Fracture Mechanics* 1995, *52*, 923–935, doi:10.1016/0013-7944(94)00320-H.

74. Arruda, E.M.; Boyce, M.C. Evolution of Plastic Anisotropy in Amorphous Polymers during Finite Straining. *International Journal of Plasticity* 1993, *9*, 697–720.

75. Du, Y.; Pei, P.; Suo, T.; Gao, G. Large Deformation Mechanical Behavior and Constitutive Modeling of Oriented PMMA. *International Journal of Mechanical Sciences* 2023, *257*, 108520, doi:10.1016/j.ijmecsci.2023.108520.

76. Zhao, W.; Liu, L.; Lan, X.; Leng, J.; Liu, Y. Thermomechanical Constitutive Models of Shape Memory Polymers and Their Composites. *Applied Mechanics Reviews* 2023, *75*, 020802, doi:10.1115/1.4056131.

77. Wang, Z.; Guo, J.; Seppala, J.E.; Nguyen, T.D. Extending the Effective Temperature Model to the Large Strain Hardening Behavior of Glassy Polymers. *Journal of the Mechanics and Physics of Solids* 2021, *146*, 104175, doi:10.1016/j.jmps.2020.104175.

78. Hong, K.; Strobl, G. Characterizing and Modeling the Tensile Deformation of Polyethylene: The Temperature and Crystallinity Dependences. *Polym. Sci. Ser. A* 2008, *50*, 483–493, doi:10.1134/S0965545X08050027.

79. Na, B.; Zhang, Q.; Fu, Q.; Men, Y.; Hong, K.; Strobl, G. Viscous-Force-Dominated Tensile Deformation Behavior of Oriented Polyethylene. *Macromolecules* 2006, *39*, 2584–2591, doi:10.1021/ma052496g.

80. Izraylit, V.; Heuchel, M.; Gould, O.E.C.; Kratz, K.; Lendlein, A. Strain Recovery and Stress Relaxation Behaviour of Multiblock Copolymer Blends Physically Cross-Linked with PLA Stereocomplexation. *Polymer* 2020, *209*, 122984, doi:10.1016/j.polymer.2020.122984.

81. Shi, F.; Ben Jar, P.-Y. Characterization of Polyethylene Using a New Test Method Based on Stress Response to Relaxation and Recovery. *Polymers* 2022, *14*, 2763, doi:10.3390/polym14142763.

82. Shi, F.; Jar, P.-Y.B. Characterization of Polyethylene Using a New Test Method Based on Stress Response to Relaxation and Recovery. *Polymers* 2022, *14*, 2763, doi:10.3390/polym14142763.

83. Haario, H.; von Hertzen, R.; Karttunen, A.T.; Jorkama, M. Identification of the Viscoelastic Parameters of a Polymer Model by the Aid of a MCMC Method. *Mechanics Research Communications* 2014, *61*, 1–6, doi:10.1016/j.mechrescom.2014.07.002.

84. Johnson, T.P.M.; Socrate, S.; Boyce, M.C. A Viscoelastic, Viscoplastic Model of Cortical Bone Valid at Low and High Strain Rates. *Acta Biomater.* 2010, *6*, 4073–4080, doi:10.1016/j.actbio.2010.04.017.

85. Christöfl, P.; Czibula, C.; Berer, M.; Oreski, G.; Teichert, C.; Pinter, G. Comprehensive Investigation of the Viscoelastic Properties of PMMA by Nanoindentation. *Polymer Testing* 2021, *93*, 106978, doi:10.1016/j.polymertesting.2020.106978.

86. Sweeney, J.; Bonner, M.; Ward, I.M. Modelling of Loading, Stress Relaxation and Stress Recovery in a Shape Memory Polymer. *Journal of the Mechanical Behavior of Biomedical Materials* 2014, *37*, 12–23, doi:10.1016/j.jmbbm.2014.05.011.

87. Wayne Chen, W.; Jane Wang, Q.; Huan, Z.; Luo, X. Semi-Analytical Viscoelastic Contact Modeling of Polymer-Based Materials. *Journal of Tribology* 2011, *133*, 041404, doi:10.1115/1.4004928.

88. Shahin, A.; Barsoum, I.; Islam, M.D. Constitutive Model Calibration of the Time and Temperature-Dependent Behavior of High Density Polyethylene. *Polymer Testing* 2020, *91*, 106800, doi:10.1016/j.polymertesting.2020.106800.

89. Xu, Q.; Engquist, B.; Solaimanian, M.; Yan, K. A New Nonlinear Viscoelastic Model and Mathematical Solution of Solids for Improving Prediction Accuracy. *Scientific reports* 2020, *10*, 2202.

90. Mierke, C.T. Viscoelasticity Acts as a Marker for Tumor Extracellular Matrix Characteristics. *Front. Cell Dev. Biol.* 2021, *9*, doi:10.3389/fcell.2021.785138.

91. Muliana, A. A Fractional Model of Nonlinear Multiaxial Viscoelastic Behaviors. *Mech Time-Depend Mater* 2022, doi:10.1007/s11043-022-09542-3.

92. Ben Jar, P.-Y. Transition of Neck Appearance in Polyethylene and Effect of the Associated Strain Rate on the Damage Generation. *Polym Eng Sci* 2014, *54*, 1871–1878, doi:10.1002/pen.23735.

93. Tan, N.; Jar, P.B. Multi-Relaxation Test to Characterize PE Pipe Performance. *Plastics Engineering* 2019, *75*, 40–45, doi:10.1002/peng.20184.

94. Zhang, Y.; Ben Jar, P.-Y. Quantitative Assessment of Deformation-Induced Damage in Polyethylene Pressure Pipe. *Polymer Testing* 2015, *47*, 42–50, doi:10.1016/j.polymertesting.2015.08.005.

95. Zhang, Y.; Jar, P.-Y.B. Phenomenological Modelling of Tensile Fracture in PE Pipe by Considering Damage Evolution. *Materials & Design* 2015, *77*, 72–82, doi:10.1016/j.matdes.2015.04.011.

96. Zhang, Y.; Ben Jar, P.-Y. Effects of Crosshead Speed on the Quasi-Static Stress–Strain Relationship of Polyethylene Pipes. *Journal of Pressure Vessel Technology* 2017, *139*, 021402, doi:10.1115/1.4033777.

97. Shi, F.; Jar, P.-Y.B. Characterization of Loading, Relaxation, and Recovery Behaviors of High-Density Polyethylene Using a Three-Branch Spring-Dashpot Model. *Polymer Engineering & Science n/a*, doi:10.1002/pen.26891.

98. Kumar, S.; Liu, G.; Schloerb, D.; Srinivasan, M. Viscoelastic Characterization of the Primate Finger Pad In Vivo by Microstep Indentation and Three-Dimensional Finite Element Models for Tactile Sensation Studies. *Journal of biomechanical engineering* 2015, *137*, doi:10.1115/1.4029985.

99. Blake, Y. Review of Viscoelastic Models Applied to Cortical Bone.

100. Heuchel, M.; Cui, J.; Kratz, K.; Kosmella, H.; Lendlein, A. Relaxation Based Modeling of Tunable Shape Recovery Kinetics Observed under Isothermal Conditions for Amorphous Shape-Memory Polymers. *Polymer* 2010, *51*, 6212–6218, doi:10.1016/j.polymer.2010.10.051.

101. López-Guerra, E.A.; Solares, S.D. Modeling Viscoelasticity through Spring–Dashpot Models in Intermittent-Contact Atomic Force Microscopy. *Beilstein J. Nanotechnol.* 2014, *5*, 2149–2163, doi:10.3762/bjnano.5.224.

102. Xu, S.; Odaira, T.; Sato, S.; Xu, X.; Omori, T.; Harjo, S.; Kawasaki, T.; Seiner, H.; Zoubková, K.; Murakami, Y.; et al. Non-Hookean Large Elastic Deformation in Bulk Crystalline Metals. *Nat Commun* 2022, *13*, 5307, doi:10.1038/s41467-022-32930-9.

103. Yang, J.-L.; Zhang, Z.; Schlarb, A.K.; Friedrich, K. On the Characterization of Tensile Creep Resistance of Polyamide 66 Nanocomposites. Part II: Modeling and Prediction of Long-Term Performance. *Polymer* 2006, *47*, 6745–6758, doi:10.1016/j.polymer.2006.07.060.

104. Alves, A.F.C.; Ferreira, B.P.; Andrade Pires, F.M. Constitutive Modeling of Amorphous Thermoplastics from Low to High Strain Rates: Formulation and Critical Comparison Employing an Optimization-Based Parameter Identification. *International Journal of Solids and Structures* 2023, *273*, 112258, doi:10.1016/j.ijsolstr.2023.112258.

105. Laheri, V.; Hao, P.; Gilabert, F.A. Constitutive Recasting of Macromolecular-Based Thermoviscoplasticity as Yield Function-Based Formulation. *International Journal of Mechanical Sciences* 2023, *250*, 108278, doi:10.1016/j.ijmecsci.2023.108278.

106. Teoh, S.H. Effect of Saline Solution on Creep Fracture of Delrin®. *Biomaterials* 1993, *14*, 132–136, doi:10.1016/0142-9612(93)90226-R.

107. Jadhao, V.; Robbins, M.O. Rheological Properties of Liquids under Conditions of Elastohydrodynamic Lubrication 2019.

108. Hong, K. A Model Treating Tensile Deformation of Semi-Crystalline Polymers. PhD Thesis, Verlag nicht ermittelbar, 2005.

109. Tan, N.; Ben Jar, P.-Y. Reanalysis of the Creep Test Data and Failure Behavior of Polyethylene and Its Copolymers. *J. of Materi Eng and Perform* 2022, *31*, 2182–2192, doi:10.1007/s11665-021-06360-5.

110. Halsey, G.; White, H.J.; Eyring, H. Mechanical Properties of Textiles, I. *Textile Research* 1945, *15*, 295–311, doi:10.1177/004051754501500901.

111. Lee, H.-N.; Paeng, K.; Swallen, S.F.; Ediger, M.D. Direct Measurement of Molecular Mobility in Actively Deformed Polymer Glasses. *Science* 2009, *323*, 231–234, doi:10.1126/science.1165995.

112. Ghorbel, E.; Hadriche, I.; Casalino, G.; Masmoudi, N. Characterization of Thermo-Mechanical and Fracture Behaviors of Thermoplastic Polymers. *Materials* 2014, *7*, 375–398, doi:10.3390/ma7010375.

113. Men, Y.; Rieger, J.; Strobl, G. Role of the Entangled Amorphous Network in Tensile Deformation of Semicrystalline Polymers. *Phys. Rev. Lett.* 2003, *91*, 095502, doi:10.1103/PhysRevLett.91.095502.

114. Nitta, K. On a Thermodynamic Foundation of Eyring Rate Theory for Plastic Deformation of Polymer Solids. *Philosophical Magazine Letters* 2023, *103*, 2186190, doi:10.1080/09500839.2023.2186190.

115. Srikanth, K.; Sreejith, P.; Arvind, K.; Kannan, K.; Pandey, M. An Efficient Mode-of-Deformation Dependent Rate-Type Constitutive Relation for Multi-Modal Cyclic Loading of Elastomers. *International Journal of Plasticity* 2023, *163*, 103517, doi:10.1016/j.ijplas.2023.103517.

116. Kakaletsis, S.; Lejeune, E.; Rausch, M.K. Can Machine Learning Accelerate Soft Material Parameter Identification from Complex Mechanical Test Data? *Biomech Model Mechanobiol* 2023, *22*, 57–70, doi:10.1007/s10237-022-01631-z.

117. Klinge, S.; Steinmann, P. Inverse Analysis for Heterogeneous Materials and Its Application to Viscoelastic Curing Polymers. *Comput Mech* 2015, *55*, 603–615, doi:10.1007/s00466-015-1126-5.

118. Polanco-Loria, M.; Daiyan, H.; Grytten, F. Material Parameters Identification: An Inverse Modeling Methodology Applicable for Thermoplastic Materials. *Polymer Engineering & Science* 2012, *52*, 438–448, doi:10.1002/pen.22102.

119. Chen, Z.; Diebels, S.; Peter, N.J.; Schneider, A.S. Identification of Finite Viscoelasticity and Adhesion Effects in Nanoindentation of a Soft Polymer by Inverse Method. *Computational Materials Science* 2013, *72*, 127–139, doi:10.1016/j.commatsci.2013.01.040.

120. Yun, G.J.; Shang, S. A Self-Optimizing Inverse Analysis Method for Estimation of Cyclic Elasto-Plasticity Model Parameters. *International Journal of Plasticity* 2011, *27*, 576–595, doi:10.1016/j.ijplas.2010.08.003.

121. Van Der Vossen, B.C.; Makeev, A.V. Mechanical Properties Characterization of Fiber Reinforced Composites by Nonlinear Constitutive Parameter Optimization in Short Beam Shear Specimens. *Journal of Composite Materials* 2021, *55*, 2985–2997, doi:10.1177/00219983211002238.

122. Saleeb, A.F.; Gendy, A.S.; Wilt, T.E. Parameter-Estimation Algorithms for Characterizing a Class of Isotropic and Anisotropic Viscoplastic Material Models. *Mechanics of Time-Dependent Materials* 2002, *6*, 323–361, doi:10.1023/A:1021268030967.

123. Maier, G.; Bocciarelli, M.; Bolzon, G.; Fedele, R. Inverse Analyses in Fracture Mechanics. *Int J Fract* 2006, *138*, 47–73, doi:10.1007/s10704-006-7153-7.

124. Lyu, Y.; Pathirage, M.; Ramyar, E.; Liu, W.K.; Cusatis, G. Machine Learning Meta-Models for Fast Parameter Identification of the Lattice Discrete Particle Model. *Comput Mech* 2023, *72*, 593–612, doi:10.1007/s00466-023-02320-z.

125. Hoerig, C.; Ghaboussi, J.; Wang, Y.; Insana, M.F. Machine Learning in Model-Free Mechanical Property Imaging: Novel Integration of Physics With the Constrained Optimization Process. *Front. Phys.* 2021, *9*, 600718, doi:10.3389/fphy.2021.600718.

126. Andrade-Campos, A.; Thuillier, S.; Pilvin, P.; Teixeira-Dias, F. On the Determination of Material Parameters for Internal Variable Thermoelastic–Viscoplastic Constitutive Models. *International Journal of Plasticity* 2007, *23*, 1349–1379, doi:10.1016/j.ijplas.2006.09.002.

127. Unger, J.F.; Könke, C. An Inverse Parameter Identification Procedure Assessing the Quality of the Estimates Using Bayesian Neural Networks. *Applied Soft Computing* 2011, *11*, 3357–3367, doi:10.1016/j.asoc.2011.01.007.

128. Xu, H.; Jiang, X. Creep Constitutive Models for Viscoelastic Materials Based on Fractional Derivatives. *Computers & Mathematics with Applications* 2017, *73*, 1377–1384, doi:10.1016/j.camwa.2016.05.002.

129. Van Den Bos, A. Nonlinear Least-Absolute-Values and Minimax Model Fitting. *IFAC Proceedings Volumes* 1985, *18*, 173–177, doi:10.1016/S1474-6670(17)60554-8.

130. Powell, M.J.D. *Approximation Theory and Methods*; Cambridge University Press: Cambridge [Eng.] ; New York, 1981; ISBN 978-0-521-22472-7.

131. Setiyoko, A.; Basaruddin, T.; Arymurthy, A.M. Minimax Approach for Semivariogram Fitting in Ordinary Kriging. *IEEE Access* 2020, *8*, 82054–82065, doi:10.1109/ACCESS.2020.2991428.

132. Boutaleb, S.; Zaïri, F.; Mesbah, A.; Naït-Abdelaziz, M.; Gloaguen, J.M.; Boukharouba, T.; Lefebvre, J.M. Micromechanics-Based Modelling of Stiffness and Yield Stress for Silica/Polymer Nanocomposites. *International Journal of Solids and Structures* 2009, *46*, 1716–1726, doi:10.1016/j.ijsolstr.2008.12.011.

133. Khan, A.S.; Lopez-Pamies, O.; Kazmi, R. Thermo-Mechanical Large Deformation Response and Constitutive Modeling of Viscoelastic Polymers over a Wide Range of Strain Rates and Temperatures. *International Journal of Plasticity* 2006, *22*, 581–601, doi:10.1016/j.ijplas.2005.08.001.

134. Kemmer, G.; Keller, S. Nonlinear Least-Squares Data Fitting in Excel Spreadsheets. *Nat Protoc* 2010, *5*, 267–281, doi:10.1038/nprot.2009.182.

135. Paetzold, M.; Andert, T.P.; Asmar, S.W.; Anderson, J.D.; Barriot, J.-P.; Bird, M.K.; Haeusler, B.; Hahn, M.; Tellmann, S.; Sierks, H.; et al. Asteroid 21 Lutetia: Low Mass, High Density. *Science* 2011, *334*, 491–492, doi:10.1126/science.1209389.

136. Messager, M.L.; Lehner, B.; Grill, G.; Nedeva, I.; Schmitt, O. Estimating the Volume and Age of Water Stored in Global Lakes Using a Geo-Statistical Approach. *Nat Commun* 2016, *7*, 13603, doi:10.1038/ncomms13603.

137. Sprave, L.; Menzel, A. A Large Strain Gradient-Enhanced Ductile Damage Model: Finite Element Formulation, Experiment and Parameter Identification. *Acta Mech* 2020, *231*, 5159–5192, doi:10.1007/s00707-020-02786-5.

138. Sweeney, J. A Comparison of Three Polymer Network Models in Current Use. *Computational and Theoretical Polymer Science* 1999, *9*, 27–33.

139. Mahnken, R.; Stein, E. Parameter Identification for Viscoplastic Models Based on Analytical Derivatives of a Least-Squares Functional and Stability Investigations. *International Journal of Plasticity* 1996, *12*, 451–479, doi:10.1016/S0749-6419(95)00016-X.

140. Khan, A.; Zhang, H. Finite Deformation of a Polymer: Experiments and Modeling. *International Journal of Plasticity* 2001, *17*, 1167–1188, doi:10.1016/S0749-6419(00)00073-5.

141. Zhang, C.; Cai, L.-H.; Guo, B.-H.; Miao, B.; Xu, J. New Kinetics Equation for Stress Relaxation of Semi-Crystalline Polymers below Glass Transition Temperature. *Chinese Journal of Polymer Science* 2022, *40*, 1662–1669.

142. Ayoub, G.; Zaïri, F.; Fréderix, C.; Gloaguen, J.M.; Naït-Abdelaziz, M.; Seguela, R.; Lefebvre, J.M. Effects of Crystal Content on the Mechanical Behaviour of Polyethylene under Finite Strains: Experiments and Constitutive Modelling. *International Journal of Plasticity* 2011, *27*, 492–511, doi:10.1016/j.ijplas.2010.07.005.

143. Drozdov, A.D.; Klitkou, R.; Christiansen, J. deC. Multi-Cycle Deformation of Semicrystalline Polymers: Observations and Constitutive Modeling. *Mechanics Research Communications* 2013, *48*, 70–75, doi:10.1016/j.mechrescom.2013.01.001.

144. Kubát, J.; Seldén, R. The Stress Dependence of Activation Volumes in Creep and Stress Relaxation. *Materials Science and Engineering* 1978, *36*, 65–69, doi:10.1016/0025-5416(78)90195-7.

145. Syrjakow, M.; Szczerbicka, H. Efficient Parameter Optimization Based on Combination of Direct Global and Local Search Methods. In *Evolutionary Algorithms*; Davis, L.D., De Jong,

K., Vose, M.D., Whitley, L.D., Eds.; The IMA Volumes in Mathematics and its Applications; Springer New York: New York, NY, 1999; Vol. 111, pp. 227–249 ISBN 978-1-4612-7185-7.

146. Renders, J.-M.; Flasse, S.P. Hybrid Methods Using Genetic Algorithms for Global Optimization. *IEEE Transactions on Systems, Man, and Cybernetics, Part B (Cybernetics)* 1996, *26*, 243–258, doi:10.1109/3477.485836.

147. Mahinthakumar, G. (Kumar); Sayeed, M. Hybrid Genetic Algorithm—Local Search Methods for Solving Groundwater Source Identification Inverse Problems. *J. Water Resour. Plann. Manage.* 2005, *131*, 45–57, doi:10.1061/(ASCE)0733-9496(2005)131:1(45).

148. Maaranen, H.; Miettinen, K.; Penttinen, A. On Initial Populations of a Genetic Algorithm for Continuous Optimization Problems. *J Glob Optim* 2007, *37*, 405–436, doi:10.1007/s10898-006-9056-6.

149. Yen, J.; Liao, J.C.; Lee, B.; Randolph, D. A Hybrid Approach to Modeling Metabolic Systems Using a Genetic Algorithm and Simplex Method. *IEEE Transactions on Systems, Man, and Cybernetics, Part B (Cybernetics)* 1998, *28*, 173–191, doi:10.1109/3477.662758.

150. Ahn, C.W.; Ramakrishna, R.S. A Genetic Algorithm for Shortest Path Routing Problem and the Sizing of Populations. *IEEE Transactions on Evolutionary Computation* 2002, *6*, 566–579, doi:10.1109/TEVC.2002.804323.

151. Pál, K.F. Genetic Algorithm with Local Optimization. *Biol. Cybern.* 1995, *73*, 335–341, doi:10.1007/BF00199469.

152. Okamoto, M.; Nonaka, T.; Ochiai, S.; Tominaga, D. Nonlinear Numerical Optimization with Use of a Hybrid Genetic Algorithm Incorporating the Modified Powell Method. *Applied Mathematics and Computation* 1998, *91*, 63–72, doi:10.1016/S0096-3003(97)10007-8.

153. Crain, T.; Bishop, R.H.; Fowler, W.; Rock, K. Interplanetary Flyby Mission Optimization Using a Hybrid Global-Local Search Method. *Journal of Spacecraft and Rockets* 2012, doi:10.2514/2.3607.

154. Attaviriyanupap, P.; Kita, H.; Tanaka, E.; Hasegawa, J. A Hybrid EP and SQP for Dynamic Economic Dispatch with Nonsmooth Fuel Cost Function. *IEEE Transactions on Power Systems* 2002, *17*, 411–416, doi:10.1109/TPWRS.2002.1007911.

155. Henz, B.J.; Mohan, R.V.; Shires, D.R. A Hybrid Global–Local Approach for Optimization of Injection Gate Locations in Liquid Composite Molding Process Simulations. *Composites Part A: Applied Science and Manufacturing* 2007, *38*, 1932–1946, doi:10.1016/j.compositesa.2007.03.005.

156. Le, T.M.; Fatahi, B. Trust-Region Reflective Optimisation to Obtain Soil Visco-Plastic Properties. *Engineering Computations* 2016, *33*, doi:10.1108/EC-11-2014-0236.

157. Schmidt, U.; Mergheim, J.; Steinmann, P. Multiscale Parameter Identification. *Int J Mult Comp Eng* 2012, *10*, 327–342, doi:10.1615/IntJMultCompEng.2012002175.

158. Ramzanpour, M.; Hosseini-Farid, M.; Ziejewski, M.; Karami, G. Particle Swarm Optimization Method for Hyperelastic Characterization of Soft Tissues.

159. Pereira, J.O.; Farias, T.M.; Castro, A.M.; (Al-Baldawi), A.A.; Secchi, A.R.; Cardozo, N.S.M. Estimation of the Nonlinear Parameters of Viscoelastic Constitutive Models Using CFD

and Multipass Rheometer Data. *Journal of Non-Newtonian Fluid Mechanics* 2020, *281*, 104284, doi:10.1016/j.jnnfm.2020.104284.

160. Wu, L.; Chen, Z.; Long, C.; Cheng, S.; Lin, P.; Chen, Y.; Chen, H. Parameter Extraction of Photovoltaic Models from Measured I-V Characteristics Curves Using a Hybrid Trust-Region Reflective Algorithm. *Applied Energy* 2018, *232*, 36–53, doi:10.1016/j.apenergy.2018.09.161.

161. Nenov, Hr.B.; Dimitrov, B.Hr.; Marinov, A.St. Algorithms for Computational Procedure Acceleration for Systems Differential Equations in Matlab. In Proceedings of the 2013 36th International Convention on Information and Communication Technology, Electronics and Microelectronics (MIPRO); May 2013; pp. 238–242.

162. Rivard, S.R.; Mailloux, J.-G.; Beguenane, R.; Bui, H.T. Design of High-Performance Parallelized Gene Predictors in MATLAB. *BMC Res Notes* 2012, *5*, 183, doi:10.1186/1756-0500-5-183.

163. Tan, N. Deformation Transitions and Their Effects on the Long-Term Performance of Polyethylene and Its Pressure Pipe. 172.

164. Zheng, J.; Li, H.; Hogan, J.D. Strain-Rate-Dependent Tensile Response of an Alumina Ceramic: Experiments and Modeling. *International Journal of Impact Engineering* 2023, *173*, 104487, doi:10.1016/j.ijimpeng.2022.104487.

165. Zheng, J.; Li, H.; Hogan, J.D. Advanced Tensile Fracture Analysis of Alumina Ceramics: Integrating Hybrid Finite-Discrete Element Modeling with Experimental Insights. *Engineering Fracture Mechanics* 2024, *302*, 110075, doi:10.1016/j.engfracmech.2024.110075.

166. Jar, P.-Y.B. Effect of Tensile Loading History on Mechanical Properties for Polyethylene. *Polym Eng Sci* 2015, *55*, 2002–2010, doi:10.1002/pen.24042.

167. Zheng, J.; Ji, M.; Zaiemyekeh, Z.; Li, H.; Hogan, J.D. Strain-Rate-Dependent Compressive and Compression-Shear Response of an Alumina Ceramic. *Journal of the European Ceramic Society* 2022, *42*, 7516–7527, doi:10.1016/j.jeurceramsoc.2022.09.004.

168. Fritsch, J.; Hiermaier, S.; Strobl, G. Characterizing and Modeling the Non-Linear Viscoelastic Tensile Deformation of a Glass Fiber Reinforced Polypropylene. *Composites Science and Technology* 2009, *69*, 2460–2466, doi:10.1016/j.compscitech.2009.06.021.

169. Rafiee, R.; Mazhari, B. Simulation of the Long-Term Hydrostatic Tests on Glass Fiber Reinforced Plastic Pipes. *Composite Structures* 2016, *136*, 56–63, doi:10.1016/j.compstruct.2015.09.058.

170. Ebert, C.; Hufenbach, W.; Langkamp, A.; Gude, M. Modelling of Strain Rate Dependent Deformation Behaviour of Polypropylene. *Polymer Testing* 2011, *30*, 183–187, doi:10.1016/j.polymertesting.2010.11.011.

171. Graba, M. Evaluation of Measurement Uncertainty in a Static Tensile Test. *Open Engineering* 2021, *11*, 709–722, doi:10.1515/eng-2021-0069.

172. Mulliken, A.D.; Boyce, M.C. Mechanics of the Rate-Dependent Elastic–Plastic Deformation of Glassy Polymers from Low to High Strain Rates. *International Journal of Solids and Structures* 2006, *43*, 1331–1356, doi:10.1016/j.ijsolstr.2005.04.016.

173. Jar, P.B. Revisiting Creep Test on Polyethylene Pipe—Data Analysis and Deformation Mechanisms. *Polym Eng Sci* 2021, *61*, 586–599, doi:10.1002/pen.25603.

174. A G Piyal Aravinna Estimation of Measurement Uncertainty in Determination of Tensile Strength of Reinforcement Steel. 2021, doi:10.13140/RG.2.2.14541.77287.

175. Hong, K.; Rastogi, A.; Strobl, G. A Model Treating Tensile Deformation of Semicrystalline Polymers: Quasi-Static Stress- Strain Relationship and Viscous Stress Determined for a Sample of Polyethylene. *Macromolecules* 2004, *37*, 10165–10173.

176. Richeton, J.; Ahzi, S.; Daridon, L.; Rémond, Y. A Formulation of the Cooperative Model for the Yield Stress of Amorphous Polymers for a Wide Range of Strain Rates and Temperatures. *Polymer* 2005, *46*, 6035–6043, doi:10.1016/j.polymer.2005.05.079.

177. Bergstrom, J.; Boyce, M.C. Constitutive Modeling of the Large Strain Time-Dependent Behavior of Elastomers. *Journal of the Mechanics and Physics of Solids* 1998, *46*, 931–954, doi:10.1016/S0022-5096(97)00075-6.

178. Natarajan, V.D. *Constitutive Behavior of a Twaron® Fabric/Natural Rubber Composite: Experiments and Modeling*; 2011;

179. Popa, C.M.; Fleischhauer, R.; Schneider, K.; Kaliske, M. Formulation and Implementation of a Constitutive Model for Semicrystalline Polymers. *International Journal of Plasticity* 2014, *61*, 128–156, doi:10.1016/j.ijplas.2014.05.010.

180. Jar, P. -Y. B. Analysis of Time-dependent Mechanical Behavior of Polyethylene. *SPE Polymers* 2024, *5*, 426–443, doi:10.1002/pls2.10134.

181. Pyrz, M.; Zairi, F. Identification of Viscoplastic Parameters of Phenomenological Constitutive Equations for Polymers by Deterministic and Evolutionary Approach. *Modelling Simul. Mater. Sci. Eng.* 2007, *15*, 85–103, doi:10.1088/0965-0393/15/2/006.

182. Zhang, Y.; Jar, P.-Y.B. Comparison of Mechanical Properties Between PE80 and PE100 Pipe Materials. *J. of Materi Eng and Perform* 2016, *25*, 4326–4332, doi:10.1007/s11665-016-2274-2.

183. Liu, X.; Zhang, H.; Xia, M.; Wu, K.; Chen, Y.; Zheng, Q.; Li, J. Mechanical Response of Buried Polyethylene Pipelines under Excavation Load during Pavement Construction. *Engineering Failure Analysis* 2018, *90*, 355–370, doi:10.1016/j.engfailanal.2018.03.027.

184. Zhang, C.; Moore, I.D. Nonlinear Mechanical Response of High Density Polyethylene. Part II: Uniaxial Constitutive Modeling. *Polym. Eng. Sci.* 1997, *37*, 414–420, doi:10.1002/pen.11684.

185. Zhang, C.; Moore, I.D. Nonlinear Mechanical Response of High Density Polyethylene. Part I: Experimental Investigation and Model Evaluation. *Polymer Engineering & Science* 1997, *37*, 404–413, doi:10.1002/pen.11683.

186. Moore, I. Profiled HDPE Pipe Response to Parallel Plate Loading. In *Buried Plastic Pipe Technology: 2nd Volume*; Eckstein, D., Ed.; ASTM International: 100 Barr Harbor Drive, PO Box C700, West Conshohocken, PA 19428-2959, 1994; pp. 25-25–16 ISBN 978-0-8031-1992-5.

187. Whelton, A. J.; Dietrich, A. M.; Gallagher, D. L. Contaminant Diffusion, Solubility, and Material Property Differences between HDPE and PEX Potable Water Pipes. *Journal of Environmental Engineering* 2010, 136 (2), 227–237, doi:10.1061/(ASCE)EE.1943-7870.0000147.

Chapter 5 Conclusions and future work

Chapter 5 concludes all the findings in this study and summarizes the future work.

5.1 Key conclusions

The primary goal of this research is to develop a novel RR test method, construct spring-dashpot models, and identify the unique model parameter values for the characterization of SCPs under tensile deformation. In this study, a new RR test, including cyclic stages of stress relaxation and recovery with increasing deformation, was proposed. The proposed RR test could generate a very small hysteresis loop for the unloading curve before recovery and loading curve after recovery. Unusual stress drop was found at the end of recovery behavior. Based on the Eyring's law, four nonlinear viscoelastic models, that is, the standard model, Parallel model, Series model, and three-branch model were constructed and examined for the analysis of the RR test results. It was found that only the three-branch spring-dashpot model could mimic closely the unusual stress drop at the recovery stages. The study concludes that the three-branch model can serve as a suitable tool for analyzing the mechanical properties of HDPE, and values for the model parameters can potentially be used to characterize the difference among PEs for their mechanical performance. Computer programs were developed to automatically determine model parameter values. Additionally, a novel analytical approach based on global optimization and local optimization was introduced for the determination of unique and accurate model parameter values as functions of deformation.

(1) Characterization of time-dependent behavior using RR tests and examination of two-branch models

A novel RR test was developed, featuring multiple cycles with six stages per cycle. The test was designed to separate the viscous component from the quasi-static counterpart during deformation. The study found that the typical hysteresis loop observed from loading-unloading of polymeric materials is hardly visible between the unloading stage before the recovery stage and

the initial loading stage after the recovery stage in the RR test. By combining springs and Eyring's dashpots, three models were constructed, which were evaluated for their ability to analyze the RR test results. The study found that the standard model could not closely reproduce the stress response during the entire relaxation stage of 10,000 s, but, the Parallel and the Series models could. The standard model could determine the long-term performance of PE and identify a transition point representing the onset of plastic deformation in the crystalline phase. Despite this, none of the three models was able to mimic the stress drop at the end of recovery phase after the maximum point.

The viscous and quasi-static stress responses of two HDPEs were characterized using the RR test, with data analysis based on three models. Stiffness calculated for each unloading stage demonstrates that the RR test has the advantage for determining the total stiffness of the materials at different deformation levels, making it useful for evaluating the mechanical performance of PE. The study demonstrates that the RR test provides a comprehensive data set that can assess the suitability of spring-dashpot models for characterizing both the time-dependent and time-independent mechanical performance of PE, and the possibility of determining the activation energies for deformation at the stress relaxation stages.

(2) Construction of three-branch spring-dashpot model and determination of the range for the model parameter values using RR tests

The study demonstrates that stress response at various stages of the RR test could be simulated very closely using the proposed three-branch model, including the unusual stress response at the end of recovery stages, with the maximum difference between observed data from experiments and simulation data from the model within 0.08 MPa. The fitting parameters $\sigma_{v,L}(0)$ and

$\sigma_{0,L}$ for the relaxation stages exhibit the same transitions in the trend of change with increasing deformation. On the other hand, the corresponding fitting parameters for the short-term viscous branch, $\sigma_{v,S}(0)$ and $\sigma_{0,S}$, showed no indication of a transition at either the relaxation or the recovery stages. This suggests that the transition indicated by the long-term branch could represent some deformation mechanism not captured by the short-term branch.

The study also shows that σ_{qs} as a function of stroke is highly consistent among predictions based on the ten sets of fitting parameter values, with the stroke for the maximum σ_{qs} closely aligning with the stroke for the yield point based on $\sigma_A(0)$. Additionally, values for $K_{v,L}$ as a function of stroke, determined using stress variation at the loading stages, showed the trend of change that indicates the occurrence of degradation from the early stage of the RR test.

Another key finding is that stress drop at the relaxation stages in the long-term viscous branch could continue after the end of the relaxation stages, which contributed to the stress variation at the following recovery stages. Stress drop in the short-term viscous branch, on the other hand, ceased before the end of the relaxation stages, similarly for its stress increase at the recovery stages. Therefore, the conventional concept for the stress response of polymers, that is, stress drop after loading and stress increase after unloading, represents only part of the stress response of HDPE to deformation, which could be represented by the short-term viscous branch of the three-branch spring-dashpot model. The long-term viscous branch showed stress drop during both the relaxation and recovery stages, offering a reasonable explanation for the 'abnormal' stress drop observed during the stress recovery that has been reported in the literature.

The study demonstrates that the three-branch spring-dashpot model is capable of describing the stress response of HDPE under complex deformation conditions. The proposed data analysis has successfully separated the applied stress into quasi-static, long-term viscous, and short-term viscous components during the deformation. The algorithms developed in the study enabled the rapid determination of ten sets of model parameter values, allowing the assessment of the variation range of these parameter.

(3) A novel approach to narrow down the variation of the model parameter values for the characterization of PE and its pipes

This study introduces a new analysis method based on the global and local optimization for the description of relaxation, recovery, and loading behaviors of PE and its pipes in the RR tests on cylindrical and NPR specimens. The three-branch model, with parameter values determined through the proposed analysis approach, accurately reproduce the results of the RR tests, and the maximum difference of stress response between the experimental data and the data generated from the model is significantly smaller than values from the results in the literature.

Using the proposed analysis method, 1000 sets of fitting parameter values were determined to mimic closely stress response as functions of time at the relaxation stages for different deformation levels, with the discrepancy of stress values between the observed data from experiments and simulation data from the model below 0.08 MPa. The 1000 sets of parameter values indicate that the $\sigma_{v,L}(0)$ values follow two distinct paths as the deformation level increases. Results from the best five fits demonstrate that the proposed method can determine consistent values and a clear trend for $\sigma_{v,L}(0)$, $\sigma_{v,S}(0)$, $\sigma_{0,L}$ and $\sigma_{0,S}$. The results also indicate that the proposed analysis method is better than any of the method reported in the literature on parameter identification of

spring-dashpot models. Results suggest that it is possible to determine a unique set of parameter values, which can then be used to characterize the viscous and quasi-static components of mechanical behavior for SCPs. It was also found that variations of the characteristic relaxation time have little impact on the variation of other fitting parameter values.

Without taking account of the resolution of the test setup using in this study, the proposed analysis approach allows the selection of the best five sets of parameter values to accurately predict changes in viscous behavior as deformation increases. The study also confirms that $K_{v,L}$ values for PE should be bigger than the $K_{v,S}$ at the same stroke.

Overall, a unique set parameter values could be identified, if the experimental data have a sufficiently high resolution to minimize uncertainty of the test results. With such experimental data, it is then possible to investigate the relationship between these parameters and microstructural changes in PE during the deformation. This study provides a reliable tool to determine the unique model parameter values for a three-branch model, if such values exist.

5.2 Future work

Overall, the research work presented in this thesis provided a novel experimental test method, RR test method, spring-dashpot models, and a novel approach for the determination of model parameter values. However, further research is needed to reveal the relation between the microstructures of the SCPs and the model parameter values.

(1) To Improve the three-branch spring-dashpot model to reproduce experimental data from creep tests on PEs

Halsey et al. [1] first proposed that the Eyring's equation can be applied to simulate the creep behavior of polymers. Hong et al. [2,3] used to describe the relaxation and creep behavior of SCPs using a spring-dashpot model with one Eyring's process. However, Tan and Jar [4,5] found standard model with one Eyring's process is not adequate to fully describe the relaxation behavior from 1 s to 10000 s of PEs. It is necessary to allow the proposed spring-dashpot model to describe more time-dependent behaviors. Simple creep tests after tensile loading will be conducted to obtain the creep data. The proposed spring-dashpot model's suitability to simulate deformation behavior in a creep mode will be evaluated, and if necessary modified. Eyring's parameters, the springs' stiffnesses, and the quasi-static stress as a function of deformation, which are calibrated from the analysis of RR tests, will be applied for the modelling of the creep tests. Additional elements (springs or dashpots) may be required for the proposed model to fully describe the creep behavior. Finally, the proposed model will be able to reproduce the experimental data of the creep tests on PEs.

(2) To develop multiple-creep tests using SCPs, and to use the results to verify the prediction ability of the spring-dashpot model

In literature, Dusunceli used the multiple-unloading-creep test to verify the VBOP model. However, this test only took into account the creep behavior after the unloading phase, and the creep behavior after the loading phase can be different from the creep behavior after the unloading phase. In future work, a multiple-creep test will be developed and used to investigate the creep behavior under different stress levels. Firstly, a new model examined by creep test will be used to predict the experimental data in the multiple-creep tests on PE. Closeness of data generated from the model to the experimental data will be

examined to verify prediction ability of the model. An expected stress-time relationship for a multiple-creep test is shown in Figure 5.1.

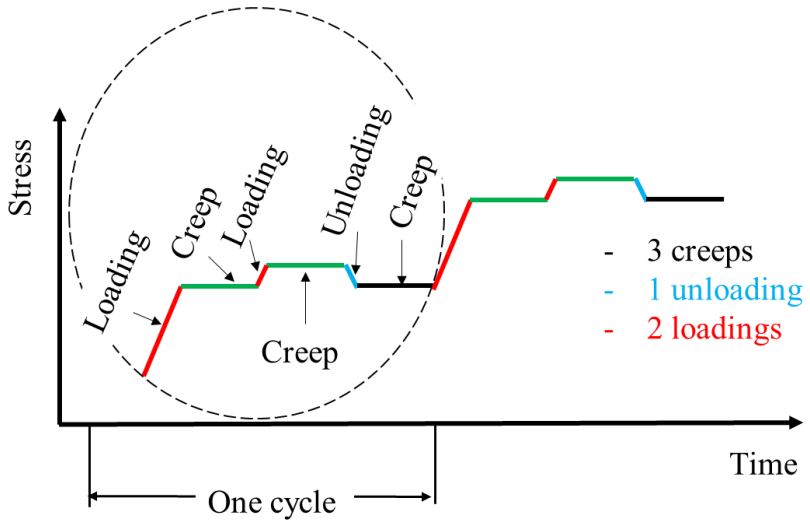

Figure 5.1. Schematic of multiple-creep test, and stress profile as a function of time.

Again, the multiple-creep test contains 6 loading modes in one cycle, including 2 loadings, 3 creeps, and 1 unloading, which are repeated cyclically to cover a wide range of stress levels, and could continue till the specimen fails through large deformation or fracture. Different types of specimens will be prepared and tested to check the difference between the experimental data and the model prediction. The prediction results will be compared to measurements and data in the literature.

(3) To improve the resolution of the experimental data for the determination of more accurate model parameter values to characterize SCPs

The current study confirms that simulation generated by the current method is consistent with the experiment within the limits of the measurement precision. However, it also indicates that

the experimental resolution should be improved to detect finer discrepancies. Advanced measurement tools and techniques with higher precision will be used to collect experimental data. This could involve the use of more sensitive sensors, high-resolution imaging, or advanced data acquisition systems to reduce noise and increase the accuracy of recorded stress and deformation data. It is also important to extend the application of the improved resolution techniques to a broader range of SCPs to validate the generalizability of the method. By applying the method to different types of SCPs, the robustness of the model parameters and the method's ability to characterize diverse materials can be assessed.

References

1. Halsey, G.; White, H.J.; Eyring, H. Mechanical Properties of Textiles, I. *Textile Research* 1945, *15*, 295–311, doi:10.1177/004051754501500901.

2. Hong, K.; Rastogi, A.; Strobl, G. Model Treatment of Tensile Deformation of Semicrystalline Polymers: Static Elastic Moduli and Creep Parameters Derived for a Sample of Polyethylene. *Macromolecules* 2004, *37*, 10174–10179, doi:10.1021/ma049172x.

3. Hong, K.; Rastogi, A.; Strobl, G. A Model Treating Tensile Deformation of Semicrystalline Polymers: Quasi-Static Stress−Strain Relationship and Viscous Stress Determined for a Sample of Polyethylene. *Macromolecules* 2004, *37*, 10165–10173, doi:10.1021/ma049174h.

4. Tan, N.; Jar, P.-Y.B. Determining Deformation Transition in Polyethylene under Tensile Loading. *Polymers* 2019, *11*, 1415, doi:10.3390/polym11091415.

5. Tan, N.; Jar, P.B. Multi-Relaxation Test to Characterize PE Pipe Performance. *Plastics Engineering* 2019, *75*, 40–45, doi:10.1002/peng.20184.

Bibliography

Sparks, T.D.; Banerjee, D. Materials Informatics and Polymer Science: Pushing the Frontiers of Our Understanding. Matter 2021, 4, 1454–1456, doi:10.1016/j.matt.2021.04.003.

Stepto, R.; Horie, K.; Kitayama, T.; Abe, A. Mission and challenges of polymer science and technology. Pure and Applied Chemistry 2003, 75, 1359–1369, doi:10.1351/pac200375101359.

Men, Y. Critical Strains Determine the Tensile Deformation Mechanism in Semicrystalline Polymers. Macromolecules 2020, 53, 9155–9157, doi:10.1021/acs.macromol.0c02076.

Felder, S.; Holthusen, H.; Hesseler, S.; Pohlkemper, F.; Gries, T.; Simon, J.-W.; Reese, S. Incorporating Crystallinity Distributions into a Thermo-Mechanically Coupled Constitutive Model for Semi-Crystalline Polymers. International Journal of Plasticity 2020, 135, 102751, doi:10.1016/j.ijplas.2020.102751.

Farge, L.; Boisse, J.; Dillet, J.; André, S.; Albouy, P.-A.; Meneau, F. Wide-Angle X-Ray Scattering Study of the Lamellar/Fibrillar Transition for a Semi-Crystalline Polymer Deformed in Tension in Relation with the Evolution of Volume Strain. J. Polym. Sci. Part B: Polym. Phys. 2015, 53, 1470–1480, doi:10.1002/polb.23790.

Uchida, M.; Tada, N. Micro-, Meso- to Macroscopic Modeling of Deformation Behavior of Semi-Crystalline Polymer. International Journal of Plasticity 2013, 49, 164–184, doi:10.1016/j.ijplas.2013.03.007.

Garcia-Gonzalez, D.; Zaera, R.; Arias, A. A Hyperelastic-Thermoviscoplastic Constitutive Model for Semi-Crystalline Polymers: Application to PEEK under Dynamic Loading Conditions. International Journal of Plasticity 2017, 88, 27–52, doi:10.1016/j.ijplas.2016.09.011.

Hao, P.; Laheri, V.; Dai, Z.; Gilabert, F.A. A Rate-Dependent Constitutive Model Predicting the Double Yield Phenomenon, Self-Heating and Thermal Softening in Semi-Crystalline Polymers. International Journal of Plasticity 2022, 153, 103233, doi:10.1016/j.ijplas.2022.103233.

Li, C.Y. The Rise of Semicrystalline Polymers and Why Are They Still Interesting. Polymer 2020, 211, 123150, doi:10.1016/j.polymer.2020.123150.

Regrain, C.; Laiarinandrasana, L.; Toillon, S.; Saï, K. Multi-Mechanism Models for Semi-Crystalline Polymer: Constitutive Relations and Finite Element Implementation. International Journal of Plasticity 2009, 25, 1253–1279, doi:10.1016/j.ijplas.2008.09.010.

Dusunceli, N.; Colak, O.U. Modelling Effects of Degree of Crystallinity on Mechanical Behavior of Semicrystalline Polymers. International Journal of Plasticity 2008, 24, 1224–1242, doi:10.1016/j.ijplas.2007.09.003.

Yeh, I.-C.; Andzelm, J.W.; Rutledge, G.C. Mechanical and Structural Characterization of Semicrystalline Polyethylene under Tensile Deformation by Molecular Dynamics Simulations. Macromolecules 2015, 48, 4228–4239, doi:10.1021/acs.macromol.5b00697.

Yang, X.; Sun, Y.; Liao, T.; Men, Y. Strain Dependent Evolution of Structure and Stress in Propylene-Based Elastomer during Stress Relaxation. Polymer 2020, 201, 122612, doi:10.1016/j.polymer.2020.122612.

Khan, F.; Yeakle, C. Experimental Investigation and Modeling of Non-Monotonic Creep Behavior in Polymers. International Journal of Plasticity 2011, 27, 512–521, doi:10.1016/j.ijplas.2010.06.007.

Lendlein, A.; Langer, R. Biodegradable, Elastic Shape-Memory Polymers for Potential Biomedical Applications. Science 2002, 296, 1673–1676, doi:10.1126/science.1066102.

Lendlein, A.; Gould, O.E. Reprogrammable Recovery and Actuation Behaviour of Shape-Memory Polymers. Nature Reviews Materials 2019, 4, 116–133.

Leterrier, Y. Durability of Nanosized Oxygen-Barrier Coatings on Polymers. Progress in materials science 2003, 48, 1–55.

Hutař, P.; Ševčík, M.; Frank, A.; Náhlík, L.; Kučera, J.; Pinter, G. The Effect of Residual Stress on Polymer Pipe Lifetime. Engineering Fracture Mechanics 2013, 108, 98–108, doi:10.1016/j.engfracmech.2013.04.014.

Kartalis, C.N.; Papaspyrides, C.D.; Pfaendner, R. Recycling of Post-Used PE Packaging Film Using the Restabilization Technique. Polymer Degradation and Stability 2000, 70, 189–197, doi:10.1016/S0141-3910(00)00106-3.

Hou, S.; Qi, S.; Hutt, D.A.; Tyrer, J.R.; Mu, M.; Zhou, Z. Three Dimensional Printed Electronic Devices Realised by Selective Laser Melting of Copper/High-Density-Polyethylene Powder Mixtures. Journal of Materials Processing Technology 2018, 254, 310–324, doi:10.1016/j.jmatprotec.2017.11.020.

Sobhan, K.; Mashnad, M. Tensile Strength and Toughness of Soil–Cement–Fly-Ash Composite Reinforced with Recycled High-Density Polyethylene Strips. Journal of Materials in Civil Engineering 2002, 14, 177–184, doi:10.1061/(ASCE)0899-1561(2002)14:2(177).

Cha, J.-H.; Kim, Y.; Sathish Kumar, S.K.; Choi, C.; Kim, C.-G. Ultra-High-Molecular-Weight Polyethylene as a Hypervelocity Impact Shielding Material for Space Structures. Acta Astronautica 2020, 168, 182–190, doi:10.1016/j.actaastro.2019.12.008.

Zaribaf, F.P. Medical-Grade Ultra-High Molecular Weight Polyethylene: Past, Current and Future. Materials Science and Technology 2018, 34, 1940–1953, doi:10.1080/02670836.2018.1469455.

Patil, A.; Patel, A.; Purohit, R. An Overview of Polymeric Materials for Automotive Applications. Materials Today: Proceedings 2017, 4, 3807–3815, doi:10.1016/j.matpr.2017.02.278.

Barba, D.; Arias, A.; Garcia-Gonzalez, D. Temperature and Strain Rate Dependences on Hardening and Softening Behaviours in Semi-Crystalline Polymers: Application to PEEK. International Journal of Solids and Structures 2020, 182–183, 205–217, doi:10.1016/j.ijsolstr.2019.08.021.

Ayoub, G.; Zaïri, F.; Naït-Abdelaziz, M.; Gloaguen, J.M. Modelling Large Deformation Behaviour under Loading–Unloading of Semicrystalline Polymers: Application to a High Density Polyethylene. International Journal of Plasticity 2010, 26, 329–347, doi:10.1016/j.ijplas.2009.07.005.

Atiq, O.; Ricci, E.; Baschetti, M.G.; De Angelis, M.G. Modelling Solubility in Semi-Crystalline Polymers: A Critical Comparative Review. Fluid Phase Equilibria 2022, 556, 113412, doi:10.1016/j.fluid.2022.113412.

Nunes dos Santos, W.; Augusto Marcondes Agnelli, J.; Mummery, P.; Wallwork, A. Effect of Recycling on the Thermal Properties of Polymers. Polymer Testing 2007, 26, 216–221, doi:10.1016/j.polymertesting.2006.10.004.

Miaudet, P.; Derre, A.; Maugey, M.; Zakri, C.; Piccione, P.M.; Inoubli, R.; Poulin, P. Shape and Temperature Memory of Nanocomposites with Broadened Glass Transition. Science 2007, 318, 1294–1296.

Li, Y.; He, Y.; Liu, Z. A Viscoelastic Constitutive Model for Shape Memory Polymers Based on Multiplicative Decompositions of the Deformation Gradient. International Journal of Plasticity 2017, 91, 300–317, doi:10.1016/j.ijplas.2017.04.004.

Liu, P.; Peng, L.; Chen, J.; Yang, B.; Chen, Y.; Luo, Z.; Han, C.C.; Huang, X.; Men, Y. Tensile Creep Failure of Isotactic Polypropylene under the Strain Criterion. Macromolecules 2022, 55, 9663–9670, doi:10.1021/acs.macromol.2c01263.

Xu, S.; Zhou, J.; Pan, P. Strain-Induced Multiscale Structural Evolutions of Crystallized Polymers: From Fundamental Studies to Recent Progresses. Progress in Polymer Science 2023, 101676.

Sedighiamiri, A.; Govaert, L.E.; Kanters, M.J.W.; van Dommelen, J.A.W. Micromechanics of Semicrystalline Polymers: Yield Kinetics and Long-Term Failure. J. Polym. Sci. B Polym. Phys. 2012, 50, 1664–1679, doi:10.1002/polb.23136.

Lim, S.D.; Rhee, J.M.; Nah, C. Predicting the Long-Term Creep Behavior of Plastics Using the Short-Term Creep Test. 2004, 7.

Kubát, J. Stress Relaxation in Solids. Nature 1965, 205, 378–379.

Janssen, R. Deformation and Failure in Semi-Crystalline Polymer Systems. 53.

Malpass, V.E. Prediction of Long-Term ABS Relaxation Behavior. Journal of Applied Polymer Science 1968, 12, 771–788, doi:10.1002/app.1968.070120415.

Moser, A.P.; Folkman, S.L. Buried Pipe Design; 3rd ed.; McGraw-Hill: New York, 2008; ISBN 978-0-07-147689-8.

Moser, A.P. Structural Performance of Buried Profile-Wall High-Density Polyethylene Pipe and Influence of Pipe Wall Geometry. Transportation Research Record 1998, 1624, 206–213, doi:10.3141/1624-24.

Frank, A.; Pinter, G.; Lang, R.W. Prediction of the Remaining Lifetime of Polyethylene Pipes after up to 30 Years in Use. Polymer Testing 2009, 28, 737–745, doi:10.1016/j.polymertesting.2009.06.004.

Frank, A.; Berger, I.J.; Arbeiter, F.; Hutař, P.; Pinter, G. Lifetime Prediction of PE100 and PE100-RC Pipes Based on Slow Crack Growth Resistance. 2016, doi:10.13140/RG.2.2.27467.80165.

Hoàng, E.M.; Lowe, D. Lifetime Prediction of a Blue PE100 Water Pipe. Polymer Degradation and Stability 2008, 93, 1496–1503, doi:10.1016/j.polymdegradstab.2008.05.008.

Brown, N. Intrinsic Lifetime of Polyethylene Pipelines. Polym. Eng. Sci. 2007, 47, 477–480, doi:10.1002/pen.20696.

Zha, S.; Lan, H.; Huang, H. Review on Lifetime Predictions of Polyethylene Pipes: Limitations and Trends. International Journal of Pressure Vessels and Piping 2022, 198, 104663, doi:10.1016/j.ijpvp.2022.104663.

Frank, A.; Arbeiter, F.J.; Berger, I.J.; Hutař, P.; Náhlík, L.; Pinter, G. Fracture Mechanics Lifetime Prediction of Polyethylene Pipes. J. Pipeline Syst. Eng. Pract. 2019, 10, 04018030, doi:10.1061/(ASCE)PS.1949-1204.0000356.

Zhang, Y.; Jar, P.-Y.B. Time-Strain Rate Superposition for Relaxation Behavior of Polyethylene Pressure Pipes. Polymer Testing 2016, 50, 292–296, doi:10.1016/j.polymertesting.2015.12.014.

Zhang, Y.; Jar, P.-Y.B.; Xue, S.; Han, L.; Li, L. Measurement of Environmental Stress Cracking Resistance of Polyethylene Pipe: A Review. In Proceedings of the ASME 2019 Asia Pacific Pipeline Conference; American Society of Mechanical Engineers: Qingdao, China, May 15 2019; p. V001T10A001.

Zhang, Y.; Jar, P.-Y.B.; Xue, S.; Li, L. Numerical Simulation of Ductile Fracture in Polyethylene Pipe with Continuum Damage Mechanics and Gurson-Tvergaard-Needleman Damage Models. Proceedings of the IMechE 2019, 233, 2455–2468, doi:10.1177/1464420719863458.

Zhang, Y.; Qiao, L.; Fan, J.; Xue, S.; Jar, P.B. Molecular Dynamics Simulation of Plastic Deformation in Polyethylene under Uniaxial and Biaxial Tension. Proceedings of the Institution of Mechanical Engineers, Part L: Journal of Materials: Design and Applications 2021, 146442072110458, doi:10.1177/14644207211045821.

Fancey, K.S. A Mechanical Model for Creep, Recovery and Stress Relaxation in Polymeric Materials. J Mater Sci 2005, 40, 4827–4831, doi:10.1007/s10853-005-2020-x.

Tan, N.; Jar, P.-Y.B. Determining Deformation Transition in Polyethylene under Tensile Loading. Polymers 2019, 11, 1415, doi:10.3390/polym11091415.

Hong, K.; Rastogi, A.; Strobl, G. Model Treatment of Tensile Deformation of Semicrystalline Polymers: Static Elastic Moduli and Creep Parameters Derived for a Sample of Polyethylene. Macromolecules 2004, 37, 10174–10179, doi:10.1021/ma049172x.

Castagnet, S. High-Temperature Mechanical Behavior of Semi-Crystalline Polymers and Relationship to a Rubber-like “Relaxed” State. Mechanics of Materials 2009, 41, 75–86, doi:10.1016/j.mechmat.2008.10.001.

Koerner, H.; Price, G.; Pearce, N.A.; Alexander, M.; Vaia, R.A. Remotely Actuated Polymer Nanocomposites—Stress-Recovery of Carbon-Nanotube-Filled Thermoplastic Elastomers. Nature materials 2004, 3, 115–120.

Shi, F. Studies on the Time-Dependent Behavior of Semi-Crystalline Polymers. Res Dev Polymer Sci 2023, 2, 1–2, doi:10.54026/RDPS/1006.

Yakimets, I.; Lai, D.; Guigon, M. Model to Predict the Viscoelastic Response of a Semi-Crystalline Polymer under Complex Cyclic Mechanical Loading and Unloading Conditions. Mech Time-Depend Mater 2007, 11, 47–60, doi:10.1007/s11043-007-9031-8.

Wilding, M.A.; Ward, I.M. Creep and Recovery of Ultra High Modulus Polyethylene. Polymer 1981, 22, 870–876, doi:10.1016/0032-3861(81)90259-7.

Wilding, M.A.; Ward, I.M. Tensile Creep and Recovery in Ultra-High Modulus Linear Polyethylenes. Polymer 1978, 19, 969–976, doi:10.1016/0032-3861(78)90208-2.

Sweeney, J.; Ward, I.M. A Unified Model of Stress Relaxation and Creep Applied to Oriented Polyethylene. J Mater Sci 1990, 25, 697–705, doi:10.1007/BF00714097.

Okereke, M.I.; Akpoyomare, A.I. Two-Process Constitutive Model for Semicrystalline Polymers across a Wide Range of Strain Rates. Polymer 2019, 183, 121818, doi:10.1016/j.polymer.2019.121818.

Detrez, F.; Cantournet, S.; Séguéla, R. A Constitutive Model for Semi-Crystalline Polymer Deformation Involving Lamellar Fragmentation. Comptes Rendus Mécanique 2010, 338, 681–687, doi:10.1016/j.crme.2010.10.008.

Olley, P.; Sweeney, J. A Multiprocess Eyring Model for Large Strain Plastic Deformation. J. Appl. Polym. Sci. 2011, 119, 2246–2260, doi:10.1002/app.32951.

Johnsen, J.; Clausen, A.H.; Grytten, F.; Benallal, A.; Hopperstad, O.S. A Thermo-Elasto-Viscoplastic Constitutive Model for Polymers. Journal of the Mechanics and Physics of Solids 2019, 124, 681–701, doi:10.1016/j.jmps.2018.11.018.

Brusselle-Dupend, N.; Lai, D.; Feaugas, X.; Guigon, M.; Clavel, M. Mechanical Behavior of a Semicrystalline Polymer before Necking. Part II: Modeling of Uniaxial Behavior. Polym. Eng. Sci. 2003, 43, 501–518, doi:10.1002/pen.10041.

DeMaio, A.; Patterson, T. Rheological Modeling of the Tensile Creep Behavior of Paper: Tensile Creep Behavior of Paper. J. Appl. Polym. Sci. 2007, 106, 3543–3554, doi:10.1002/app.26895.

Duxbury, J.; Ward, I.M. The Creep Behaviour of Ultra-High Modulus Polypropylene. J Mater Sci 1987, 22, 1215–1222, doi:10.1007/BF01233111.

Guedes, R.M.; Singh, A.; Pinto, V. Viscoelastic Modelling of Creep and Stress Relaxation Behaviour in PLA-PCL Fibres. Fibers Polym 2017, 18, 2443–2453, doi:10.1007/s12221-017-7479-y.

Daneshyar, A.; Ghaemian, M.; Du, C. A Fracture Energy–Based Viscoelastic–Viscoplastic–Anisotropic Damage Model for Rate-Dependent Cracking of Concrete. Int J Fract 2023, 241, 1–26, doi:10.1007/s10704-022-00685-5.

Jordan, B.; Gorji, M.B.; Mohr, D. Neural Network Model Describing the Temperature- and Rate-Dependent Stress-Strain Response of Polypropylene. International Journal of Plasticity 2020, 135, 102811, doi:10.1016/j.ijplas.2020.102811.

Nechad, H.; Helmstetter, A.; El Guerjouma, R.; Sornette, D. Andrade and Critical Time-to-Failure Laws in Fiber-Matrix Composites: Experiments and Model. Journal of the Mechanics and Physics of Solids 2005, 53, 1099–1127.

Naraghi, M.; Kolluru, P.V.; Chasiotis, I. Time and Strain Rate Dependent Mechanical Behavior of Individual Polymeric Nanofibers. Journal of the Mechanics and Physics of Solids 2014, 62, 257–275, doi:10.1016/j.jmps.2013.10.006.

Xu, P.; Zhou, Z.; Liu, T.; Pan, S.; Tan, X.; Chen, Z. The Investigation of Viscoelastic Mechanical Behaviors of Bolted GLARE Joints: Modeling and Experiments. International Journal of Mechanical Sciences 2020, 175, 105538.

Agbossou, A.; Cohen, I.; Muller, D. Effects of Interphase and Impact Strain Rates on Tensile Off-Axis Behaviour of Unidirectional Glass Fibre Composite: Experimental Results. Engineering Fracture Mechanics 1995, 52, 923–935, doi:10.1016/0013-7944(94)00320-H.

Arruda, E.M.; Boyce, M.C. Evolution of Plastic Anisotropy in Amorphous Polymers during Finite Straining. International Journal of Plasticity 1993, 9, 697–720.

Du, Y.; Pei, P.; Suo, T.; Gao, G. Large Deformation Mechanical Behavior and Constitutive Modeling of Oriented PMMA. International Journal of Mechanical Sciences 2023, 257, 108520, doi:10.1016/j.ijmecsci.2023.108520.

Zhao, W.; Liu, L.; Lan, X.; Leng, J.; Liu, Y. Thermomechanical Constitutive Models of Shape Memory Polymers and Their Composites. Applied Mechanics Reviews 2023, 75, 020802, doi:10.1115/1.4056131.

Wang, Z.; Guo, J.; Seppala, J.E.; Nguyen, T.D. Extending the Effective Temperature Model to the Large Strain Hardening Behavior of Glassy Polymers. Journal of the Mechanics and Physics of Solids 2021, 146, 104175, doi:10.1016/j.jmps.2020.104175.

Hong, K.; Strobl, G. Characterizing and Modeling the Tensile Deformation of Polyethylene: The Temperature and Crystallinity Dependences. Polym. Sci. Ser. A 2008, 50, 483–493, doi:10.1134/S0965545X08050027.

Na, B.; Zhang, Q.; Fu, Q.; Men, Y.; Hong, K.; Strobl, G. Viscous-Force-Dominated Tensile Deformation Behavior of Oriented Polyethylene. Macromolecules 2006, 39, 2584–2591, doi:10.1021/ma052496g.

Izraylit, V.; Heuchel, M.; Gould, O.E.C.; Kratz, K.; Lendlein, A. Strain Recovery and Stress Relaxation Behaviour of Multiblock Copolymer Blends Physically Cross-Linked with PLA Stereocomplexation. Polymer 2020, 209, 122984, doi:10.1016/j.polymer.2020.122984.

Shi, F.; Ben Jar, P.-Y. Characterization of Polyethylene Using a New Test Method Based on Stress Response to Relaxation and Recovery. Polymers 2022, 14, 2763, doi:10.3390/polym14142763.

Shi, F.; Jar, P.-Y.B. Characterization of Polyethylene Using a New Test Method Based on Stress Response to Relaxation and Recovery. Polymers 2022, 14, 2763, doi:10.3390/polym14142763.

Haario, H.; von Hertzen, R.; Karttunen, A.T.; Jorkama, M. Identification of the Viscoelastic Parameters of a Polymer Model by the Aid of a MCMC Method. Mechanics Research Communications 2014, 61, 1–6, doi:10.1016/j.mechrescom.2014.07.002.

Johnson, T.P.M.; Socrate, S.; Boyce, M.C. A Viscoelastic, Viscoplastic Model of Cortical Bone Valid at Low and High Strain Rates. Acta Biomater. 2010, 6, 4073–4080, doi:10.1016/j.actbio.2010.04.017.

Christöfl, P.; Czibula, C.; Berer, M.; Oreski, G.; Teichert, C.; Pinter, G. Comprehensive Investigation of the Viscoelastic Properties of PMMA by Nanoindentation. Polymer Testing 2021, 93, 106978, doi:10.1016/j.polymertesting.2020.106978.

Sweeney, J.; Bonner, M.; Ward, I.M. Modelling of Loading, Stress Relaxation and Stress Recovery in a Shape Memory Polymer. Journal of the Mechanical Behavior of Biomedical Materials 2014, 37, 12–23, doi:10.1016/j.jmbbm.2014.05.011.

Wayne Chen, W.; Jane Wang, Q.; Huan, Z.; Luo, X. Semi-Analytical Viscoelastic Contact Modeling of Polymer-Based Materials. Journal of Tribology 2011, 133, 041404, doi:10.1115/1.4004928.

Shahin, A.; Barsoum, I.; Islam, M.D. Constitutive Model Calibration of the Time and Temperature-Dependent Behavior of High Density Polyethylene. Polymer Testing 2020, 91, 106800, doi:10.1016/j.polymertesting.2020.106800.

Xu, Q.; Engquist, B.; Solaimanian, M.; Yan, K. A New Nonlinear Viscoelastic Model and Mathematical Solution of Solids for Improving Prediction Accuracy. Scientific reports 2020, 10, 2202.

Mierke, C.T. Viscoelasticity Acts as a Marker for Tumor Extracellular Matrix Characteristics. Front. Cell Dev. Biol. 2021, 9, doi:10.3389/fcell.2021.785138.

Muliana, A. A Fractional Model of Nonlinear Multiaxial Viscoelastic Behaviors. Mech Time-Depend Mater 2022, doi:10.1007/s11043-022-09542-3.

Ben Jar, P.-Y. Transition of Neck Appearance in Polyethylene and Effect of the Associated Strain Rate on the Damage Generation. Polym Eng Sci 2014, 54, 1871–1878, doi:10.1002/pen.23735.

Tan, N.; Jar, P.B. Multi-Relaxation Test to Characterize PE Pipe Performance. Plastics Engineering 2019, 75, 40–45, doi:10.1002/peng.20184.

Zhang, Y.; Ben Jar, P.-Y. Quantitative Assessment of Deformation-Induced Damage in Polyethylene Pressure Pipe. Polymer Testing 2015, 47, 42–50, doi:10.1016/j.polymertesting.2015.08.005.

Zhang, Y.; Jar, P.-Y.B. Phenomenological Modelling of Tensile Fracture in PE Pipe by Considering Damage Evolution. Materials & Design 2015, 77, 72–82, doi:10.1016/j.matdes.2015.04.011.

Zhang, Y.; Ben Jar, P.-Y. Effects of Crosshead Speed on the Quasi-Static Stress–Strain Relationship of Polyethylene Pipes. Journal of Pressure Vessel Technology 2017, 139, 021402, doi:10.1115/1.4033777.

Shi, F.; Jar, P.-Y.B. Characterization of Loading, Relaxation, and Recovery Behaviors of High-Density Polyethylene Using a Three-Branch Spring-Dashpot Model. Polymer Engineering & Science n/a, doi:10.1002/pen.26891.

Kumar, S.; Liu, G.; Schloerb, D.; Srinivasan, M. Viscoelastic Characterization of the Primate Finger Pad In Vivo by Microstep Indentation and Three-Dimensional Finite Element Models for Tactile Sensation Studies. Journal of biomechanical engineering 2015, 137, doi:10.1115/1.4029985.

Blake, Y. Review of Viscoelastic Models Applied to Cortical Bone.

Heuchel, M.; Cui, J.; Kratz, K.; Kosmella, H.; Lendlein, A. Relaxation Based Modeling of Tunable Shape Recovery Kinetics Observed under Isothermal Conditions for Amorphous Shape-Memory Polymers. Polymer 2010, 51, 6212–6218, doi:10.1016/j.polymer.2010.10.051.

López-Guerra, E.A.; Solares, S.D. Modeling Viscoelasticity through Spring–Dashpot Models in Intermittent-Contact Atomic Force Microscopy. Beilstein J. Nanotechnol. 2014, 5, 2149–2163, doi:10.3762/bjnano.5.224.

Xu, S.; Odaira, T.; Sato, S.; Xu, X.; Omori, T.; Harjo, S.; Kawasaki, T.; Seiner, H.; Zoubková, K.; Murakami, Y.; et al. Non-Hookean Large Elastic Deformation in Bulk Crystalline Metals. Nat Commun 2022, 13, 5307, doi:10.1038/s41467-022-32930-9.

Yang, J.-L.; Zhang, Z.; Schlarb, A.K.; Friedrich, K. On the Characterization of Tensile Creep Resistance of Polyamide 66 Nanocomposites. Part II: Modeling and Prediction of Long-Term Performance. Polymer 2006, 47, 6745–6758, doi:10.1016/j.polymer.2006.07.060.

Alves, A.F.C.; Ferreira, B.P.; Andrade Pires, F.M. Constitutive Modeling of Amorphous Thermoplastics from Low to High Strain Rates: Formulation and Critical Comparison Employing an Optimization-Based Parameter Identification. International Journal of Solids and Structures 2023, 273, 112258, doi:10.1016/j.ijsolstr.2023.112258.

Laheri, V.; Hao, P.; Gilabert, F.A. Constitutive Recasting of Macromolecular-Based Thermoviscoplasticity as Yield Function-Based Formulation. International Journal of Mechanical Sciences 2023, 250, 108278, doi:10.1016/j.ijmecsci.2023.108278.

Teoh, S.H. Effect of Saline Solution on Creep Fracture of Delrin®. Biomaterials 1993, 14, 132–136, doi:10.1016/0142-9612(93)90226-R.

Jadhao, V.; Robbins, M.O. Rheological Properties of Liquids under Conditions of Elastohydrodynamic Lubrication 2019.

Hong, K. A Model Treating Tensile Deformation of Semi-Crystalline Polymers. PhD Thesis, Verlag nicht ermittelbar, 2005.

Tan, N.; Ben Jar, P.-Y. Reanalysis of the Creep Test Data and Failure Behavior of Polyethylene and Its Copolymers. J. of Materi Eng and Perform 2022, 31, 2182–2192, doi:10.1007/s11665-021-06360-5.

Halsey, G.; White, H.J.; Eyring, H. Mechanical Properties of Textiles, I. Textile Research 1945, 15, 295–311, doi:10.1177/004051754501500901.

Lee, H.-N.; Paeng, K.; Swallen, S.F.; Ediger, M.D. Direct Measurement of Molecular Mobility in Actively Deformed Polymer Glasses. Science 2009, 323, 231–234, doi:10.1126/science.1165995.

Ghorbel, E.; Hadriche, I.; Casalino, G.; Masmoudi, N. Characterization of Thermo-Mechanical and Fracture Behaviors of Thermoplastic Polymers. Materials 2014, 7, 375–398, doi:10.3390/ma7010375.

Men, Y.; Rieger, J.; Strobl, G. Role of the Entangled Amorphous Network in Tensile Deformation of Semicrystalline Polymers. Phys. Rev. Lett. 2003, 91, 095502, doi:10.1103/PhysRevLett.91.095502.

Nitta, K. On a Thermodynamic Foundation of Eyring Rate Theory for Plastic Deformation of Polymer Solids. Philosophical Magazine Letters 2023, 103, 2186190, doi:10.1080/09500839.2023.2186190.

Srikanth, K.; Sreejith, P.; Arvind, K.; Kannan, K.; Pandey, M. An Efficient Mode-of-Deformation Dependent Rate-Type Constitutive Relation for Multi-Modal Cyclic Loading of Elastomers. International Journal of Plasticity 2023, 163, 103517, doi:10.1016/j.ijplas.2023.103517.

Kakaletsis, S.; Lejeune, E.; Rausch, M.K. Can Machine Learning Accelerate Soft Material Parameter Identification from Complex Mechanical Test Data? Biomech Model Mechanobiol 2023, 22, 57–70, doi:10.1007/s10237-022-01631-z.

Klinge, S.; Steinmann, P. Inverse Analysis for Heterogeneous Materials and Its Application to Viscoelastic Curing Polymers. Comput Mech 2015, 55, 603–615, doi:10.1007/s00466-015-1126-5.

Polanco-Loria, M.; Daiyan, H.; Grytten, F. Material Parameters Identification: An Inverse Modeling Methodology Applicable for Thermoplastic Materials. Polymer Engineering & Science 2012, 52, 438–448, doi:10.1002/pen.22102.

Chen, Z.; Diebels, S.; Peter, N.J.; Schneider, A.S. Identification of Finite Viscoelasticity and Adhesion Effects in Nanoindentation of a Soft Polymer by Inverse Method. Computational Materials Science 2013, 72, 127–139, doi:10.1016/j.commatsci.2013.01.040.

Yun, G.J.; Shang, S. A Self-Optimizing Inverse Analysis Method for Estimation of Cyclic Elasto-Plasticity Model Parameters. International Journal of Plasticity 2011, 27, 576–595, doi:10.1016/j.ijplas.2010.08.003.

Van Der Vossen, B.C.; Makeev, A.V. Mechanical Properties Characterization of Fiber Reinforced Composites by Nonlinear Constitutive Parameter Optimization in Short Beam Shear Specimens. Journal of Composite Materials 2021, 55, 2985–2997, doi:10.1177/00219983211002238.

Saleeb, A.F.; Gendy, A.S.; Wilt, T.E. Parameter-Estimation Algorithms for Characterizing a Class of Isotropic and Anisotropic Viscoplastic Material Models. Mechanics of Time-Dependent Materials 2002, 6, 323–361, doi:10.1023/A:1021268030967.

Maier, G.; Bocciarelli, M.; Bolzon, G.; Fedele, R. Inverse Analyses in Fracture Mechanics. Int J Fract 2006, 138, 47–73, doi:10.1007/s10704-006-7153-7.

Lyu, Y.; Pathirage, M.; Ramyar, E.; Liu, W.K.; Cusatis, G. Machine Learning Meta-Models for Fast Parameter Identification of the Lattice Discrete Particle Model. Comput Mech 2023, 72, 593–612, doi:10.1007/s00466-023-02320-z.

Hoerig, C.; Ghaboussi, J.; Wang, Y.; Insana, M.F. Machine Learning in Model-Free Mechanical Property Imaging: Novel Integration of Physics With the Constrained Optimization Process. Front. Phys. 2021, 9, 600718, doi:10.3389/fphy.2021.600718.

Andrade-Campos, A.; Thuillier, S.; Pilvin, P.; Teixeira-Dias, F. On the Determination of Material Parameters for Internal Variable Thermoelastic–Viscoplastic Constitutive Models. International Journal of Plasticity 2007, 23, 1349–1379, doi:10.1016/j.ijplas.2006.09.002.

Unger, J.F.; Könke, C. An Inverse Parameter Identification Procedure Assessing the Quality of the Estimates Using Bayesian Neural Networks. Applied Soft Computing 2011, 11, 3357–3367, doi:10.1016/j.asoc.2011.01.007.

Xu, H.; Jiang, X. Creep Constitutive Models for Viscoelastic Materials Based on Fractional Derivatives. Computers & Mathematics with Applications 2017, 73, 1377–1384, doi:10.1016/j.camwa.2016.05.002.

Van Den Bos, A. Nonlinear Least-Absolute-Values and Minimax Model Fitting. IFAC Proceedings Volumes 1985, 18, 173–177, doi:10.1016/S1474-6670(17)60554-8.

Powell, M.J.D. Approximation Theory and Methods; Cambridge University Press: Cambridge [Eng.] ; New York, 1981; ISBN 978-0-521-22472-7.

Setiyoko, A.; Basaruddin, T.; Arymurthy, A.M. Minimax Approach for Semivariogram Fitting in Ordinary Kriging. IEEE Access 2020, 8, 82054–82065, doi:10.1109/ACCESS.2020.2991428.

Boutaleb, S.; Zaïri, F.; Mesbah, A.; Naït-Abdelaziz, M.; Gloaguen, J.M.; Boukharouba, T.; Lefebvre, J.M. Micromechanics-Based Modelling of Stiffness and Yield Stress for Silica/Polymer Nanocomposites. International Journal of Solids and Structures 2009, 46, 1716–1726, doi:10.1016/j.ijsolstr.2008.12.011.

Khan, A.S.; Lopez-Pamies, O.; Kazmi, R. Thermo-Mechanical Large Deformation Response and Constitutive Modeling of Viscoelastic Polymers over a Wide Range of Strain Rates and Temperatures. International Journal of Plasticity 2006, 22, 581–601, doi:10.1016/j.ijplas.2005.08.001.

Kemmer, G.; Keller, S. Nonlinear Least-Squares Data Fitting in Excel Spreadsheets. Nat Protoc 2010, 5, 267–281, doi:10.1038/nprot.2009.182.

Paetzold, M.; Andert, T.P.; Asmar, S.W.; Anderson, J.D.; Barriot, J.-P.; Bird, M.K.; Haeusler, B.; Hahn, M.; Tellmann, S.; Sierks, H.; et al. Asteroid 21 Lutetia: Low Mass, High Density. Science 2011, 334, 491–492, doi:10.1126/science.1209389.

Messager, M.L.; Lehner, B.; Grill, G.; Nedeva, I.; Schmitt, O. Estimating the Volume and Age of Water Stored in Global Lakes Using a Geo-Statistical Approach. Nat Commun 2016, 7, 13603, doi:10.1038/ncomms13603.

Sprave, L.; Menzel, A. A Large Strain Gradient-Enhanced Ductile Damage Model: Finite Element Formulation, Experiment and Parameter Identification. Acta Mech 2020, 231, 5159–5192, doi:10.1007/s00707-020-02786-5.

Sweeney, J. A Comparison of Three Polymer Network Models in Current Use. Computational and Theoretical Polymer Science 1999, 9, 27–33.

Mahnken, R.; Stein, E. Parameter Identification for Viscoplastic Models Based on Analytical Derivatives of a Least-Squares Functional and Stability Investigations. International Journal of Plasticity 1996, 12, 451–479, doi:10.1016/S0749-6419(95)00016-X.

Khan, A.; Zhang, H. Finite Deformation of a Polymer: Experiments and Modeling. International Journal of Plasticity 2001, 17, 1167–1188, doi:10.1016/S0749-6419(00)00073-5.

Zhang, C.; Cai, L.-H.; Guo, B.-H.; Miao, B.; Xu, J. New Kinetics Equation for Stress Relaxation of Semi-Crystalline Polymers below Glass Transition Temperature. Chinese Journal of Polymer Science 2022, 40, 1662–1669.

Ayoub, G.; Zaïri, F.; Fréderix, C.; Gloaguen, J.M.; Naït-Abdelaziz, M.; Seguela, R.; Lefebvre, J.M. Effects of Crystal Content on the Mechanical Behaviour of Polyethylene under Finite Strains: Experiments and Constitutive Modelling. International Journal of Plasticity 2011, 27, 492–511, doi:10.1016/j.ijplas.2010.07.005.

Drozdov, A.D.; Klitkou, R.; Christiansen, J. deC. Multi-Cycle Deformation of Semicrystalline Polymers: Observations and Constitutive Modeling. Mechanics Research Communications 2013, 48, 70–75, doi:10.1016/j.mechrescom.2013.01.001.

Kubát, J.; Seldén, R. The Stress Dependence of Activation Volumes in Creep and Stress Relaxation. Materials Science and Engineering 1978, 36, 65–69, doi:10.1016/0025-5416(78)90195-7.

Syrjakow, M.; Szczerbicka, H. Efficient Parameter Optimization Based on Combination of Direct Global and Local Search Methods. In Evolutionary Algorithms; Davis, L.D., De Jong, K., Vose, M.D., Whitley, L.D., Eds.; The IMA Volumes in Mathematics and its Applications; Springer New York: New York, NY, 1999; Vol. 111, pp. 227–249 ISBN 978-1-4612-7185-7.

Renders, J.-M.; Flasse, S.P. Hybrid Methods Using Genetic Algorithms for Global Optimization. IEEE Transactions on Systems, Man, and Cybernetics, Part B (Cybernetics) 1996, 26, 243–258, doi:10.1109/3477.485836.

Mahinthakumar, G. (Kumar); Sayeed, M. Hybrid Genetic Algorithm—Local Search Methods for Solving Groundwater Source Identification Inverse Problems. J. Water Resour. Plann. Manage. 2005, 131, 45–57, doi:10.1061/(ASCE)0733-9496(2005)131:1(45).

Maaranen, H.; Miettinen, K.; Penttinen, A. On Initial Populations of a Genetic Algorithm for Continuous Optimization Problems. J Glob Optim 2007, 37, 405–436, doi:10.1007/s10898-006-9056-6.

Yen, J.; Liao, J.C.; Lee, B.; Randolph, D. A Hybrid Approach to Modeling Metabolic Systems Using a Genetic Algorithm and Simplex Method. IEEE Transactions on Systems, Man, and Cybernetics, Part B (Cybernetics) 1998, 28, 173–191, doi:10.1109/3477.662758.

Ahn, C.W.; Ramakrishna, R.S. A Genetic Algorithm for Shortest Path Routing Problem and the Sizing of Populations. IEEE Transactions on Evolutionary Computation 2002, 6, 566–579, doi:10.1109/TEVC.2002.804323.

Pál, K.F. Genetic Algorithm with Local Optimization. Biol. Cybern. 1995, 73, 335–341, doi:10.1007/BF00199469.

Okamoto, M.; Nonaka, T.; Ochiai, S.; Tominaga, D. Nonlinear Numerical Optimization with Use of a Hybrid Genetic Algorithm Incorporating the Modified Powell Method. Applied Mathematics and Computation 1998, 91, 63–72, doi:10.1016/S0096-3003(97)10007-8.

Crain, T.; Bishop, R.H.; Fowler, W.; Rock, K. Interplanetary Flyby Mission Optimization Using a Hybrid Global-Local Search Method. Journal of Spacecraft and Rockets 2012, doi:10.2514/2.3607.

Attaviriyanupap, P.; Kita, H.; Tanaka, E.; Hasegawa, J. A Hybrid EP and SQP for Dynamic Economic Dispatch with Nonsmooth Fuel Cost Function. IEEE Transactions on Power Systems 2002, 17, 411–416, doi:10.1109/TPWRS.2002.1007911.

Henz, B.J.; Mohan, R.V.; Shires, D.R. A Hybrid Global–Local Approach for Optimization of Injection Gate Locations in Liquid Composite Molding Process Simulations. Composites Part A: Applied Science and Manufacturing 2007, 38, 1932–1946, doi:10.1016/j.compositesa.2007.03.005.

Le, T.M.; Fatahi, B. Trust-Region Reflective Optimisation to Obtain Soil Visco-Plastic Properties. Engineering Computations 2016, 33, doi:10.1108/EC-11-2014-0236.

Schmidt, U.; Mergheim, J.; Steinmann, P. Multiscale Parameter Identification. Int J Mult Comp Eng 2012, 10, 327–342, doi:10.1615/IntJMultCompEng.2012002175.

Ramzanpour, M.; Hosseini-Farid, M.; Ziejewski, M.; Karami, G. Particle Swarm Optimization Method for Hyperelastic Characterization of Soft Tissues.

Pereira, J.O.; Farias, T.M.; Castro, A.M.; (Al-Baldawi), A.A.; Secchi, A.R.; Cardozo, N.S.M. Estimation of the Nonlinear Parameters of Viscoelastic Constitutive Models Using CFD and Multipass Rheometer Data. Journal of Non-Newtonian Fluid Mechanics 2020, 281, 104284, doi:10.1016/j.jnnfm.2020.104284.

Wu, L.; Chen, Z.; Long, C.; Cheng, S.; Lin, P.; Chen, Y.; Chen, H. Parameter Extraction of Photovoltaic Models from Measured I-V Characteristics Curves Using a Hybrid Trust-Region Reflective Algorithm. Applied Energy 2018, 232, 36–53, doi:10.1016/j.apenergy.2018.09.161.

Nenov, Hr.B.; Dimitrov, B.Hr.; Marinov, A.St. Algorithms for Computational Procedure Acceleration for Systems Differential Equations in Matlab. In Proceedings of the 2013 36th International Convention on Information and Communication Technology, Electronics and Microelectronics (MIPRO); May 2013; pp. 238–242.

Rivard, S.R.; Mailloux, J.-G.; Beguenane, R.; Bui, H.T. Design of High-Performance Parallelized Gene Predictors in MATLAB. BMC Res Notes 2012, 5, 183, doi:10.1186/1756-0500-5-183.

Tan, N. Deformation Transitions and Their Effects on the Long-Term Performance of Polyethylene and Its Pressure Pipe. 172.

Zheng, J.; Li, H.; Hogan, J.D. Strain-Rate-Dependent Tensile Response of an Alumina Ceramic: Experiments and Modeling. International Journal of Impact Engineering 2023, 173, 104487, doi:10.1016/j.ijimpeng.2022.104487.

Zheng, J.; Li, H.; Hogan, J.D. Advanced Tensile Fracture Analysis of Alumina Ceramics: Integrating Hybrid Finite-Discrete Element Modeling with Experimental Insights. Engineering Fracture Mechanics 2024, 302, 110075, doi:10.1016/j.engfracmech.2024.110075.

Jar, P.-Y.B. Effect of Tensile Loading History on Mechanical Properties for Polyethylene. Polym Eng Sci 2015, 55, 2002–2010, doi:10.1002/pen.24042.

Zheng, J.; Ji, M.; Zaiemyekeh, Z.; Li, H.; Hogan, J.D. Strain-Rate-Dependent Compressive and Compression-Shear Response of an Alumina Ceramic. Journal of the European Ceramic Society 2022, 42, 7516–7527, doi:10.1016/j.jeurceramsoc.2022.09.004.

Fritsch, J.; Hiermaier, S.; Strobl, G. Characterizing and Modeling the Non-Linear Viscoelastic Tensile Deformation of a Glass Fiber Reinforced Polypropylene. Composites Science and Technology 2009, 69, 2460–2466, doi:10.1016/j.compscitech.2009.06.021.

Rafiee, R.; Mazhari, B. Simulation of the Long-Term Hydrostatic Tests on Glass Fiber Reinforced Plastic Pipes. Composite Structures 2016, 136, 56–63, doi:10.1016/j.compstruct.2015.09.058.

Ebert, C.; Hufenbach, W.; Langkamp, A.; Gude, M. Modelling of Strain Rate Dependent Deformation Behaviour of Polypropylene. Polymer Testing 2011, 30, 183–187, doi:10.1016/j.polymertesting.2010.11.011.

Graba, M. Evaluation of Measurement Uncertainty in a Static Tensile Test. Open Engineering 2021, 11, 709–722, doi:10.1515/eng-2021-0069.

Mulliken, A.D.; Boyce, M.C. Mechanics of the Rate-Dependent Elastic–Plastic Deformation of Glassy Polymers from Low to High Strain Rates. International Journal of Solids and Structures 2006, 43, 1331–1356, doi:10.1016/j.ijsolstr.2005.04.016.

Jar, P.B. Revisiting Creep Test on Polyethylene Pipe—Data Analysis and Deformation Mechanisms. Polym Eng Sci 2021, 61, 586–599, doi:10.1002/pen.25603.

A G Piyal Aravinna Estimation of Measurement Uncertainty in Determination of Tensile Strength of Reinforcement Steel. 2021, doi:10.13140/RG.2.2.14541.77287.

Hong, K.; Rastogi, A.; Strobl, G. A Model Treating Tensile Deformation of Semicrystalline Polymers: Quasi-Static Stress- Strain Relationship and Viscous Stress Determined for a Sample of Polyethylene. Macromolecules 2004, 37, 10165–10173.

Richeton, J.; Ahzi, S.; Daridon, L.; Rémond, Y. A Formulation of the Cooperative Model for the Yield Stress of Amorphous Polymers for a Wide Range of Strain Rates and Temperatures. Polymer 2005, 46, 6035–6043, doi:10.1016/j.polymer.2005.05.079.

Bergstrom, J.; Boyce, M.C. Constitutive Modeling of the Large Strain Time-Dependent Behavior of Elastomers. Journal of the Mechanics and Physics of Solids 1998, 46, 931–954, doi:10.1016/S0022-5096(97)00075-6.

Natarajan, V.D. Constitutive Behavior of a Twaron® Fabric/Natural Rubber Composite: Experiments and Modeling; 2011;

Popa, C.M.; Fleischhauer, R.; Schneider, K.; Kaliske, M. Formulation and Implementation of a Constitutive Model for Semicrystalline Polymers. International Journal of Plasticity 2014, 61, 128–156, doi:10.1016/j.ijplas.2014.05.010.

Jar, P. -Y. B. Analysis of Time-dependent Mechanical Behavior of Polyethylene. SPE Polymers 2024, 5, 426–443, doi:10.1002/pls2.10134.

Pyrz, M.; Zairi, F. Identification of Viscoplastic Parameters of Phenomenological Constitutive Equations for Polymers by Deterministic and Evolutionary Approach. Modelling Simul. Mater. Sci. Eng. 2007, 15, 85–103, doi:10.1088/0965-0393/15/2/006.

Zhang, Y.; Jar, P.-Y.B. Comparison of Mechanical Properties Between PE80 and PE100 Pipe Materials. J. of Materi Eng and Perform 2016, 25, 4326–4332, doi:10.1007/s11665-016-2274-2.

Liu, X.; Zhang, H.; Xia, M.; Wu, K.; Chen, Y.; Zheng, Q.; Li, J. Mechanical Response of Buried Polyethylene Pipelines under Excavation Load during Pavement Construction. Engineering Failure Analysis 2018, 90, 355–370, doi:10.1016/j.engfailanal.2018.03.027.

Zhang, C.; Moore, I.D. Nonlinear Mechanical Response of High Density Polyethylene. Part II: Uniaxial Constitutive Modeling. Polym. Eng. Sci. 1997, 37, 414–420, doi:10.1002/pen.11684.

Zhang, C.; Moore, I.D. Nonlinear Mechanical Response of High Density Polyethylene. Part I: Experimental Investigation and Model Evaluation. Polymer Engineering & Science 1997, 37, 404–413, doi:10.1002/pen.11683.

Moore, I. Profiled HDPE Pipe Response to Parallel Plate Loading. In Buried Plastic Pipe Technology: 2nd Volume; Eckstein, D., Ed.; ASTM International: 100 Barr Harbor Drive, PO Box C700, West Conshohocken, PA 19428-2959, 1994; pp. 25-25–16 ISBN 978-0-8031-1992-5.

Whelton, A. J.; Dietrich, A. M.; Gallagher, D. L. Contaminant Diffusion, Solubility, and Material Property Differences between HDPE and PEX Potable Water Pipes. Journal of Environmental Engineering 2010, 136 (2), 227–237, doi:10.1061/(ASCE)EE.1943-7870.0000147.

Appendix

The algorithm flow chart for determining the fitting parameters is shown in Figure S1(a) for the relaxation stages, Figure S1(b) for the recovery stages, and Figure S1(c) for the first loading stages. Figure S1(d) presents the flow chart for the algorithm that is based on GA in Matlab. Note that index k in all of the above flow charts is the loop counter for narrowing down the range of $\tau_{v,L}$ and $\tau_{v,S}$ values until their variation for the entire RR test is less than 1 s, i.e., remaining constant for all relaxation or recovery stages in the entire RR test. Index h refers to the data point in the loading stages. In addition, index i in the flow charts is used to represent the cycle number for the RR test so that the fitting parameters of each cycle of RR tests can be determined. In the flow chart, 'max', 'min', 'avg' denotes finding the maximum, minimum, and average value of an array, respectively.

As specified in Figure S1(a), initial value ranges for the fitting parameters are [0.1, 20] (in MPa) for $\sigma_{v,L}(0)$, $[\sigma_{0,ci} - 0.2, \sigma_{0,ci} + 0.2]$ (in MPa) for $\sigma_{0,L}$ where value for reference stress ($\sigma_{0,ci}$), with subscript ci denoting cycle i of RR test, was determined based on the method described in[1], [1000, 90000] (in s) for $\tau_{v,L}$, [0.1, 20] (in MPa) for $\sigma_{v,S}(0)$, [0.01, 2] (in MPa) for $\sigma_{0,S}$, and [1, 900] (in s) for $\tau_{v,S}$. Note that in[1], $\sigma_{0,i}$ was determined based on the fitting of the stress drop of a relaxation stage at relaxation time longer than 1000 s, using a model with a single dashpot.

In view that σ_{qs} is expected to be the same from the relaxation and the recovery processes at the same stroke[2,3] and that the maximum difference of the strokes for the relaxation and recovery stages in the same cycle was less than 0.005 mm, σ_{qs} value determined from the relaxation stage was used in the data analysis as the σ_{qs} value for the recovery stage in the same cycle, as

shown in the algorithm depicted in Figure S1(b). Furthermore, in view of the small stroke increment applied at the loading stages, with the maximum increments of 0.187 and 0.037 mm for the 1st and the 2nd loading stages, respectively, $K_{v,L}$ and $K_{v,S}$ values were treated as constant at a given loading stage, but values for $\sigma_{0,L}$, $\sigma_{0,S}$, and $\tau_{v,S}$ were allowed to change, though only in a monotonic manner with the increase of the stroke. Additionally, the simulation process at the loading stages started from the last point recorded at each loading stage, that is, before the commencement of relaxation. In other words, $h = 24$ in Figure S1(c) represents the last point at the loading stage.

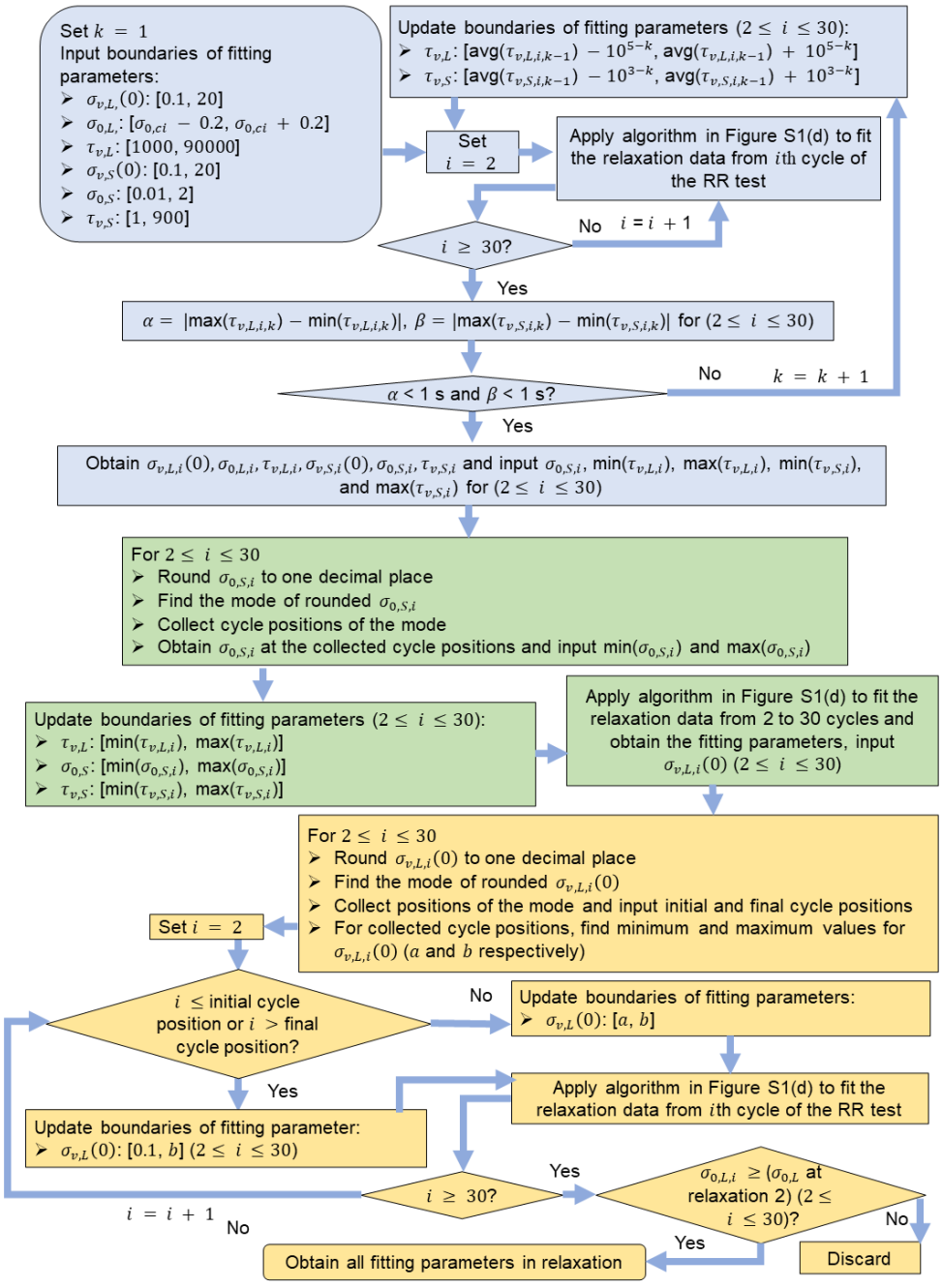
Set $k = 1$
Input boundaries of fitting parameters:
$\sigma_{v,L,}(0)$: [0.1, 20]
$\sigma_{0,L,}$: [$\sigma_{0,ci} - 0.2$, $\sigma_{0,ci} + 0.2$]
$\tau_{v,L}$: [1000, 90000]
$\sigma_{v,S}(0)$: [0.1, 20]
$\sigma_{0,S}$: [0.01, 2]
$\tau_{v,S}$: [1, 900]
Update boundaries of fitting parameters ($2 \leq i \leq 30$):
$\tau_{v,L}$: [avg($\tau_{v,L,i,k-1}$) $- 10^{5-k}$, avg($\tau_{v,L,i,k-1}$) $+ 10^{5-k}$]
$\tau_{v,S}$: [avg($\tau_{v,S,i,k-1}$) $- 10^{3-k}$, avg($\tau_{v,S,i,k-1}$) $+ 10^{3-k}$]
Set $i = 2$
Apply algorithm in Figure S1(d) to fit the relaxation data from ith cycle of the RR test
$i \geq 30$?
No
$i = i + 1$
Yes
$\alpha = |\max(\tau_{v,L,i,k}) - \min(\tau_{v,L,i,k})|$, $\beta = |\max(\tau_{v,S,i,k}) - \min(\tau_{v,S,i,k})|$ for $(2 \leq i \leq 30)$
α < 1 s and β < 1 s?
No
$k = k + 1$
Yes
Obtain $\sigma_{v,L,i}(0)$, $\sigma_{0,L,i}$, $\tau_{v,L,i}$, $\sigma_{v,S,i}(0)$, $\sigma_{0,S,i}$, $\tau_{v,S,i}$ and input $\sigma_{0,S,i}$, $\min(\tau_{v,L,i})$, $\max(\tau_{v,L,i})$, $\min(\tau_{v,S,i})$, and $\max(\tau_{v,S,i})$ for $(2 \leq i \leq 30)$
For $2 \leq i \leq 30$
Round $\sigma_{0,S,i}$ to one decimal place
Find the mode of rounded $\sigma_{0,S,i}$
Collect cycle positions of the mode
Obtain $\sigma_{0,S,i}$ at the collected cycle positions and input $\min(\sigma_{0,S,i})$ and $\max(\sigma_{0,S,i})$
Update boundaries of fitting parameters ($2 \leq i \leq 30$):
$\tau_{v,L}$: [$\min(\tau_{v,L,i})$, $\max(\tau_{v,L,i})$]
$\sigma_{0,S}$: [$\min(\sigma_{0,S,i})$, $\max(\sigma_{0,S,i})$]
$\tau_{v,S}$: [$\min(\tau_{v,S,i})$, $\max(\tau_{v,S,i})$]
Apply algorithm in Figure S1(d) to fit the relaxation data from 2 to 30 cycles and obtain the fitting parameters, input $\sigma_{v,L,i}(0)$ $(2 \leq i \leq 30)$
For $2 \leq i \leq 30$
Round $\sigma_{v,L,i}(0)$ to one decimal place
Find the mode of rounded $\sigma_{v,L,i}(0)$
Collect positions of the mode and input initial and final cycle positions
For collected cycle positions, find minimum and maximum values for $\sigma_{v,L,i}(0)$ (a and b respectively)
Set $i = 2$
$i \leq$ initial cycle position or $i >$ final cycle position?
No
Update boundaries of fitting parameters:
$\sigma_{v,L}(0)$: [a, b]
Yes
Update boundaries of fitting parameter:
$\sigma_{v,L}(0)$: [0.1, b] $(2 \leq i \leq 30)$
Apply algorithm in Figure S1(d) to fit the relaxation data from ith cycle of the RR test
$i \geq 30$?
Yes
$\sigma_{0,L,i} \geq (\sigma_{0,L}$ at relaxation 2) $(2 \leq i \leq 30)$?
No
$i = i + 1$
No
Yes
Obtain all fitting parameters in relaxation
Discard

(a)

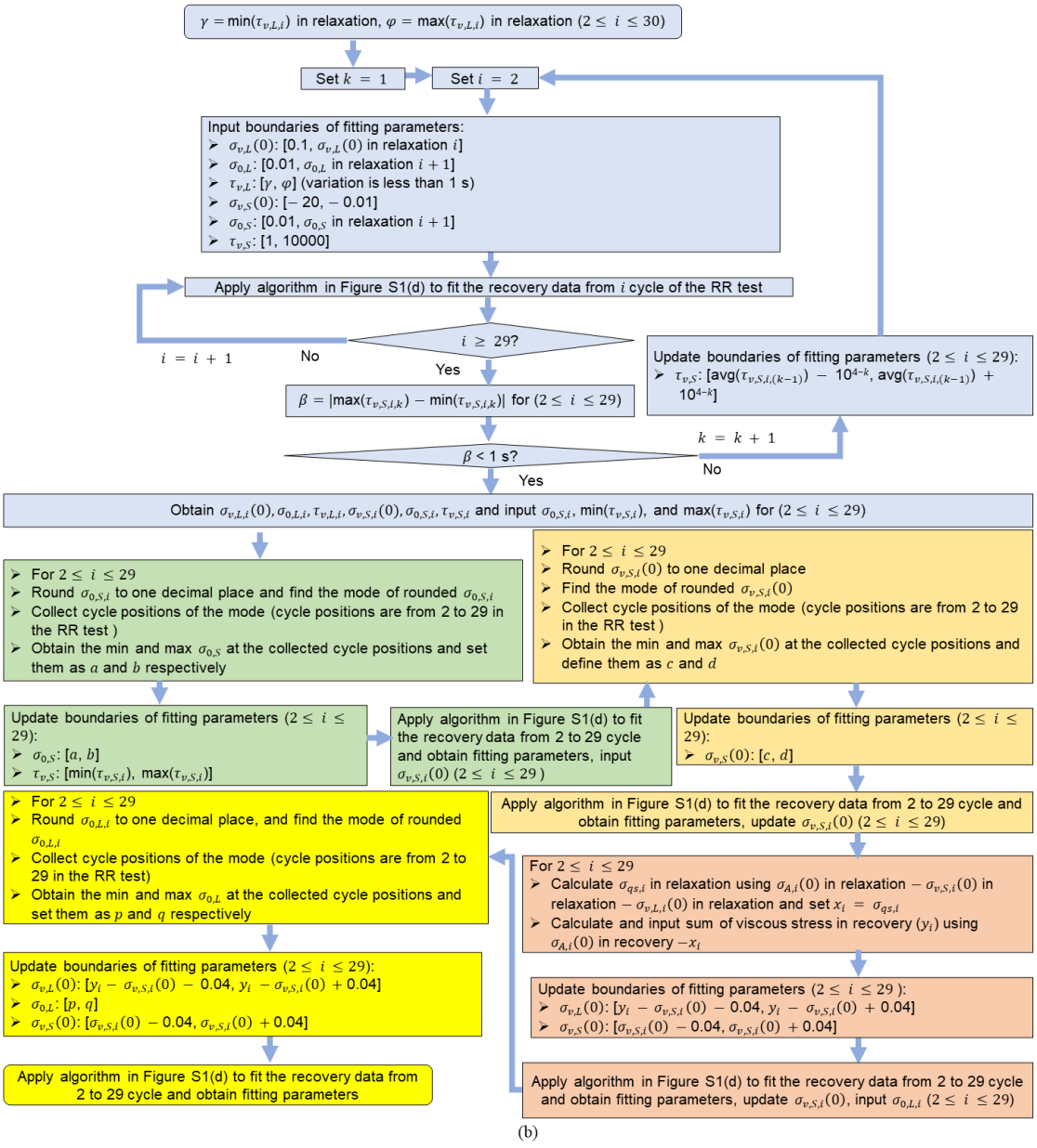
$\gamma = \min(\tau_{v,L,i})$ in relaxation, $\varphi = \max(\tau_{v,L,i})$ in relaxation $(2 \le i \le 30)$
Set $k = 1$
Set $i = 2$
Input boundaries of fitting parameters:
$\sigma_{v,L}(0)$: [0.1, $\sigma_{v,L}(0)$ in relaxation i]
$\sigma_{0,L}$: [0.01, $\sigma_{0,L}$ in relaxation $i+1$]
$\tau_{v,L}$: [γ, φ] (variation is less than 1 s)
$\sigma_{v,S}(0)$: [-20, -0.01]
$\sigma_{0,S}$: [0.01, $\sigma_{0,S}$ in relaxation $i+1$]
$\tau_{v,S}$: [1, 10000]
Apply algorithm in Figure S1(d) to fit the recovery data from i cycle of the RR test
$i \ge 29$?
No
$i = i + 1$
Yes
$\beta = |\max(\tau_{v,S,i,k}) - \min(\tau_{v,S,i,k})|$ for $(2 \le i \le 29)$
$\beta < 1$ s?
No
$k = k + 1$
Yes
Update boundaries of fitting parameters $(2 \le i \le 29)$:
$\tau_{v,S}$: [avg$(\tau_{v,S,i,(k-1)}) - 10^{4-k}$, avg$(\tau_{v,S,i,(k-1)}) + 10^{4-k}$]
Obtain $\sigma_{v,L,i}(0), \sigma_{0,L,i}, \tau_{v,L,i}, \sigma_{v,S,i}(0), \sigma_{0,S,i}, \tau_{v,S,i}$ and input $\sigma_{0,S,i}$, $\min(\tau_{v,S,i})$, and $\max(\tau_{v,S,i})$ for $(2 \le i \le 29)$
For $2 \le i \le 29$
Round $\sigma_{0,S,i}$ to one decimal place and find the mode of rounded $\sigma_{0,S,i}$
Collect cycle positions of the mode (cycle positions are from 2 to 29 in the RR test)
Obtain the min and max $\sigma_{0,S}$ at the collected cycle positions and set them as a and b respectively
For $2 \le i \le 29$
Round $\sigma_{v,S,i}(0)$ to one decimal place
Find the mode of rounded $\sigma_{v,S,i}(0)$
Collect cycle positions of the mode (cycle positions are from 2 to 29 in the RR test)
Obtain the min and max $\sigma_{v,S,i}(0)$ at the collected cycle positions and define them as c and d
Update boundaries of fitting parameters $(2 \le i \le 29)$:
$\sigma_{0,S}$: $[a, b]$
$\tau_{v,S}$: [$\min(\tau_{v,S,i})$, $\max(\tau_{v,S,i})$]
Apply algorithm in Figure S1(d) to fit the recovery data from 2 to 29 cycle and obtain fitting parameters, input $\sigma_{v,S,i}(0)$ $(2 \le i \le 29)$
Update boundaries of fitting parameters $(2 \le i \le 29)$:
$\sigma_{v,S}(0)$: $[c, d]$
For $2 \le i \le 29$
Round $\sigma_{0,L,i}$ to one decimal place, and find the mode of rounded $\sigma_{0,L,i}$
Collect cycle positions of the mode (cycle positions are from 2 to 29 in the RR test)
Obtain the min and max $\sigma_{0,L}$ at the collected cycle positions and set them as p and q respectively
Apply algorithm in Figure S1(d) to fit the recovery data from 2 to 29 cycle and obtain fitting parameters, update $\sigma_{v,S,i}(0)$ $(2 \le i \le 29)$
For $2 \le i \le 29$
Calculate $\sigma_{qs,i}$ in relaxation using $\sigma_{A,i}(0)$ in relaxation $- \sigma_{v,S,i}(0)$ in relaxation $- \sigma_{v,L,i}(0)$ in relaxation and set $x_i = \sigma_{qs,i}$
Calculate and input sum of viscous stress in recovery (y_i) using $\sigma_{A,i}(0)$ in recovery $-x_i$
Update boundaries of fitting parameters $(2 \le i \le 29)$:
$\sigma_{v,L}(0)$: [$y_i - \sigma_{v,S,i}(0) - 0.04$, $y_i - \sigma_{v,S,i}(0) + 0.04$]
$\sigma_{0,L}$: $[p, q]$
$\sigma_{v,S}(0)$: [$\sigma_{v,S,i}(0) - 0.04$, $\sigma_{v,S,i}(0) + 0.04$]
Update boundaries of fitting parameters $(2 \le i \le 29)$:
$\sigma_{v,L}(0)$: [$y_i - \sigma_{v,S,i}(0) - 0.04$, $y_i - \sigma_{v,S,i}(0) + 0.04$]
$\sigma_{v,S}(0)$: [$\sigma_{v,S,i}(0) - 0.04$, $\sigma_{v,S,i}(0) + 0.04$]
Apply algorithm in Figure S1(d) to fit the recovery data from 2 to 29 cycle and obtain fitting parameters
Apply algorithm in Figure S1(d) to fit the recovery data from 2 to 29 cycle and obtain fitting parameters, update $\sigma_{v,S,i}(0)$, input $\sigma_{0,L,i}$ $(2 \le i \le 29)$

(b)

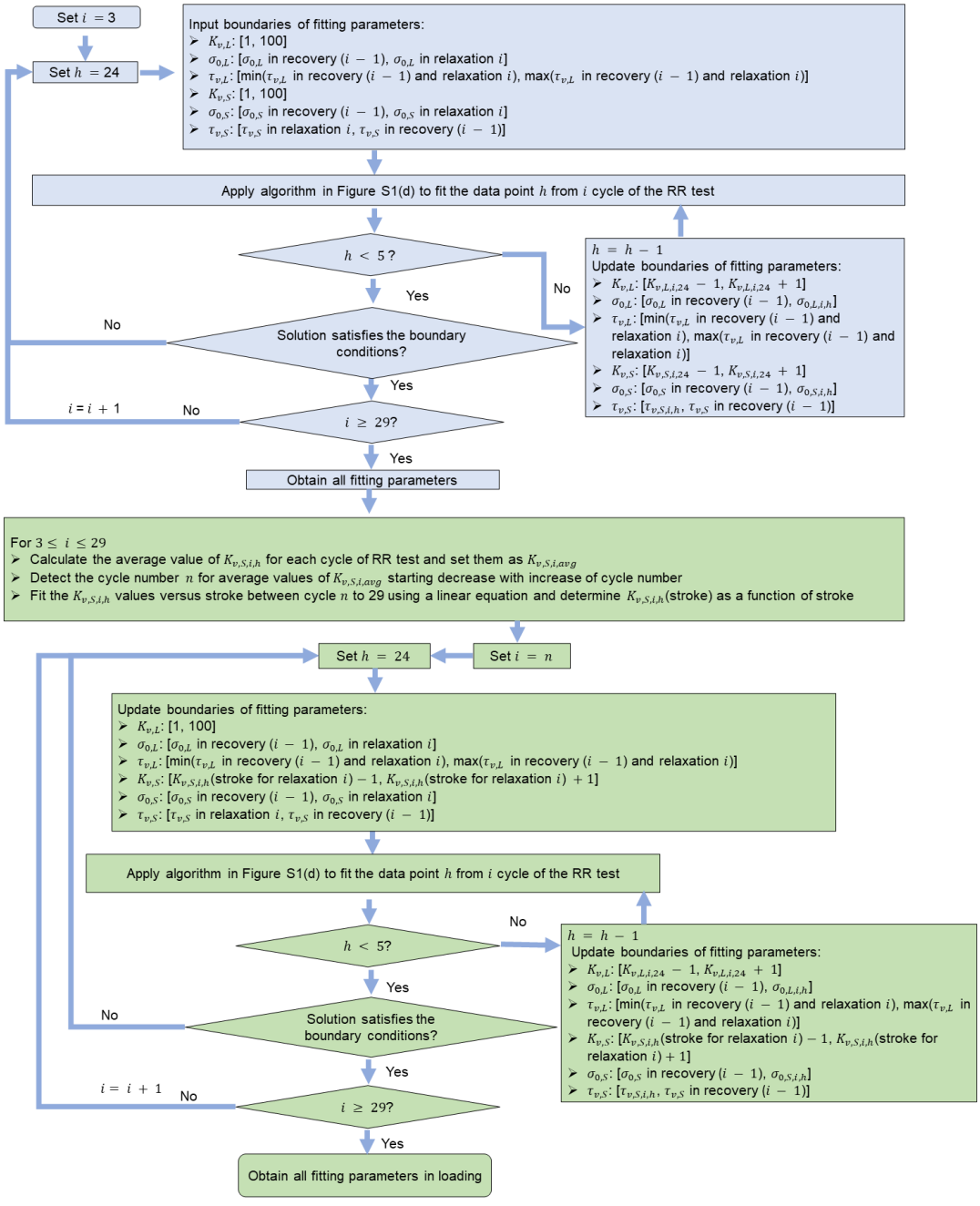
Set $i = 3$
Set $h = 24$
Input boundaries of fitting parameters:
$K_{v,L}$: [1, 100]
$\sigma_{0,L}$: [$\sigma_{0,L}$ in recovery $(i-1)$, $\sigma_{0,L}$ in relaxation i]
$\tau_{v,L}$: [min($\tau_{v,L}$ in recovery $(i-1)$ and relaxation i), max($\tau_{v,L}$ in recovery $(i-1)$ and relaxation i)]
$K_{v,S}$: [1, 100]
$\sigma_{0,S}$: [$\sigma_{0,S}$ in recovery $(i-1)$, $\sigma_{0,S}$ in relaxation i]
$\tau_{v,S}$: [$\tau_{v,S}$ in relaxation i, $\tau_{v,S}$ in recovery $(i-1)$]
Apply algorithm in Figure S1(d) to fit the data point h from i cycle of the RR test
$h < 5$?
No
Yes
$h = h - 1$
Update boundaries of fitting parameters:
$K_{v,L}$: [$K_{v,L,i,24} - 1$, $K_{v,L,i,24} + 1$]
$\sigma_{0,L}$: [$\sigma_{0,L}$ in recovery $(i-1)$, $\sigma_{0,L,i,h}$]
$\tau_{v,L}$: [min($\tau_{v,L}$ in recovery $(i-1)$ and relaxation i), max($\tau_{v,L}$ in recovery $(i-1)$ and relaxation i)]
$K_{v,S}$: [$K_{v,S,i,24} - 1$, $K_{v,S,i,24} + 1$]
$\sigma_{0,S}$: [$\sigma_{0,S}$ in recovery $(i-1)$, $\sigma_{0,S,i,h}$]
$\tau_{v,S}$: [$\tau_{v,S,i,h}$, $\tau_{v,S}$ in recovery $(i-1)$]
No
Solution satisfies the boundary conditions?
Yes
$i = i + 1$
No
$i \geq 29$?
Yes
Obtain all fitting parameters
For $3 \leq i \leq 29$
Calculate the average value of $K_{v,S,i,h}$ for each cycle of RR test and set them as $K_{v,S,i,avg}$
Detect the cycle number n for average values of $K_{v,S,i,avg}$ starting decrease with increase of cycle number
Fit the $K_{v,S,i,h}$ values versus stroke between cycle n to 29 using a linear equation and determine $K_{v,S,i,h}$(stroke) as a function of stroke
Set $h = 24$
Set $i = n$
Update boundaries of fitting parameters:
$K_{v,L}$: [1, 100]
$\sigma_{0,L}$: [$\sigma_{0,L}$ in recovery $(i-1)$, $\sigma_{0,L}$ in relaxation i]
$\tau_{v,L}$: [min($\tau_{v,L}$ in recovery $(i-1)$ and relaxation i), max($\tau_{v,L}$ in recovery $(i-1)$ and relaxation i)]
$K_{v,S}$: [$K_{v,S,i,h}$(stroke for relaxation i) $- 1$, $K_{v,S,i,h}$(stroke for relaxation i) $+ 1$]
$\sigma_{0,S}$: [$\sigma_{0,S}$ in recovery $(i-1)$, $\sigma_{0,S}$ in relaxation i]
$\tau_{v,S}$: [$\tau_{v,S}$ in relaxation i, $\tau_{v,S}$ in recovery $(i-1)$]
Apply algorithm in Figure S1(d) to fit the data point h from i cycle of the RR test
$h < 5$?
No
Yes
$h = h - 1$
Update boundaries of fitting parameters:
$K_{v,L}$: [$K_{v,L,i,24} - 1$, $K_{v,L,i,24} + 1$]
$\sigma_{0,L}$: [$\sigma_{0,L}$ in recovery $(i-1)$, $\sigma_{0,L,i,h}$]
$\tau_{v,L}$: [min($\tau_{v,L}$ in recovery $(i-1)$ and relaxation i), max($\tau_{v,L}$ in recovery $(i-1)$ and relaxation i)]
$K_{v,S}$: [$K_{v,S,i,h}$(stroke for relaxation i) $- 1$, $K_{v,S,i,h}$(stroke for relaxation i) $+ 1$]
$\sigma_{0,S}$: [$\sigma_{0,S}$ in recovery $(i-1)$, $\sigma_{0,S,i,h}$]
$\tau_{v,S}$: [$\tau_{v,S,i,h}$, $\tau_{v,S}$ in recovery $(i-1)$]
No
Solution satisfies the boundary conditions?
Yes
$i = i + 1$
No
$i \geq 29$?
Yes
Obtain all fitting parameters in loading

(c)

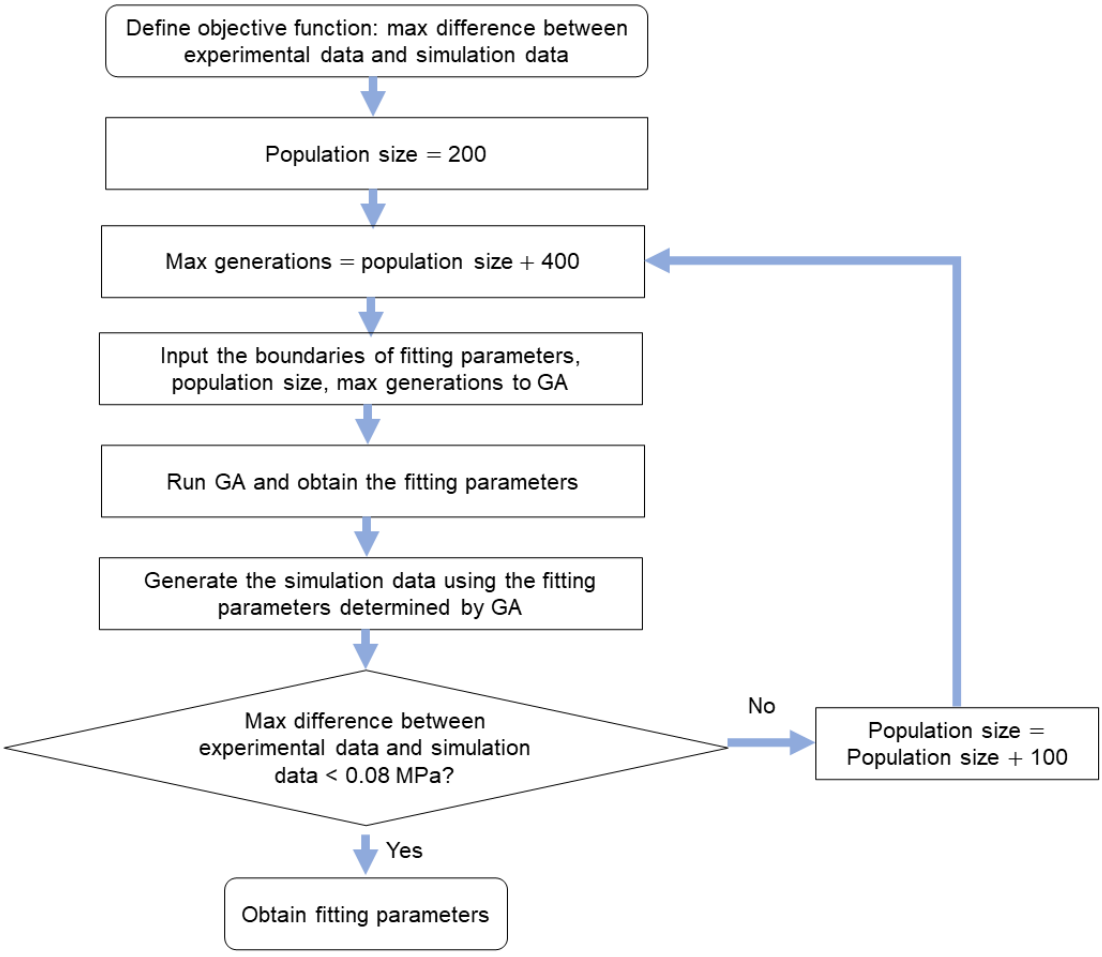

(d)

Figure S1. Flow charts for algorithms used to simulate the stress from the experimental data: (a) at relaxation stages, (b) at recovery stages, (c) at the first loading stages, and (d) details of the curve fitting using the GA in the Matlab.

Figures S2 and S3 summarize the ten sets of the fitting parameter values for the recovery stages. These figures suggest that for the recovery stages, the six fitting parameters show slightly more scattering values than their counterparts for the relaxation stages. Because of the increase in the scattering, it is not clear whether Figures S2(a) and S2(c), for $\sigma_{v,L}(0)$ and $\sigma_{0,L}$ respectively,

indicate any transitional phenomenon for the long-term viscous branch. On the other hand, Figures S2(b) and S2(d) show reasonably small coefficients of variation for $\sigma_{v,S}(0)$ and $\sigma_{0,S}$ respectively. Since these two figures do not show any transition, similar to their values for the relaxation stages, it is believed that in the RR test, transition did not occur in the deformation behavior that is represented by the short-term viscous branch. Works in the literature[1,4] have suggested that under tensile loading, transition of SCP's deformation behavior could be caused by the onset of local yielding in the crystalline phase. It, therefore, raises a question on whether the long-term viscous branch represents the viscous deformation from the interaction between the crystalline and the amorphous phases, and the short-term viscous branch the other types of viscous deformation, such as deformation of the network structure[4]. Further study on this issue is being planned when this manuscript is prepared.

Figure S2(b) also shows that after the small amount of unloading, $\sigma_{v,S}(0)$ for the following recovery stage was negative though the overall deformation of the specimen was in tension. This suggests that the spring in the short-term viscous branch could have been completely recovered before the unloading to result in the negative stress through the unloading stage. This phenomenon is consistent with the small $\tau_{v,S}$ value for the relaxation stage which allows the spring in the short-term viscous branch to be completely recovered from deformation during the relaxation stage. According to the literature[5–7], the negative stress generated by the unloading should represent the stress response from the amorphous phase, which will be examined in the near future.

For $\tau_{v,L}$ and $\tau_{v,S}$ at the recovery stages, Figures S3(a) and S3(b) suggest that their values which allow the spring-dashpot model used in the study to fit the experimental data, could vary quite significantly. Therefore, $\tau_{v,L}$ and $\tau_{v,S}$ should have little influence on the ability of the

spring-dashpot model to fit the experimental data from the RR test, consistent with the work suggested in the literature[8].

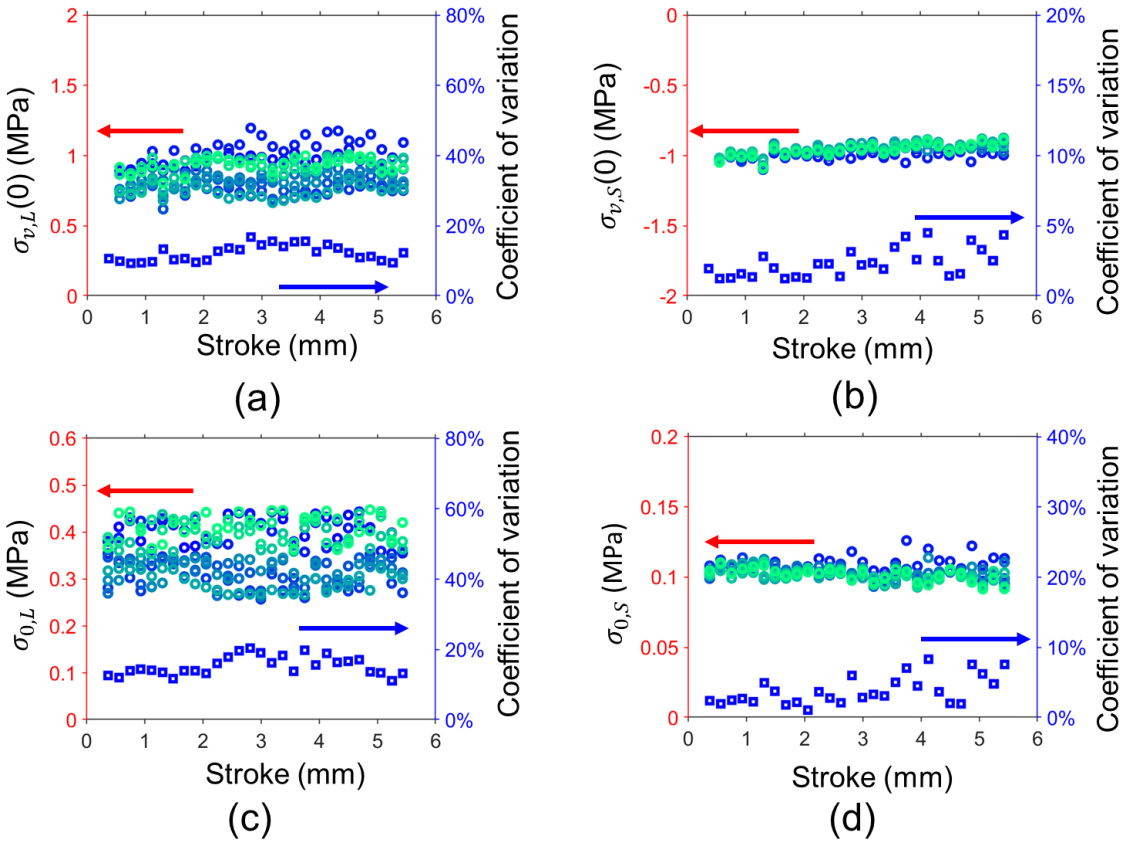

Figure S2. Summary of ten sets of values (in open circles) for fitting parameters of the spring-dashpot model in Figure 2 of the main text, and the corresponding coefficient of variation (in open squares) at the recovery stages: (a) $\sigma_{v,L}(0)$, (b) $\sigma_{v,S}(0)$, (c) $\sigma_{0,L}$, and (d) $\sigma_{0,S}$.

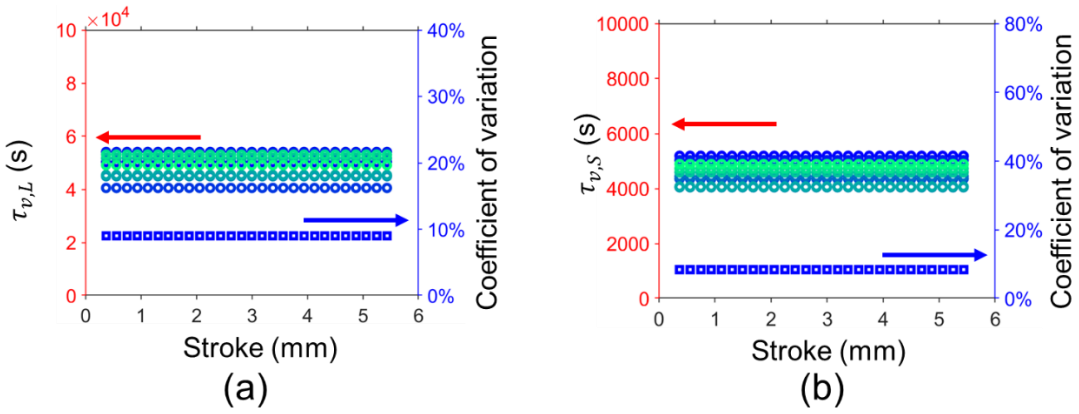

Figure S3. Summary of ten sets of values (in open circles) for fitting parameters of the spring-dashpot model, and the corresponding coefficient of variation (in open squares) at the recovery stages: (a) $\tau_{v,L}$, and (b) $\tau_{v,S}$.

References

1. Tan, N.; Jar, P.-Y.B. Determining Deformation Transition in Polyethylene under Tensile Loading. *Polymers* 2019, *11*, 1415, doi:10.3390/polym11091415.

2. Castagnet, S. High-Temperature Mechanical Behavior of Semi-Crystalline Polymers and Relationship to a Rubber-like "Relaxed" State. *Mechanics of Materials* 2009, *41*, 75–86, doi:10.1016/j.mechmat.2008.10.001.

3. Bergstrom, J.; Boyce, M.C. Constitutive Modeling of the Large Strain Time-Dependent Behavior of Elastomers. *Journal of the Mechanics and Physics of Solids* 1998, *46*, 931–954, doi:10.1016/S0022-5096(97)00075-6.

4. Hong, K.; Rastogi, A.; Strobl, G. A Model Treating Tensile Deformation of Semicrystalline Polymers: Quasi-Static Stress−Strain Relationship and Viscous Stress Determined for a Sample of Polyethylene. *Macromolecules* 2004, *37*, 10165–10173, doi:10.1021/ma049174h.

5. Drozdov, A.D.; Dusunceli, N. Two-phase model in viscoelasticity and viscoplasticity of semicrystalline polymers. *Int. J. Comp. Mat. Sci. Eng.* 2012, *01*, 1250015, doi:10.1142/S2047684112500157.

6. Drozdov, A.D.; Christiansen, J. deC. Time-Dependent Response of Polypropylene/Clay Nanocomposites under Tension and Retraction. *Polymer Engineering & Science* 2013, *53*, 931–940, doi:10.1002/pen.23340.

7. Dusunceli, N.; Drozdov, A.D.; Theilgaard, N. Influence of Temperature on Viscoelastic–Viscoplastic Behavior of Poly(Lactic Acid) under Loading–Unloading. *Polymer Engineering & Sci* 2017, *57*, 239–247, doi:10.1002/pen.24404.

8. Fritsch, J.; Hiermaier, S.; Strobl, G. Characterizing and Modeling the Non-Linear Viscoelastic Tensile Deformation of a Glass Fiber Reinforced Polypropylene. *Composites Science and Technology* 2009, *69*, 2460–2466, doi:10.1016/j.compscitech.2009.06.021.